

The background of the cover is a dark blue, starry field. Scattered throughout are numerous bright green, glowing structures that resemble cross-sections of biological tissue or cells. These structures vary in size and shape, some appearing as simple rings or circles, while others are more complex and irregular. The overall effect is that of a microscopic or cellular view of a tissue, with the green fluorescence highlighting specific components against the dark background.

FLUORESCENCE-ENHANCED
SURGICAL NAVIGATION
Towards tailored tumor detection

L.S.F. BOOGERD



FLUORESCENCE-ENHANCED SURGICAL NAVIGATION

Towards tailored tumor detection

FLUORESCENCE-ENHANCED SURGICAL NAVIGATION

Towards tailored tumor detection

Design: Caroline de Lint, Voorburg (caro@delint.nl)

All rights reserved. No part from this thesis may be reproduced, distributed or transmitted in any form or by any means, without prior written permission of the author.

Publication of this thesis was financially supported by the foundation Centre for Human Drug Research, Leiden, the Netherlands.

PROEFSCHRIFT

ter verkrijging van de graad van Doctor
aan de universiteit Leiden, op gezag van
Rector Magnificus prof. mr. C.J.J.M. Stolker,
volgens besluit van het College voor Promoties
te verdedigen donderdag 4 april 2019
klokke 16:15 uur

DOOR

Leonora Sophia Francesca Boogerd
geboren te Haarlem
in 1987

PROMOTORES

Prof. dr. C.J.H. van de Velde
Prof. dr. J. Burggraaf

CO-PROMOTOR

Dr. A.L. Vahrmeijer

LEDEN PROMOTIECOMMISSIE

Prof. dr. L.F. de Geus-Oei
Prof. dr. C.W.G.M. Löwik (Erasmus Medisch Centrum, Rotterdam)
Prof. dr. H.J. Bonjer (Amsterdam UMC, locatie VUMC, Amsterdam)
Prof. dr. C. Verhoef (Erasmus Medisch Centrum, Rotterdam)

	1	General introduction and outline of the thesis – 7
PART I		FLUORESCENCE-GUIDED HEPATO-PANCREATICO-BILIARY SURGERY USING NON-TARGETED DYES
	2	The best approach for laparoscopic fluorescence cholangiography: overview of the literature and optimization of dose and dosing time – 21
	3	Application of near-infrared fluorescence imaging during modified associating liver partition and portal vein ligation for staged hepatectomy – 39
	4	Laparoscopic detection and resection of occult liver tumors of multiple cancer types using real-time near-infrared fluorescence guidance – 43
PART II		PRECLINICAL EVALUATION OF TUMOR TARGETS FOR FLUORESCENCE IMAGING
	5	Concordance of folate receptor- α expression between biopsy, primary tumor and metastasis in breast and lung cancer patients – 61
	6	Fluorescence-guided tumor detection with a novel anti-EPCAM targeted antibody fragment: preclinical validation – 83
	7	Correlation between preoperative serum carcinoembryonic antigen levels and expression on pancreatic and rectal cancer tissue – 105
	8	Biomarker expression in rectal cancer tissue before and after neoadjuvant therapy – 119
PART III		CLINICAL TRANSLATION OF TUMOR-TARGETED FLUORESCENT TRACERS
	9	Folate receptor- α targeted near-infrared fluorescence imaging in high-risk endometrial cancer patients: a tissue microarray and clinical feasibility study – 139
	10	Safety and effectiveness of SGM-101, a fluorescent antibody targeting carcinoembryonic antigen, for intraoperative detection of colorectal cancer: a dose-escalation, pilot study – 155
PART IV		SUMMARY AND APPENDICES
	11	Summary, discussion and future perspectives – 183
	12	Nederlandse samenvatting – 195
		List of publications – 200
		Curriculum Vitae – 205
		Dankwoord – 206

CHAPTER I

GENERAL INTRODUCTION AND OUTLINE OF THE THESIS

Adapted from: Image-Guided Surgery. Poston G,
Audisio R and Wild L (editors), chapter in *Surgical Oncology*, 2016

LSF BOOGERD, HJM HANDGRAAF, MC BOONSTRA,
AL VAHRMEIJER AND CJH VAN DE VELDE

The diagnostic accuracy of preoperative imaging modalities such as magnetic resonance imaging (MRI) and computed tomography (CT)-scan has improved considerably over the last decades, but their ability to detect small sized tumor lesions remains suboptimal¹. In addition, translation of these images to the surgical theatre is challenging as these images do commonly not depict the actual situation in the patient's body. Image-guided surgery (IGs) using near-infrared (NIR) fluorescence is a promising intraoperative imaging modality that can assist surgeons to identify tumor tissue, lymph nodes and vital structures². This imaging modality gives real-time information during surgical procedures by revealing the location of targeted tissue. Hence it may improve patient outcome, e.g. by reducing the number of positive resection margins or by decreasing the risk of iatrogenic damage to vital structures. Here, we describe an overview of the technique, applications and perspectives of NIR fluorescence IGs.

NEAR-INFRARED FLUORESCENCE IMAGING

TECHNIQUE ••• NIR fluorescence IGs uses fluorophores that emit light after excitation³. Especially fluorophores emitting light in the NIR wavelength spectrum (700–900nm) are of interest, because autofluorescence and light absorbance of normal tissue structures, such as blood or fatty tissue, are low at these wavelength spectra⁴. Consequently, relatively deep tissue penetration can be achieved enabling visualisation of structures up to a depth of 10mm^{5,6}. Furthermore, this light is invisible for the human eye and therefore does not alter the surgical field.

Next to an optimal fluorophore, a fluorescence imaging system consisting of a light source that is able to excite fluorophores combined with a camera that can detect the emitted fluorescence is required (fig. 1). Since the introduction of IGs in 1998, various commercially available NIR fluorescence imaging systems have been developed, either for open, laparoscopic or robotic surgery⁷. All imaging systems have to overcome specific challenges to optimize their utility, such as enabling sufficient fluorescence excitation, low-attenuation optics for NIR light and enough sensitivity to detect low concentrations of NIR fluorophores⁵. High fluence rates of the excitation light would be optimal to achieve deep tissue penetration. However, safety of the technique is partly dependent on illumination levels. High power levels can burn tissue and photobleach contrast agents⁸. Therefore, fluence rates are currently restricted to the range of 10–25mW/cm².

Most fluorescence imaging systems are capable to show normal white light images next to NIR fluorescence images⁷. Some imaging systems have the ability to display a real-time overlay of the fluorescence and normal light image, which enhances

anatomical orientation of the origin of the fluorescent signal. Overall, important factors varying between all produced NIR imaging systems are wavelength of the excitation light, internal optics, usability and costs. No widely used fluorescence imaging standard is yet available resulting in difficulties to compare performance of imaging devices in an objective manner⁹.

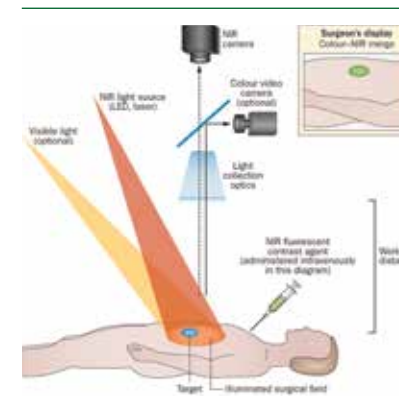


Figure 1 The mechanism of fluorescence IGs

After injection of a fluorophore, either intravenously, peritumorally or topically, its localization can be visualized by NIR fluorescence imaging. During surgery, the NIR light source can be positioned above the surgical field with a distance of approximately 20–30cm, or can be encased within a fiberscope for minimally invasive and robotic surgery. Some NIR fluorescence imaging system can simultaneously display color-, NIR fluorescence-, and overlay images in real-time during surgery and thereby enhance anatomical orientation.

Image reprinted by permission from Macmillan Publishers Ltd.: Nature medicine². Copyright © 2013

CLINICAL INDICATIONS

SENTINEL LYMPH NODE MAPPING ••• The sentinel lymph node (SLN) procedure can be improved by using NIR fluorescence IGs². Currently, SLN mapping is performed by a peritumoral injection of a radiotracer and/or blue dye. The radioactive tracer is injected the day before surgery, after which SLNs can be detected using Single Photon Emission Computed Tomography (SPECT)/CT or lymphoscintigraphy. The radioactive signal can be traced using a handheld gamma probe during surgery. Blue dye is injected peritumorally prior to the first incision and provides visual guidance shortly thereafter. However, not all SLNs stain blue; for example in only 69% of vulvar cancer patients blue SLNs could be identified¹⁰. Nonetheless, the combined approach results in high SLN detection rates and low numbers of false negative lymph nodes and is currently standard-of-care in surgery for melanoma, breast and vulvar cancer patients^{11–13}. However, high costs of using radioactivity, the risk of radiation exposure, discoloration of the surgical field and long-lasting tattooing of the skin by using blue dye, emphasize the need for improvements.

Indocyanine green (ICG) is used as the preferred NIR fluorescent dye for SLN mapping. For decades, ICG has been registered and used to determine cardiac output, hepatic function and ophthalmic perfusion¹⁴. Application of ICG as lymphatic tracer

was initially based on its intrinsic green color resulting in relatively low contrast and consequently low SLN detection rates^{15,16}. However, its fluorescent characteristics have resulted in superior SLN detection rates compared to blue dye alone¹⁷. After peritumoral injection of a low dose of ICG (1.6mL of 500µM), the lymphatic drainage could be traced in real-time using a NIR fluorescence imaging system. Lymphatic vessels and lymph nodes can sometimes even be identified percutaneously, which facilitates the procedure and may decrease incisional length and postoperative morbidity¹⁸. The use of ICG as NIR fluorescent tracer has been studied in SLN procedures in head-and-neck, breast, skin, gastro-intestinal, urological and gynaecological cancer patients (fig. 2a)^{10, 19-23}. ICG emits light with a wavelength of 820 nm, is cleared almost exclusively by the liver and has an elimination half-life in blood of approximately 3 minutes²⁴. Allergic reactions after administration are rare and have been documented in less than 1:10,000 patients, but only in doses above 0.5mg/kg¹⁴. The doses used in NIR fluorescence imaging are lower: between 0.1-0.5mg/kg²⁵. Although use of NIR fluorescence light results in deeper tissue penetration (up to 10mm) than use of a conventional blue dye (1mm), the relatively superficial tissue penetration still remains a problem for SLN detection in obese patients. Furthermore, injection of ICG alone as lymphatic tracer has been shown to result in fluorescent staining of second tier nodes. Therefore, ICG has been non-covalently absorbed to albumin nanocolloid assuming that a larger hydrodynamic diameter would lead to less staining of higher tier nodes and a better retention in the SLN^{2,26}. In Europe, an albumin-based tracer is most commonly used since ICG already shows high affinity for albumin, while in the USA a sulphur based colloid is commonly used²⁷. A hybrid tracer, combining ICG and 99mTechnetium nanocolloid (ICG:99mTc) has been studied in feasibility trials for SLN mapping²⁸. Although those studies were intended as feasibility studies, ICG outperformed blue dye as tracer. Moreover, one combined preoperative injection of ICG:99mTc resulted in similar sensitivity rates.

IDENTIFICATION OF VITAL STRUCTURES ••• Morbidity after surgery depends partly on the extent of damage to vital structures, such as nerves, ureters and bile ducts. Although laparoscopic and robotic surgery have decreased morbidity rates, iatrogenic damage is sometimes inevitable. One step closer to preservation of vital structures is highlighting these structures using NIR fluorescence imaging. Currently, nerves are identified during surgery by inspection, potentially in combination with electromyographic (EMG) monitoring. However, nerve damage is still frequently observed, resulting in pain, numbness, weakness or paralysis. Preclinical studies already showed accurate identification of nerves as small as 50µm using the specific peptide NP41 and Oxazine 4, but none of these agents are clinically evaluated or approved²⁹⁻³¹.

Bile duct imaging can be achieved by low dose (2.5-20 mg) intravenous ICG injection prior to surgery³². Since ICG is almost exclusively cleared by the liver via biliary secretion, it can be used to explore the biliary anatomy with NIR fluorescence imaging. Preferably ICG is administered 24 hrs before surgery because injection directly prior to, or during surgery results in highly fluorescent liver tissue, concealing the bile ducts³³. The optimal dose of ICG and time of dosing is yet to be defined. When applied appropriately, ICG improves anatomical orientation and may decrease complication rates particularly in patients with an aberrant biliary anatomy, severe adhesions or patients undergoing major liver surgery.

Another delicate structure that is sensitive to damage is the ureter. In a clinical feasibility study, the ureter was successfully visualized with methylene blue (MB) as NIR fluorophore (fig. 2b)³⁴. MB is fluorescent at 700 nm and is partly cleared by the kidneys. Alike ICG, MB was first used for its intrinsic blue color³⁵. However, this requires high doses (7.5mg/kg) and may result in serious adverse events, such as toxic metabolic encephalopathy³⁶. In strongly diluted concentrations, MB reveals its fluorescent properties³⁷. Intravenous injection of doses of 0.5-1.0 mg/kg MB resulted in good visualization of the ureters and no serious adverse events are reported at these low dose levels³⁴. However, as MB is a suboptimal fluorophore, improvement can be expected when novel 800nm fluorophores, such as ZW800-1, will become available for clinical use. The quantum yield, i.e. brightness of the fluorescent signal, of ZW800-1 is four times higher and ZW800-1 is cleared exclusively by the kidneys, potentially resulting in a much brighter signal in the ureters³⁸. Clinical evaluation of this new agent is currently ongoing.

PERFUSION ANGIOGRAPHY ••• Sufficient blood supply is of vital importance in the creation of intestinal anastomosis. Although complications such as stricture or leakage have multifactorial causes, any means to minimize or avoid these is desirable³⁹. A reliable, relatively easy and low-risk method to assess vascularization of anastomosis is NIR fluorescence angiography. Several studies have shown the feasibility of NIR fluorescence angiography during intestinal surgery by using low doses of ICG⁴⁰⁻⁴². Intravenous injection of 2.5-7.5mg ICG led to real-time feedback about the perfusion of the organ of interest. A randomized controlled trial to evaluate the use of intraoperative fluorescence angiography to prevent anastomotic leakage in rectal cancer surgery is currently ongoing⁴³. Objective criteria for insufficient blood flow are yet to be determined, because quantification of the fluorescence signal is not directly correlated to the actual perfusion. Nonetheless, in the hands of an experienced surgeon, NIR fluorescence angiography may contribute to reduced anastomotic complication rates. Fluorescence angiography has also been proven to be

helpful in reconstructive cancer surgery⁴⁴. By intraoperative identification of vascular perfusion to free or pedicled flaps, selection of well-vascularized flaps can be performed and venous outflow can be monitored⁴⁵.

TUMOR IDENTIFICATION USING CLINICALLY AVAILABLE FLUOROPHORES

Tumor imaging is already feasible by using the nonspecific dyes ICG and MB. Liver metastases and hepatocellular carcinoma (HCC) can be identified due to the inherent properties of ICG. Metastases are identifiable by a fluorescent rim, caused by stasis of ICG in compressed liver parenchyma. Healthy hepatocytes clear ICG within approximately 24h. Compression by tumor tissue causes obstructed bile canaliculi. In addition, compression and inflammation lead to an increased presence of immature hepatocytes, in which ICG tends to accumulate. As a result, superficially located liver metastases, even as small as 1 mm, can be identified by a characteristic fluorescent rim pattern surrounding the metastases (fig. 2c). Van der Vorst et al. showed that with NIR fluorescence imaging, 24 or 48 hours after intravenous injection of either 10 or 20mg ICG, superficial liver metastases that were otherwise undetectable were identified in 5 out of 40 patients with colorectal cancer during open surgery⁴⁶. Also in patients with pancreatic cancer additional metastases were identified in 8 out of 49 patients (16%)⁴⁷. Especially small, superficially located liver metastases can be more readily detected by use of NIR fluorescence imaging, since intraoperative ultrasound (IOUS) has more added value in detection of more deeply located metastases (>6mm)⁴⁸. In addition, the resolution of CT is too low to accurately detect lesions smaller than 10mm⁴⁹.

Ishizawa et al. were the first to demonstrate NIR fluorescence detection of HCC after a preoperative injection of ICG, resulting in a clear fluorescence signal throughout the tumor⁵⁰. Currently, three types of fluorescence can be classified in HCC patients: uniform, partial and rim-type. The type of fluorescence is associated with tumor pathology. Well- or moderately differentiated HCCs show mostly uniform fluorescence, whereas poorly differentiated HCCs show partly or rim-type fluorescence⁵¹. Besides NIR fluorescence detection of liver metastases and HCCs, tumor imaging after an intravenous injection of ICG has been investigated in pancreatic cancer patients assuming that accumulation of the NIR fluorophore in tumorous lesions would occur because of the enhanced permeation and retention (EPR) effect⁵². Due to a combination of newly formed, porous blood vessels and poorly developed lymphatic vessels in tumor tissue, large molecules such as ICG retain in the tumor⁵³. The EPR effect mainly depends on physical characteristics of injected macromolecules and therefore leads to non-specific targeting⁵⁴. Although in breast cancer patients the EPR effect did result in tumor detection, pancreatic cancer lesions nor metastatic

ovarian cancer lesions could be identified after systemic injection of ICG. A possible explanation for this failure might be the difference in tumor biology^{52,55}.

MB was initially used to visualize enlarged parathyroid adenomas and neuroendocrine tumors; administration of a high dose of MB (up to 7.5mg/kg) resulted in macroscopically visible blue staining of the tumor^{35,36}. After dilution, using its fluorescent characteristics, NIR fluorescence detection of various types of (neuro-) endocrine tumors by administration of 1mg/kg MB appeared feasible^{56,57}. However, the exact mechanism of tracer uptake in these tumors remains unclear. A recent study showed visualization of hyperparathyroid adenomas after a single injection of 0.5mg/kg and MB has also been successfully used for tumor identification in breast cancer patients^{56,58}.

Since the first report of intraoperative use of fluorescein for detection of brain tumors in 1948, fluorescence imaging is applied in neurosurgical procedures⁵⁹. Oral administration three hours before surgery of 5-aminolevulinic acid (5-ALA), a precursor of the hemoglobin synthesis pathway, results in accumulation of fluorescing protoporphyrin IX (PPIX) in malignant tissue^{60,61}. By using a specifically modified neurosurgical microscope, 5-ALA can be identified by excitation with violet-blue light. In a large phase III multicentre randomized controlled trial (RCT) in 2006, Stummer et al. demonstrated the benefit of fluorescence-guided resection of malignant gliomas using 5-ALA compared to conventional white light resection. 5-ALA resulted in a higher number of complete tumor resections (65% vs. 36%) and significantly prolonged 6-month progression-free survival (41% vs. 21%)⁶¹. Application of 5-ALA is nowadays approved for resection of high-grade malignant gliomas.

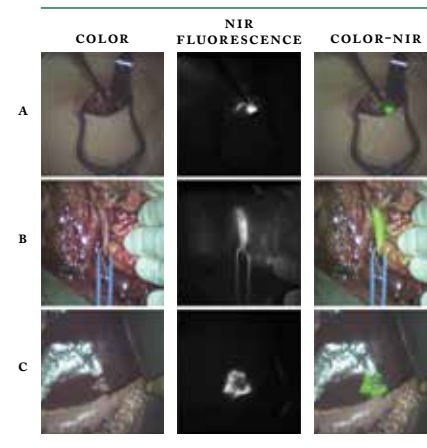


Figure 2 Applications of fluorescence ICG

Displayed from left to right (A, B, C) are color, NIR fluorescence and color-NIR overlay images.

- A Example of sentinel lymph node detection in a patient with breast cancer after periareolar-injection of 1.6mL 0.5 mM indocyanine green. A lymphatic vessel leading to the SLN is clearly visible. The surgical field is not altered by staining of any dye.
- B Example of ureter visualisation after intravenous administration of 1mg/kg methylene blue.
- C Example of colorectal liver metastasis identification after preoperative injection (24h before surgery) of 10mg indocyanine green. A fluorescent rim pattern surrounding the colorectal liver metastasis clearly marks the border of the tumor.

TUMOR IDENTIFICATION USING TUMOR-TARGETED FLUORESCENT DYES ••• Although broadly applied clinically, 5-ALA nor ICG or MB are tumor-specific fluorophores. Identification of novel targets, based on the various hallmarks of cancer, have paved the way to develop tumor-specific fluorophores⁶². To accomplish tumor-specific targeting, a tumor recognizing ligand, such as an antibody or nanobody, has to be conjugated to a (NIR) fluorescent dye. Both ICG and MB cannot easily be conjugated due to their chemical properties, but relatively novel conjugatable NIR fluorophores include IRDYE800CW (LI-COR, Biosciences, Lincoln, NE) and ZW800-1 (Curadel Surgical Innovations, Wayland, MA). They share favourable characteristics such as emission at a wavelength range of 800nm, small size and low toxicity.

A milestone in tumor-targeted fluorescence imaging was the first in-human trial with Folate-FITC for visualization of metastatic ovarian cancer⁶³. The folate receptor is upregulated in ovarian cancer and targeting of this receptor with Folate-FITC, i.e. folate conjugated to a 500nm fluorophore, resulted in intraoperative detection of otherwise undetected tumor lesions. Since then, various tumor-targeted imaging agents have been tested in first-in-human trials⁶⁴⁻⁶⁷. Vehicles can either be antibodies, but other ligands such as fragments of antibodies, nanobodies, small peptides or much larger nanoparticles are currently also evaluated for clinical use. Although results are promising, there appears to be substantial variation in the quality of fluorescence tumor detection as shown by the varying fluorescence intensity of tumors between patients. This may be due to the heterogeneity of expression of tumor molecules between patients, heterogeneity in the tumor itself, anatomical location of the tumor or combinations thereof. Further, it appears that variability is due to differences caused by physico-chemical properties of the ligands and differences between imaging systems and the machine settings used for imaging. It is therefore of utmost importance to identify what patients can benefit most from particular types of tumor-specific agents, before these (vulnerable oncological) patients are exposed to possibly harmful novel agents. At the mean time, the quest for the optimal tumor target to use for IGS continues.

OUTLINE OF THE THESIS

This thesis is divided in three parts; PART I describes the clinical use of the non-targeted fluorescent dye ICG during hepato-pancreatico-biliary (HPB) surgery, PART II focuses on the preclinical development and evaluation of novel tracers for fluorescence-guided surgery and PART III describes the clinical introduction of newly developed tumor-specific fluorescent contrast agents for intraoperative tumor

detection. PART I, chapter two describes an overview of all clinical studies describing different strategies for fluorescence cholangiography and a clinical trial to identify the optimal dose and timing of administration of ICG for bile duct identification. Chapter three explores the use of ICG during a (relatively) novel surgical procedure as treatment option for patients with initially unresectable liver tumors: associating liver partition and portal vein ligation for staged hepatectomy (ALPPS). Chapter four demonstrates the added value of ICG during laparoscopic resection of multiple types of liver tumors.

PART II, chapter five describes the expression of Folate Receptor- α (FR- α) in breast cancer and non-small cell lung cancer and investigates the concordance between preoperative biopsies, primary tumor tissues and metastases. Chapter 6 describes the preclinical development and validation of a novel EPCAM-targeted fluorescent imaging agent as pluripotent tumor imaging target. In chapter 7, preoperative serum CEA is compared with the expression of CEA on tumor tissue derived from patients with pancreatic or rectal cancer. Chapter 8 investigates expression of EPCAM, CEA and C-MET on rectal cancer tissue, derived from patients who did or did not receive preoperative (chemo)radiotherapy and compared the differences in expression patterns between these groups.

PART III, chapter 9 demonstrates FR- α expression in tissues derived from high-risk endometrial cancer patients and shows the first clinical experience with OTL-38 (a folate targeting NIR fluorescent agent) in endometrial cancer patients. Chapter 10 describes the clinical translation of a novel tumor-specific CEA-targeted NIR fluorescent tracer for intraoperative detection of primary, recurrent and metastatic colorectal cancer.

PART IV contains a summary of the thesis and a general discussion on the future perspectives of fluorescence-enhanced surgical navigation.

REFERENCES

- 1 Frangioni JV. New technologies for human cancer imaging. *J Clin Oncol* 2008; 26(24): 4012-21.
- 2 Vahrmeijer AL, Hutteman M, van der Vorst JR, van de Velde CJ, Frangioni JV. Image-guided cancer surgery using near-infrared fluorescence. *Nat Rev Clin Oncol* 2013; 10(9): 507-18.
- 3 Vahrmeijer AL, Frangioni JV. Seeing the invisible during surgery. *Br J Surg* 2011; 98(6): 749-50.
- 4 Frangioni JV. In vivo near-infrared fluorescence imaging. *Curr Opin Chem Biol* 2003; 7(5): 626-34.
- 5 Keerweeer S, Van Driel PB, Snoeks TJ, et al. Optical image-guided cancer surgery: challenges and limitations. *Clin Cancer Res* 2013; 19(14): 3745-54.
- 6 Chance B. Near-infrared (NIR) optical spectroscopy characterizes breast tissue hormonal and age status. *Acad Radiol* 2001; 8(3): 209-10.
- 7 Zhu B, Sevick-Muraca EM. A review of performance of near-infrared fluorescence imaging devices used in clinical studies. *Br J Radiol* 2015; 88(1045): 20140547.
- 8 Gioux S, Choi HS, Frangioni JV. Image-guided surgery using invisible near-infrared light: fundamentals of clinical translation. *Mol Imaging* 2010; 9(5): 237-55.
- 9 Snoeks TJ, van Driel PB, Keerweeer S, et al. Towards a successful clinical implementation of fluorescence-guided surgery. *Mol Imaging Biol* 2014; 16(2): 147-51.
- 10 Handgraaf HJ, Verbeek FP, Tummers QR, et al. Real-time near-infrared fluorescence guided surgery in gynecological oncology: a review of the current state of the art. *Gynecol Oncol* 2014; 135(3): 606-13.
- 11 Morton DL, Thompson JF, Cochran AJ, et al. Sentinel-node biopsy or nodal observation in melanoma. *N Engl J Med* 2006; 355(13): 1307-17.
- 12 Giuliano AE, Kirgan DM, Guenther JM, Morton DL. Lymphatic mapping and sentinel lymphadenectomy for breast cancer. *Ann Surg* 1994; 220(3): 391-8; 8-401.
- 13 Van der Zee AG, Oonk MH, De Hullu JA, et al. Sentinel node dissection is safe in the treatment of early-stage vulvar cancer. *J Clin Oncol* 2008; 26(6): 884-9.
- 14 Schaafsma BE, Mieog JS, Hutteman M, et al. The clinical use of indocyanine green as a near-infrared fluorescent contrast agent for image-guided oncologic surgery. *J Surg Oncol* 2011; 104(3): 323-32.
- 15 Motomura K, Inaji H, Komoike Y, et al. Combination technique is superior to dye alone in identification of the sentinel node in breast cancer patients. *J Surg Oncol* 2001; 76(2): 95-9.
- 16 Motomura K, Inaji H, Komoike Y, et al. Sentinel Node Biopsy in Breast Cancer Patients with Clinically Negative Lymph-Nodes. *Breast Cancer* 1999; 6(3): 259-62.
- 17 van der Vorst JR, Schaafsma BE, Verbeek FP, et al. Randomized comparison of near-infrared fluorescence imaging using indocyanine green and 99(m) technetium with or without patent blue for the sentinel lymph node procedure in breast cancer patients. *Ann Surg Oncol* 2012; 19(13): 4104-11.
- 18 Hutteman M, van der Vorst JR, Gaarenstroom KN, et al. Optimization of near-infrared fluorescence sentinel lymph node mapping for vulvar cancer. *Am J Obstet Gynecol* 2012; 206(1): 89 e1-5.
- 19 van der Vorst JR, Schaafsma BE, Verbeek FP, et al. Near-infrared fluorescence sentinel lymph node mapping of the oral cavity in head and neck cancer patients. *Oral Oncol* 2013; 49(1): 15-9.
- 20 Tong M, Guo W, Gao W. Use of Fluorescence Imaging in Combination with Patent Blue Dye versus Patent Blue Dye Alone in Sentinel Lymph Node Biopsy in Breast Cancer. *J Breast Cancer* 2014; 17(3): 250-5.
- 21 Cloyd JM, WapNIR IL, Read BM, Swetter S, Greco RS. Indocyanine green and fluorescence lymphangiography for sentinel lymph node identification in cutaneous melanoma. *J Surg Oncol* 2014; 110(7): 888-92.
- 22 Can MF, Yagci G, Cetiner S. Systematic review of studies investigating sentinel node navigation surgery and lymphatic mapping for gastric cancer. *J Laparoendosc Adv Surg Tech A* 2013; 23(8): 651-62.
- 23 Schaafsma BE, Verbeek FP, Elzevier HW, et al. Optimization of sentinel lymph node mapping in bladder cancer using near-infrared fluorescence imaging. *J Surg Oncol* 2014; 110(7): 845-50.
- 24 Shimizu S, Kamiike W, Hatanaka N, et al. New method for measuring ICG Rmax with a clearance meter. *World J Surg* 1995; 19(1): 113-8; 8.
- 25 Boni L, David G, Mangano A, et al. Clinical applications of indocyanine green (ICG) enhanced fluorescence in laparoscopic surgery. *Surg Endosc* 2015; 29(7): 2046-55.
- 26 Buckle T, van Leeuwen AC, Chin PT, et al. A self-assembled multimodal complex for combined pre- and intraoperative imaging of the sentinel lymph node. *Nanotechnology* 2010; 21(35): 355101.
- 27 Morton DL, Bostick PJ. Will the true sentinel node please stand? *Ann Surg Oncol* 1999; 6(1): 12-4.
- 28 Brouwer OR, Buckle T, Vermeeren L, et al. Comparing the hybrid fluorescent-radioactive tracer indocyanine green-99mTc-nanocolloid with 99mTc-nanocolloid for sentinel node identification: a validation study using lymphoscintigraphy and SPECT/CT. *J Nucl Med* 2012; 53(7): 1034-40.
- 29 Whitney MA, Crisp JL, Nguyen LT, et al. Fluorescent peptides highlight peripheral nerves during surgery in mice. *Nat Biotechnol* 2011; 29(4): 352-6.
- 30 Park MH, Hyun H, Ashitate Y, et al. Prototype nerve-specific near-infrared fluorophores. *Theranostics* 2014; 4(8): 823-33.
- 31 Barth CW, Gibbs SL. Direct Administration of Nerve-Specific Contrast to Improve Nerve Sparing Radical Prostatectomy. *Theranostics* 2017; 7(3): 573-93.
- 32 Schols RM, Connell NJ, Stassen LP. Near-infrared fluorescence imaging for real-time intraoperative anatomical guidance in minimally invasive surgery: a systematic review of the literature. *World J Surg* 2015; 39(5): 1069-79.
- 33 Verbeek FP, Schaafsma BE, Tummers QR, et al. Optimization of near-infrared fluorescence cholangiography for open and laparoscopic surgery. *Surg Endosc* 2014; 28(4): 1076-82.
- 34 Verbeek FP, van der Vorst JR, Schaafsma BE, et al. Intraoperative near infrared fluorescence guided identification of the ureters using low dose methylene blue: a first in human experience. *J Urol* 2013; 190(2): 574-9.
- 35 Dudley NE. Methylene blue for rapid identification of the parathyroids. *Br Med J* 1971; 3(5776): 680-1.
- 36 Keaveny TV, Tawes R, Belzer FO. A new method for intra-operative identification of insulinomas. *Br J Surg* 1971; 58(3): 233-4.
- 37 Winer JH, Choi HS, Gibbs-Strauss SL, et al. Intraoperative localization of insulinoma and normal pancreas using invisible near-infrared fluorescent light. *Ann Surg Oncol* 2010; 17(4): 1094-100.
- 38 Choi HS, Gibbs SL, Lee JH, et al. Targeted zwitterionic near-infrared fluorophores for improved optical imaging. *Nat Biotechnol* 2013; 31(2): 148-53.
- 39 Girard E, Messager M, Sauvanet A, et al. Anastomotic leakage after gastrointestinal surgery: diagnosis and management. *J Visc Surg* 2014; 151(6): 441-50.
- 40 Ris F, Hompes R, Cunningham C, et al. Near-infrared (NIR) perfusion angiography in minimally invasive colorectal surgery. *Surg Endosc* 2014; 28(7): 2221-6.
- 41 Diana M, Noll E, Diemunsch P, et al. Enhanced-reality video fluorescence: a real-time assessment of intestinal viability. *Ann Surg* 2014; 259(4): 700-7.
- 42 Jafari MD, Wexner SD, Martz JE, et al. Perfusion assessment in laparoscopic left-sided/anterior resection (PILLAR 11): a multi-institutional study. *J Am Coll Surg* 2015; 220(1): 82-92 e1.
- 43 Armstrong G, Croft J, Corrigan N, et al. IntAct: intra-operative fluorescence angiography to prevent anastomotic leak in rectal cancer surgery: a randomized controlled trial. *Colorectal Dis* 2018; 20(8): 226-234.
- 44 Lee BT, Hutteman M, Gioux S, et al. The FLARE intraoperative near-infrared fluorescence imaging system: a first-in-human clinical trial in perforator flap breast reconstruction. *Plast Reconstr Surg* 2010; 126(5): 1472-81.
- 45 Newman MI, Samson MC, Tamburrino JF, Swartz KA. Intraoperative laser-assisted indocyanine green angiography for the evaluation of mastectomy flaps in immediate breast reconstruction. *J Reconstr Microsurg* 2010; 26(7): 487-92.
- 46 van der Vorst JR, Schaafsma BE, Hutteman M, et al. Near-infrared fluorescence-guided resection of colorectal liver metastases. *Cancer* 2013; 119(18): 3411-8.
- 47 Yokoyama N, Otani T, Hashidate H, et al. Real-time detection of hepatic micrometastases from pancreatic cancer by intraoperative fluorescence imaging: preliminary results of a PROSPECTIVE study. *Cancer* 2012; 118(11): 2813-9.
- 48 Nomura K, Kadoya M, Ueda K, et al. Detection of hepatic metastases from colorectal carcinoma: comparison of histopathologic features of anatomically resected liver with results of preoperative imaging. *J Clin Gastroenterol* 2007; 41(8): 789-95.
- 49 Nickel MC, Bipat S, Stoker J. Diagnostic imaging of colorectal liver metastases with CT, MR imaging, FDG PET, and/or FDG PET/CT: a meta-analysis of prospective studies including patients who have not previously undergone treatment. *Radiology* 2010; 257(3): 674-84.
- 50 Ishizawa T, Fukushima N, Shibahara J, et al. Real-time identification of liver cancers by using indocyanine green fluorescent imaging. *Cancer* 2009; 115(11): 2491-504.
- 51 Ishizawa T, Masuda K, Urano Y, et al. Mechanistic background and clinical applications of indocyanine green fluorescence imaging of hepatocellular carcinoma. *Ann Surg Oncol* 2014; 21(2): 440-8.
- 52 Hutteman M, van der Vorst JR, Mieog JS, et al. Near-infrared fluorescence imaging in patients undergoing pancreaticoduodenectomy. *Eur Surg Res* 2011; 47(2): 90-7.
- 53 Matsumura Y, Maeda H. A new concept for macromolecular therapeutics in cancer chemotherapy: mechanism of tumorotropic accumulation of proteins and the antitumor agent smancs. *Cancer Res* 1986; 46(12 Pt 1): 6387-92.
- 54 Maeda H, Wu J, Sawa T, Matsumura Y, et al. Tumor vascular permeability and the EPR effect in macromolecular therapeutics: a review. *J Control Release* 2000; 65(1-2): 271-84.
- 55 Hagen A, Grosenick D, MacDonald R, et al. Late-fluorescence mammography assesses tumor capillary permeability and differentiates malignant from benign lesions. *Opt Express* 2009; 17(19): 17016-33.
- 56 van der Vorst JR, Schaafsma BE, Verbeek FP, et al. Intraoperative near-infrared fluorescence imaging of parathyroid adenomas with use of low-dose methylene blue. *Head Neck* 2014; 36(6): 853-8.
- 57 van der Vorst JR, Vahrmeijer AL, Hutteman M, et al. Near-infrared fluorescence imaging of a solitary fibrous tumor of the pancreas using methylene blue. *World J Gastrointest Surg* 2012; 4(7): 180-4.
- 58 Tummers QR, Verbeek FP, Schaafsma BE, et al. Real-time intraoperative detection of breast cancer using near-infrared fluorescence imaging and Methylene Blue. *Eur J Surg Oncol* 2014; 40(7): 850-8.
- 59 Moore GE, Peyton WT, et al. The clinical use of fluorescein in neurosurgery; the localization of brain tumors. *J Neurosurg* 1948; 5(4): 392-8.
- 60 Stummer W, Stocker S, Novotny A, et al. In vitro and in vivo porphyrin accumulation by C6 glioma cells after exposure to 5-aminolevulinic acid. *J Photochem Photobiol B* 1998; 45(2-3): 160-9.
- 61 Stummer W, Pichlmeier U, Meinel T, et al. Fluorescence-guided surgery with 5-aminolevulinic acid for resection of malignant glioma: a randomised controlled multicentre phase III trial. *Lancet Oncol* 2006; 7(5): 392-401.

- 62 Keereweer S, Van Driel PB, Robinson DJ, Lowik CW. Shifting focus in optical image-guided cancer therapy. *Mol Imaging Biol* 2014; 16(1): 1-9.
- 63 van Dam GM, Themelis G, Crane LM, et al. Intraoperative tumor-specific fluorescence imaging in ovarian cancer by folate receptor-alpha targeting: first in-human results. *Nat Med* 2011; 17(10): 1315-9.
- 64 Burggraaf J, Kamerling IM, Gordon PB, et al. Detection of colorectal polyps in humans using an intravenously administered fluorescent peptide targeted against c-Met. *Nat Med* 2015; 21(8): 955-61.
- 65 Hoogstins CE, Tummers QR, Gaarenstroom KN, et al. A Novel Tumor-Specific Agent for Intraoperative Near-Infrared Fluorescence Imaging: A Translational Study in Healthy Volunteers and Patients with Ovarian Cancer. *Clin Cancer Res* 2016; 22(12): 2929-38.
- 66 Harlaar NJ, Koller M, de Jongh SJ, et al. Molecular fluorescence-guided surgery of peritoneal carcinomatosis of colorectal origin: a single-centre feasibility study. *Lancet Gastroenterol Hepatol* 2016; 1(4): 283-90.
- 67 Gao RW, Teraphongphom N, de Boer E, et al. Safety of panitumumab-IRDYE800CW and cetuximab-IRDYE800CW for fluorescence-guided surgical navigation in head and neck cancers. *Theranostics* 2018; 8(9): 2488-95.

PART I

FLUORESCENCE-GUIDED HEPATO-PANCREATICO-BILIARY SURGERY USING NON-TARGETED DYES

CHAPTER 2

THE BEST APPROACH FOR LAPAROSCOPIC FLUORESCENCE CHOLANGIOGRAPHY: OVERVIEW OF THE LITERATURE AND OPTIMIZATION OF DOSE AND DOSING TIME

Surg Innov. 2017 Aug;24(4):386-396

LSF BOOGERD, HJM HANDGRAAF, VAL HUURMAN, JSD MIEOG,
H LAM, WJ VAN DER MADE, CJH VAN DE VELDE
AND AL VAHRMEIJER

ABSTRACT

BACKGROUND ¶ Fluorescence cholangiography using indocyanine green (ICG) can enhance orientation of bile duct anatomy during laparoscopic cholecystectomy. To ensure clear discrimination between bile ducts and liver, the fluorescence ratio between both should be sufficient. This ratio is influenced by the ICG dose and timing of fluorescence imaging. We first systematically identified all strategies for fluorescence cholangiography. Second, we aimed to optimize the dose of ICG and time in a prospective clinical trial.

METHODS ¶ PUBMED was searched for clinical trials studying fluorescence cholangiography. Furthermore, 28 patients planned to undergo laparoscopic cholecystectomy were divided into 7 groups, receiving different intravenous doses (5 or 10mg ICG) at different time points (0.5, 2, 4, 6 or 24h prior to surgery).

RESULTS ¶ The systematic review revealed 27 trials including 1,057 patients. The majority of studies used 2.5mg administered within 1h before imaging. Imaging 3 to 24h after ICG administration was never studied. The clinical trial demonstrated that the highest bile duct-to-liver ratio was achieved 3-7h after administration of 5mg and 5-25h after administration of 10mg ICG. Up to 3h after administration of 5mg and up to 5h after administration of 10mg ICG, the liver was equally or more fluorescent than the cystic duct, resulting in a ratio ≤ 1.0 .

CONCLUSION ¶ This study shows for the first time that the interval between ICG administration and intraoperative fluorescence cholangiography should be extended. Administering 5mg ICG at least 3h before imaging is easy to implement in everyday clinical practice and results in bile duct-to-liver ratios > 1 .

INTRODUCTION

Iatrogenic bile duct injury after laparoscopic cholecystectomy is a rare but serious complication with an incidence ranging from 0.08% to 1.5%¹⁻³. Bile duct injuries are mostly the result of misidentification of the common bile duct (CBD) or the common hepatic duct (CHD) for the cystic duct (CD). Transection of the CBD or CHD leads to severe complications, long-term mortality rates up to 21%, and significant costs⁴. Important contributing factors are the learning curve associated with laparoscopic surgery and the presence of (misinterpreted) aberrant bile duct anatomy. Because laparoscopic cholecystectomy is currently one of the most performed surgeries worldwide, safer approaches are desirable. Use of the critical view of safety – a method of intraoperative identification of the CD and cystic artery – has been developed to minimize the risk of bile duct injury⁵. Although this strategy is now implemented worldwide, bile duct injuries still occur.

Identification of bile ducts during laparoscopic cholecystectomies can be enhanced by intraoperative cholangiography (IOC). This imaging technique requires injection of radio-opaque contrast into the CD, whereupon a series of x-rays are taken. IOC can accurately depict biliary anatomy and some advocate that it should be performed routinely^{6,7}. However, this technique is expensive, time-consuming, and exposes patients and health care personnel to radiation. Moreover, bile duct cannulation may cause bile duct injury itself and images can be difficult to interpret^{8,9}.

An alternative intraoperative imaging technique that is less invasive, does not require radiation, and is not time-consuming, is near-infrared (NIR) fluorescence cholangiography. Feasibility of real-time NIR fluorescence imaging of bile ducts using indocyanine green (ICG) was first described in 2008¹⁰. After intravenous administration, ICG is cleared via the liver, enabling visualization of liver tumors and bile duct anatomy^{11,13}. ICG has a favorable safety profile; side effects are reported in less than 1 out of 40,000 patients¹⁴.

Several studies have described fluorescence cholangiography during open, laparoscopic, and robotic cholecystectomy¹⁵⁻²⁰. However, only few tried to optimize the dose and timing of administration^{15,20}. This is important, because if fluorescence imaging is performed directly after administration of ICG, the liver will be highly fluorescent while bile ducts do not yet contain ICG. Optimal would be a high fluorescence signal in bile ducts, while liver tissue in the background stains dark. Excretion of ICG into the bile reaches a peak approximately 2 h after dosing and remains detectable long after injection²¹. Yet, most studies inject ICG within the first hour prior to imaging. It is already shown that discrimination between bile ducts and liver is enhanced when the time interval between ICG injection and fluorescence imaging is prolonged

to 24 h instead of 30 min¹⁵. Additionally, a recent study showed that a dose of 0.25 mg/kg, administered at least 45 min prior to fluorescence imaging facilitates accurate bile duct identification²⁰. Although several ICG doses were tested (up to 0.25 mg/kg) in this study, fluorescence cholangiography was performed only up to 180 min after ICG administration. The optimal dose for laparoscopic fluorescence cholangiography after an extended interval between dosing and imaging as determined by Verbeek et al.¹⁵, i.e. 10mg ICG, was not studied. Moreover, dosing times between 3 h and 6 h prior to surgery have never been studied, while these are clinically relevant.

In the current study, we first performed a systematic literature research to identify all used strategies for fluorescence cholangiography in clinical studies. Second, we optimized the dose of ICG and dosing time, ranging from 0.5 h to 24 h prior to surgery, to distinguish bile ducts from adjacent liver tissue.

MATERIALS AND METHODS

SYSTEMATIC REVIEW OF THE LITERATURE.... We systematically searched PUBMED for clinical trials about fluorescence cholangiography performed during open, laparoscopic, or robotic surgery since 2008. Only articles written in English and describing 3 or more patients were included. Selection of relevant titles was performed independently by two reviewers. Subsequently, all included articles were scanned on the content of the abstract, again by two independent reviewers.

CLINICAL TRIAL.... This study was approved by the Medical Ethics Committee of the Leiden University Medical Center and performed in accordance with the ethical standards of the Helsinki Declaration of 1975 (Netherlands Trial Registry: NTR5623). Twenty-eight patients suffering from cholecystolithiasis and/or cholecystitis, and planned for laparoscopic cholecystectomy, were included. Exclusion criteria were based on contraindications for ICG: renal impairment (eGFR <55); allergy for iodine, shellfish, or ICG; hyperthyroidism and pregnancy. All patients provided informed consent.

Patients were first assigned into 2 dose groups receiving either 5 mg or 10 mg ICG. Patients assigned to the 5 mg group, were planned to receive their ICG dose 30 min, 2, 4, or 6 h prior to surgery (4 patients per time interval). Patients assigned to the 10 mg group, were planned to receive their ICG dose 4, 6, or 24 h prior to surgery. Patients were distributed over the different groups based on their order in the surgical program. Patients scheduled early in the morning were allocated in the brief interval groups, while patients late in the afternoon were allocated into the longer interval groups. Patients were selected for the 24 h interval group if their procedure was

scheduled on Tuesday until Friday. Standard-of-care laparoscopic cholecystectomy was performed. When the surgeon considered it to be necessary, IOC was performed. Fluorescence imaging of bile ducts and adjacent structures was performed at least 3 times before the critical view of safety was assessed.

INTRAOPERATIVE NEAR-INFRARED FLUORESCENCE IMAGING SYSTEM

Laparoscopic imaging was performed using a high definition (HD) fluorescence laparoscope (Karl Storz Endoscopes, Germany) through a standard 12 mm subumbilical trocar port. The system was equipped with a visible and 760 nm (ICG modus) light source. No overlay of visible and ICG images was possible, but anatomical orientation could be maintained due to easy and fast switching between both channels using a foot pedal.

PREPARATION AND ADMINISTRATION OF INDOCYANINE GREEN

Twenty-five mg ICG (Pulsion Medical Systems, Munich, Germany) was resuspended in 10 cc sterile water to yield a concentration of 2.5 mg/mL. To obtain doses of 5 mg and 10 mg ICG, respectively 2 and 4 mL of the solution was intravenously administered.

POSTOPERATIVE QUESTIONNAIRE FOR SURGEONS

After surgery, the surgeon completed a questionnaire to score the following statements about fluorescence imaging: (I) it could decrease the number of bile duct complications; (II) it led to better detection of bile ducts; (III) the technique was of added value for this procedure; (IV) it needs to be standard-of-care during laparoscopic cholecystectomy (V) it delays surgery. Surgeons scored these statements ranging from totally disagree, somewhat disagree, neutral, somewhat agree and totally agree.

DATA ANALYSIS

Data was analyzed using GraphPad Prism Software (Version 5.01, La Jolla, CA). Bile duct to liver ratios (BLR) were calculated by dividing the fluorescence signal of the CD by the fluorescence signal of the liver. Intraoperative fluorescence images of 3 different time points were analyzed using Image J (version 1.49b, National Institutes of Health, Bethesda, MD).

RESULTS

SYSTEMATIC REVIEW.... A total of 242 articles were identified (Figure 1). After reviewing all titles and subsequently, content of the abstracts, 27 eligible clinical studies were reviewed (Table 1)^{10, 15-20, 22-42}. Used ICG doses ranged from 0.025 mg

in total to 0.25 mg/kg. Most studies (17/27) used 2.5 mg administered within 1 h prior to FI. Timing of ICG administration differed from 0 (intraoperatively) up to 24 h. No clinical trial studied fluorescence cholangiography 3 to 24 h after ICG administration. The majority of studies (24/27) performed ICG injection 30 to 60 min prior to surgery. Successful identification of the CD by fluorescence imaging was achieved in 98% (range: 48–100%) of all included patients (N=1,057). Two studies investigated fluorescence cholangiography using different doses of ICG and time of administration^{15,20}. They studied the doses 5 or 10 mg and 0.025 or 0.25 mg/kg, and time points of 10 to 180 min and 30 min or 24 h prior to surgery.

PATIENT CHARACTERISTICS ••• A total of 28 patients were included. No adverse events related to ICG occurred. Sixteen patients received 5 mg ICG and 12 patients 10 mg ICG. Patient characteristics are summarized in Table 2. Three patients were excluded: one patient due to failed ICG administration, one due to technical issues during saving of images, and one patient with a history of Roux-en-Y gastric bypass who had a percutaneous drain in situ. In 3 patients, an IOC was performed. One patient, with a history of Roux-en-Y gastric bypass, underwent a transgastric ERCP because of choledocholithiasis. Fluorescence cholangiography, performed 30 min after injection of 5 mg ICG, did not provide an overview of the bile duct anatomy (BLR 0.3). Another IOC was performed in a patient whose surgery was postponed. Fluorescence imaging 10 h post dosing of 5 mg ICG was not optimal (BLR 0.4). The third IOC was performed in a patient who received 10 mg ICG 24 h preoperatively. Fluorescence imaging showed the CBD (BLR 1.1), which was confirmed by IOC. No aberrant bile ducts were detected in the current study, but two patients showed aberrant arterial structures in close proximity to the gallbladder. Due to the lack of fluorescence, these structures could be identified as vasculature instead of bile ducts.

OPTIMIZATION OF DOSE AND TIME INTERVAL ••• Identification of the CD by fluorescence imaging was successful in 24 out of 25 patients (96%). The patient with unsuccessful bile duct identification was a patient who suffered from cirrhosis and Mirizzi syndrome and previously underwent stent placement and ERCP. During the laparoscopic surgery, strong adhesions between stomach, duodenum and gallbladder were found. No clear overview of bile duct anatomy could be obtained, neither by normal inspection nor using fluorescence imaging. After conversion, the gallbladder appeared completely fused with the proximal duodenum and a fistula between gallbladder and duodenum, and a cyst originating from the CBD was found.

Of the remaining 24 patients, 14 patients received 5 mg ICG and 10 patients 10 mg ICG. Patients were intended to be divided in different groups based on time of

fluorescence imaging after ICG injection, but it turned out to be difficult to time the exact moment between ICG administration and surgery due to the unpredictable course of the surgical program. In Figure 2, the BLR is plotted for every individual patient. In the 5 mg dose group, all BLRs between 3 to 7 h post dosing were >1, with a mean ratio of 1.8 ± 0.5 (video 1). Up to 3 h after dosing, all measurements showed equally or more fluorescent liver tissue compared to the CD (BLR 0.8 ± 0.2), which was significantly lower ($p=0.004$, Figure 3). In the 10 mg dose group, all BLRs between 5 and 25 h were >1, with mean ratios of 1.4 ± 0.3 . Up to 5 h after dosing, the liver showed to be equally or more fluorescent than the CD (BLR 0.9 ± 0.2 , respectively), which was again significant ($p=0.02$, Figure 4). BLRs 3 to 7 h post dosing of 5 mg and 5 to 25 h post dosing of 10 mg were not statistically different ($p=0.12$)

ADDITIONAL FINDING ••• A patient planned to undergo a laparoscopic cholecystectomy and defenestration of a liver cyst received 10 mg ICG. Fluorescence cholangiography was performed at 3.5 h post dosing. Although bile duct detection was hampered by the intense fluorescence of the liver (BLR 0.7), the liver cyst could be clearly demarcated by the lack of fluorescence inside the cyst (video clip 2).

EVALUATION OF FLUORESCENCE CHOLANGIOGRAPHY PER SURGEON
Results of the questionnaire among all operating surgeons are displayed in Figure 5.

DISCUSSION

Fluorescence cholangiography can improve orientation of bile duct anatomy during laparoscopic cholecystectomies and potentially lead to a reduced risk of bile duct injury. This study is the first showing that the interval between administration of ICG and intraoperative fluorescence imaging should be prolonged to 3 to 6 h post dosing of 5 mg, or 5 to 23 h post dosing of 10 mg. By doing so, bile ducts are more fluorescent than liver tissue, resulting in improved discrimination of bile duct anatomy. Consequently, also unexpected aberrant bile ducts can be detected⁴³. This may make laparoscopic cholecystectomy safer. Large studies focusing on patient outcome should demonstrate if fluorescence imaging reduces bile duct injuries.

In our systematic review, none of the identified manuscripts studied fluorescence imaging at the optimal time points. Only two studies focused on optimizing the dose of ICG and timing of fluorescence imaging. Zarrinpar et al.²⁰ performed a study in patients undergoing laparoscopic hepatic or biliary operations and injected doses ranging between 0.02 and 0.25 mg/kg, 10 to 180 min prior to fluorescence imaging. In this study, the authors also concluded that a prolonged interval appeared optimal

for fluorescence cholangiography, but they did not study longer time intervals. Our group previously studied fluorescence cholangiography during open and laparoscopic surgery 0.5 and 24 h after ICG administration¹⁵. The latter resulted in much better discrimination between bile ducts and liver tissue. However, administering ICG 24 h prior to surgery is less feasible in everyday clinical practice; most patients arrive in the morning prior to surgery at the hospital. According to our study results, we can advise a dose of 5 mg ICG, administered 3 to 7 h prior to surgery, which is much more practical in everyday clinical practice. Although this study is performed with a relatively small group of patients, we believe these results should form the basis for larger studies that focus on the added value of fluorescence cholangiography. Currently, three large, multicenter, randomized clinical studies are ongoing to assess the potential added value of fluorescence cholangiography (Table 3). Unfortunately, probably due to logistical reasons, researchers choose to inject ICG directly prior to surgery. Prevention of bile duct injuries is a very difficult endpoint that requires huge amount of patients, but other useful endpoints could be reduced OR time, cost effectiveness, less use of radiation for IOC, etc.

A commonly mentioned drawback of fluorescence-guided surgery is the lack of standardization of fluorescence imaging systems⁴⁴. Standardization is important for the determination of objective assessments during oncological fluorescence-guided surgery trials⁴⁵, but differences in fluorescence imaging systems also hinder comparison between fluorescence cholangiography studies. Different lasers, LEDs, filters, image sensors, and image processing all make a fair comparison difficult. A recent study compared five different fluorescence laparoscopic imaging systems for fluorescence cholangiography: a prototype and an improved version of the Hamamatsu Photonics laparoscope, the fluorescence imaging system of Olympus Medical Systems, the Karl Storz HD fluorescence laparoscope and the fluorescence imaging system of Novadaq¹⁹. An important conclusion from this study was that the contrast of ICG was significantly different among all the used laparoscopic imaging systems. Outcomes of studies (e.g., BLR) are therefore difficult to compare. The system used in the present study, the Karl Storz HD fluorescence laparoscope, showed not to be optimal for ICG detection and therefore, ratios obtained in the current study are expected to be even higher when other imaging systems are used.

The intensity of the fluorescence signal depends on several factors, including the distance from the tip of the laparoscope to its target and the amount of covering tissue. For this reason, we chose in the current study to calculate a ratio between the fluorescence signal in the cystic duct and liver, instead of measuring solely fluorescence intensity in the bile duct or liver. Moreover, to make the results more accurate, we analyzed the BLR at 3 different time points during surgery.

Intraoperative assessment of biliary anatomy can be improved using several techniques⁴⁶. IOC, still the most frequent applied technique for bile duct clarification, is investigated in large cohort studies. A forest plot of the six largest population-based studies showed an odds ratio for bile duct injury of 0.60 (95% confidence interval 0.52–0.70) when using IOC⁴⁶. No randomized trial studying the effect of IOC exists and is almost impossible to conduct. Still, the association between reduced risk of bile duct injury and use of IOC has been shown convincingly⁴⁷. An important disadvantage of IOC is however that obtained radiographic images can be difficult to interpret and IOC is a technically challenging procedure⁴⁸. Moreover, costs of IOC are high, caused by prolonged surgery time of 10–23 min, requirement of an additional medical specialist and use of equipment⁴⁹. On the other hand, treating patients with bile duct injuries is a financial burden for the health care system. Some physicians state therefore that routinely use of IOC is cost effective⁴⁷. As indicated by our surgeons, fluorescence imaging does not prolong OR time. Furthermore, it does not require another medical specialist or the use of radiation, and it certainly cannot cause bile duct injury³⁵. We therefore advocate that fluorescence imaging should be an important part of laparoscopic cholecystectomy.

A limiting factor of fluorescence cholangiography compared to IOC is the inability to detect CBD stones. Moreover, the CBD is not always identified, due to the limited penetration depth of approximately 1 cm of light in the NIR spectrum¹². Structures beneath a layer of (periductal) fat, especially in obese patients, are therefore more difficult to identify using NIR fluorescence imaging^{12,42}. Fluorescence cholangiography can however easily be combined with IOC, as shown in the current study. An advantage of fluorescence cholangiography is that it can be performed at all time during surgery without significant delay.

Intravenous ICG administration can also be valuable to assess intraoperative identification of (bile duct) vasculature^{28,31}. Because ICG binds to plasma proteins, it remains intravascular⁵⁰. This in combination with its short half-life of approximately 3 minutes makes it a very useful contrast agent for perfusion angiography. When doubt exists about aberrant vasculature or identification of the cystic artery, an additional injection of ICG can be given. One should however bear in mind that intravenous ICG administration during surgery will result in intense fluorescence of the liver and thus, should only be performed when bile duct anatomy is already clarified.

In conclusion, this study shows that a prolonged interval (at least 3 h) between ICG injection and intraoperative fluorescence cholangiography results in better contrast between bile ducts and liver tissue. Although this study was performed in a small group of patients, we believe that when the optimal dose and timing are used, fluorescence cholangiography can be of added value for both patients and surgeons.

REFERENCES

1. Nuzzo G, Giulianti F, Giovannini I, et al. Bile duct injury during laparoscopic cholecystectomy: results of an Italian national survey on 56 591 cholecystectomies. *Archives of surgery (Chicago, Ill : 1960)* 2005;140(10):986-92.
2. Tornqvist B, Stromberg C, Persson G, et al. Effect of intended intraoperative cholangiography and early detection of bile duct injury on survival after cholecystectomy: population based cohort study. *BMJ* 2012;345:e6457.
3. Halbert C, Pagkratis S, Yang J, et al. Beyond the learning curve: incidence of bile duct injuries following laparoscopic cholecystectomy normalize to open in the modern era. *Surgical endoscopy* 2016;30(6):2239-43.
4. Halbert C, Altieri MS, Yang J, et al. Long-term outcomes of patients with common bile duct injury following laparoscopic cholecystectomy. *Surgical endosc* 2016;30(10):4294-9.
5. Vettoretto N, Saronni C, Harbi A, et al. Critical view of safety during laparoscopic cholecystectomy. *JLS* 2011;15(3):322-5.
6. Polat FR, Abci I, Coskun I, et al. The importance of intraoperative cholangiography during laparoscopic cholecystectomy. *JLS* 2000;4(2):103-7.
7. Halawani HM, Tamim H, Khalifeh F, et al. Impact of intraoperative cholangiography on postoperative morbidity and readmission: analysis of the NSQIP database. *Surgical endosc* 2016;30(12):5395-5403.
8. El Shallaly G, Seow C, Sharp C, et al. Intraoperative cholangiography time in laparoscopic cholecystectomy: timing the radiographer. *Surg Endosc* 2005;19(10):1370-2.
9. Way LW, Stewart L, Gantert W, et al. Causes and prevention of laparoscopic bile duct injuries: analysis of 252 cases from a human factors and cognitive psychology perspective. *Ann Surg* 2003;237(4):460-9.
10. Mitsuhashi N, Kimura F, Shimizu H, et al. Usefulness of intraoperative fluorescence imaging to evaluate local anatomy in hepatobiliary surgery. *Journal of hepatobiliary-pancreatic surgery* 2008;15(5):508-14.
11. Schaafsma BE, Mieog JS, Hutteman M, et al. The clinical use of indocyanine green as a near-infrared fluorescent contrast agent for image-guided oncologic surgery. *J Surg Oncol* 2011;104(3):323-32.
12. Vahrmeijer AL, Hutteman M, van der Vorst JR, et al. Image-guided cancer surgery using near-infrared fluorescence. *Nat Rev Clin Oncol* 2013;10(9):507-18.
13. Boogerd LS, Handgraaf HJ, Lam HD, et al. Laparoscopic detection and resection of occult liver tumors of multiple cancer types using real-time near-infrared fluorescence guidance. *Surgical endosc* 2017;31(2):952-961.
14. Benya R, Quintana J, Brundage B. Adverse reactions to indocyanine green: a case report and a review of the literature. *Cathet Cardiovasc Diagn* 1989;17(4):231-3.
15. Verbeek FP, Schaafsma BE, Tummers QR, et al. Optimization of near-infrared fluorescence cholangiography for open and laparoscopic surgery. *Surg Endosc* 2014;28(4):1076-82.
16. Buchs NC, Hagen ME, Pugin F, et al. Intra-operative fluorescent cholangiography using indocyanine green during robotic single site cholecystectomy. *The international journal of medical robotics + computer assisted surgery: MRCAS* 2012;8(4):436-40.
17. Ishizawa T, Kaneko J, Inoue Y, et al. Application of fluorescent cholangiography to single-incision laparoscopic cholecystectomy. *Surgical endosc* 2011;25(8):2631-6.
18. Daskalaki D, Fernandes E, Wang X, et al. Indocyanine green (ICG) fluorescent cholangiography during robotic cholecystectomy: results of 184 consecutive cases in a single institution. *Surgical innov* 2014;21(6):615-21.
19. Kono Y, Ishizawa T, Tani K, et al. Techniques of Fluorescence Cholangiography During Laparoscopic Cholecystectomy for Better Delineation of the Bile Duct Anatomy. *Medicine* 2015;94(25):1005.
20. Zarrinpar A, Dutson EP, Mobley C, et al. Intraoperative Laparoscopic Near-Infrared Fluorescence Cholangiography to Facilitate Anatomical Identification: When to Give Indocyanine Green and How Much. *Surg Innov* 2016;23(4):360-5.
21. Cherrick GR SS, Leevy CM, et al. Indocyanine green: observations on its physical properties, plasma decay, and hepatic extraction. *J Clin Invest* 1960;39:592-600.
22. Ishizawa T, Tamura S, Masuda K, et al. Intraoperative fluorescent cholangiography using indocyanine green: a biliary road map for safe surgery. *Journal of the American College of Surgeons* 2009;208(1):e1-4.
23. Aoki T, Murakami M, Yasuda D, et al. Intraoperative fluorescent imaging using indocyanine green for liver mapping and cholangiography. *Journal of hepatobiliary-pancreatic sciences* 2010;17(5):590-4.
24. Ishizawa T, Bandai Y, Ijichi M, et al. Fluorescent cholangiography illuminating the biliary tree during laparoscopic cholecystectomy. *BJs* 2010;97(9):1369-77.
25. Tagaya N, Shimoda M, Kato M, et al. Intraoperative exploration of biliary anatomy using fluorescence imaging of indocyanine green in experimental and clinical cholecystectomies. *Journal of hepatobiliary-pancreatic sciences* 2010;17(5):595-600.
26. Hutteman M, van der Vorst JR, Mieog JS, et al. Near-infrared fluorescence imaging in patients undergoing pancreaticoduodenectomy. *European surgical research* 2011;47(2):90-7.
27. Ishizawa T, Fukushima N, Shibahara J, et al. Real-time identification of liver cancers by using indocyanine green fluorescence imaging. *Cancer* 2009;115(11):2491-504.
28. Kaneko J, Ishizawa T, Masuda K, et al. Indocyanine green reinjection technique for use in fluorescent angiography concomitant with cholangiography during laparoscopic cholecystectomy. *Surgical laparoscopy, endoscopy & percutaneous techniques* 2012;22(4):341-4.
29. Buchs NC, Pugin F, Azagury DE, et al. Real-time near-infrared fluorescent cholangiography could shorten operative time during robotic single-site cholecystectomy. *Surgical endosc* 2013;27(10):3897-901.
30. Schols RM, Bouvy ND, Masclee AA, et al. Fluorescence cholangiography during laparoscopic cholecystectomy: a feasibility study on early biliary tract delineation. *Surgical endosc* 2013;27(5):1530-6.
31. Schols RM, Bouvy ND, van Dam RM, et al. Combined vascular and biliary fluorescence imaging in laparoscopic cholecystectomy. *Surgical endosc* 2013;27(12):4511-7.
32. Spingoglio G, Piora F, Bianchi PP, et al. Real-time near-infrared (NIR) fluorescent cholangiography in single-site robotic cholecystectomy (SSRC): a single-institutional prospective study. *Surgical endosc* 2013;27(6):1516-62.
33. Prevot F, Rebibo L, Cosse C, et al. Effectiveness of intraoperative cholangiography using indocyanine green (versus contrast fluid) for the correct assessment of extrahepatic bile ducts during day-case laparoscopic cholecystectomy. *Journal of gastrointestinal surgery* 2014;18(8):1462-8.
34. Larsen SS, Schulze S, Bisgaard T. Non-radiographic intraoperative fluorescent cholangiography is feasible. *Danish medical journal* 2014;61(8):A4891.
35. Dip FD, Asbun D, Rosales-Velderrain A, et al. Cost analysis and effectiveness comparing the routine use of intraoperative fluorescence cholangiography with fluoroscopic cholangiogram in patients undergoing laparoscopic cholecystectomy. *Surgical endosc* 2014;28(6):1838-43.
36. Dip F, Roy M, Lo Menzo E, et al. Routine use of fluorescent incisionless cholangiography as a new imaging modality during laparoscopic cholecystectomy. *Surgical endosc* 2015;29(6):1621-6.
37. Dip F, Nguyen D, Montorfano L, et al. Accuracy of Near Infrared-Guided Surgery in Morbidly Obese Subjects Undergoing Laparoscopic Cholecystectomy. *Obesity surgery* 2016;26(3):525-30.
38. Boni L, David G, Mangano A, et al. Clinical applications of indocyanine green (ICG) enhanced fluorescence in laparoscopic surgery. *Surgical endosc* 2015;29(7):2046-55.
39. Kawaguchi Y, Velayutham V, Fuks D, et al. Usefulness of Indocyanine Green-Fluorescence Imaging for Visualization of the Bile Duct During Laparoscopic Liver Resection. *Journal of the American College of Surgeons* 2015;221(6):e113-7.
40. Osayi SN, Wendling MR, Drosdeck JM, et al. Near-infrared fluorescent cholangiography facilitates identification of biliary anatomy during laparoscopic cholecystectomy. *Surgical endosc* 2015;29(2):368-75.
41. van Dam DA, Ankersmit M, van de Ven P, et al. Comparing Near-Infrared Imaging with Indocyanine Green to Conventional Imaging During Laparoscopic Cholecystectomy: A Prospective Crossover Study. *Journal of laparoendoscopic & advanced surgical techniques Part A* 2015;25(6):486-92.
42. Igami T, Nojiri M, Shinohara K, et al. Clinical value and pitfalls of fluorescent cholangiography during single-incision laparoscopic cholecystectomy. *Surg Today* 2016;46(12):1443-1450.
43. Calatayud D, Milone L, Elli EF, et al. ICG-fluorescence identification of a small aberrant biliary canalculus during robotic cholecystectomy. *Liver international* 2012;32(4):602.
44. Snoeks TJ, van Driel PB, Keereweer S, et al. Towards a successful clinical implementation of fluorescence-guided surgery. *Mol Imaging Biol* 2014;16(2):147-51.
45. Rosenthal EL, Warram JM, de Boer E, et al. Successful Translation of Fluorescence Navigation During Oncologic Surgery: A Consensus Report. *J Nucl Med* 2016;57(1):144-50.
46. Buddingh KT, Nieuwenhuijs VB, van Buuren L, et al. Intraoperative assessment of biliary anatomy for prevention of bile duct injury: a review of current and future patient safety interventions. *Surgical endosc* 2011;25(8):2449-61.
47. Flum DR, Flowers C, Veenstra DL. A cost-effective analysis of intraoperative cholangiography in the prevention of bile duct injury during laparoscopic cholecystectomy. *J Am Coll Surg* 2003;196(3):385-93.
48. Buddingh KT, Weersma RK, Savenije RA, et al. Lower rate of major bile duct injury and increased intraoperative management of common bile duct stones after implementation of routine intraoperative cholangiography. *J Am Coll Surg* 2011;213(2):267-74.
49. Ford JA, Soop M, Du J, et al. Systematic review of intraoperative cholangiography in cholecystectomy. *BJs* 2012;99(2):160-7.
50. Schaafsma BE, Mieog JS, Hutteman M, et al. The clinical use of indocyanine green as a near-infrared fluorescent contrast agent for image-guided oncologic surgery. *J Surg Oncol* 2011;104(3):323-32.

Figure 1 Flowchart of the literature search

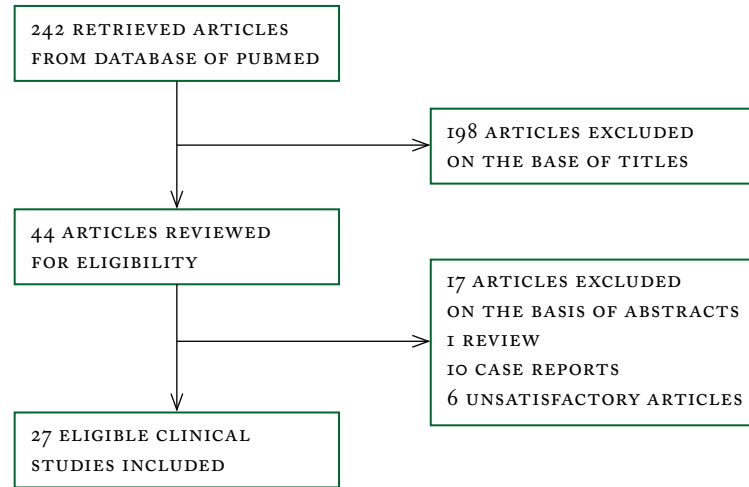


Figure 2 Fluorescence intensity of bile duct compared to adjacent liver tissue for each individual patient. The parabolic lines show our expectation of the mean BLRS over time.

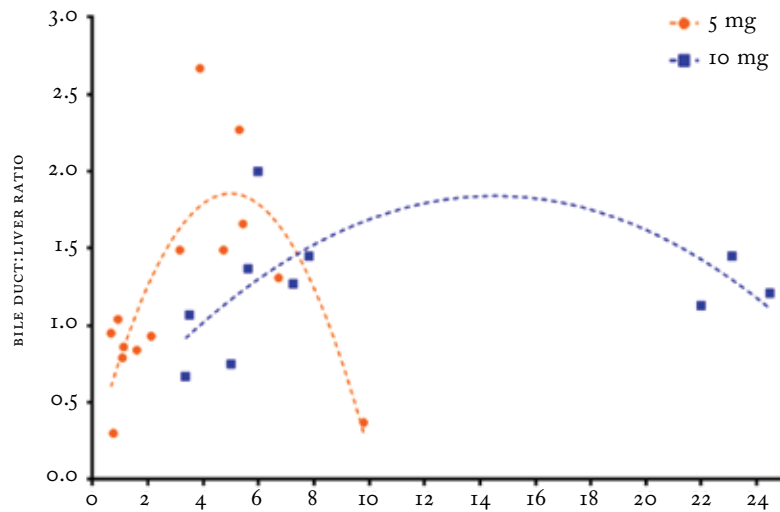


Figure 3 Fluorescence cholangiography over time after administration of 5 mg ICG

Shown are images of fluorescence detection of the cystic duct (arrow) and adjacent liver tissue (pyramid) over time. Bile duct-to-liver ratios were sufficient (i.e. >1) in patients who received 5 mg ICG 3 to 7 h prior to surgery. BLR was ≤ 1 when fluorescence imaging was performed less than 3 h after administration.

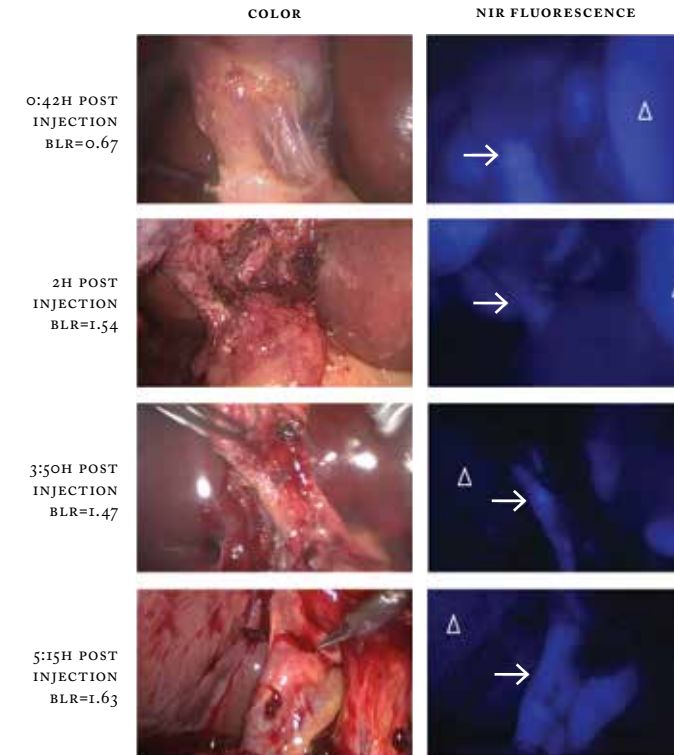


Figure 4 Fluorescence cholangiography over time after administration of 10 mg ICG

Shown are images of fluorescence detection of cystic duct (arrow) and adjacent liver tissue (pyramid) over time. Bile duct-to-liver ratios were sufficient (i.e. >1) between 5 to 25 h post dosing of 10 mg ICG.

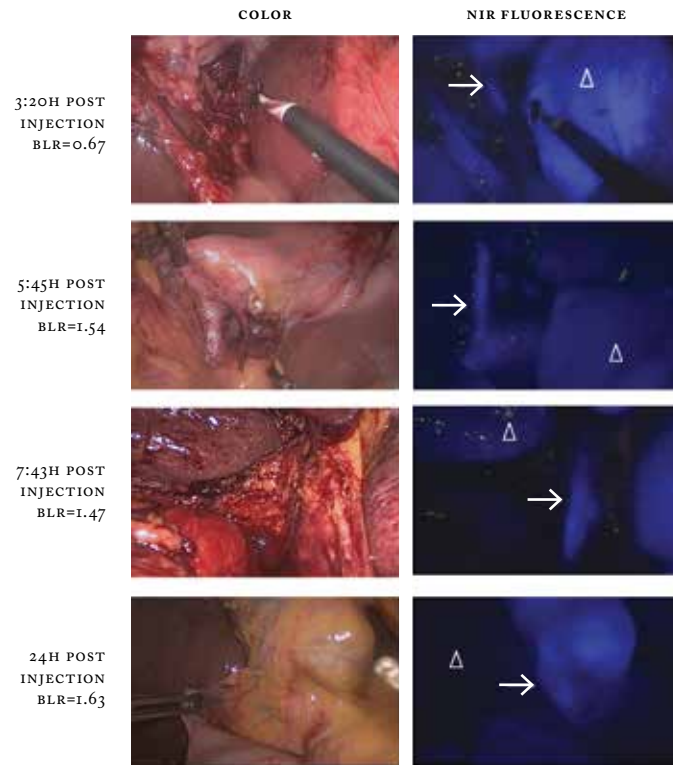
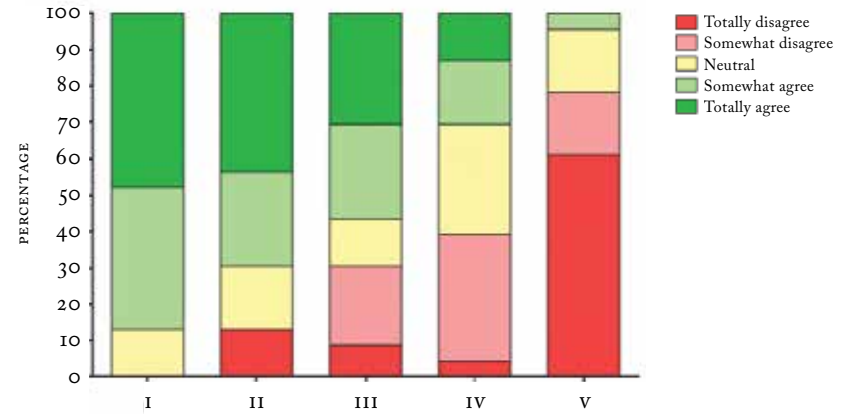


Figure 5 Results of questionnaire

Shown are all the scores that were given by surgeons after they performed a laparoscopic cholecystectomy with use of fluorescence cholangiography. The statements that were scored were respectively (i) it could decrease the number of bile duct complications; (ii) it led to better detection of bile ducts; (iii) the technique was of added value for this procedure; (iv) it needs to be standard-of-care during laparoscopic cholecystectomy (v) it delays surgery.



Video 1 Fluorescence cholangiography during laparoscopic cholecystectomy, performed 5 hours after injection of 5 mg ICG (*online available*)

Video 2 Fluorescence imaging of bile ducts and liver cysts during laparoscopic cholecystectomy and liver cyst defenestration (*online available*)

Table 1 Relevant articles about fluorescence cholangiography

Study	Year	N	Procedure	Fluorescence imaging system	Dose of ICG (mg)	Timing of injection	IR of CD (%)
Mitsuhashi et al. ¹⁰	2008	5	oc	Photo Dynamic Eye	2.5 mg	30min prior to surgery	5/5 (100%)
Ishizawa et al. ²²	2009	10	oc	Photo Dynamic Eye	2.5 mg	60min prior to surgery / during conversion	10/10 (100%)
Aoki et al. ²³	2010	14	LC	Hamamatsu laparoscope	12.5 mg	30min prior to surgery	10/14 (71%)
Tagaya et al. ²⁵	2010	12	oc (N=4)/LC (N=8)	Prototype laparoscope and Photo Dynamic Eye	2.5 mg	60min-120min prior to surgery	12/12 (100%)
Ishizawa et al. ²⁴	2010	52	LC	Hamamatsu laparoscope	2.5 mg	30min prior to surgery	52/52 (100%)
Hutteman et al. ²⁶	2011	8	oc*	Mini-flare	5 mg or 10 mg	during surgery	8/8 (100%)
Ishizawa et al. ¹⁷	2011	7	SILC	Hamamatsu laparoscope	2.5 mg	after intubation	7/7 (100%)
Buchs et al. ¹⁶	2012	12	SIRC	da Vinci s1 System (Intuitive Surgical)	2.5 mg	45min prior to surgery	12/12 (100%)
Kaneko et al. ²⁸	2012	28	LC	Hamamatsu laparoscope	2.5 mg	15min prior to surgery and during surgery***	27/28 (96%)
Buchs et al. ²⁹	2013	23	SIRC	da Vinci s1 System (Intuitive Surgical)	2.5 mg	after intubation	NA
Schols et al. ³¹	2013	30	LC	Karl Storz HD fluorescence endoscopy system	2.5 mg	after intubation and during surgery***	29/30 (97%)
Schols et al. ³⁰	2013	15	LC	Karl Storz HD fluorescence endoscopy system	2.5 mg	after intubation	15/15 (100%)
Spinoglio et al. ³²	2013	45	SIRC	da Vinci s1 System (Intuitive Surgical)	2.5 mg	30min prior to surgery	44/45 (98%)
Verbeek et al. ¹⁵	2014	41	oc (N=27)/LC (N=14)	Mini-flare / Karl Storz	5 mg or 10 mg	24h or 30min prior to surgery	41/41 (100%)
Prevot et al. ³³	2014	23	LC	Karl Storz HD fluorescence endoscopy system	0.05 mg/kg	after intubation	23/23 (100%)
Daskalaki et al. ¹⁸	2014	184	RC	da Vinci s1 System (Intuitive Surgical)	2.5 mg	45min prior to surgery	184/188 (98%)
Larsen et al. ³⁴	2014	35	LC	Olympus laparoscopic imaging system	0.3-0.4 mg/mL/kg in 5 mL	after intubation	35/35 (100%)
Boni et al. ³⁸	2015	52	LC	Karl Storz HD fluorescence endoscopy system	0.4 mg/mL/kg	15min prior to surgery and during surgery***	52/52 (100%)
Dip et al. ³⁵	2014	43	LC	Karl Storz HD fluorescence endoscopy system	0.05 mg/kg	60min prior to surgery	43/43 (100%)
Kawaguchi et al. ³⁹	2015	24	LLR	Olympus laparoscopic imaging system	0.025 mg	after intubation	24/24 (100%)
Osayi et al. ⁴⁰	2015	82	LC	Stryker Infrared Fluorescence (IRF) Imaging System	2.5 mg	60min prior to surgical incision	78/82 (95%)
Dip et al. ³⁶	2015	45	LC	Karl Storz HD fluorescence endoscopy system	0.05 mg/kg	60min prior to surgery	45/45 (100%)
van Dam et al. ⁴¹	2015	30	LC	Olympus laparoscopic imaging system	0.05 mg/kg	after intubation	29/30 (97%)
Kono et al. ¹⁹	2015	108	LC	5 fluorescence laparoscopic imaging systems**	2.5 mg	30min prior to surgery and during surgery	99/108 (92%)
Dip et al. ³⁷	2015	71	LC	Karl Storz HD fluorescence endoscopy system	0.05 mg/kg	60min prior to surgery	100/100 (100%)
Zarrinpar et al. ²⁰	2016	37	LC + LLR	PinPoint	0.025 mg/kg-0.25mg/kg	10 to 180min prior to surgery	NA
Igami et al. ⁴²	2016	21	LC	Karl Storz HD fluorescence endoscopy system	2.5 mg	After intubation	10/21 (48%)
TOTAL		1057					984/1009 (98%)

OC = open cholecystectomy; LC = laparoscopic cholecystectomy; SILC = single-incision laparoscopic cholecystectomy; SIRC = single-incision robotic cholecystectomy; LLR = laparoscopic liver resection; IR = identification rate; CD = cystic duct

* Open cholecystectomy performed during pancreaticoduodenectomy

** 5 fluorescence laparoscopic imaging systems include (1) prototype and (2) improved version of the Hamamatsu Photonics laparoscope, the fluorescence imaging system of Olympus Medical Systems (3), the Karl Storz HD fluorescence laparoscope (4) and the fluorescence imaging system of Novadaq (5)

*** An additional ICG injection during surgery was given to evaluate fluorescence angiograph

Table 2 Patients' characteristics

Characteristics	5 mg dose group	10 mg dose group
Number of included patients (n)	16	12
Age (median, range)	61 (20-75)	61 (40-76)
Gender (n (%))		
Female	10 (63%)	9 (75%)
Male	6 (37%)	3 (25%)
Body Mass Index (kg/m ²)(median, range)	29 (22-37)	27 (22-36)
ASA classification (n (%))		
ASA class I	4 (25%)	3 (25%)
ASA class II	12 (75%)	9 (75%)
Preoperative diagnosis		
cholelithiasis	14	11
choledocholithiasis	5	5
gallbladder polyp	1	1
Mirizzi syndrome	1	0
Preoperative imaging technique us	16	12
MRCP	2	4
ERCP	5	6

US = ultrasound; MRCP = magnetic resonance cholangio-pancreaticography;
ERCP = endoscopic retrograde cholangio-pancreaticography

Table 3 Recruiting randomized controlled trials using fluorescence cholangiography

Study coordinator nct No.	Participating country	No. of pts	Start accrual	Main Outcome	Comparator	Dose ICG	Timing
L. Lehrs-kov-Schmidt <i>NCT02344654</i>	Denmark	120	May 2015	Identification BD	x-ray chol- angiography	0.05 mg/kg	after intubation
J. van den Bos <i>NCT02558556</i>	The Netherlands	308	Jan 2016	Time to visual- ization cvs	White light	2.5 mg	after intubation
R. Rosenthal <i>NCT02702843</i>	USA	1000	April 2016	Identification BD	White light	0.05 mg/kg	>45 min prior to surgery

No. = number; pts = patients; BD = bile ducts; cvs = critical view of safety

CHAPTER 3

APPLICATION OF NEAR-INFRARED FLUORESCENCE IMAGING DURING MODIFIED ASSOCIATING LIVER PARTITION AND PORTAL VEIN LIGATION FOR STAGED HEPATECTOMY

Surgery, 2016 May; 159(5): 1481-2

LSF BOOGERD, HJM HANDGRAAF, H LAM, AE BRAAT,
RJ SWIJNENBURG, JV FRANGIONI, AL VAHRMEIJER
AND J RINGERS

Associating Liver Partition and Portal vein ligation for Staged hepatectomy (ALPPS) emerged as a novel curative treatment option for patients suffering from initially unresectable liver tumors¹. The goal of ALPPS is an R0 resection with maximal preservation of liver function. The technique remains controversial among hepatobiliary surgeons due to high morbidity and mortality rates². Different adaptations have been proposed to reduce these rates. The preferred method at the Leiden University Medical Center (LUMC) is to perform first only the liver partition, followed by a selective percutaneous portal vein embolization when the patient is sufficiently recovered, usually after four to five days. We hypothesize that the inflammatory state will be decreased after a few days and that this approach therefore results in lower complication rates. The international ALPPS registry showed a 2-year disease-free survival rate of 42%³. These data also showed that incomplete resection – usually the result of hampered demarcation due to tumor size and location – was accountable for only 9% of the recurrent tumors. This may indicate that other small tumors remain undetected during surgery. Current pre- and intraoperative imaging modalities all suffer serious drawbacks. CT and MRI have low sensitivity for lesions <10 mm and intraoperative ultrasonography (IOUS) has low resolution within the first millimeters below the liver surface due to reflection artifacts. In 2009, it was reported that intravenous administration of indocyanine green (ICG) enables intraoperative identification of hepatic tumors using near-infrared (NIR) fluorescence⁴. Accumulation of ICG in liver tissue affected or compressed by invasive growth of tumors results in bright signals in and around tumors, while healthy liver tissue clears ICG within hours. Based on our previous experiences, we currently apply fluorescence imaging (FI) routinely during oncologic liver surgery. We believe that FI could become an important component of ALPPS and other liver procedures. In support, we illustrate two recent cases.

Both patients provided informed consent and received an IV administration of 10 mg ICG one day prior to the first stage. Intraoperative FI was performed using the Mini-Fluorescence-Assisted Resection and Exploration (Mini-FLARE®) system⁵. In the first patient, FI was of great value in determining the transection line. Contrary to preoperative imaging, the tumor was identified beyond the falciform ligament (Fig. 1a). Liver parenchyma was partitioned guided by the fluorescent signal. Histopathological analysis after the second stage revealed no tumor involvement in the resection margin. The second patient suffered from a large solitary tumor in the right liver lobe. Differential diagnosis (based on radiological findings) included HCC, fibrolamellar HCC and cholangiocarcinoma. No biopsy was performed to prevent needle tract metastases. Two lesions of approximately 5 mm in the left liver lobe were identified by FI during the procedure (Fig. 1b). Only one of these

lesions could be visualized in the second instance by IOUS. Frozen section analysis was inconclusive, but additional histological staining revealed an adenocarcinoma.

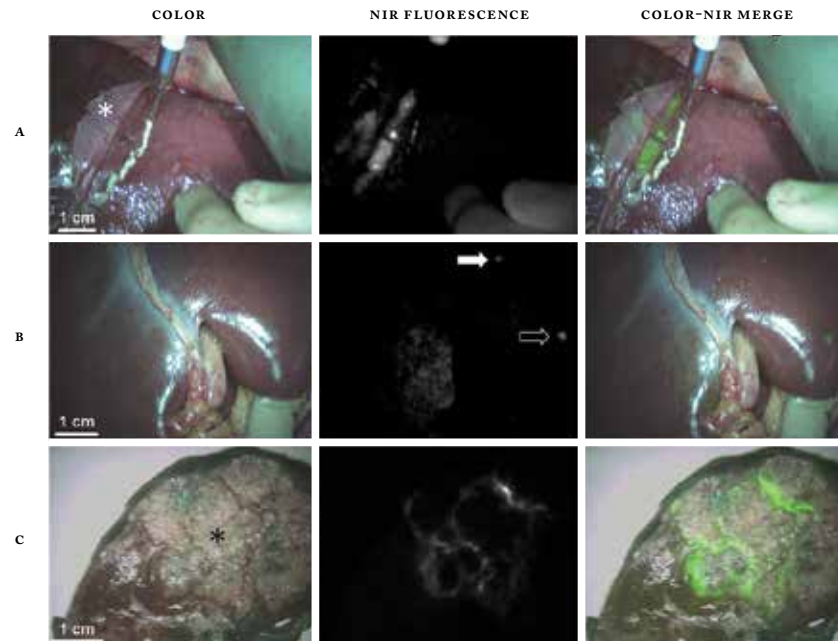
These cases illustrate the added value of FI during ALPPS. First, it provides real-time tumor margin assessment during resection (video 1). This in contrast to intraoperative ligation of vasculature, where discoloration of liver tissue observed by the naked eye only represents the ischemic part and not the tumor itself. Secondly, it can identify otherwise undetectable lesions and serve as a complimentary intraoperative diagnostic modality. FI is an easy, effective, and safe method. The only requirement is a NIR fluorescence imaging system, several of which are clinically available. Large series will have to define if fluorescence imaging truly improves patient outcomes, but we believe this technology could become an important component of ALPPS and other liver procedures.

REFERENCES

- 1 Schnitzbauer AA, Lang SA, Goessmann H, Nadalin S, Baumgart J, Farkas SA, et al. Right portal vein ligation combined with in situ splitting induces rapid left lateral liver lobe hypertrophy enabling 2-staged extended right hepatic resection in small-for-size settings. *Ann Surg* 2012 Mar;255(3):405-14.
- 2 Aloia TA. Insights into ALPPS. *Eur J Surg Oncol* 2015 May;41(5):610-1.
- 3 Schadde E, Ardiles V, Robles-Campos R, Malago M, Machado M, Hernandez-Alejandro R, et al. Early survival and safety of ALPPS: first report of the International ALPPS Registry. *Ann Surg* 2014 Nov;260(5):829-36.
- 4 Gotoh K, Yamada T, Ishikawa O, Takahashi H, Eguchi H, Yano M, et al. A novel image-guided surgery of hepatocellular carcinoma by indocyanine green fluorescence imaging navigation. *J Surg Oncol* 2009 Jul 1;100(1):75-9.
- 5 van der Vorst JR, Schaafsma BE, Hutteman M, Verbeek FP, Liefers GJ, Hartgrink HH, et al. Near-infrared fluorescence-guided resection of colorectal liver metastases. *Cancer* 2013 Sep 15;119(18):3411-8.

Figure 1 Near-infrared fluorescence imaging of liver tumors

- A Fluorescence-guided transection of the liver; the plane of transection can be marked beyond the falciform ligament (white star) based on fluorescent signal (Patient #1).
- B Fluorescence detection of two additional lesions (both arrows) in the left liver lobe (Patient #2). Only one lesion could be identified by ICG (segment 3; open arrow). This lesion was resected and histopathologic examination revealed adenocarcinoma after additional staining.
- C *Ex vivo* fluorescence imaging of resected specimen, 21 days after pre- and intraoperative ICG administration (Patient #2). Fluorescence is still clearly visible surrounding the tumor (tumor is highlighted by black star).



CHAPTER 4

LAPAROSCOPIC DETECTION AND RESECTION OF OCCULT LIVER TUMORS OF MULTIPLE CANCER TYPES USING REAL-TIME NEAR-INFRARED FLUORESCENCE GUIDANCE

Surg Endosc. 2017 Feb; 31(2):952-961

LSF BOOGERD*, HJM HANDGRAAF*, H LAM, VAL HUURMAN,
A FARIÑA-SARASQUETA, JV FRANGIONI, CJH VAN DE VELDE,
AE BRAAT AND AL VAHRMEIJER

**shared first authorship*

ABSTRACT

BACKGROUND † Tumor recurrence after radical resection of hepatic tumors is not uncommon, suggesting that malignant lesions are missed during surgery. Intraoperative navigation using fluorescence guidance is an innovative technique enabling real-time identification of (sub)capsular liver tumors. The objective of the current study was to compare fluorescence imaging (FI) and conventional imaging modalities for laparoscopic detection of both primary and metastatic tumors in the liver.

METHODS † Patients undergoing laparoscopic resection of a malignant hepatic tumor were eligible for inclusion. Patients received standard-of-care, including preoperative CT and/or MRI. In addition, 10 mg indocyanine green was intravenously administered one day prior to surgery. After introduction of the laparoscope, inspection, FI, and laparoscopic ultrasonography (LUS) were performed. Histopathological examination of resected suspect tissue was considered the gold standard.

RESULTS † Twenty-two patients suspected to have hepatocellular carcinoma (N=4), cholangiocarcinoma (N=2) or liver metastases from colorectal carcinoma (N=12), uveal melanoma (N=2) and breast cancer (N=2) were included. Two patients were excluded because their surgery was unexpectedly postponed several days. Twenty-six malignancies were resected in the remaining 20 patients. Sensitivity for various modalities was 80% (CT), 84% (MRI), 62% (inspection), 86% (LUS) and 92% (FI), respectively. Three metastases (12%) were identified solely by FI. All 26 malignancies could be detected by combining LUS and FI (100% sensitivity).

CONCLUSION † This study demonstrates added value of FI during laparoscopic resections of several hepatic tumors. Although larger series will be needed to confirm long-term patient outcome, the technology already aids the surgeon by providing real-time fluorescence guidance.

INTRODUCTION

Major advances have been achieved in the treatment of patients with liver-only metastases and primary liver tumors. Several studies and meta-analyses show improved overall survival after aggressive resection¹⁻³. Recurrence-free survival, however, is rather low. Up to 69% of patients with colorectal liver metastases develop local recurrence or new metastases, with the majority in the first year⁴. Similar rates are reported in patients undergoing resection of hepatocellular carcinoma (HCC)⁵. These numbers are not entirely explained by incomplete resections and support the hypothesis that small malignant lesions are missed during resection.

It is well known that preoperative imaging modalities, including computed tomography (CT) and magnetic resonance imaging (MRI), have relatively low sensitivity for sub-centimeter lesions due to their limited spatial resolution. Moreover, altered body position during surgery and time interval between preoperative imaging and surgery make translation of preoperative images challenging. Extensive intraoperative inspection and palpation of the liver is therefore of vital importance. Palpation, however, is impossible during minimally invasive procedures. Laparoscopic ultrasonography (LUS) can assist in detecting tumors, but acoustic reflection artifacts can obscure tumors in the first millimeters below the liver capsule⁶. In short, surgeons need a highly-sensitive, real-time intraoperative imaging modality to identify small superficial tumors in the liver.

Ishizawa and colleagues⁷ reported in 2009 that an intravenous injection of the safe and widely used dye indocyanine green (ICG) causes “bullseyes” of fluorescence to be formed around primary or metastatic tumors in the liver. Defective biliary clearance in the transition area between tumor and normal liver tissue and in primary liver tumors results in ICG retention, which can be visualized using a near-infrared (NIR) fluorescence imaging system. Our group showed that this method of detection is feasible during resection of hepatocellular carcinoma (HCC) and hepatic metastases of uveal melanoma (UMLM) and colorectal cancer (CRLM)^{8,9,10}. The added value of fluorescence imaging during oncological liver surgery is twofold: 1) it can demarcate liver tumors and provide real-time resection margin assessment, and 2) it can identify otherwise undetectable, i.e., occult, (sub)capsular liver tumors. NIR fluorescence imaging can be especially valuable during minimally invasive procedures, because surgeons are deprived of tactile feedback. Based on previous study results, fluorescence imaging is now routinely performed during laparoscopic liver surgery in our hospital if patients provide informed consent. The purpose of the present study was to compare sensitivity and positive predictive values of fluorescence imaging with CT, MRI, visual inspection, and LUS during laparoscopic resection of several tumor types in the liver.

MATERIALS AND METHODS

PATIENTS ••• The local Medical Ethics Committee and the Departments of Surgery and Anesthesiology approved implementation of NIR fluorescence imaging during oncologic liver surgery as standard-of-care. Informed consent from all patients was obtained. ICG (25 mg vials, Pulsion Medical Systems, Munich, Germany) was dissolved in 10 mL sterile water to yield a 2.5 mg/L (3.2 mM) concentration. Subsequently, a bolus of 4 mL containing 10 mg ICG was administered intravenously 24 h prior to surgery. Dose and time of administration were optimized in our previous study⁸.

All patients undergoing laparoscopic staging or resection of a liver tumor were eligible for inclusion. Exclusion criteria were EGFR <55, pregnancy, lactation, and an allergy to iodine, shellfish, or ICG. Preoperative imaging was performed using computed tomography (CT) with or without positron emission tomography (PET) and in most cases also using magnetic resonance imaging (MRI), all within 6 weeks prior to surgery.

NEAR-INFRARED FLUORESCENCE IMAGING ••• Intraoperative imaging during surgery was performed using the laparoscopic high definition fluorescence imaging system (Karl Storz GmbH & Co. KG, Tuttlingen, Germany). The system includes a light source for visible and 760 nm (ICG mode) light, a plasma light guide and a 30°, 10 mm laparoscope containing optical filters. The system allows easy switching between white light and ICG modes using a foot pedal. Images were recorded using a charge-coupled camera device.

Ex vivo fluorescence imaging of resected tissue specimens was performed at the pathology department using the previously described Fluorescence-Assisted Resection and Exploration (FLARE[®], Beth Israel Deaconess Medical Center, Boston, MA, USA) prototype surgical imaging system¹¹. In addition, the location of ICG in resected tissue was assessed using fluorescence microscopy. Digital images were made using the Leica DM5500B digital microscope (Leica Microsystems B.V., Son, The Netherlands) equipped with a Leica DFC365FX camera and LAS X software (version 2.6.0) for image acquisition and processing.

PROCEDURE ••• The procedure started with inspection of the abdominal cavity for presence of extrahepatic metastases. When none were found, the liver capsule was inspected, followed by NIR fluorescence imaging. Subsequently, LUS was performed with a dedicated radiologist. Each suspect lesion detected by inspection, fluorescence imaging, and/or LUS, was resected when the surgeon considered it to be safe and relevant.

All resected liver lesions were routinely analyzed at the pathology department and the method of detection was correlated with histopathological findings. Histopathological diagnosis was considered the gold standard. Sensitivity and positive predictive value of every resected lesion was calculated for all imaging modalities. Only malignant lesions were considered true positives. Statistical analysis was performed using SPSS version 22.0 software (SPSS, ©IBM Corporation, Somers NY, USA).

RESULTS

PATIENT CHARACTERISTICS ••• Twenty-two patients planned to undergo laparoscopic staging (N=4) or resection (N=19) of one or multiple tumors confined to the liver were included from April 2013 to November 2015. Patient characteristics are shown in Table 1. One patient, with a suspected intrahepatic cholangiocarcinoma, was included twice. First, he underwent a diagnostic laparoscopy followed by resection of the liver tumor 2 months later.

Preoperative working diagnosis differed from final histopathological diagnosis in 4 patients. One patient presented with a large, atypical mass in segments 2 and 3 was suspected to have (fibrolamellar) HCC by radiological imaging. Final diagnosis demonstrated focal nodular hyperplasia (FNH). The second patient, with a history of laparoscopic cholecystectomy, presented with abdominal pain and preoperative images showed a liver lesion suspicious for HCC. This lesion was found to be liver tissue herniated through one of the old trocar incisions. The third patient presented with a history of breast cancer and a FDG-PET-positive lesion in segment 4b, suspicious for metastasis. Instead, the final diagnosis was intrahepatic cholangiocarcinoma. The fourth patient was suspected to have an intrahepatic cholangiocarcinoma and simultaneous liver metastases of a non-small cell lung carcinoma (NSCLC). The large liver tumor suspicious for cholangiocarcinoma was not biopsied during the first procedure. Two other suspect lesions in the liver, either metastases of NSCLC or hepatic adenomas, were biopsied and diagnosed as hepatic adenomas. The large tumor was resected in a second procedure and final histopathological evaluation indeed showed an intrahepatic cholangiocarcinoma.

PRE- AND INTRAOPERATIVE TUMOR DETECTION ••• No adverse events occurred due to ICG administration. Two patients (suffering from UMLM and CRLM) were excluded, because their procedure was postponed 3 and 6 days after ICG administration due to fever and logistical reasons. This delay resulted in intraoperative fluorescence signals too weak for sufficient guidance. In all other patients, fluorescence imaging of all types of tumors was successful (Figure 1).

A total of 46 lesions, including 26 malignant tumors with a median size of 20 mm, were resected in the remaining 20 patients (Table 2). Sensitivity and positive predictive values of the imaging modalities are shown in Figure 2. Of all resected malignancies, 20% were missed by CT-scan, 16% by MRI-scan, 38% by inspection, 12% by LUS, and 8% by NIR fluorescence imaging. Sensitivity of all imaging modalities of lesions sized <10 mm dropped considerably. However, these differences were not statistically significant. The lesions missed by LUS were all superficially located. The lesions missed by intraoperative NIR fluorescence imaging (a CRLM and UMLM) were located >8 mm below the liver capsule. During gross examination at the pathology department, the resected CRLM did show rim-type fluorescence (Figure 3). The other false-negative lesion was located several centimeters below the liver capsule and diagnosis was confirmed after biopsy. A sensitivity of 100% was reached when fluorescence imaging and LUS were combined.

No additional malignancies were identified only by intraoperative inspection. LUS alone identified one additional malignant tumor (Figure 3B). NIR Fluorescence imaging solely identified 3 additional malignancies in 2 patients suffering from CRLM. The first patient presented with a synchronous, solitary CRLM in segment 6, which partially responded to neo-adjuvant chemotherapy. During laparoscopic metastasectomy, 2 additional lesions in segment 3 were visualized by typical rim-type fluorescence, whereupon resection of these lesions was performed (see Video 1). Histopathological analysis confirmed the diagnosis of 2 metastatic intestinal type adenocarcinomas of 1 and 3 mm respectively. The second patient suffered from multiple CRLM resected by bi-segmentectomy. The additional occult lesion, sized 2 mm, was identified within the planned resection area.

Positive predictive values were 71% (CT), 80% (MRI), 52% (inspection), 77% (LUS), 75% (NIR fluorescence imaging), and 70% (LUS combined with NIR fluorescence imaging). The differences did not reach statistical significance. Lesions that appeared suspicious by NIR fluorescence imaging included a bile duct hamartoma, steatotic liver tissue, necrosis (3 times), cholestatic and inflamed liver tissue, FNH, and a biliary adenofibroma (Figure 4). Other benign lesions, such as cysts and fibrosis, were negative for NIR fluorescence. In hindsight, 4 benign lesions were unnecessarily removed because inspection alone was positive. One benign lesion was removed because NIR fluorescence imaging alone was positive.

Fluorescence imaging resulted in clear intra-operative demarcation of tumors. Resection could be performed more accurately using fluorescence guidance (see Video 2). Prior to resection, the planned margins could be checked again by LUS. Histopathological evaluation of all resected malignant tumors revealed a radical resection rate of 88% (22/25). One large UMLM was only biopsied to confirm diagnosis,

since multiple similar liver lesions were detected during surgery. In one patient, intraoperative NIR fluorescence imaging after resection showed a fluorescent margin, located on the right portal vein. LUS and inspection did not show any remaining tumor. Based on the latter results, and the goal of preserving as much liver volume as possible, it was decided not to extend the resection to a full hemihepatectomy. *Ex vivo* evaluation of the resected tissue showed a tumor positive resection margin, suggesting that a full hemihepatectomy should have been considered.

In the second patient, the positive resection margin was in retrospect visible during surgery (Figure 5). The positive resection margin in the third patient, suffering from a multinodular HCC, was not visible during surgery.

DISCUSSION

The present study describes the largest series of intra-operative fluorescence imaging during minimally-invasive oncological liver surgery. Laparoscopic resection of liver tumors is believed to have several advantages over open surgery: less intraoperative blood loss, lower morbidity rates, and decreased length of hospital stay^{12,13}. Importantly, overall and disease-free survival remains similar for patients with HCC and CRLM. However, implementation of the laparoscopic technique occurs slowly. In France for instance, currently approximately 15% of all liver resections are performed laparoscopically¹⁴. The main concerns include technical feasibility, safety of the technique, and the substantial learning curve¹⁵. Indeed, depth perception and the range of motion are hampered by a lack of tactile feedback and three-dimensional vision, as well as by altered orientation and scale of the surgical field¹⁶. No randomized controlled trials exist, but one can imagine that, compared to open procedures, the more technically demanding laparoscopic approach may expose patients to a higher risk of R1 resection. A recent meta-analysis showing a significant lower incidence of R1 resections after laparoscopic resection of CRLM may be the result of a selection bias, as some tumor locations with a higher risk of incomplete resection, such as the posterior segments, make an open approach preferable¹⁷. NIR fluorescence guidance during laparoscopic oncologic liver surgery reveals the localization of the tumor, enhances demarcation, and hopefully results in fewer incomplete resections. The current study showed that no NIR fluorescence should be visible at the resection margin to ensure a surgical margin of at least 8 mm. The radical resection rate was 88% (22 of 25 malignancies) which is comparable with the literature¹⁸. All 3 incompletely removed tumors were located in the technically more demanding segments 6, 7, and/or 8.

Two patients from the current study were excluded because fluorescence imaging several days after ICG injection resulted in fluorescence signals that were too low. Other studies described adequate fluorescence imaging up to 2 weeks after ICG administration¹⁹. Patients included in these studies underwent a standard-of-care ICG clearance test to assess liver function and received a dose of 0.5 mg/kg ICG. In The Netherlands, this test is not standard-of-care. Moreover, we have previously optimized dose and timing of administration resulting in a lower dose by a factor of 3 to 5⁸. The 2 excluded patients demonstrate that if a procedure is postponed, adequate fluorescence imaging demands a repeated dose of ICG, a higher initial dose of ICG, or a more sensitive fluorescence imaging system.

The appearance of the fluorescence signal during surgery depends not only on ICG dose and timing of administration, but also on tumor type and localization. Superficial metastases are recognizable by rim-type fluorescence, while deeper located metastases are completely surrounded by liver tissue and thus show total staining. In the current study, *ex vivo* fluorescence imaging showed rim-type fluorescence of all liver metastases and of the intrahepatic cholangiocarcinoma, while HCC also showed partial fluorescence. After intravenous administration, ICG is rapidly eliminated from the blood via the liver with a half-life of 2-3 min. Retention of ICG around liver tumors is not only due to simple mechanical compression of bile ducts. Recent studies revealed an underlying molecular mechanism. The transition zone between tumor and healthy liver tissue is composed of dedifferentiated hepatocytes with a keratine-7-positive immature phenotype⁸. These hepatocytes show down-regulation of anion transporters and are consequently unable to transport ICG into biliary canaliculi²⁰. ICG is thus entrapped around tumors in these immature hepatocytes. Normally differentiated hepatocytes throughout the liver have already excreted their ICG and appear dark, just like metastases from extrahepatic tumors and poorly differentiated HCC, resulting in high contrast ratios. In differentiated HCC, the portal uptake function is preserved, leading to accumulation of ICG in the tumor itself²¹. A similar mechanism may play a role in ICG retention in FNH and biliary adenofibroma, as shown in this study (Figure 4). Observations in resected liver tumors showed that ICG is not only preserved in fresh tissue, but also in paraffin-embedded tissue²². *Ex vivo* fluorescence imaging remains possible in samples as old as 3 years.

The laparoscopic imaging system used in this study, i.e. the Karl Storz HD fluorescence laparoscope, allows easy switching between white light modus and fluorescence modus using a foot pedal. A drawback of this system is that no overlay of fluorescence and white light images is available. This makes orientation during fluorescence imaging sometimes challenging. Several other laparoscopic fluorescence imaging systems are available, including the commercially-available Pinpoint

endoscopic fluorescence imaging system (Novadaq Technologies Inc, Toronto, Canada)²³ and FireFly fluorescence imaging for the da Vinci Si surgical robot (Intuitive Surgical, Inc., Sunnyvale, CA, USA)²⁴. These two systems do possess an overlay function, which may improve ease of use.

Near-infrared light (700-900 nm) has the advantage of higher photon penetration into tissue and lower autofluorescence compared to the visible light spectrum (400-700 nm). The reported depth penetration is however limited to a maximum of ≈ 8 mm²⁵. In the present study, both lesions missed by fluorescence imaging were located >8 mm below the liver surface. Although the missed CRLM did show rim-type fluorescence *ex vivo* (Figure 3B), these lesions were intraoperatively only visible using LUS. This finding demonstrates that fluorescence imaging must be seen as a complementary technique to LUS. The combination of LUS and fluorescence imaging reached a sensitivity of 100%. However, only suspect lesions were resected and this value is therefore not accurate, just like specificity and negative predictive value. No significant differences were found because this study was not designed and powered to do so. Deeper located liver tumors may also be visualized using intraoperative photoacoustic tomography²⁶. This technique combines the specific uptake of ICG by some liver tumors with enhanced depth penetration of ultrasonography. Although feasible, technical improvements are required to make this technique available for clinical use.

Multiple studies illustrated the highly sensitive intraoperative detection of HCC and CRLM using fluorescence imaging^{8,21,27,10}. However, only 1 small study and 3 case reports describe this technique during minimally-invasive liver surgery^{9,28,29,30}. Our group previously reported feasibility of UMLM detection in 3 patients during laparoscopic resection⁹. Additional metastases were identified in 2 patients. Kudo et al. showed fluorescent detection of 12 out of 16 HCCs and 11 out of 16 CRLM in 17 patients²⁸. Contrary to our current study, no comparison was made between lesions detected by fluorescence imaging and by other imaging modalities. Moreover, no information was provided about false positive lesions detected by fluorescence imaging. The rather disappointing results of this study may be the result of a less sensitive imaging system, a suboptimal ICG dose, or variations in timing of ICG administration. To improve homogeneity, we chose to use a fixed ICG dose and to administer the dose the day before surgery. This strategy allowed visualization of all included tumors *in vivo* or *ex vivo*.

Fluorescence imaging can assist in differentiating between benign and malignant lesions, such as cysts, fibrosis, and hemangiomas. In the current study, 4 necrotic lesions were suspicious using fluorescence imaging. These lesions were resected in 2 CRLM patients who received neoadjuvant therapy. It may be that these lesions were

in fact tumors that fully responded to the chemotherapy. In addition, two other resected lesions (a biliary adenofibroma and FNH) were considered false-positive, because they were benign. Nonetheless, imaging of these large lesions (18 – 84 mm) was still relevant as these lesions were preoperatively planned to be resected. Other studies describing fluorescence imaging during laparoscopic resection of liver tumors do not mention false positivity rates.

Three occult, otherwise undetected, liver tumors (12%) were identified in 2 patients suffering from CRLM. Other studies describe similar results. Van der Vorst et al.⁸ identified additional lesions in 12.5% (5 of 40) of patients suffering from CRLM. Ishizawa et al.²¹ examined resected liver specimens of patients with HCC and identified 7.7% (21 of 273) additional HCCs that were not identified by gross examination. A key unanswered question is whether these additional lesions are “harbingers” of even more tumors not yet visible by any means or the only sites of disease that would otherwise have not been resected. One patient in the current study developed multiple liver metastases 3 months after surgery. The second patient is still disease-free after 6 months. Of the 5 patients with additional detected tumors in the study of van der Vorst et al.⁸, 2 developed hepatic recurrence within 1 year, but 3 are currently still disease-free after a period of 3 to 6 years. Although these results should be interpreted cautiously, it appears that NIR fluorescence imaging can indeed prevent recurrence in some patients.

This study demonstrates the added value of intraoperative navigation using NIR fluorescence imaging during laparoscopic resection of a broad variety of malignant liver tumors. It is an easy, effective, and safe method. NIR fluorescence imaging can assist in localization and demarcation of known tumors, as well as identification of otherwise undetectable occult liver tumors. Large studies are required to confirm whether fluorescence-guided resection of liver tumors can improve radical resection rates and patient outcomes, but based on our results we believe this method could quickly be an important component of laparoscopic resection of liver tumors.

REFERENCES

- Nuzzo G, Giulianti F, Giovannini I, et al. Bile duct injury during laparoscopic cholecystectomy: results of an Italian national survey on 56 591 cholecystectomies. *Archives of surgery (Chicago, Ill : 1960)* 2005;140(10):986-92.
- Tornqvist B, Stromberg C, Persson G, et al. Effect of intended intraoperative cholangiography and early detection of bile duct injury on survival after cholecystectomy: population based cohort study. *BMJ* 2012;345:e6457.
- Halbert C, Pagkratis S, Yang J, et al. Beyond the learning curve: incidence of bile duct injuries following laparoscopic cholecystectomy normalize to open in the modern era. *Surgical endoscopy* 2016;30(6):2239-43.
- Halbert C, Altieri MS, Yang J, et al. Long-term outcomes of patients with common bile duct injury following laparoscopic cholecystectomy. *Surgical endoscopy* 2016;30(10):4294-9.
- Vettoretto N, Saronni C, Harbi A, et al. Critical view of safety during laparoscopic cholecystectomy. *JSL S* 2011;15(3):322-5.
- Polat FR, Abci I, Coskun I, et al. The importance of intraoperative cholangiography during laparoscopic cholecystectomy. *JSL S* 2000;4(2):103-7.
- Halawani HM, Tamim H, Khalifeh F, et al. Impact of intraoperative cholangiography on postoperative morbidity and readmission: analysis of the NSQIP database. *Surgical endoscopy* 2016;30(12):5395-5403.
- El Shallaly G, Seow C, Sharp C, et al. Intraoperative cholangiography time in laparoscopic cholecystectomy: timing the radiographer. *Surg Endosc* 2005;19(10):1370-2.
- Way LW, Stewart L, Gantert W, et al. Causes and prevention of laparoscopic bile duct injuries: analysis of 252 cases from a human factors and cognitive psychology perspective. *Ann Surg* 2003;237(4):460-9.
- Mitsuhashi N, Kimura F, Shimizu H, et al. Usefulness of intraoperative fluorescence imaging to evaluate local anatomy in hepatobiliary surgery. *Journal of hepatobiliary-pancreatic surgery* 2008;15(5):508-14.
- Schaafsma BE, Mieog JS, Hutteman M, et al. The clinical use of indocyanine green as a near-infrared fluorescent contrast agent for image-guided oncologic surgery. *J Surg Oncol* 2011;104(3):323-32.
- Vahrmeijer AL, Hutteman M, van der Vorst JR, et al. Image-guided cancer surgery using near-infrared fluorescence. *Nat Rev Clin Oncol* 2013;10(9):507-18.
- Boogerd LS, Handgraaf HJ, Lam HD, et al. Laparoscopic detection and resection of occult liver tumors of multiple cancer types using real-time near-infrared fluorescence guidance. *Surgical endoscopy* 2017;31(2):952-961.
- Benya R, Quintana J, Brundage B. Adverse reactions to indocyanine green: a case report and a review of the literature. *Cathet Cardiovasc Diagn* 1989;17(4):231-3.
- Verbeek FP, Schaafsma BE, Tummers QR, et al. Optimization of near-infrared fluorescence cholangiography for open and laparoscopic surgery. *Surg Endosc* 2014;28(4):1076-82.
- Buchs NC, Hagen ME, Pugin F, et al. Intra-operative fluorescent cholangiography using indocyanine green during robotic single site cholecystectomy. *The international journal of medical robotics + computer assisted surgery: MRCAS* 2012;8(4):436-40.
- Ishizawa T, Kaneko J, Inoue Y, et al. Application of fluorescent cholangiography to single-incision laparoscopic cholecystectomy. *Surgical endoscopy* 2011;25(8):2631-6.
- Daskalaki D, Fernandes E, Wang X, et al. Indocyanine green (ICG) fluorescent cholangiography during robotic cholecystectomy: results of 184 consecutive cases in a single institution. *Surgical innov* 2014;21(6):615-21.
- Kono Y, Ishizawa T, Tani K, et al. Techniques of Fluorescence Cholangiography During Laparoscopic Cholecystectomy for Better Delineation of the Bile Duct Anatomy. *Medicine* 2015;94(25):1005.
- Zarrinpar A, Dutton EP, Mobley C, et al. Intraoperative Laparoscopic Near-Infrared Fluorescence Cholangiography to Facilitate Anatomical Identification: When to Give Indocyanine Green and How Much. *Surg Innov* 2016;23(4):360-5.
- Cherrick GR SS, Leevy CM, et al. Indocyanine green: observations on its physical properties, plasma decay, and hepatic extraction. *J Clin Invest* 1960;39:592-600.
- Ishizawa T, Tamura S, Masuda K, et al. Intraoperative fluorescent cholangiography using indocyanine green: a biliary road map for safe surgery. *Journal of the American College of Surgeons* 2009;208(1):e1-4.
- Aoki T, Murakami M, Yasuda D, et al. Intraoperative fluorescent imaging using indocyanine green for liver mapping and cholangiography. *Journal of hepatobiliary-pancreatic sciences* 2010;17(5):590-4.
- Ishizawa T, Bandai Y, Ijichi M, et al. Fluorescent cholangiography illuminating the biliary tree during laparoscopic cholecystectomy. *BJ S* 2010;97(9):1369-77.
- Tagaya N, Shimoda M, Kato M, et al. Intraoperative exploration of biliary anatomy using fluorescence imaging of indocyanine green in experimental and clinical cholecystectomies. *Journal of hepatobiliary-pancreatic sciences* 2010;17(5):595-600.
- Hutteman M, van der Vorst JR, Mieog JS, et al. Near-infrared fluorescence imaging in patients undergoing pancreaticoduodenectomy. *European surgical research* 2011;47(2):90-7.
- Ishizawa T, Fukushima N, Shibahara J, et al. Real-time identification of liver cancers by using indocyanine green fluorescent imaging. *Cancer* 2009;115(11):2491-504.
- Kaneko J, Ishizawa T, Masuda K, et al. Indocyanine green reinjection technique for use in fluorescent angiography concomitant with cholangiography during laparoscopic cholecystectomy. *Surgical laparoscopy, endoscopy & percutaneous techniques* 2012;22(4):341-4.

29. Buchs NC, Pugin F, Azagury DE, et al. Real-time near-infrared fluorescent cholangiography could shorten operative time during robotic single-site cholecystectomy. *Surgical endosc* 2013;27(10):3897-901.

30. Schols RM, Bouvy ND, Masclee AA, et al. Fluorescence cholangiography during laparoscopic cholecystectomy: a feasibility study on early biliary tract delineation. *Surgical endosc* 2013;27(5):1530-6.

31. Schols RM, Bouvy ND, van Dam RM, et al. Combined vascular and biliary fluorescence imaging in laparoscopic cholecystectomy. *Surgical endosc* 2013;27(12):4511-7.

32. Spinoglio G, Piora F, Bianchi PP, et al. Real-time near-infrared (NIR) fluorescent cholangiography in single-site robotic cholecystectomy (SSRC): a single-institutional prospective study. *Surgical endosc* 2013;27(6):2156-62.

33. Prevot F, Rebibo L, Cosse C, et al. Effectiveness of intraoperative cholangiography using indocyanine green (versus contrast fluid) for the correct assessment of extrahepatic bile ducts during day-case laparoscopic cholecystectomy. *Journal of gastrointestinal surgery* 2014;18(8):1462-8.

34. Larsen SS, Schulze S, Bisgaard T. Non-radiographic intraoperative fluorescent cholangiography is feasible. *Danish medical journal* 2014;61(8):A4891.

35. Dip FD, Asbun D, Rosales-Velderrain A, et al. Cost analysis and effectiveness comparing the routine use of intraoperative fluorescent cholangiography with fluoroscopic cholangiogram in patients undergoing laparoscopic cholecystectomy. *Surgical endosc* 2014;28(6):1838-43.

36. Dip F, Roy M, Lo Menzo E, et al. Routine use of fluorescent incisionless cholangiography as a new imaging modality during laparoscopic cholecystectomy. *Surgical endosc* 2015;29(6):1621-6.

37. Dip F, Nguyen D, Montorfano L, et al. Accuracy of Near Infrared-Guided Surgery in Morbidly Obese Subjects Undergoing Laparoscopic Cholecystectomy. *Obesity surgery* 2016;26(3):525-30.

38. Boni L, David G, Mangano A, et al. Clinical applications of indocyanine green (ICG) enhanced fluorescence in laparoscopic surgery. *Surgical endosc* 2015;29(7):2046-55.

39. Kawaguchi Y, Velayutham V, Fuks D, et al. Usefulness of Indocyanine Green-Fluorescence Imaging for Visualization of the Bile Duct During Laparoscopic Liver Resection. *Journal of the American College of Surgeons* 2015;221(6):1113-7.

40. Osayi SN, Wendling MR, Drosdeck JM, et al. Near-infrared fluorescent cholangiography facilitates identification of biliary anatomy during laparoscopic cholecystectomy. *Surgical endosc* 2015;29(2):368-75.

41. van Dam DA, Ankersmit M, van de Ven P, et al. Comparing Near-Infrared Imaging with Indocyanine Green to Conventional Imaging During Laparoscopic Cholecystectomy: A Prospective Crossover Study. *Journal of laparoendoscopic & advanced surgical techniques Part A* 2015;25(6):486-92.

42. Igami T, Nojiri M, Shinohara K, et al. Clinical value and pitfalls of fluorescent cholangiography during single-incision laparoscopic cholecystectomy. *Surg Today* 2016;46(12):1443-1450.

43. Calatayud D, Milone L, Elli EF, et al. ICG-fluorescence identification of a small aberrant biliary canaliculus during robotic cholecystectomy. *Liver international* 2012;32(4):602.

44. Snoeks TJ, van Driel PB, Keereweer S, et al. Towards a successful clinical implementation of fluorescence-guided surgery. *Mol Imaging Biol* 2014;16(2):147-51.

45. Rosenthal EL, Warram JM, de Boer E, et al. Successful Translation of Fluorescence Navigation During Oncologic Surgery: A Consensus Report. *J Nucl Med* 2016;57(1):144-50.

46. Buddingh KT, Nieuwenhuijs VB, van Buuren L, et al. Intraoperative assessment of biliary anatomy for prevention of bile duct injury: a review of current and future patient safety interventions. *Surgical endosc* 2011;25(8):2449-61.

47. Flum DR, Flowers C, Veenstra DL. A cost-effective analysis of intraoperative cholangiography in the prevention of bile duct injury during laparoscopic cholecystectomy. *J Am Coll Surg* 2003;196(3):385-93.

48. Buddingh KT, Weersma RK, Savenije RA, et al. Lower rate of major bile duct injury and increased intraoperative management of common bile duct stones after implementation of routine intraoperative cholangiography. *J Am Coll Surg* 2011;213(2):267-74.

49. Ford JA, Soop M, Du J, et al. Systematic review of intraoperative cholangiography in cholecystectomy. *BJs* 2012;99(2):160-7.

50. Schaafsma BE, Mieog JS, Hutteman M, et al. The clinical use of indocyanine green as a near-infrared fluorescent contrast agent for image-guided oncologic surgery. *J Surg Oncol* 2011;104(3):323-32.

Figure 1 Representative images of intraoperative NIR fluorescence identification of liver tumors

A well-differentiated hepatocellular carcinoma shows uptake of ICG in and around the tumor. A cholangiocarcinoma shows a rim-type fluorescence, similar to hepatic metastases of colorectal and breast cancer and uveal melanoma. As the breast cancer and uveal melanoma liver metastases are located below the liver surface, the fluorescence does not show a rim. However, *ex vivo* a distinctive rim-type fluorescence signal is visible (data not shown). Of note, the fluorescence laparoscope does not possess an overlay function; the images are therefore not always aligned.

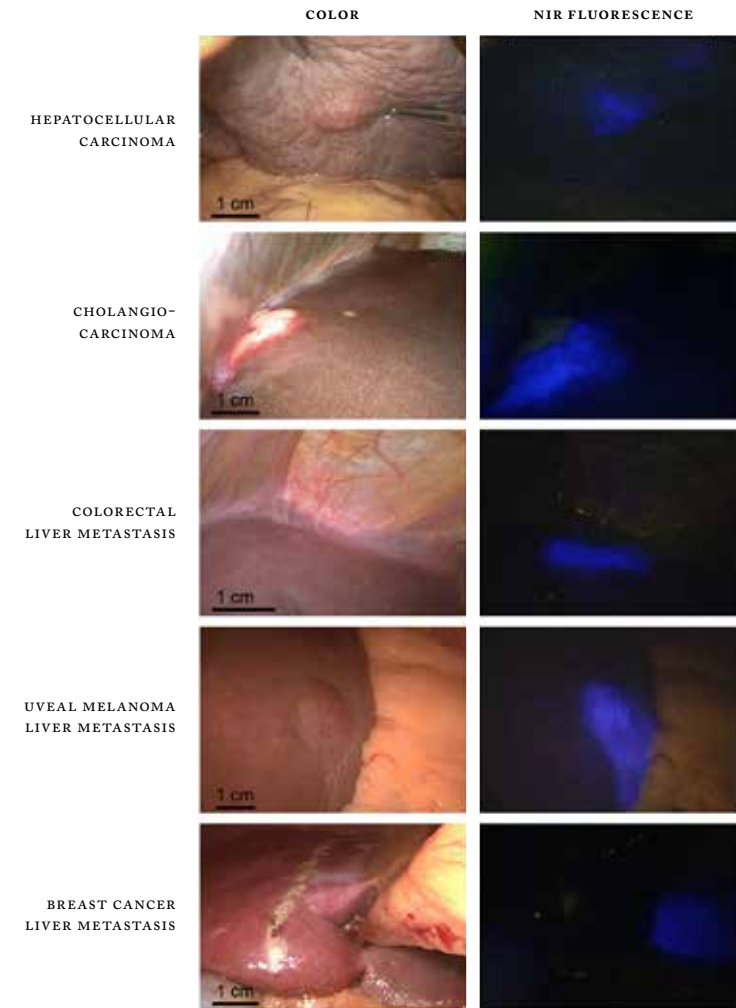


Figure 2 Sensitivity of all imaging modalities employed

Sensitivity and positive predictive value of computed tomography (CT), magnetic resonance imaging (MRI), visual inspection, laparoscopic ultrasonography (LUS), near-infrared fluorescence imaging (NIRF) and combination of LUS and NIRF. NIRF has the highest sensitivity rate amongst all imaging modalities. Combination of NIRF + LUS results in detection of all hepatic tumors (100% detection). The graph shows the sensitivity for all lesions together and divided into <10 mm and ≥10 mm. Sensitivity of all imaging modalities drops considerably for detection of lesions <10 mm. However, all small lesions could still be detected by combining NIRF and LUS. Differences are not statistically.

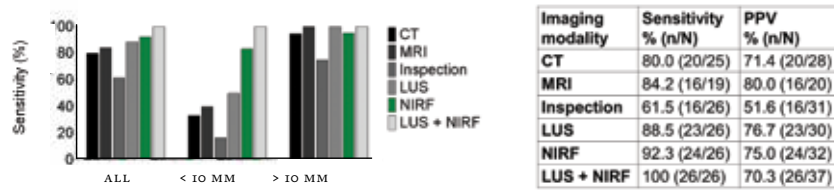


Figure 3 Ex vivo fluorescence imaging of resected tumors

Rim-type fluorescence surrounding a cholangiocarcinoma (CHC, image A) and a colorectal liver metastasis (CRLM, image B) imaged using a FLARE® prototype. The CRLM was not visible using fluorescence imaging during surgery, because it was located >8 mm below the liver surface. Matching microscopic images (magnification 2X and 40X) of hematoxylin & eosin and DAPI staining sections were made of CHC (image C) and CRLM (image D). Fluorescence shows a sharp demarcation between normal liver tissue and fibrosis or tumor tissue. Image D also shows fluorescence in a biliary duct, probably due to mechanic obstruction by the tumor.

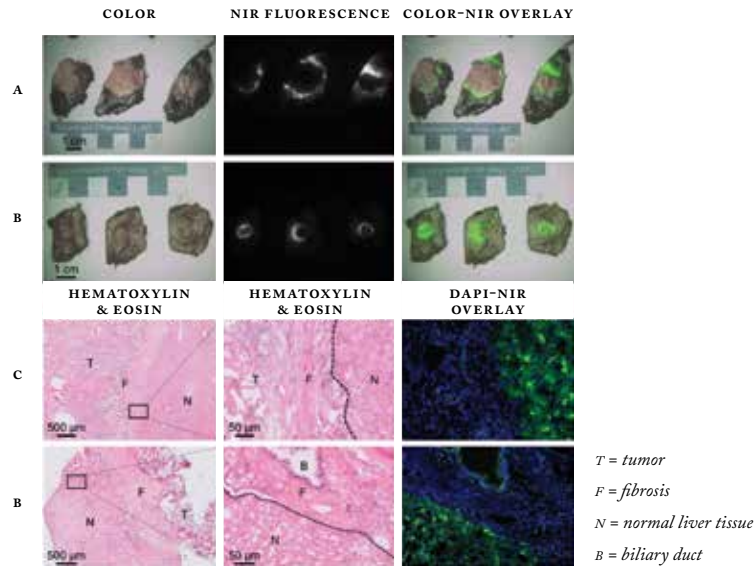


Figure 4 Fluorescence imaging of benign lesions

- A Intraoperative imaging of a cyst (white arrow) and a bile duct hamartoma (dashed arrow). The cyst is not visible using fluorescence imaging, but the bile duct hamartoma is. The weak fluorescence signal does not show a distinctive rim-type fluorescence and can thereby be discriminated from a malignancy.
- B Benign, large focal nodular hyperplasia also shows NIR fluorescence. The mechanism of ICG uptake is unknown, but potentially its biliary excretion is disturbed.

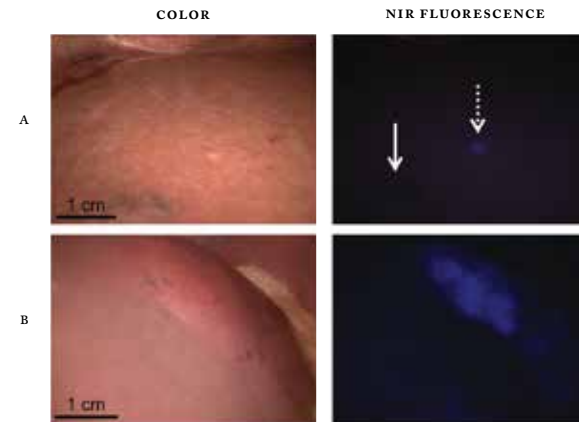


Figure 5 Intraoperative visualization of a positive resection margin of a colorectal liver metastasis

In vivo fluorescence is visible in the resection margin (white arrow), indicating a tumor-free margin of less than 8 mm. *Ex vivo*, the distinctive fluorescent rim is interrupted (dashed arrow) at the positive resection margin.

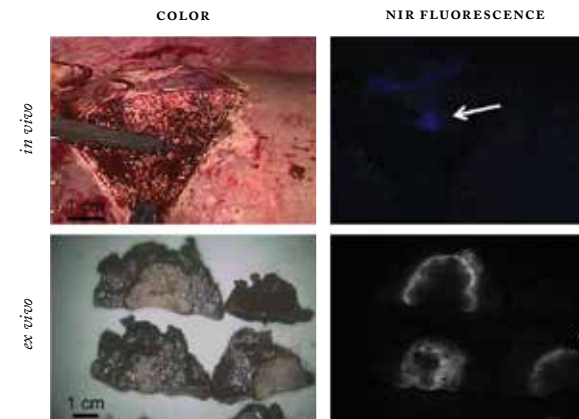


Table 1 Patient characteristics

Total patients, n	22	
Age at surgery, median [range]	65 [28 – 76]	
Gender, % (n)	Female	45 [5]
	Male	55 [11]
BMI, median [range]	23.0 [18.8 – 36.6]	
ASA classification, % (n)	1	9 [16]
	2	82 (18)
	3	9 [16]
	4	0 (0)
Liver cirrhosis, % (n)	14 [15]	
Neo-adjuvant therapy, % (n)	27 [31]	

ASA = American Society of Anesthesiologists

Table 2 Characteristics of resected lesions

	Histopathological diagnosis	N	Size (mm)	Method of detection, n/N*					
				CT	MRI	Insp	LUS	NIRF	LUS + NIRF
Malignant	HCC	3	45 [25-58]	3/3	1/1	2/3	3/3	3/3	3/3
	CHC	2	32 [30-33]	1/1	1/1	2/2	2/2	2/2	2/2
	CRLM	18	18 [1-35]	14/18	11/14	10/18	15/18	17/18	18/18
	UMLM	2	16 [14-18]	2/2	2/2	1/2	2/2	1/2	2/2
	BCLM	1	11	0/1	1/1	1/1	1/1	1/1	1/1
	total	26	20 [1-58]	20/25	16/19	16/26	23/26	24/26	26/26
Benign	Adenoma	1	20	1/1	-	1/1	1/1	0/1	1/1
	FNH	1	84	1/1	-	1/1	1/1	1/1	1/1
	Biliary adenofibroma	1	18	1/1	-	1/1	1/1	1/1	1/1
	Bile duct hamartoma	6	4 [2-15]	1/6	1/5	5/6	1/5	1/6	2/6
	Necrosis	4	13 [8-37]	2/4	2/4	3/4	2/4	3/4	3/4
	No lesion identified**	2	-	1/2	1/2	1/2	0/2	0/2	0/2
	Other***	5	-	1/3	0/4	3/5	1/5	2/5	3/5
	Total	20	13 [2-84]	8/18	4/15	15/20	7/19	8/20	11/20

Insp. = inspection; HCC = hepatocellular carcinoma; CHC = intrahepatic cholangiocarcinoma; CRLM = colorectal liver metastasis; UMLM = uveal melanoma liver metastasis; BCLM = breast cancer liver metastasis; FNH = focal nodular hyperplasia.

* Not all lesions were imaged by all imaging modalities.

** After gross examination, the pathologist could not identify any abnormal lesion in two specimens.

*** Includes cholestasis, cirrhotic tissue, fibrosis and steatosis.

PART II

PRECLINICAL EVALUATION OF TUMOR TARGETS FOR FLUORESCENCE IMAGING

CHAPTER 5

CONCORDANCE OF FOLATE RECEPTOR- α EXPRESSION BETWEEN BIOPSY, PRIMARY TUMOR AND METASTASIS IN BREAST AND LUNG CANCER PATIENTS

Oncotarget, 2016; Mar 2, Oncotarget. 2016 Apr 5;7(14):17442-54

LSF BOOGERD*, MC BOONSTRA*, ACC BECK, A CHAREHBILI, CES HOOGSTINS,
HAJM PREVOO, S SINGHAL, PS LOW, CJH VAN DE VELDE
AND AL VAHRMEIJER

**shared first authorship*

ABSTRACT

Folate receptor alpha (FR α) is known to be upregulated in a variety of cancers, including non-small-cell lung cancer (NSCLC) and breast cancer. To ensure reliable implementation of diagnostic- and therapeutic agents, concordance of FR α expression between biopsy, primary tumor and metastases is important. Using immunohistochemistry (MAB 2B3.F2) these concordances were investigated in 60 NSCLC and 40 breast cancer patients. False positivity of FR α expression on breast and lung cancer biopsies was limited to less than 5%. In NSCLC, FR α expression was shown in 21/34 adenocarcinomas and 4/26 squamous cell carcinomas (SCC). Concordance of FR α expression between biopsy and primary tumor was achieved in respectively 83% and 91% of adenocarcinomas and SCCs. Approximately 80% of all local and distant metastases of NSCLC patients showed concordant FR α expression as their corresponding primary tumor. In breast cancer, FR α positivity was shown in 12/40 biopsies, 20/40 lumpectomies and 6/20 LN metastases, with concordance of 68% between biopsy and primary tumor and 60% between primary tumor and LN metastases. In conclusion, this study shows high concordance rates of FR α expression between biopsies and metastases compared to primary NSCLC and breast cancers, underscoring the applicability of FR α -targeted agents in these patients.

INTRODUCTION

The introduction of molecular targeted oncologic therapies has created the need to select patients with the right expression patterns to achieve optimal results¹. Currently, the molecular markup of tumors can be determined using (real-time or quantitative reverse transcription) polymerase chain reaction, microRNA detection, or immunohistochemistry (IHC). Immunohistochemical staining of tumor tissue is the preferred method, since it provides insight about the expression pattern of specific membrane-bound proteins and, in addition, is a relatively easy and inexpensive technique. Immunohistochemical staining of tumor biopsies is already implemented in clinical practice and used as an efficient selection method in cancer care in, for example, breast cancer patients². Concordance of biomarker expression between biopsy, primary tumor and (distant) metastasis is important for appropriate application of tumor-targeted modalities; e.g. Positron Emission Tomography (PET) or Single Photon Emission Computed Tomography (SPECT)-targeted agents or targeted therapies. For example, a biopsy can turn out to be positive for a certain biomarker while the distant metastasis showed to be negative in most of the cases, resulting in suboptimal applications/results of the targeted approaches. In this study, we investigate these concordances in NSCLC and breast cancer patients and generate insight for the reliable application of FR α -targeted agents in these patients.

In the past decades, several membrane-located proteins were discovered that could successfully be targeted, i.e. estrogen/progesterone receptor (ER/PR) in breast cancer patients and epidermal growth factor receptor (EGFR) in lung cancer patients^{2,3}. Another potential target that holds great promise is folate receptor alpha (FR α). This glycosylphosphatidylinositol (GPI)-anchored cell membrane protein was first described on a human ovarian cancer cell line in 1991 and is part of the folate receptor (FR) family^{4,5}. Folic acid and 5-methyltetrahydrofolate, the major circulating form of folate, bind with high affinity to these FRs⁶. Folate, the water-soluble vitamin B₉, is involved in one-carbon metabolic reactions and is therefore required in the biosynthesis of the nucleotide bases thymine and uracil. The essential role of folate in growth, proliferation and survival of cells reflects the importance of folate during growth and sustenance of tumor cells^{7,8}. In total, four isoforms of FR are described of which FR β and FR γ are sited on hematopoietic cells and overexpressed on cancer cells of hematopoietic origin⁷. The isoform FR β is also found on activated macrophages, while the function of FR δ remains unclear. FR α is normally located on the apical surface of a restricted number of healthy epithelial tissues, such as proximal kidney tubules, fallopian tube and type I and II pneumocytes of the lung⁹. Research on FR α has focused on identification of tumor types that show FR α

overexpression and a recent study showed that 40% of epithelial tumors show *FRα* overexpression, including (non-mucinous) ovarian, kidney, uterine, colon, lung and breast cancer¹⁰.

Lung cancer is the number one cause of cancer death worldwide with a poor five-year survival estimated at 15%. This disease can be divided in non-small cell lung cancer (NSCLC), contributing to 85% of all lung cancers, and small cell lung cancer (SCLC). NSCLC is further subdivided by histological subtype, of which adenocarcinoma (40%), squamous cell carcinoma (25-30%) and large-cell carcinoma (10-15%) are the most prevalent¹¹. Tumor-targeted therapies have already been extensively studied in lung cancer patients, which resulted in implementation of such therapies, e.g. bevacizumab, erlotinib and gefitinib, in the treatment guideline of lung cancer disease¹². Overexpression of *FRα* in lung cancer is mainly restricted to NSCLC and can therefore be an interesting target for many lung cancer patients^{13,14}. In breast cancer, treatment is already personalized by molecular protein expression of the tumor². The outcome of breast cancer patients is significantly improved by targeted treatment focused on hormone receptor (HR) positive, or human epidermal growth factor receptor 2 (HER2) positive tumors. However, 15% of all breast cancers show no expression of either ER/PR or HER2 and are considered triple negative (TN) breast cancers. This type of breast cancer has the worst prognosis amongst all breast cancers¹⁵. Previous studies reported *FRα* overexpression on especially the majority of TN breast cancers and therefore, *FRα* could be an interesting target for this specific group of patients¹⁶.

The aim of the present study is to determine *FRα* expression on both NSCLC and breast cancers and to determine concordance between *FRα* expression on biopsy, primary tumor and corresponding local and distant metastatic tissue.

RESULTS

PATIENT AND TUMOR CHARACTERISTICS ••• Patient- and histopathological characteristics of all NSCLC and breast cancer patients are summarized in Table 1. In short, mean age of breast and NSCLC patients was respectively 56 and 63.5 years at diagnosis. The majority of breast cancer patients displayed pT1 or pT2 stage tumors and all of them underwent a lumpectomy. The majority of NSCLC patients displayed pT4 tumors and IASLC stage IV. Of both NSCLC and breast cancer patients approximately 70% showed lymph node involvement, i.e. nodal stage N1-2. The cohort of breast cancer patients consisted of 15 TN breast cancers with a majority of high-grade tumors, e.g. 21 out of 40 tumors showed differentiation grade III.

FRα EXPRESSION AND CONCORDANCE BETWEEN BIOPSY, PRIMARY TUMOR AND METASTASES IN NSCLC PATIENTS ••• Of all primary tumors containing adenocarcinoma (N=34), 21 out of 34 tumors showed *FRα* expression of which the majority (>80%) showed overexpression (Figure 1, Table 2). Heterogeneity of *FRα* expression was seen in 16 out of 21 *FRα*-expressing adenocarcinomas. Of all primary tumors containing SCC (N=26), only 4 out of 26 tumors showed *FRα* expression. Overexpression was seen in 1 SCC and a heterogeneous staining pattern in 3 out of 4 SCCs. Of all biopsy specimens (N=23), 8 out of 12 adenocarcinomas showed *FRα* expression whereas only 2 out of 11 SCCs showed *FRα* expression. Of all 60 metastatic LNS, obtained from 33 patients, 26 out of 42 LNS containing adenocarcinoma showed *FRα* expression, whereas 3 out of 18 LNS containing SCC showed *FRα* expression. Of all distant metastases (N=23), *FRα* expression was shown in 5 out of 15 adenocarcinomas but in none of the 8 SCCs.

Concordance of *FRα* expression between biopsy and primary tumor was shown in 20 out of 23 biopsies (Figure 2, Table 3). Two of the discordances (one adenocarcinoma and one SCC) were attributed to loss of *FRα* expression in biopsy specimens, while primary tumors did show expression. The other discordance was due to upregulation of *FRα* expression on the biopsy specimen, containing adenocarcinoma. In conclusion, only one biopsy specimen showed false positivity. Concordance between local metastasis, e.g. metastatic LNS, and primary tumor was shown in 31 out of 42 LNS containing adenocarcinoma, within 14 of 18 patients. All discordances could be attributed to loss of *FRα* expression in metastatic LNS. In SCC, concordance of *FRα* expression between metastatic LNS and primary tumor was achieved in 13 out of 18 LNS, within 12 of 15 patients. In 3 LNS discordance was attributed to upregulation of *FRα* expression, while 2 LNS showed downregulation compared to *FRα* expression in the primary tumor. Concordance between primary tumors and corresponding distant metastases was seen in 12 out of 15 adenocarcinomas and in 7 out of 8 SCC (Figure 3). Discordance in 2 of the metastatic adenocarcinomas and in the metastasis that contained SCC was attributed to downregulation of the distant metastases compared to the primary tumor. The other bone metastasis containing adenocarcinoma showed upregulation compared to the corresponding primary tumor.

FRα EXPRESSION AND CONCORDANCE BETWEEN BIOPSY, PRIMARY TUMOR AND METASTASES IN BREAST CANCER PATIENTS ••• Of the total cohort of breast cancer patients in this study (N=40), a positive *FRα* expression was seen in 12 of the 40 biopsy specimens, 20 of the 40 lumpectomy specimens and 6 of the 20 metastatic LNS (Figure 1, Table 4). Overexpression of *FRα* was seen in the

majority of biopsies, lumpectomy specimens and metastatic LNs, however, almost no homogeneous staining patterns were detected. In total, only 5 of the 20 primary tumors showed a homogeneous staining pattern. Of all tissue, the hormone receptor (HR) status was known and correlated with FRA expression. As described in Table 4, the HR status, e.g. ER/PR status, showed to correlate negatively with FRA expression of biopsies ($P=0.002$) and lumpectomy specimens ($P=0.010$). Of all the 15 TN breast cancers that were included in this study, e.g. ER-PR-HER2-, respectively 7 biopsies ($P=0.091$) and 12 primary tumor specimens ($P=0.008$) showed a positive FRA expression. In addition, 3 out of 7 metastatic LNs of TN breast cancers showed FRA positivity ($P=0.613$). Of all biopsy and lumpectomy tissue, a subdivision of FRA expression per LN status was made. Of all specimens of patients with LN metastases ($N=27$), 7 out of 27 biopsies showed a positive FRA expression and 12 out of 27 lumpectomy specimens.

Concordance of FRA expression between biopsy and primary tumor was shown in 27 out of 40 specimens (Figure 2, Table 3). Discordance was attributed to downregulation of FRA on the biopsy specimens compared to the primary tumor in 11 of the 13 tissue sections and upregulation in 2 tissue sections. In conclusion, based on concordance of biopsy and primary tumor tissue, only 2 of the 40 evaluated tissue specimens showed false positivity. Furthermore, in 50% of all tissues, a similar FRA expression was shown in biopsy, lumpectomy and metastatic LN. Concordance between primary tumor and metastatic LN, in the cohort with LN metastases, was seen in 12 out of 20 specimens. Subanalysis showed that 6 out of these 8 discordances were attributed to downregulation of FRA expression on metastatic LNs compared to the primary tumor. The remaining two LNs showed a positive FRA expression, whereas the corresponding lumpectomy specimen did not show FRA expression. Separate analysis of the 6 patients that received neoadjuvant therapy showed in 4 out of these 6 patients concordant FRA expression between primary tumor and biopsy specimen. All these 4 patients showed no FRA expression in biopsy nor in primary tumor. The other two patients both showed a positive FRA expression on the primary tumor, but no expression on corresponding biopsy. In 5 of the 6 patients who received neoadjuvant therapy, metastatic LNs were available for evaluation of FRA expression. Only one metastatic LN showed FRA positivity, which was not concordant with the absent FRA expression of the primary tumor.

DISCUSSION

Since FRA has emerged as target for imaging and treatment purposes, several clinical trials have been conducted with promising results^{10,17}. Diagnostic and

therapeutic agents can be delivered intracellularly through FRA-mediated endocytosis¹⁸. During this process, an endosome (containing a FRA-targeted agent bound to FRA) is formed which moves to the recycling center, close to the nucleus. Here, the folate-agent detaches from its receptor and is released, in contrast to the receptor that is brought back to the cell surface. This pathway is mainly responsible for accumulation of FRA-targeted agents in malignant cells. However, absorption of folate in normal tissue such as duodenum and jejunum is facilitated by the proton-coupled folate transporter and the reduced folate carrier (RFC). This anion exchanger is responsible for transport of the majority of folate in healthy tissues, while folate-coupled agents show no affinity for this RFC nor the proton-coupled folate transporter^{7,19}.

As reported by Hilgenbrink and Low et al.²⁰, folate has been linked to a wide variation of substances used in cancer therapy, including protein toxins, enzymes to activate prodrugs, chemotherapeutics, immunotherapeutic agents, drug-comprising liposomes and nanoparticles. Currently, farletuzumab, vintafolide and IMG853 are the three FRA-targeting agents that show the most potential in clinical cancer trials, among other as treatment strategy for lung cancer^{10,21}. Detection of malignancies by FRA-targeted imaging approaches is studied broadly using folate linked to radio-nuclides, PET agents, MRI contrast agents and fluorescent dyes. In NSCLC, a recent study of Okusanya et al. showed feasibility of intraoperative detection of small sub-pleural lung tumors using a fluorescent FRA-targeted molecular agent, e.g. folate-FITC (Figure 5)²². An excellent sensitivity and specificity was shown, resulting in the start of a novel study with the same targeting ligand but optimized fluorophore, e.g. OTL-38 (clinicaltrials.gov). Analysis of a similar clinical trial in breast cancer patients is currently ongoing to determine tumor detection during breast cancer surgery using folate-FITC (clinicaltrials.gov).

In order to efficiently apply both FRA-targeted therapeutic and imaging agents, adequate patient selection regarding FRA expression is required. In addition, knowledge about the concordance of FRA expression between biopsy, primary tumor specimen and (possible) metastasis is pivotal to estimate efficacy and usability of these approaches. Based on results from the current study, selection of breast- and NSCLC patients who might benefit from FRA-targeted approaches can be performed reliably via biopsy staining. Although the majority of tumor specimens showed heterogeneity of FRA expression, less than 5% of all biopsies showed false positivity. In a clinical setting, this suggests that 1 out of 20 included breast cancer or NSCLC patients in a FRA-targeted trial would show no FRA expression in the primary tumor while the biopsy stained FRA-positive. Regarding the targeting of disseminated malignant cells, this study shows high concordance rates of local/distant metastases

with corresponding primary tumors. Although concordance rates were relatively lower for breast cancer than for NSCLC, e.g. 68% vs. >80%, these results still suggest that the majority of metastases can be targeted when the primary tumor shows FRA expression.

Overall, discordance was mainly due to downregulation of FRA in biopsy- and metastatic tissue compared to primary NSCLC and breast cancer, which could be a result of tissue sampling or of heterogeneity of FRA expression. In this study, whole tissue slides were used to overcome the difficulty in evaluating heterogeneity as is experienced with the generally used TMA²³. Of all 266 evaluated tumor tissue specimens, heterogeneity of FRA was shown in the majority (>80%) of the stained sections.

Several IHC studies investigated FRA expression on primary lung (NSCLC) and breast cancers. Two lung studies applied the same monoclonal antibody as used in this study, i.e. 2B3.F2, and displayed similar expression rates, underscoring the validity of the used staining: more than 70% of adenocarcinomas expressed FRA and less than 15% of SCCs^{14,24}. In the current study, a significant association between FRA expression and histological subtype was shown in biopsies ($P=0.036$), primary tumors ($P<0.001$) and metastatic LNS ($P=0.004$). The distinction between FRA expression in adenocarcinoma and SCC is caused by the type of cancer cell they derive from; adenocarcinoma originates from FRA-expressing type 1 and 2 pneumocytes and SCC from more centrally positioned tracheal cells which do not express the receptor^{14,25}.

Other IHC studies using a different monoclonal antibody (MAB343) showed expression rates in adenocarcinoma and SCC ranging from 72% to 87% and 15% to 57% respectively^{13,26}. The difference in percentages of positive FRA expressing tumors between studies may be partially contributed to a variation in applied antibodies. For example, relatively high percentages of FRA expression in patients with SCC obtained using MAB343 may be a result of non-specific binding^{13,26}. Furthermore, cut-off values for defining FRA positivity and scoring methods are diverse amongst studies. Nunez et al.¹³ examined FRA expression in NSCLC patients ($N=320$) by using the H-score, which offers a separate score for both cytoplasmic and membranous staining. In breast cancer, cut-off values for defining FRA positivity differed from 5-15%. Scoring using the M-score has been described in which both membranous tumor cell staining and the proportion and staining intensity of FRA positive cells are captured¹⁶. Hartmann et al.²⁷ assessed FRA expression using MAB343 on a tissue micro array (TMA) containing samples of 63 invasive breast cancers with either poor or good outcome. An association between strong FRA expression and a poor outcome, defined as median time to recurrence of 1.9 years, was shown. These results are in line with other studies describing a significant association between FRA expression and

worse (disease-free) survival^{16,28}. Increased folate storage in FRA-expressing tumors may cause accelerated growth and consequently, a more aggressive tumor. However, a recent study describing FRA expression in breast cancer brain metastases was unable to show any association between FRA expression and survival, possibly due to small sample size²⁹. In lung cancer, results from studies investigating survival and FRA expression also vary. Several IHC studies and a study investigating FRA gene expression using RT-PCR, reported an improved overall survival when FRA expression is high^{14,30}. However, Nunez et al. could not show any correlation between FRA expression and overall- or recurrence free survival in a cohort of 320 patients¹³. It still remains unclear why high levels of FRA are correlated with a favorable prognosis; further research is warranted to explain this.

Recent studies showed that FRA expressing breast cancers represented a novel molecular subtype associated with ER-/PR-/HER2NEU- and ER- breast cancers^{16,28}. The current study endorses these conclusions as 12 out of 15 primary tumors of TN breast cancers showed a positive FRA expression and a significant correlation between HR status and FRA expression on both biopsy specimens ($P=0.002$) and primary tumors ($P=0.010$) was found. It is known that estrogens are involved in the regulation of FRA expression and 17 β estradiol via the P4 promoter, resulting in down-regulation of FRA^{31,32}. Positive FRA expression was shown in respectively 30%, 50% and 30% of biopsy-, lumpectomy- and metastatic LN tissue. Although this percentage is higher than described in literature, it must be noted that 67.5% of the included patients had LN metastases (N1-2) and 37.5% were TN breast cancer patients. Furthermore, tumors displayed a relatively high tumor grade. In the study of Zhang et al.²⁸, a significant association between FRA positive expression and high histologic grade, high nodal stage and subgroups of ER/PR- and TN breast cancers was shown. In an extra cohort of metastatic stage IV, HER2 negative breast cancer patients, O'Shannessy et al.¹⁶ described that the percentage of FRA positive tumors in early stage disease is retained in late stage metastatic disease, as 36% of samples showed FRA positive expression of whom 86% were TN breast cancers.

In an additional cohort of NSCLC patients ($N=23$), concordance of FRA expression between primary tumor and corresponding distant metastases was assessed. In the literature, little is known about FRA expression on distant metastases. In a study of O'Shannessy et al.¹⁴, 9 fine needle aspirates comprising LN metastases of lung adenocarcinoma showed 63% FRA positivity. Furthermore, Nunez et al.¹³ reported no significant difference in FRA expression between 27 NSCLC and 15 derived metastatic sites. We show concordance rates between primary tumor and distant metastases of respectively 80% and 88% for adenocarcinomas and SCCs. In addition, all metastatic LNS showed concordant FRA expression with the corresponding distant metastases.

On the contrary, Kikuchi et al.³³ showed downregulation of *FR α* gene expression in 16 metastatic brain tumors compared to 22 primary lung adenocarcinomas using cDNA microarray. However, as this study investigated gene expression and non-corresponding metastases, results have to be interpreted with caution.

Finally, normal breast and lung cells showed *FR α* expression (Figure 3). In particular the luminal border of secretory cells (due to the secretion of folate in milk) and the myoepithelial layers of normal epithelial breast tissue stained positive. Nonetheless, *FR α* expression on normal breast and lung tissue will not significantly interfere when *FR α* -targeted agents are intravenously administered, since the receptor is confined to the luminal side of polarized epithelial cells. The lack of cellular polarity on malignant cells on the other hand, will lead to binding of *FR α* -targeted agents through the whole tumor¹⁸.

In conclusion, this study shows high concordance rates of *FR α* expression between primary tumor and corresponding biopsy and metastatic tissue of both breast cancer and NSCLC patients, underscoring applicability of *FR α* -targeted agents in these patients. Moreover, an association between *FR α* expression and histological/molecular subtype of tumors was shown. Importantly, false positivity of *FR α* expression on biopsies was limited to less than 5%. Although this study is performed with a relatively small amount of tissue specimens, the current results provide rationale for the use of biopsies to select lung and breast cancer patients for *FR α* -targeted agents, eventually leading to optimal personalized medicine.

MATERIAL AND METHODS

TISSUE SAMPLES ••• The total cohort of NSCLC patients consisted of 38 patients who received curative surgery between 2011–2013 and 22 patients with distant metastases (2000–2013). Of all 60 NSCLC patients, 34 primary tumors containing adenocarcinoma and 26 SCCs were included as shown in Table 1. To assess the correlation between *FR α* expression on primary tumor and preoperatively obtained biopsy tissue, all available biopsy specimens, obtained via mediastinal biopsy, were collected. However, in some patients a transesophageal endoscopic ultrasound fine needle aspiration (EUS-FNA) or endobronchial ultrasound transbronchial needle aspiration (EBUS-TBNA) was performed and some patients were referred to our academic center, of whom biopsy specimen could not be obtained. In total, 23 biopsies were collected: 12 biopsies containing adenocarcinoma and 11 biopsies containing SCC (Table 2). Moreover, 60 metastatic LNS of 33 patients were stained for *FR α* . Adenocarcinoma was present in 42 of these LNS, while SCC was present in the remaining 18 metastatic LNS. Fifteen of the distant metastases contained

adenocarcinoma, whereas 8 of them contained scc. Of one patient who suffered from adenocarcinoma, tissues from two different metastatic sites were included. Metastases originated mostly from the brain (N=10), followed by metastases from bone (N=7), liver (N=3), skin (N=1), adrenal gland (N=1) and jejunum (N=1).

The total cohort of breast cancer patients consisted of 40 patients, who had undergone a breast conserving surgery (lumpectomy) for a cT1 or cT2 stage tumor between 2000–2014. In total, 6 of the 40 patients received neoadjuvant chemotherapy, of whom obtained results are separately described. The first cohort of breast cancer patients consisted of 20 patients of whom biopsy specimen and lumpectomy tissue was stained. In addition, a second cohort of 20 patients was included to assess concordance of *FR α* expression between biopsy specimen, lumpectomy and metastatic LNS. Of all patients, the receptor status of the tumor tissue was known, e.g. ER, PR and HER2 status.

IMMUNOHISTOCHEMISTRY ••• IHC was performed using formalin-fixed, paraffin-embedded (FFPE) tissue, obtained from the Pathology archive from the Leiden University Medical Center, Diaconessen Hospital and Rijnland Hospital. All samples were handled in an anonymous fashion according to the national ethical guidelines ('Code for Proper Secondary Use of Human Tissue,' Dutch Federation of Medical Scientific Societies) and approved by the Institutional Ethics Committee of the Leiden University Medical Center. Tissue samples were stained using the monoclonal antibody (MAB) 26B3.F2 (certified Folate Receptor alpha IHC Assay Kit, Biocare Medical) and subsequently scored for staining. The MAB26B3.F2 is highly specific for *FR α* without cross-reactivity to the other FR, e.g. FR β , FR γ or FR δ . Validation of the staining protocol was performed by using (the recommended) lung adenocarcinoma as positive control and normal liver as negative control. Immunohistochemical staining was performed on 4 μ m paraffin sections on adhesive slides. Slides were deparaffinized in xylene and rehydrated in decreasing concentrations of ethanol. After rinsing in distilled water, endogenous peroxidase was blocked with hydrogen peroxide for five minutes. Slides were rinsed in water and antigen retrieval was performed in the DAKO PT Link, Target Retrieval Solution pH6.0 at 95°C for 10 minutes. After rinsing in PBS, nonspecific sites were blocked with a protein block (Background Punisher) for 5 minutes and the secondary antibody was incubated for 30 minutes on room temperature. As a negative control, one control slide was incubated with negative control reagent. After three washes the slides were incubated with MACH4 Mouse Probe Primary Antibody Enhancer (Biocare Medical) for 10 minutes. Again slides were washed in PBS, followed by incubation with MACH4 HRP Polymer for 10 minutes. Subsequently, the slides were

washed and antibody binding was visualized by using 3,3'-diaminobenzidine (DAB, DAKO). Sections were counterstained with haematoxylin, dehydrated and mounted with pertex.

SCORING METHOD ••• FRA expression was assessed in both lung and breast cancer tissue by using a membranous scoring method with a scale ranging from 0 to 3+, as described by O'Shannessy et al.¹⁴. A score of 0 corresponded with absence of staining; 1+ equaled faint staining on luminal borders; 2+ equaled moderate staining on apical and sometimes lateral borders and 3+ indicated strong circumferential staining (Figure 1). The tumor was considered positive when more than 10% of malignant cells were positively stained (>0). Overexpression of FRA was defined as a score of 2+ or 3+. Heterogeneity was described when FRA expression was detectable on all malignant cells. Concordance was achieved when the expression score of one of the stained tissues, i.e. biopsy or corresponding LN or distant metastasis, matched the score of the primary tumor and both displayed either positive or negative expression of FRA. In general, FRA expression of the primary tumor specimen was considered as golden standard. Concordance between either biopsy or metastatic tissue with the primary tumor was described as down- or upregulation of FRA. False positive expression was determined as positive FRA expression on biopsy or metastatic tissue without FRA expression on the primary tumor. Evaluation of the immunohistochemical staining was performed blinded independently by two observers. Disagreements were resolved by consensus after reviewing the relevant slide with the pathologist.

STATISTICAL ANALYSIS ••• The statistical analysis was performed using SPSS version 22.0 software (SPSS, ©IBM Corporation, Somers NY, USA). FRA expression per histopathological subgroup was calculated by the Fishers exact test. A P-value of <0.05 was considered statistically significant.

REFERENCES

- Maitland M.L., Schilsky R.L. Clinical trials in the era of personalized oncology. *CA Cancer J Clin*;61:365-81;2011
- Kourea H.P., Zolota V., Scopa C.D. Targeted pathways in breast cancer: molecular and protein markers guiding therapeutic decisions. *Curr Mol Pharmacol*;7:4-21;2014
- Roengvoraphoj M., Tsongalis G.J., Dragnev K.H., Rigas J.R. Epidermal growth factor receptor tyrosine kinase inhibitors as initial therapy for non-small cell lung cancer: focus on epidermal growth factor receptor mutation testing and mutation-positive patients. *Cancer Treat Rev*;39:839-50;2013
- Coney L.R., Tomassetti A., Carayannopoulos L., Frasca V., Kamen B.A., Colnaghi M.I. et al. Cloning of a tumor-associated antigen: MOV18 and MOV19 antibodies recognize a folate-binding protein. *Cancer Res*;51:6125-32;1991
- Ross J.F., Chaudhuri P.K., Ratnam M. Differential regulation of folate receptor isoforms in normal and malignant tissues in vivo and in established cell lines. *Physiology and clinical implications. Cancer*;73:2432-43;1994
- Della-Longa S., Arcovito A. Structural and functional insights on folate receptor alpha (FRA) by homology modeling, ligand docking and molecular dynamics. *J Mol Graph Model*;44:197-207;2013
- Elnakat H., Ratnam M. Distribution, functionality and gene regulation of folate receptor isoforms: implications in targeted therapy. *Adv Drug Deliv Rev*;56:1067-84;2004
- Gonen N., Assaraf Y.G. Antifolates in cancer therapy: structure, activity and mechanisms of drug resistance. *Drug Resist Updat*;15:183-210;2012
- Weitman S.D., Lark R.H., Coney L.R., Fort D.W., Frasca V., Zurawski V.R., Jr. et al. Distribution of the folate receptor GP38 in normal and malignant cell lines and tissues. *Cancer Res*;52:3396-401;1992
- Assaraf Y.G., Leamon C.P., Reddy J.A. The folate receptor as a rational therapeutic target for personalized cancer treatment. *Drug Resist Updat*;17:89-95;2014
- de G.P., Munden R.F. Lung cancer epidemiology, risk factors, and prevention. *Radiol Clin North Am*;50:863-76;2012
- Gadgeel S.M., Ramalingam S.S., Kalemkerian G.P. Treatment of lung cancer. *Radiol Clin North Am*;50:961-74;2012
- Nunez M.I., Behrens C., Woods D.M., Lin H., Suraoakar M., Kadara H. et al. High expression of folate receptor alpha in lung cancer correlates with adenocarcinoma histology and EGFR corrected mutation. *J Thorac Oncol*;7:833-40;2012
- O'Shannessy D.J., Yu G., Smale R., Fu Y.S., Singhal S., Thiel R.P. et al. Folate receptor alpha expression in lung cancer: diagnostic and prognostic significance. *Oncotarget*;3:414-25;2012
- Chen L., Linden H.M., Anderson B.O., Li C.I. Trends in 5-year survival rates among breast cancer patients by hormone receptor status and stage. *Breast Cancer Res Treat*;147:609-16;2014
- O'Shannessy D.J., Somers E.B., Maltzman J., Smale R., Fu Y.S. Folate receptor alpha (FRA) expression in breast cancer: identification of a new molecular subtype and association with triple negative disease. *Springerplus*;1:22;2012
- Sega E.L., Low P.S. Tumor detection using folate receptor-targeted imaging agents. *Cancer Metastasis Rev*;27:655-64;2008
- Low P.S., Kularatne S.A. Folate-targeted therapeutic and imaging agents for cancer. *Curr Opin Chem Biol*;13:256-62;2009
- Matherly L.H., Hou Z. Structure and function of the reduced folate carrier: a paradigm of a major facilitator superfamily mammalian nutrient transporter. *Vitam Horm*;79:145-84;2008
- Hilgenbrink A.R., Low P.S. Folate receptor-mediated drug targeting: from therapeutics to diagnostics. *J Pharm Sci*;94:2135-46;2005
- Shi H., Guo J., Li C., Wang Z. A current review of folate receptor alpha as a potential tumor target in non-small-cell lung cancer. *Drug Des Devel Ther*;9:4989-96;2015
- Okusanya O.T., DeJesus E.M., Jiang J.X., Judy R.P., Venegas O.G., Deshpande C.G. et al. Intraoperative molecular imaging can identify lung adenocarcinomas during pulmonary resection. *J Thorac Cardiovasc Surg*;150:28-35;2015
- Kyndi M., Sorensen F.B., Knudsen H., Overgaard M., Nielsen H.M., Andersen J. et al. Tissue microarrays compared with whole sections and biochemical analyses. A subgroup analysis of DBCG 82 B & C. *Acta Oncol*;47:591-9;2008
- Bremer R.E., Scoggins T.S., Somers E.B., O'Shannessy D.J., Tacha D.E. Interobserver agreement and assay reproducibility of folate receptor alpha expression in lung adenocarcinoma: a prognostic marker and potential therapeutic target. *Arch Pathol Lab Med*;137:1747-52;2013
- Sutherland K.D., Berns A. Cell of origin of lung cancer. *Mol Oncol*;4:397-403;2010
- Cagle P.T., Zhai Q.J., Murphy L., Low P.S. Folate receptor in adenocarcinoma and squamous cell carcinoma of the lung: potential target for folate-linked therapeutic agents. *Arch Pathol Lab Med*;137:241-4;2013
- Hartmann L.C., Keeney G.L., Lingle W.L., Christianson T.J., Varghese B., Hillman D. et al. Folate receptor overexpression is associated with poor outcome in breast cancer. *Int J Cancer*;121:938-42;2007
- Zhang Z., Wang J., Tacha D.E., Li P., Bremer R.E., Chen H. et al. Folate receptor alpha associated with triple-negative breast cancer and poor prognosis. *Arch Pathol Lab Med*;138:890-5;2014

- 29 Leone J.P., Bhargava R., Theisen B.K., Hamilton R.L., Lee A.V., Brufsky A.M. Expression of high affinity folate receptor in breast cancer brain metastasis. *Oncotarget*;6:30327-33;2015
- 30 Iwakiri S., Sonobe M., Nagai S., Hirata T., Wada H., Miyahara R. Expression status of folate receptor alpha is significantly correlated with prognosis in non-small-cell lung cancers. *Ann Surg Oncol*;15:889-99;2008
- 31 Rochman H., Selhub J., Karrison T. Folate binding protein and the estrogen receptor in breast cancer. *Cancer Detect Prev*;8:71-5;1985
- 32 Kelley K.M., Rowan B.G., Ratnam M. Modulation of the folate receptor alpha gene by the estrogen receptor: mechanism and implications in tumor targeting. *Cancer Res*;63:2820-8;2003
- 33 Kikuchi T., Daigo Y., Ishikawa N., Katagiri T., Tsunoda T., Yoshida S. et al. Expression profiles of metastatic brain tumor from lung adenocarcinomas on cDNA microarray. *Int J Oncol*;28:799-805;2006
- 34 van Driel P.B., van de Giessen M., Boonstra M.C., Snoeks T.J., Keereweer S., Oliveira S. et al. Characterization and evaluation of the artemis camera for fluorescence-guided cancer surgery. *Mol Imaging Biol*;17:413-23;2015

Figure 1 Staining intensities of FR α in NSCLC and breast cancer samples using immunohistochemistry (IHC)

The staining score (0 to 3+) was obtained by assessment of membrane intensity. A score of 0 equals no membrane staining, a score of 1+ a faint apical membrane staining, a score of 2+ a moderate apical and occasional lateral membrane staining and a score of 3+ equals a strong circumferential membrane staining. NSCLC FR α expression on biopsy (1A), primary tumor (1B) and metastatic LN tissue (1C) in a NSCLC patient, containing adenocarcinoma (20x)

1A-D Staining intensity of respectively 0, 1+, 2+ and 3+ in adenocarcinoma samples of NSCLC patients (40x).
2A-D Staining intensity of respectively 0, 1+, 2+ and 3+ in breast cancer samples (40x).

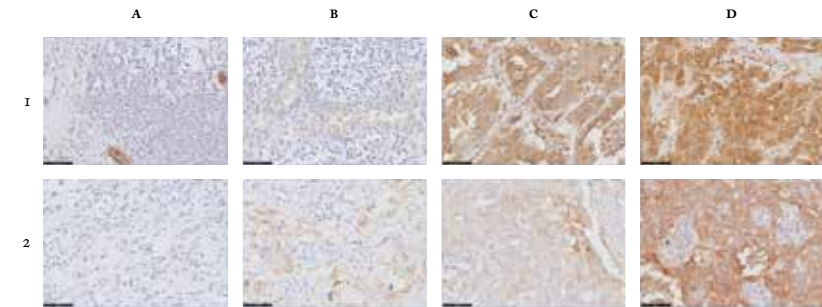


Figure 2 Examples of (dis)concordance in FR α staining in biopsy-, primary tumor-, and metastatic LN tissue in NSCLC and breast cancer patients

- 1A-C Example of concordance between positive FR α expression on biopsy (1A), primary tumor (1B) and metastatic LN tissue (1C) in a NSCLC patient, containing adenocarcinoma (20x)
- 2A-C Example of discordance between FR α expression on biopsy (2A), primary tumor (2B) and metastatic LN tissue (2C) in a NSCLC patient, containing scc (20x)
- 3A-C Example of concordance between positive FR α expression on biopsy (3A), primary tumor (3B) and metastatic LN tissue (3C) in a breast cancer patient (20x)

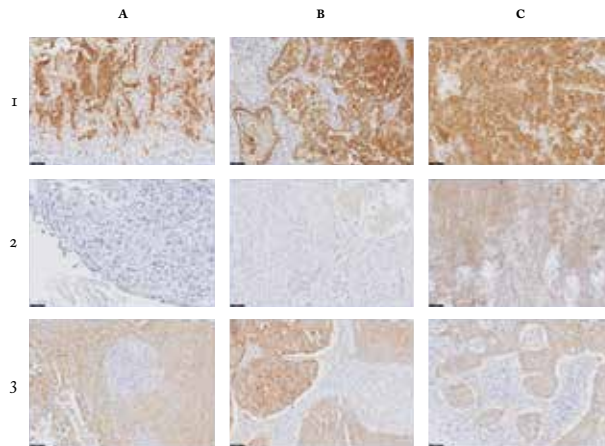


Figure 3 FR α expression in NSCLC and corresponding distant metastases

- 1A Primary tumor containing adenocarcinoma without FR α expression (20x)
- 1B Corresponding distant metastasis of the bone with positive FR α expression (20x)
- 2A Primary tumor containing adenocarcinoma with positive FR α expression (20x)
- 2B Corresponding distant metastasis of the brain with positive FR α expression (20x)

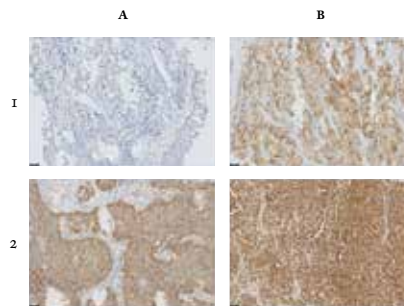


Figure 4 Example of FR α -targeted detection of an adenocarcinoma using EC-17, i.e. fluorescent FR α -targeted molecular agent, in a patient suffering from NSCLC.

In vivo fluorescence imaging was performed using the Artemis imaging system.³⁴

- A Prior to pulmonary resection, a tumor of 3 cm in the upper lobe of the left lung is detected by CT- and PET-scan
- B *In vivo* fluorescence imaging shows clear tumor delineation
- C *Ex vivo* fluorescence imaging of the tumor in the resected specimen
- D After resection, the wound bed was inspected with λ_{ex} 490 nm and demonstrated no residual fluorescence at the surgical margins
- E FR α upregulation was confirmed by fluorescence microscopy and immunohistochemical staining

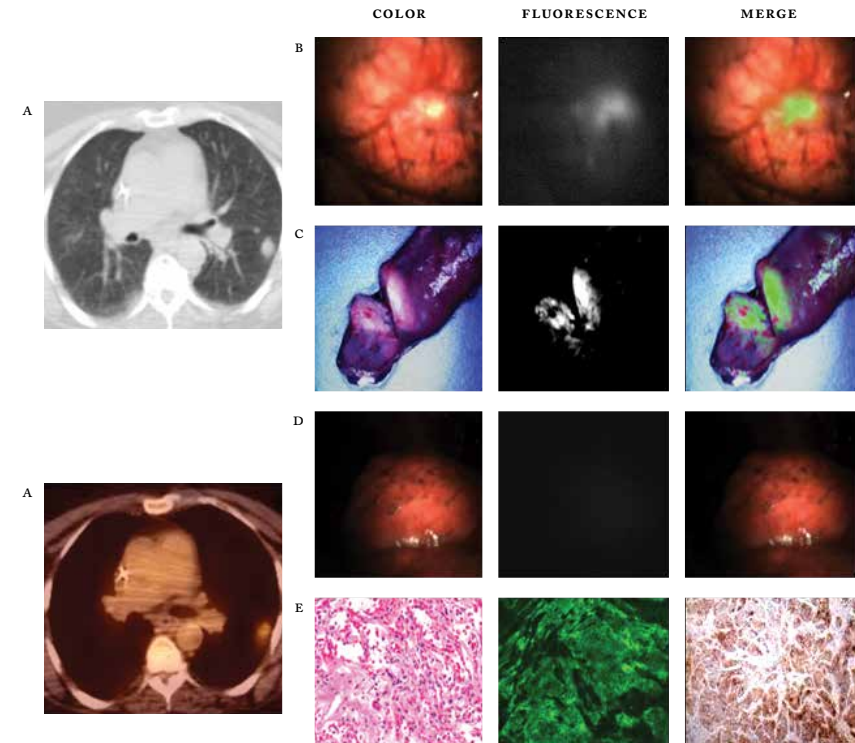


Figure 5 Examples of FR α staining in normal lung and breast tissue

- A Staining of FR α at the luminal border of normal lung tissue in an adenocarcinoma patient (10x)
- B Staining of FR α at the luminal border of normal lung tissue in an scc patient (10x)
- C Staining of FR α in normal breast tissue: staining at the luminal border of secretory cells (10x)

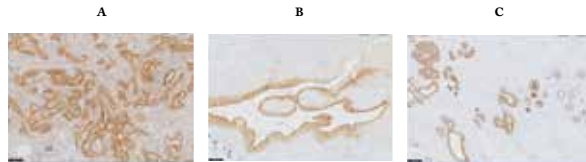


Table 1 Patient and tumor characteristics

Variable	NSCLC, adenocarcinoma No. (%)	NSCLC, SCC No. (%)	Breast cancer No. (%)
All patients	34 (57)	26 (43)	40
Mean age at diagnosis (years)	64.5	62.5	56
Sex			
male	21 (87.5)	20 (77)	0 (0)
female	13 (12.5)	6 (23)	40 (100)
Tumor size			
PT1	10 (29)	3 (12)	23 (57.5)
PT2	5 (15)	6 (23)	16 (40)
PT3	4 (12)	4 (15)	1 (2.5)
PT4	15 (44)	13 (50)	0 (0)
Nodal Stage			
NX	0 (0)	0 (0)	1 (2.5)
NO	7 (21)	5 (19)	12 (30)
NI-2	27 (79)	21 (81)	27 (67.5)
IASCL stage			
IA	4 (12)	1 (4)	
IB	2 (6)	2 (8)	
IIA	3 (9)	4 (15)	
IIB	2 (6)	0 (0)	
IIIA	7 (20)	10 (38)	
IIIB	1 (3)	1 (4)	
IV	15 (44)	8 (31)	
Marker status			
HR status			
positive			19 (47.5)
negative			21 (52.5)
HER2 status			
positive			17 (42.5)
negative			23 (57.5)
TN			
yes			15 (37.5)
no			25 (62.5)
Histology			
Ductal			36 (90)
Lobular			4 (10)
Tumor grade			
NE			4 (10)
Grade 1			2 (5)
Grade 2			13 (32.5)
Grade 3			21 (52.5)
Neo-adjuvant therapy			
Yes	14 (41)	8 (31)	6 (15)
No	20 (59)	18 (69)	34 (85)

NSCLC non-small-cell lung cancer; SCC squamous cell carcinoma; pT pathological tumor stage, N node status, IASCL International Association for the Study of Lung Cancer; HR hormone receptor, including progesterone and estrogen receptor status; Her2 human epidermal growth factor receptor 2; NE not evaluable; Tumor grade, according to Bloom & Richardson scoring method

Table 2 Folate receptor- α expression in NSCLC patients

	Total No.	FRA(+) No. (%)	FRA(-) No. (%)	p-value
Biopsies				
Total	23			
Adenocarcinoma	12	8 (67)	4 (33)	0.036
SCC	11	2 (18)	9 (82)	
Primary tumor				
Total	60			
Adenocarcinoma	34	21 (62)	13 (38)	<0.001
SCC	26	4 (15)	22 (85)	
Lymph node metastases				
Total	60 (in 33 pts)			
Adenocarcinoma	42 (in 18 pts)	26 (62)	16 (38)	0.004
SCC	18 (in 15 pts)	3 (17)	15 (83)	
Distant metastasis				
Total	23			
Adenocarcinoma	15	5 (33)	10 (67)	0.122
SCC	8	0 (0)	8 (100)	

SCC squamous cell carcinoma; FRA Folate receptor α ; pts patients

Table 3 Concordance between biopsy, primary tumor and corresponding disseminated lymph nodes and distant metastases in patients with breast cancer and NSCLC

Degree of concordance	Breast cancer patients No. (%)	NSCLC patients, adenocarcinoma No. (%)	NSCLC patients, scc, No. (%)
Concordance of FRA status			
Biopsy = Primary tumor	27 out of 40 (67.5)	10 out of 12 (83)	10 out of 11 (91)
Primary tumor = Local metastasis	12 out of 20 (60)	31 out of 42 (78)*	13 out of 18 (80)*
Primary tumor = Distant metastases		12 out of 15 (80)	7 out of 8 (88)
Disconcordance of FRA status			
Biopsy > Primary tumor	2	1	0
Biopsy < Primary tumor	11	1	1
Primary tumor > Local metastasis	6	4	2
Primary tumor < Local metastasis	2	0	3
Primary tumor > Distant metastasis		2	1
Primary tumor < Distant metastasis		1	0

SCC squamous cell carcinoma; FRA Folate receptor α ; pos LN positive lymph node

* LN expression was assessed in 33 patients, in respectively 18 patients with adenocarcinoma and 15 patients with SCC; concordance was seen in 14 out of 18 adenocarcinoma patients (31/42 LNs) and 12 out of 15 SCC patients (13/18 LNs).

Table 4 Folate receptor- α expression in breast cancer patients

Biopsy	Biomarker status	FRA (+) No. (%)	FRA (-) No. (%)	p-value
Total				
HR status	positive	1 (8)	18 (64)	0.002
	negative	11 (92)	10 (36)	
HER2 status	positive	5 (42)	12 (43)	1.000
	negative	7 (58)	16 (57)	
TN	yes	7 (58)	8 (29)	0.091
	no	5 (42)	20 (72)	
Node status	positive	7 (58)	20 (71)	0.476
	negative	5 (42)	8 (29)	
Lumpectomy specimen				
Total		20	20	
HR status	positive	5 (25)	6 (30)	0.010
	negative	15 (75)	14 (70)	
HER2 status	positive	7 (35)	10 (50)	0.523
	negative	13 (65)	10 (50)	
TN	yes	12 (60)	3 (15)	0.008
	no	8 (40)	17 (85)	
Node status	positive	12 (60)	15 (75)	0.501
	negative	8 (40)	5 (25)	
Lymph node metastasis				
Total		6	14	
HR status	positive	2 (33)	7 (50)	0.642
	negative	4 (67)	7 (50)	
HER2 status	positive	2 (33)	8 (57)	0.628
	negative	4 (67)	6 (43)	
TN	yes	3 (50)	4 (29)	0.613
	no	3 (50)	10 (71)	

FRA Folate receptor α ; HR hormone receptor including estrogen- and progesterone receptor; HER2 human epidermal growth factor receptor 2; TN triple negative

CHAPTER 6

FLUORESCENCE-GUIDED TUMOR DETECTION WITH A NOVEL ANTI-EPCAM TARGETED ANTIBODY FRAGMENT: PRECLINICAL VALIDATION

Surgical Oncology, 2019 (in press)

LSF BOOGERD*, MC BOONSTRA*, HAJM PREVOO, HJM HANDGRAAF,
PJK KUPPEN, GC MACDONALD, J CIZEAU, A PREMSUKH,
ML VINKENBURG, CFM SIER, CJH VAN DE VELDE, J BURGGRAAF
AND AL VAHRMEIJER

**shared first authorship*

ABSTRACT

Tumor-specific fluorescent imaging agents are moving towards the clinic, supporting surgeons with real-time intraoperative feedback about tumor locations. The epithelial cell adhesion molecule (EPCAM) is considered as one of the most promising tumor-specific proteins due to its high overexpression on epithelial-derived cancers. This study describes the development and evaluation of EPCAM-F800, a novel fluorescent anti-EPCAM antibody fragment, for intraoperative tumor imaging.

Fab production, conjugation to the fluorophore IRDYE800CW, and binding capacities were determined and validated using HPLC, spectrophotometry and cell-based assays. *In vivo*, dose escalation-, blocking-, pharmacokinetic- and biodistribution studies (using both fluorescence and radioactivity) were performed, next to imaging of clinically relevant orthotopic xenografts for breast and colorectal cancer.

EPCAM-F800 targets EPCAM with high specificity *in vitro*, which was validated using *in vivo* blocking experiments with a 10x higher dose of unlabeled Fab. The optimal dose range for fluorescence tumor detection in mice was 1-5 nmol (52-260µg), which corresponds to a human equivalent dose of 0.2-0.8 mg/kg. Biodistribution showed high accumulation of EPCAM-F800 in tumors and metabolizing organs. Breast and colorectal tumors could clearly be visualized within 8 h post-injection and up to 96 h, while the agent already showed homogeneous tumor distribution within 4 h. The blood half-life was 4.5 h.

This study describes the development and evaluation of a novel EPCAM-targeting agent and the feasibility to visualize breast and colorectal tumors by fluorescence imaging during resections. EPCAM-F800 will be translated for clinical use, considering its abundance in a broad range of tumor types.

INTRODUCTION

Prognosis after cancer surgery mainly depends on the completeness of the surgical resection¹⁻⁴. Accurate detection of tumor margins during surgery can be difficult due to the lack of visual distinction between tumor and normal or inflamed/fibrotic tissue. This can be problematic especially after neoadjuvant chemo- and/or radiotherapy (CRT), which is frequently used in rectal cancer patients⁵. Targeted fluorescence-guided surgery (FGS) is an intraoperative imaging technique that allows real-time tumor identification. FGS is based on (near-infrared, NIR) fluorescent dyes in combination with a dedicated imaging system and is already widely investigated for sentinel lymph node mapping, liver tumor detection and bile duct imaging using the non-targeted fluorescent dye indocyanine green⁶. Conjugating fluorescent dyes to specific tumor-recognizing ligands, such as antibodies or peptides, enhances the specificity of this technique for tumor imaging considerably. Various tumor-specific agents have already shown feasibility in early phase clinical trials⁷⁻¹¹.

Not all tumor-associated biomarkers are suitable targets for imaging purposes; prerequisite is expression on the cellular membrane with several fold higher densities compared to surrounding normal cells¹². The Epithelial Cell Adhesion Molecule (EPCAM) was among the first human tumor-associated antigens discovered and was identified by a number of independently developed monoclonal antibodies (mAb) 17-1A, 323/A3, and MOC31¹³. EPCAM is a 40KD type I transmembrane glycoprotein involved in cell-to-cell interactions and adhesions¹⁴. The molecule is under physiological conditions minimally expressed on the basolateral surface of epithelial cells and in undifferentiated pluripotent stem cells¹⁵. However, it is overexpressed in virtually all epithelial cancers and expression is conserved with cancer progression and metastasis¹⁶. EPCAM is associated with cellular signaling processes and plays a prominent role in tumor cell migration, proliferation and differentiation¹⁷. Very high overexpression (100-1000 fold) of EPCAM has been found in colorectal, gastric, esophageal, head-and-neck, breast and gynecological cancers with cell surface copy numbers ranging between 100,000 and 300,000¹⁸⁻²⁰. Consequently, EPCAM-targeting therapeutic antibodies were studied in phase I, II and III trials in various cancer types including ovarian-, gastric- and head-and-neck cancer and peritonitis carcinomatosa²¹⁻²³.

In this study, we combined two well-known clinically tested components: an antigen binding fragment (FAB) derived from the antibody MOC31²⁴ and the fluorophore IRDYE800CW^{25,26}. The first iteration of the antibody FAB fragment has already been tested in preclinical and clinical studies as the immunotoxin VB6-845, constructed as a recombinant fusion protein²⁷. The fluorophore IRDYE800CW

has previously been conjugated to cetuximab and bevacizumab, and showed visualization of respectively head-and-neck cancer and breast cancer in early phase clinical trials^{9, 10}.

The aim of this study was to develop and validate a clinical translatable EPCAM-specific NIR fluorescent imaging agent that can be used for visualization of multiple tumor types. Application of EPCAM-F800 during oncological surgeries can potentially aid real-time detection of tumors, assist clinical decision making and improve treatment strategies for cancer patients in the near future.

MATERIALS AND METHODS

HUMAN SAMPLES AND STAINING ••• Paraffin-embedded tissue blocks from 10 patients who underwent surgical resection of rectal cancer between 2014 and 2015 were obtained at the Pathology Department of the Leiden University Medical Center (LUMC) to study the effect of neoadjuvant therapy on EPCAM expression in rectal cancer tissue. Five patients did and five patients did not receive neoadjuvant CRT. Tissue blocks containing tumor tissue and blocks containing adjacent normal rectal tissue were obtained. After sectioning, slides were stained for EPCAM using MAB MOC31 (Millipore Sigma, Saint Louis, MO, USA) in a predetermined optimal dilution of 1:10,000. After overnight incubation, DAKO envision + HRP anti-mouse was added for 30 min (K4001; DAKO Cytomation, Glostrup, Denmark) followed by diaminobenzidine solution (DAB+; DAKO Kit) to visualize EPCAM expression. All sections were counterstained with hematoxylin, dehydrated and finally mounted with pertex. All samples were handled in an anonymous fashion according to the National Ethical Guidelines ('Code for Proper Secondary Use of Human Tissue', Dutch Federation of Medical Scientific Societies) and were approved by the Institutional Ethics Committee of the LUMC.

FAB PRODUCTION, CONJUGATION AND STABILITY ••• VB5-845D (Viventia, Winnipeg, Canada) is a T-cell epitope depleted FAB version of the anti-EPCAM FAB deBouganin fusion protein, VB6-845. To express VB5-845D in *E. coli* supernatant, a dicistronic unit was created where the heavy and light chains were preceded by a PelB leader sequence. The insert was placed under the control of the arabinose promoter and cloned into a PING plasmid. The resulting VB5-845D/PING plasmid was then transformed into *E. coli* strain ET.04. After L-arabinose induction, the presence of soluble VB5-845D FAB protein in the supernatant was detected by western blot using a human anti-Kappa antibody coupled to HRP (Sigma, St Louis, MO).

In a 20 L Bioreactor containing 15 L of glycerol minimum media, transformed *E. coli* ET04 cells were grown to an OD600 of 50 and induced with L-arabinose. Following induction, the supernatant was collected by centrifugation, clarified by microfiltration, concentrated and diafiltrated prior to loading onto a KappaSelect column (GE Healthcare Life Sciences, Mississauga, Canada). After the column was washed with equilibration buffer, bound VB5-845D was eluted with 0.1 M Glycine-HCl, pH 2.5 and neutralized to pH 7.0 with Tris buffer. The fractions containing VB5-845D were then flowed-through a Q-sepharose column (GE Healthcare Life Sciences, Mississauga, Canada) and the effluent loaded on to an SP-sepharose (GE Healthcare Life Sciences, Mississauga, Canada). Bound VB5-845D was eluted, filter sterilized and frozen at -20°C. Purity and stability was confirmed by Coomassie staining and SE-HPLC and identity by Western blot analysis. Protein concentration was determined by BCA (Thermo Fisher Scientific, Waltham, MA, USA).

The 800CW NHS-ester (excitation peak at 773 nm, emission peak at 792 nm) and DOTA were both stored according to manufacturer protocol. Anti-EPCAM FAB VB5-845D was covalently conjugated to 800CW (EPCAM-F800) or DOTA (EPCAM-F-DOTA) using N-Hydroxysuccinimide (NHS) ester chemistry against primary amines following manufacturer protocol (Thermo Fisher Scientific, MA, USA) and as briefly described in the supplementary data. For 800CW, MALDI-TOF analyses were performed using a Microflex (BRUKER) and sinnapinic acid as matrix to evaluate labelling ratios.

The affinity of anti-EPCAM FAB and EPCAM-F800 to recombinant His-tagged EPCAM (Sino Biological) was determined using a Biacore T200 (GE Life Science). The EPCAM protein was immobilized using the His-tag on the flow cell 2 of the NTA-Chip to the level of ~150 RU. FABs were injected in five sequential increasing concentration over flow cells 1 and 2 with flow cell 1 used as the binding reference. After each experiment the surface of the chip was regenerated from bound FAB and immobilized EPCAM using SDS and EDTA solutions. The data was fitted according to the 1:1 Binding kinetics model using Biacore T200 evaluation software.

HUMAN CANCER CELL LINES ••• After evaluation of a panel of human cancer cell lines for EPCAM expression, four human cancer cell lines were selected; two from colorectal cancer origin (HT-29 and COLO320) and two from breast cancer origin (MCF-7 and MDA-MB-231). The latter was a kind gift from Drs J. Gostner and G. Spizzo, (Medical Universität Innsbruck). All cell lines were free of mycoplasma and were cultured in RPMI1640 (PAA) supplemented with 10% fetal bovine serum (Gibco) and 100 I.U./mL penicillin/streptomycin (PAA) in a humidified incubator at 37°C and 5% CO₂. The HT-29-LUC2 cell-line was established and validated by our own research group²⁸.

FLOWCYTOMETRY AND FLUORESCENT AFFINITY ASSAYS ••• Identical protocols for flowcytometry and fluorescent affinity assays were used as recently described²⁸ and are described in detail in the supplementary materials. The number of EPCAM molecules per cell were established using the Qifkit (DAKO) as described before using anti-EPCAM monoclonal antibodies 323/A3²⁹.

ANIMAL MODELS ••• The Animal Welfare Committee of the LUMC assessed all animal experiments for animal health, ethics, and research goals and approved the studies. All animals received humane care and maintenance in compliance with the 'Code of Practice Use of Laboratory Animals in Cancer Research'. Similar animal models were used as previously described³⁰ and are extensively described in the supplementary materials. In short, six-week-old, athymic, female mice were either injected subcutaneously with HT-29-LUC2 cells (5.0×10^5 cells per spot) at 4-sides on the back, to induce subcutaneously colorectal tumors, or were inoculated with 2.5×10^5 MCF-7-LUC2-CGFP cells in two contralateral mammary fat pads, to induce orthotopic breast tumors. For the colorectal orthotopic model, subcutaneously growing HT-29-LUC2 tumors were harvested, cut in small fragments, and transplanted onto the cecal wall.

NIR FLUORESCENCE IMAGING SYSTEMS••• Imaging was performed using the Pearl® Impulse small animal imager (LI-COR, Lincoln, NE, USA) and the Artemis imaging system (Quest Medical Imaging, the Netherlands). Identical imaging set-ups were used as previously described³⁰. Detailed information is provided in the supplementary material section.

IN VIVO SPECIFICITY ••• The binding specificity of EPCAM-F800 was explored using an *in vivo* blocking experiment. Mice bearing subcutaneous colorectal tumors (HT-29-LUC2) received 4 h prior to IV injection of 1 nmol (52 µg) EPCAM-F800 an intra-peritoneal injection of a 10 times higher dose of unlabeled FAB (10 nmol, 520 µg, N=4). NIR fluorescence images were acquired at 24 and 72 h post-injection with both the Pearl and the Artemis imaging system. After the last measurement, animals were sacrificed. Tumor-to-background ratios (TBRs) were generated by drawing regions of interest (ROIs) on tumors and surrounding tissue, at the back of the mice between the tumors, on fluorescence images. TBRs were calculated by dividing the mean fluorescence signals detected in tumor by the mean signals in the surrounding tissue.

IN VIVO BINDING CHARACTERISTICS, DOSE FINDING AND BIODISTRIBUTION ••• When subcutaneous HT-29 colorectal tumors were sized $36 \pm 6 \text{ mm}^2$, either 1/16 nmol (3.3 µg), 1/4 nmol (13 µg), 1 nmol (52 µg), 5 nmol (260 µg), 10 nmol (520 µg) or 20 nmol (1040 µg) EPCAM-F800 was intravenously injected (N=3 per dose group). At 4, 8, 24, 48, 72 and 96 h post injection, fluorescence was measured using the Pearl® and the Artemis imaging system. Biodistribution was studied measuring the fluorescence signal in mice bearing HT-29-LUC2 tumors with either EPCAM-MAB800 or EPCAM-F800 or control mice without injection of EPCAM-F800. In total, 6 mice were injected with 1 nmol of EPCAM-MAB800 (150 µg) and sacrificed at 24 (N=3) or 72 h (N=3) post injection. The same experiment was performed in mice injected with EPCAM-F800 (52 µg, N=6) and control mice (N=6). Biodistribution was calculated by measuring the fluorescence intensity of all excised organs, as well as of blood, urine and feces²⁹.

RADIOLABELING AND BIODISTRIBUTION ••• Radiolabeling was performed by dissolving EPCAM-FAB-DOTA in 0.1M HEPES buffer (10 µg/100 µL) and adding indium-III chloride ($35 \text{ MBq}^{111} \text{ InCl}_3$, Covidien-Mallinckrodt, Dublin, Ireland). After 30 min of incubation on the shaker, labelling was validated by HPLC (JASCO, Easton, USA). In all cases, labelling efficacy was >90%. To study the biodistribution, 6 mice were intravenously injected with 1 nmol (50 µg)¹¹¹ IN-EPCAM-F-DOTA. Mice were sacrificed 24 (N=3) or 72 h (N=3) post injection and organs were excised, weighted, and measured for radioactivity with a gamma counter (Wizard2 2470 automatic gamma scintillation counter, Perkin Elmer, USA). Activity was divided by the weight of each tissue to calculate the percentage injected dose per gram (%ID/g).

PHARMACOKINETIC ANALYSIS ••• Pharmacokinetic analysis was performed as previously described³⁰. Briefly, EPCAM-F800 was diluted in human whole blood to the concentrations 2.0, 1.0, 0.5, 0.25, 0.13, 0.06, 0.03, 0.02, 7.81×10^{-3} , 3.90×10^{-3} , 1.95×10^{-3} , 9.76×10^{-4} µM. A calibration curve was created by measuring each concentration in a 75 µl capillary tube using the Pearl® imaging system. Data was plotted in fluorescence intensity over concentration (µM). Subsequently, four mice were injected with 5 nmol EPCAM-F800 via the lateral tail vein. The contralateral lateral tail vein was used to draw blood 5 min before and 1, 30, 60, 90, 120, 180, 240, 360 and 1440 min post injection. Blood samples were absorbed using 75 µl capillary tubes and immediately measured using the Pearl® imaging system. Each measurement was extrapolated to its concentration using the calibration curve. Data were plotted in logarithmic concentration (µM) over time (min).

HISTOLOGY AND NIR FLUORESCENCE MICROSCOPY ••• Tumor penetration of EPCAM-F800 was assessed in colorectal tumors, obtained from 8 mice bearing subcutaneous HT-29-LUC2 tumors. Mice were sacrificed at 1 (N=2), 4 (N=2), 8 (N=2) or 24 hours (N=2) after injection of either 1 or 10 nmol EPCAM-F800. Tumors were snap frozen in isopentane and stored at -80°C. Tissues were sectioned at 10 µm, stained with DAPI and subsequently fluorescence imaging was performed using a Leica DM5500B digital microscope (Leica Microsystems B.V., Son, the Netherlands). Adjacent slides were hematoxylin-eosin (HE) stained.

Specificity of EPCAM targeted fluorescence in HT-29 tumors after injection of EPCAM-F800 was confirmed by immunohistochemical staining of EPCAM using a 323/A3, an anti-EPCAM MAB targeting a different epitope. HT-29 tumors were resected 24 h post injection of 5 nmol EPCAM-F800 and snapfrozen in isopentane. Subsequently, fluorescence imaging of 5 µm tissue sections on slides was performed using the Odyssey imager (LI-COR, Lincoln, NE, USA) at 800 nm after which they were HE-stained. Adjacent slides were used for fluorescence microscopy and immunohistochemistry. To confirm the presence of EPCAM, slides were stained using 323/A3-ALEXA488 by fixation in acetone for 10 min and incubation with 5 µg/ml of the antibody, followed by washing. Slides stained for EPCAM, and unstained slides, were mounted with Prolong Gold with DAPI and analyzed with a Leica DM5500B digital microscope using L5 and Y7 filter cubes for detecting ALEXA488 and 800CW respectively.

CALCULATIONS AND STATISTICAL ANALYSES ••• Statistical analysis and generation of graphs were performed using GraphPad Prism software (version 5.01, GraphPad Software Inc, La Jolla, CA, USA). Differences between groups in the *in vitro* binding assays were analyzed using the Mann-Whitney U test. Tumor-to-background ratios (TBR) were calculated by drawing regions of interest (ROIs) on fluorescence images from the Pearl® small animal imager or Artemis imaging system to extract mean signal for tumors and all major organs. Organ-to-blood ratios were calculated by dividing each value by the mean fluorescence signal detected in the tissue and blood and reported as mean and standard deviation. The two-way repeated measurement ANOVA, used to assess the relation between TBRS in different dose groups and time points, was corrected for multiple comparisons using the Bonferroni correction.

RESULTS

EPCAM EXPRESSION ON HUMAN RECTAL (CANCER) TISSUES AND CELL LINES ••• Normal rectal tissue showed weak/moderate expression of EPCAM, which was mostly limited to enterocytes located at the tip of the villi (Figure 1A). All rectal cancer tissues showed an intense, homogeneous EPCAM expression with a circumferential staining pattern (Figure 1B and 1D). EPCAM expression on tumor tissue and adjacent normal epithelium did not differ between tissues derived from patients who were not (Figure 1B and 1C) and who were (Figure 1D and 1E) treated with neoadjuvant CRT.

The selection of cell lines for the *in vivo* studies was based on flow cytometry of panels of breast and colon cancer cell lines (for the latter see Suppl. Figure S0). Cell lines MCF-7 and HT-29, both with intermediate EPCAM expression were selected. The number of EPCAM molecules per cell, as determined using 2 different monoclonal antibodies in combination with Qifkit, confirmed the data obtained by plain flow cytometry: The positive colon cancer cell line HT-29 expressed 195,000-197,000 copies (323/A3 versus MOC31) and the breast cancer cell line MCF-7 255,000-265,000 copies. The control cell lines COLO320 and MDA-MB-231 showed numbers under the detection limit of the assay (<1,000).

FAB CONJUGATION, BINDING CAPACITY AND STABILITY ••• Little to no expression of EPCAM was seen on the control COLO-320 and MDA-MB-231 cell lines using FAB VB5-845D and positive control MOC31, while high expression of EPCAM was measured on HT-29 and MCF-7 cell lines (Figure 2A). Conjugation was evaluated using SDS-PAGE showing EPCAM-F800 at approximately 45 kDa by silver staining (Figure 2B-I) and by NIR fluorescence imaging (Figure 2B-II). No degradation products were seen. Before conjugation, the FAB showed >98% purity (Figure 2C-I) and after conjugation, MALDI-TOF analysis indicated that the majority of FAB molecules were conjugated with an average of 1-4 dye molecules (Figure 2C-II). Higher concentrations of EPCAM-F800 resulted in higher signals on the EPCAM expressing cell lines, while almost no signal was measured in the low expressing control cell lines (Figure 2D). The calculated KD of anti-EPCAM FAB was with 90 pM comparable to those of MOC31 and 323/A. Although conjugation with the fluorescent dye 800CW diminished the affinity approximately 25 times, this is still considered high affinity.

IN VIVO BIODISTRIBUTION ••• At 24 h post injection, the liver, kidneys and urine showed higher fluorescence signals than the tumor (Figure 3A). Compared to EPCAM-F800, injection of EPCAM-MAB800 resulted both at 24 and 72 h in a

significantly higher signal in the liver (Figure 3A and 3B). Due to the smaller size of EPCAM-F800 and renal clearance, fluorescence in the kidneys was higher after 24 h than EPCAM-MAB800. In contrast, 72 h after injection of EPCAM-MAB800 all measured organs showed higher signal intensity compared to EPCAM-F800 (Figure 3B). At 24 h and 72 h post injection of EPCAM-MAB800, the intensity of fluorescence in blood was respectively 3 and 6 times higher than the fluorescence measured after injection of EPCAM-F800. Biodistribution of all organs after injection of EPCAM-MAB800, EPCAM-F800 and of control mice, without injection of any dye, are shown in Figure S1 and S2. TBRS were significantly higher for EPCAM-F800 compared to its full size variant EPCAM-MAB800 at both 24 h and 72 h post-injection (Figure 3C).

Quantitative measurements of the biodistribution were performed using ^{111}In -EPCAM-F-DOTA (1 nmol). The total mean activities for the mice sacrificed at 24 h post injection were $5.7 \pm 0.1\% \text{ID/g}$ and at 72 h were $5.2 \pm 0.3\% \text{ID/g}$ (MBQ, mean \pm SD). The biodistribution study confirmed accumulation of ^{111}In -EPCAM-F-DOTA in subcutaneous colorectal tumors and the kidneys at 24h, with significant lower values at the 72 h time-point (selection in Figure 3D and full in Figure S3). Compared to the signal intensity from the intestine, relatively high intensity signals were observed in the skin, thereby influencing TBRS, as also seen with NIR fluorescence in this subcutaneous model. Mean tumor-to-colon (TC) ratio was 11.5 ± 1.5 at 24 h and 8.9 ± 0.7 at 72 h and mean tumor-to-muscle (TM) ratio was 29.6 ± 12.8 at 24 h and 29.0 ± 12.5 at 72 h.

IN VIVO BLOCKING AND DOSE OPTIMIZATION STUDY ••• Tumor binding of EPCAM-F800 was further validated using a blocking experiment by competing with the unlabeled FAB fragment. The group with a pre-injection of unlabeled FAB showed significant lower TBRS at 24 h post injection compared to the group without the pre-injection (2.1 ± 0.4 vs. 6.8 ± 1.7 , $p < 0.05$) and the difference increased further at 72 h (3.0 ± 0.6 vs. 10.0 ± 3.5 , $p < 0.05$) (Figure 4A).

Dose optimization studies showed increasing TBRS for all doses at 4h post injection (Figure 4B & S4). For the 24 h time-point, a significant difference was observed between 1 nmol versus 1/16 nmol ($p < 0.05$) and no significant differences were seen between 1 nmol and higher doses, possibly due to saturation of the receptors (Figure 4B). For the 48 h time-point, TBRS measured with 1 nmol only differed significant from 1/16 ($p < 0.05$) and 1/4 nmol ($p < 0.05$). Absolute signals in both tumor and background decreased significantly within the first 4 h after injection of 1 and 5 nmol (Figure S4). The maximal concentration of EPCAM-F800 in blood measured at 1 min post injection was $59 \mu\text{M}$ (Figure 4C). Decrease of EPCAM-F800 blood concentrations followed a biphasic pattern with a distribution and elimination phase with a mean terminal half-life of 4.5 h, and with an area under the curve (AUC) of

approximately $63 \mu\text{g}^* \text{h/mL}$. Mean systemic clearance was $0.08 \pm 0.03 \text{ mL/min}$. Figure 4D shows examples of images captured with the intraoperative Artemis imaging system. Increasing the dose over 5 nmol resulted in higher fluorescence signals in both tumors and background, but not in higher TBRS (Figure S5).

CLINICAL RELEVANT ORTHOTOPIC MODELS ••• In the orthotopic breast cancer (MCF-7) model TBRS increased significantly up to 48 h (Figure 5A) after injection of 1 nmol EPCAM-F800. Due to the relatively short blood half-life, absolute signals in the background decreased faster than signals in the tumor. Figure 5B shows an example of *in vivo* breast tumor detection using the Artemis imaging system. Tumors could be recognized at 24 h and 72 h post injection and images from all time points are shown in Figure S6. In the colorectal tumor model, mean TBRS increased significantly between 24 h and 72 h time-points (4.2 ± 0.2 at 24 h vs. 6.6 ± 0.8 at 72 h, $p < 0.05$) after injection of 1 nmol of EPCAM-F800 (Figure 5C). Similar to the breast cancer model, absolute signals in the background decreased faster than the signals in the tumors between 24 h and 72 h (46% versus 72%). Figure 5D shows an example of images captured by the Artemis imaging system and bioluminescence (BLI), confirming the presence of tumor tissue. Moreover, millimeter-sized fluorescent nodules could be visualized and confirmed by BLI.

HISTOLOGY AND NIR FLUORESCENCE MICROSCOPY ••• Fluorescence microscopy revealed a clear difference in penetration pattern and intensity after 1 and 4 h post injection (Figure 6A). After 1 h fluorescence was mainly present in a rim around the tumor cells. After 4 h, fluorescence was seen throughout the whole tumor indicating full penetration of EPCAM-F800 in tumors between 1 and 4 h after injection. Moreover, the level of fluorescence intensity retained in tumors between 4 and 24 h, possibly due to internalization of the agent. NIR fluorescence microscopy images of colorectal tumors revealed co-localization of EPCAM-F800 and 323/A3-ALEXA488, indicating that EPCAM-F800 targets EPCAM (Figure 6B).

DISCUSSION

This study investigates an anti-EPCAM FAB fluorescent agent that can demarcate multiple tumor types *in vivo* using real-time fluorescence imaging. Due to the generally high overexpression on carcinomas, EPCAM is considered as one of the most promising generic tumor targets which is also recognized by the National Cancer Institute^{23,31}. Highest expression patterns are found in colorectal cancers as well as their metastasis¹⁹. The reported levels of EPCAM overexpression around

200,000-300,000 copies per cell are confirmed for the positive cell lines used in this study, reaching the low-end range of the gene-amplification based tumor marker HER2/NEU (200,000 to 10 million copies per cell). We show that EPCAM overexpression is preserved in rectal cancer tissue after neoadjuvant therapy, a crucial characteristic for a potential candidate oncotarget. Various EPCAM specific antibodies are clinically tested for their therapeutic effect, with dosages far above the dose suggested for tumor imaging. Unfortunately, little or no overall survival benefit was shown and affinity related side effects were observed hampering their clinical utility³². However, this does not make EPCAM a useless target for imaging purposes. After all, imaging tracers require a much lower dose compared to therapeutic agents, which usually avoids potential side effects.

EPCAM has been evaluated as a target for imaging applications utilizing antibodies, antibody fragments and aptamers conjugated to fluorescent dyes, radio-nuclides or both³³⁻³⁵. Zhu et al. described the use of an EPCAM-specific NIR fluorescent imaging agent for the recognition of tumor margins in a human prostate cancer orthotopic mouse model and showed accurate detection of both primary and metastatic lesions³⁵. We recently conjugated the monoclonal antibody 323/A3 to IRDYE800CW and showed clear tumor demarcation in breast, head-and-neck and colorectal cancer xenograft models at 72h post injection³⁴. Although antibodies are believed to possess superior binding characteristics compared to smaller molecules^{36,37}, their relatively large size (~150kDa) might result in heterogeneous tumor distribution, complex pharmacokinetics, and long imaging lead-times (up to 72 h) as shown in this and our previous study³⁰. On the other hand, Fab fragments are three times smaller and show more homogeneous tumor penetration. Moreover, they display shorter half-life times, a decreased immunotoxicity potential^{38,39} while they are large enough to maintain high plasma levels for optimal (tumor) distribution⁴⁰⁻⁴³. Although smaller vehicles like nanobodies or peptides may result in even better pharmacokinetic properties (e.g. faster clearance), they can have lower stability and affinity (for example, linear peptides vs. scFv fragments), and are more compromised by conjugation compared with antibodies or antibody fragments. EPCAM-F800 is being produced for clinical use and experiments were therefore performed with a clinically validated imaging system and an already clinically tested NIR fluorescent dye, in order to expedite clinical translation. The antibody fragment we specifically developed is a Fab fragment of its full antibody variant, 4D5 MOC-B⁴⁴. It is deimmunized, to tackle potential immunogenicity. A non-deimmunized variant was already used in a first-in-human clinical trial, where it was fused with a deimmunized variant of the plant-derived toxin bouganin²⁷. Deimmunization is important because it lowers the chance of an immune response. Hence, it allows

repeated use in patients undergoing multiple surgeries or participating in tumor screening programs. Conjugation with the dye was performed using the generally accepted NHS-method, with conditions leading to stable dye/protein-labeling ratios of around 1.5. Preclinical studies showed that IRDYE800CW is not immunogenic with a no adverse effect level (NOAEL) of 20 mg/kg²⁵. The advantage of IRDYE800CW with respect to other NIR fluorescent dyes is its water-solubility in combination with high signal intensity. Water-solubility enables conjugation in water-based solutions, which simplifies the purification process substantially and simplifies production under current Good Manufacturing Practices (cGMP) conditions.

The limited effect of the enhanced permeability and retention (EPR) effect was shown in the *in vivo* blocking experiment, where a 3-4 times lower TBR was measured after pre-injection with the unlabeled agent. The stagnating TBRs in the higher dose groups (5-20 nmol) clearly show the concentration at which saturation of available EPCAM binding places occurred. The optimal dose range of EPCAM-F800 for fluorescence tumor detection, i.e. 1-5 nmol in mice (52-260 µg), corresponds with a dose of 0.16-0.8 mg/kg in humans, adjusted for body surface area⁴⁵.

Biodistribution showed a classical Fab distribution pattern with high TBRs and high signals in the tumor and excreting organs. Due to the glomerular-filtration cut-off of 60 kDa, most of the agent is excreted via the kidneys. The observed high fluorescence signals in the liver may be explained by the lipophilicity and negative charge of IRDYE800CW, which leads to increased albumin binding and adjacent liver accumulation. This is underscored by the fact that no significant liver uptake could be measured with ¹¹¹In-EPCAM-F-DOTA⁴⁶. One should bear in mind that certain factors influence fluorescence intensity during biodistribution studies, such as absorbance of photons by adjacent tissue and scattering properties.

The half-life time of EPCAM-F800 in mice was estimated at 4.5 h, which is in concordance with VB6-845 in humans²⁷. Although the total circulation time of EPCAM-F800 is relatively short (10-20 h), it is sufficient to allow adequate tumor penetration; homogeneous signals throughout the tumor were seen at 4 h post injection.

Two clinically relevant orthotopic mouse models were investigated using the Artemis imaging system. In this set-up real-time tumor-specific visualization of colorectal and breast tumors was shown with high TBRs between 8 and 24 h. Besides these tumor types, application of EPCAM-F800 may aid detection of multiple other epithelial-derived cancers due to overexpression of EPCAM. Prior to the clinical introduction of EPCAM-F800, toxicology studies need to be performed. Our preliminary data of a generic single extended dose toxicology study in rats show no test item-related mortality, clinical signs and effects on body weight, food consumption,

clinical pathology and organ weight after injection of approximately 50 and 100 times the intended human dose of EPCAM-F800. Following the promising preclinical and toxicology results, EPCAM-F800 first-in-human studies can be designed as first step towards clinical translation. After successful first-in-human studies, a possible additional study design might be to detect tumor growth during fluorescence endoscopy in patients previously treated with neoadjuvant CRT. Suitable patients can be straightforwardly selected preoperatively with immunohistochemistry on biopsy specimens using either MOC31 or the Fab fragment.

In conclusion, we demonstrate the successful development, evaluation and feasibility of EPCAM-F800 for intra-operative tumor detection using fluorescence imaging. Although only breast and colorectal tumor models were described, application of EPCAM-F800 is expected to provide surgeons with a highly sensitive imaging tool to improve intraoperative visualization of multiple tumor types. Wide implementation of tumor-specific (NIR) fluorescence imaging has the potential to make surgery safer and more precise.

REFERENCES

- Mois E, Graur F, Hajar NA et al. The influence of circumferential resection margins on survival following rectal cancer surgery. *Ann Ital Chir* 2017; 88.
- Swindle P, Eastham JA, Ohoi M et al. Do margins matter? The prognostic significance of positive surgical margins in radical prostatectomy specimens. *J Urol* 2008; 179: s47-51.
- Haque R, Contreras R, McNicoll MP et al. Surgical margins and survival after head and neck cancer surgery. *BMC Ear Nose Throat Disord* 2006; 6: 2.
- Singletary SE. Surgical margins in patients with early-stage breast cancer treated with breast conservation therapy. *Am J Surg* 2002; 184: 383-393.
- van de Velde CJ, Boelens PG, Borras JM et al. EURECCA colorectal: multidisciplinary management: European consensus conference colon & rectum. *Eur J Cancer* 2014; 50: 1 e1-1 e34.
- Vahrmeijer AL, Hutteman M, van der Vorst JR et al. Image-guided cancer surgery using near-infrared fluorescence. *Nat. Rev. Clin. Oncol* 2013; 10: 507-518.
- van Dam GM, Themelis G, Crane LM et al. Intraoperative tumor-specific fluorescence imaging in ovarian cancer by folate receptor- α targeting: first in-human results. *Nat. Med* 2011; 17: 1315-1319.
- Hoogstins CE, Tummers QR, Gaarenstroom KN et al. A Novel Tumor-Specific Agent for Intraoperative Near-Infrared Fluorescence Imaging: A Translational Study in Healthy Volunteers and Patients with Ovarian Cancer. *Clin Cancer Res* 2016; 22: 2929-2938.
- Lamberts LE, Koch M, de Jong JS et al. Tumor-Specific Uptake of Fluorescent BevacizumAb-IRDYE800CW Microdosing in Patients with Primary Breast Cancer: A Phase 1 Feasibility Study. *Clin Cancer Res* 2017; 23: 2730-2741.
- Rosenthal EL, Warram JM, de Boer E et al. Safety and Tumor Specificity of CetuximAb-IRDYE800 for Surgical Navigation in Head and Neck Cancer. *Clin Cancer Res* 2015; 21: 3658-3666.
- Boogerd LSF, Hoogstins CES, Schaap DP et al. Safety and effectiveness of SGM-101, a fluorescent antibody targeting carcinoembryonic antigen, for intraoperative detection of colorectal cancer: a dose-escalation pilot study. *Lancet Gastroenterol Hepatol*. 2018 Mar; 3(3):181-191
- van Oosten M, Crane LM, Bart J et al. Selecting Potential Targetable Biomarkers for Imaging Purposes in Colorectal Cancer Using Target Selection Criteria (TASC): A Novel Target Identification Tool. *Transl Oncol* 2011; 4: 71-82.
- Herlyn M, Steplewski Z, Herlyn D, Koprowski H. Colorectal carcinoma-specific antigen: detection by means of monoclonal antibodies. *Proc Natl Acad Sci USA* 1979; 76: 1438-1442.
- Patriarca C, Macchi RM, Marschner AK, Mellstedt H. Epithelial cell adhesion molecule expression (CD326) in cancer: a short review. *Cancer Treat. Rev* 2012; 38: 68-75.
- Balzar M, Winter MJ, de Boer CJ, Litvinov SV. The biology of the 17-1a antigen (EP-CAM). *J. Mol. Med. (Berl)* 1999; 77: 699-712.
- Winter MJ, Nagtegaal ID, van Krieken JH, Litvinov SV. The epithelial cell adhesion molecule (EP-CAM) as a morphoregulatory molecule is a tool in surgical pathology. *Am J Pathol* 2003; 163: 2139-2148.
- Trzpis M, McLaughlin PM, de Leij LM, Harmsen MC. Epithelial cell adhesion molecule: more than a carcinoma marker and adhesion molecule. *Am J Pathol* 2007; 171: 386-395.
- Went P, Vasei M, Bubendorf L et al. Frequent high-level expression of the immunotherapeutic target EP-CAM in colon, stomach, prostate and lung cancers. *Br. J. Cancer* 2006; 94: 128-135.
- Spizzo G, Fong D, Wurm M et al. EPCAM expression in primary tumour tissues and metastases: an immunohistochemical analysis. *J. Clin. Pathol* 2011; 64: 415-420.
- Osta WA, Chen Y, Mikhitarian K et al. EPCAM is overexpressed in breast cancer and is a potential target for breast cancer gene therapy. *Cancer Res* 2004; 64: 5818-5824.
- Riethmuller G, Schneider-Gadicke E, Schlimok G et al. Randomised trial of monoclonal antibody for adjuvant therapy of resected Duke's C colorectal carcinoma. German Cancer Aid 17-1A Study Group. *Lancet* 1994; 343: 1177-1183.
- Seimetz D, Lindhofer H, Bokemeyer C. Development and approval of the trifunctional antibody catumaxoab (anti-EPCAM x anti-CD3) as a targeted cancer immunotherapy. *Cancer Treat Rev* 2010; 36: 458-467.
- Gires O, Bauerle PA. EPCAM as a target in cancer therapy. *J Clin Oncol* 2010; 28: e239-240; author reply e241-232.
- Macdonald GC, Rasamoeliso M, Entwistle J et al. A phase 1 clinical study of VB4-845: weekly intratumoral administration of an anti-EPCAM recombinant fusion protein in patients with squamous cell carcinoma of the head and neck. *Drug Des Devel. Ther* 2009; 2: 105-114.
- Marshall MV, Draney D, Sevick-Muraca EM, Olive DM. Single-dose intravenous toxicity study of IRDYE 800CW in Sprague-Dawley rats. *Mol. Imaging Biol* 2010; 12: 583-594.
- Zinn KR, Korb M, Samuel S et al. IND-directed safety and biodistribution study of intravenously injected cetuximab-IRDYE800 in cynomolgus macaques. *Mol. Imaging Biol* 2015; 17: 49-57.
- Entwistle J, Brown JG, Chooniedass S et al. Preclinical evaluation of VB6-845: an anti-EPCAM immunotoxin with reduced immunogenic potential. *Cancer Biother. Radiopharm* 2012; 27: 582-592.
- Boonstra MC, Tolner B, Schaafsma BE et al. Pre-clinical evaluation of a novel CEA-targeting near-infrared fluorescent tracer delineating colorectal and pancreatic tumors. *Int J Cancer*. 2015 Oct 15; 137(8):1910-20.
- Handgraaf HJM, Boonstra MC, Prevo0 H et al. Real-time near-infrared fluorescence imaging using CRGD-zw800-1 for intraoperative visualization of multiple cancer types. *Oncotarget* 2017; 8: 21054-21066.

- 30 Boonstra MC, Van Driel PB, van Willigen DM et al. UPAR-targeted multimodal tracer for pre- and intraoperative imaging in cancer surgery. *Oncotarget* 2015; Jun 10;6(16):14260-73.
- 31 Cheever MA, Allison JP, Ferris AS et al. The prioritization of cancer antigens: a national cancer institute pilot project for the acceleration of translational research. *Clin Cancer Res* 2009; 15: 5323-5337.
- 32 Munz M, Murr A, Kvesic M et al. Side-by-side analysis of five clinically tested anti-EPCAM monoclonal antibodies. *Cancer Cell Int* 2010; 10: 44.
- 33 Meijs WE, Haisma HJ, Klok RP et al. Zirconium-labeled monoclonal antibodies and their distribution in tumor-bearing nude mice. *J Nucl Med* 1997; 38: 112-118.
- 34 van Driel PB, Boonstra MC, Prevo HA et al. EPCAM as multi-tumour target for near-infrared fluorescence guided surgery. *BMC Cancer* 2016; 16: 884.
- 35 Zhu B, Wu G, Robinson H et al. Tumor margin detection using quantitative NIRF molecular imaging targeting EPCAM validated by far red gene reporter IRFP. *Mol. Imaging Biol* 2013; 15: 560-568.
- 36 Wittrup KD, Thurber GM, Schmidt MM, Rhoden JJ. Practical theoretic guidance for the design of tumor-targeting agents. *Methods Enzymol* 2012; 503: 255-268.
- 37 Freise AC, Wu AM. In vivo imaging with antibodies and engineered fragments. *Mol. Immunol* 2015 OCT;67(2 Pt A):142-52.
- 38 Gratz S, Reize P, Kemke B et al. Targeting of osteomyelitis with IgG and Fab' Monoclonal Antibodies Labeled with 99mTc: kinetic evaluations. *Q. J. Nucl. Med. Mol. Imaging* 2016 Dec;60(4):413-23.
- 39 Kosaka N, Ogawa M, Paik DS et al. Semiquantitative assessment of the microdistribution of fluorescence-labeled monoclonal antibody in small peritoneal disseminations of ovarian cancer. *Cancer Sci* 2010; 101: 820-825.
- 40 Pak KY, Nedelman MA, Fogler WE et al. Evaluation of the 323/A3 monoclonal antibody and the use of technetium-99m-labeled 323/A3 Fab' for the detection of pan adenocarcinoma. *Int. J. Rad. Appl. Instrum. B* 1991; 18: 483-497.
- 41 Watanabe R, Hanaoka H, Sato K et al. Photoimmunotherapy targeting prostate-specific membrane antigen: are antibody fragments as effective as antibodies? *J. Nucl. Med* 2015; 56: 140-144.
- 42 Mendler CT, Friedrich L, Laitinen I et al. High contrast tumor imaging with radio-labeled antibody Fab fragments tailored for optimized pharmacokinetics via Pasylation. *MAbs* 2015; 7: 96-109.
- 43 Li D, Liu S, Liu R et al. EphB4-targeted imaging with antibody h131, h131-F(ab')2 and h131-Fab. *Mol. Pharm* 2013; 10: 4527-4533.
- 44 Willuda J, Honegger A, Waibel R et al. High thermal stability is essential for tumor targeting of antibody fragments: engineering of a humanized anti-epithelial glycoprotein-2 (epithelial cell adhesion molecule) single-chain Fv fragment. *Cancer Res* 1999; 59: 5758-5767.
- 45 Reagan-Shaw S, Nihal M, Ahmad N. Dose translation from animal to human studies revisited. *FASEB J* 2008; 22: 659-661.
- 46 Valko K, Nunhuck S, Bevan C et al. Fast gradient HPLC method to determine compounds binding to human serum albumin. Relationships with octanol/water and immobilized artificial membrane lipophilicity. *J. Pharm. Sci* 2003; 92: 2236-2248.

Figure 1

- A Example of EPCAM expression on normal rectal tissue; EPCAM expression is confined to the luminal side of the epithelium.
- B Example of EPCAM expression on a distal rectal cancer of a patient who was not treated with neoadjuvant therapy.
- C EPCAM expression on the corresponding normal rectal tissue of the same patient.
- D EPCAM expression on a proximal rectal cancer of a patient who has been treated with neoadjuvant therapy.
- E EPCAM expression on the corresponding normal rectal tissue of the same patient. (5x and 40x enlargements).

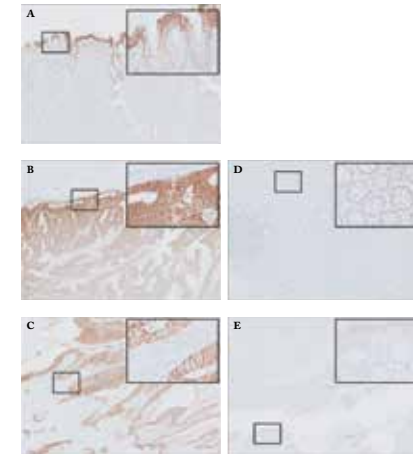


Figure 2

- A Binding capacity of FAB for EPCAM using flow-cytometry. As positive control, the anti-human EPCAM monoclonal antibody MOC31 was used confirming the high and low expression levels of EPCAM on the tumor cells. Enhancing the concentration of Fab resulted in an increase in signal on the cells with high EPCAM expression.
- B Conjugation was evaluated using SDS-PAGE gel (4-20%). Unconjugated FAB in lane 1 (10µg) and lane 2 (1µg) and EPCAM-F800 in lane 4 (10 µg), lane 5 (5 µg), lane 6 (5 µg) and lane 7 (5 µg) while lane 3 and lane 8 are empty. EPCAM-F800 was clearly visible at approximately 45kDa both with silver staining and fluorescence.
- C I, MALDI-TOF analysis of FAB showed one clear peak at 46870 DA with a purity of >98%. II, extra peaks appeared at 47816DA (1), 48795DA (2), 49820DA (3) and 50761DA (4) representing respectively 1, 2, 3 and 4 IRDYE800CW labels per FAB.
- D Plate assay analysis showed retained binding capacity of EPCAM-F800 on all four cell lines after conjugation. Increasing the concentration increased the fluorescent intensity for the high expressing cell lines.

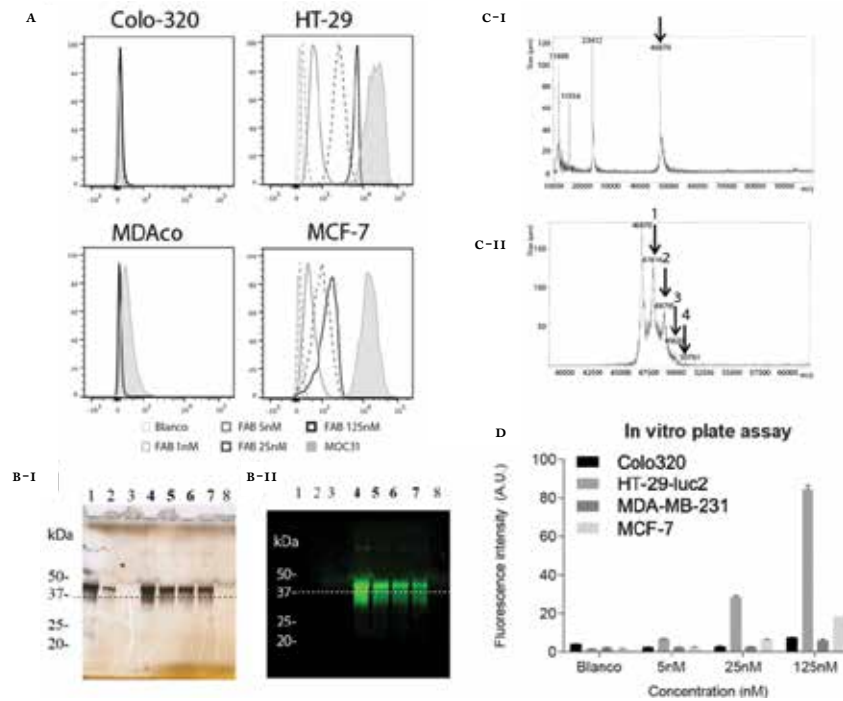


Figure 3

- A Biodistribution of EPCAM-MAB800 and EPCAM-F800 presented as organ-to-tumor ratio at 24 h post injection of 1 nmol. High fluorescence was seen in metabolizing organs and in the urine. Intensity of the fluorescence signal in the liver was significantly higher after injection of EPCAM-MAB800 compared to EPCAM-F800. Higher fluorescence signals in the kidneys after injection of EPCAM-F800 are most probably the result of renal clearance of the FAB fragment. (* = p<0.05).
- B Biodistribution of EPCAM-MAB800 and EPCAM-F800 presented as organ-to-tumor ratio at 72 h post injection of 1 nmol. All organs showed higher fluorescence signals after injection of EPCAM-MAB800 compared to EPCAM-F800. Fluorescence in the liver was significantly higher compared to EPCAM-F800.
- C Significant higher TBRS were measured for EPCAM-F800 both at 24 h and 72 h post injection compared to EPCAM-MAB800. The fluorescence signal measured at the back of the mice, between tumors, was considered as background signal.
- D Biodistribution of ¹¹¹In-EPCAM-F-DOTA shown as %ID/GRAM at 24 h and 72 h post injection.

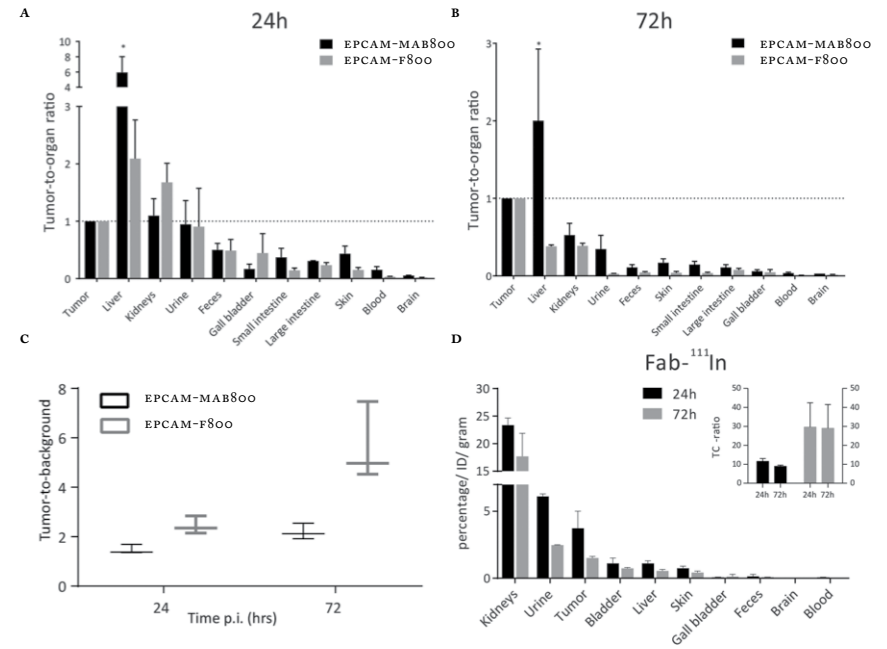


Figure 4

- A Blocking with unlabeled FAB fragments significantly ($p < 0.05$) decreased the tumor-to-background ratios at both the 24 h (6.81 ± 1.65 vs. 2.34 ± 0.42) and 72h (10.01 ± 3.544 vs. 2.96 ± 0.638) time-point.
- B Tumor-to-background ratios (TBR) are shown over time for the 1/16 to 5 nmol dose groups.
- C Pharmacokinetic results, displayed in a logarithmic scale. A mean blood half-life time of 4.5 h was measured.
- D Examples of *in vivo* images of mice bearing subcutaneous tumors acquired at 24 and 72h post injection with EPCAM-MAB800 or different doses of EPCAM-F800. The white regions of interest are used as background to calculate TBRs. All images are normalized and acquired with the Artemis imaging system. (# tumors of different sizes).

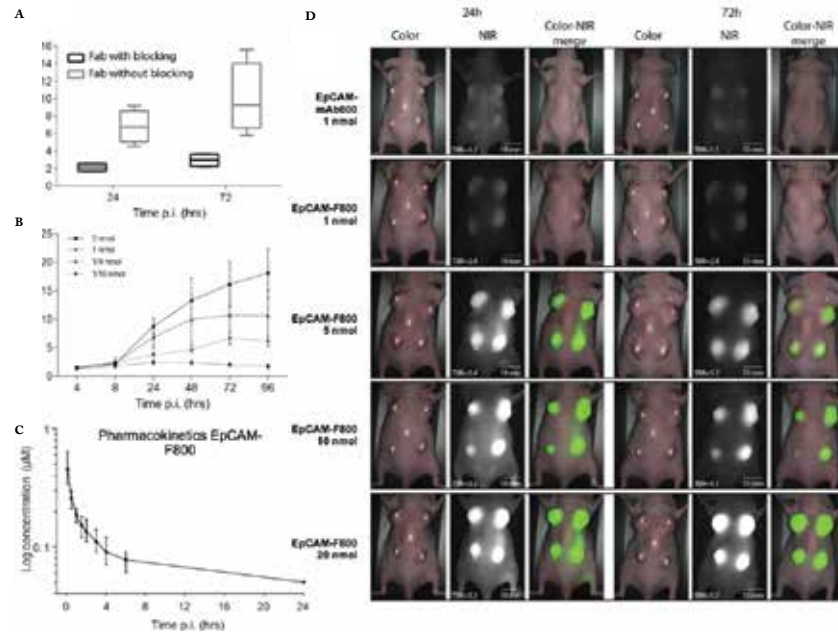


Figure 5

- A Tumor-to-background ratios and absolute signals of EPCAM-F800 in the orthotopic MCF-7 model over time.
- B Examples of images acquired with the Artemis imaging system at 24 and 72 h. In white, the background regions are shown used to calculate TBRs.
- C TBRs at 24 and 72 h and mean absolute signals at these time-points of 0.51 ± 0.08 and 0.12 ± 0.02 at 24 h post injection (shown as 100%) for respectively the tumor and the background, and 0.28 ± 0.07 and 0.04 ± 0.01 at the 72 h time point are shown.
- D Examples of images taken with the Artemis imaging system and BLI showing the co-localization of the fluorescent lesions with the colorectal tumors (Organs were slightly altered between fluorescent and BLI measurements). The background regions used to calculate TBRs are indicated by white stars (# tumors of different sizes).

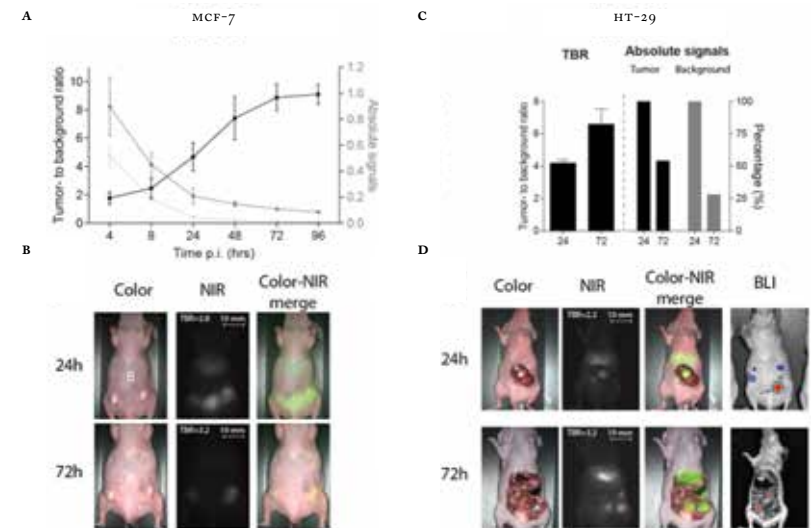
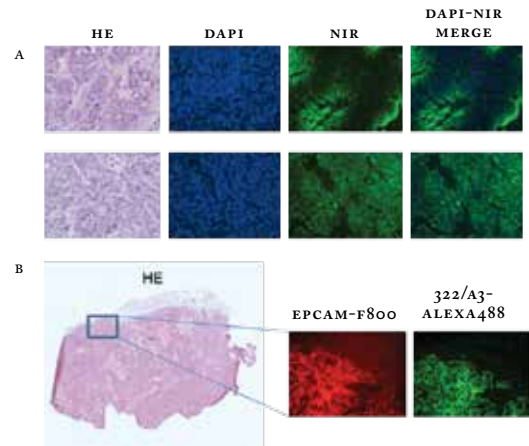


Figure 6

- A Fluorescence histology of HT29-tumors, obtained 1 and 4 h after injection of 10 nmol EPCAM-F800. Shown are respectively HE staining, DAPI staining, fluorescence microscopy images and overlay images (DAPI and fluorescence) of representative tumor slices 1 and 4 h after injection of EPCAM-F800. After 1 h, tumor penetration of EPCAM-F800 is limited to the tumor borders, while fluorescence is seen throughout the complete tumor after 4 h.
- B Fluorescence histology of a HT-29 tumor, harvested from a mouse injected with 5 nmol EPCAM-F800, shows co-localization of EPCAM-F800 and 323/A3-ALEXA488.



CHAPTER 7

CORRELATION BETWEEN PREOPERATIVE SERUM CARCINOEMBRYONIC ANTIGEN LEVELS AND EXPRESSION ON PANCREATIC AND RECTAL CANCER TISSUE

Biomark Cancer. 2017 May 7;9:1179299

LSF BOOGERD, F VUIJK, CES HOOGSTINS, HJM HANDGRAAF,
MJM VAN DER VALK, CJH VAN DE VELDE, J BURGGRAAF,
A FARIÑA-SARASQUETA AND AL VARHMEIJER

ABSTRACT

Carcinoembryonic antigen (CEA)-targeted imaging and therapeutic agents are being tested in clinical trials. If CEA overexpression in malignant tissue corresponds with elevated serum CEA, serum CEA could assist in selecting patients who may benefit from CEA-targeted agents. This study aims to assess the relationship between serum CEA and CEA expression in pancreatic (N=20) and rectal cancer tissues (N=35) using histopathology. According to local laboratory standards, a serum CEA >3ng/mL was considered elevated. In pancreatic cancer patients a significant correlation between serum CEA and percentage of CEA-expressing tumor cells was observed ($p=0.04$, $\rho=0.47$). All 6 patients with homogeneous CEA expression in the tumor had a serum CEA >3ng/mL. Most rectal cancer tissues (32/35) showed homogeneous CEA expression, independent of serum CEA levels. This study suggests that selection of pancreatic cancer patients for CEA-targeted agents via serum CEA appears adequate. For selection of rectal cancer patients, serum CEA levels are not informative.

INTRODUCTION

Carcinoembryonic antigen (CEA) is a glycoprotein produced by gastrointestinal tissue under control of the cell adhesion molecule 5 (CEACAM5) gene¹. CEA is anchored on the cell membrane via glycosylphosphatidylinositol (GPI), which makes it vulnerable for shedding into the lumen, where it is cleared via the faeces. In many cancer types, including pancreatic ductal adenocarcinoma (PDAC) and (colo)rectal cancer (CRC), CEA is found to be overexpressed, playing a role in cell recognition, adhesion, angiogenesis and tumor suppression²⁻⁴. A substantial part of CEA, shedded from tumor cells, derives into the bloodstream and enhanced serum CEA is therefore used as sensitive biomarker indicating growth or recurrence of CRC⁵.

Since the recognition of serum CEA as a valuable cancer biomarker, multiple CEA-targeted agents have been developed. Therapeutic antibodies directed towards CEA-overexpressing tumors are currently tested in various phase I-III trials^{6,7}, but also anti-CEA based radioimmunotherapy and CEA-targeted vaccins are investigated^{8,9}. In addition to the rapidly expanding field of CEA-targeted anticancer therapeutics, several imaging agents have become available for clinical testing. These agents can be labelled with radioisotopes for PET or SPECT imaging^{10,11}, with near-infrared (NIR) fluorescent dyes^{12,13}, or they can provide both molecular imaging and targeted therapy of CEA-expressing tumors¹⁴.

Especially in early phase clinical trials investigating CEA-targeted tumor imaging, it would be beneficial to identify patients with homogeneous CEA overexpression in the tumor prior to inclusion. For example, patient selection is pivotal in the recently initiated phase I study (Netherlands Trial Register ID: 5673) assessing the safety and feasibility of SGM-101, a monoclonal CEA-targeted antibody conjugated to a NIR fluorescent dye, utilized for intraoperative detection of PDAC and CRC. Selecting eligible PDAC and rectal patients for CEA-targeted applications might be feasible using serum CEA levels. Since CEA expression on normal epithelium is confined to the apical surface of polarized cells², it can be hypothesized that CEA in serum of cancer patients originates mostly from shedding by CEA-overexpressing malignant cells that lose their polarity. The aim of the current study was to investigate if elevated serum CEA levels can predict overexpression of CEA on pancreatic and rectal cancer tissue.

METHODS

This study was approved by the Institutional Ethics Committee of the Leiden University Medical Center (LUMC) and performed following the Code for Proper Secondary Use of Human Tissue, Dutch Federation of Medical Scientific Society.

Tissue samples of twenty patients with PDAC and thirty-five patients with rectal adenocarcinoma, undergoing surgery at the LUMC between 2013 and 2016, were retrospectively collected. Patients were selected on availability of preoperative serum CEA values. Based on hematoxylin-eosin-stained (HE) slides, a single representative tumor containing formalin-fixed paraffin-embedded (FFPE) tissue block from each patient was chosen by a board certified pathologist (A.F.S.). Serum CEA was measured using routine methodology (Elecsys, Roche Diagnostics) and according to local laboratory standards, serum CEA levels $>3\text{ng/mL}$ were considered elevated.

IMMUNOHISTOCHEMISTRY ••• Immunohistochemical staining for CEA was performed on FFPE tissue. Tissue samples were stained using a monoclonal mouse antibody against CEACAM5 (clone number C1-P83-1, Santa Cruz Biotechnology). Validation of the staining protocol was performed by using human colon cancer tissue as a positive control. Sections (thickness $4\ \mu\text{m}$) were cut from paraffin blocks and mounted on adhesive slides (Starfrost). Slides were deparaffinized using xylene and rehydrated in decreasing concentrations of ethanol. Subsequently, slides were rinsed with distilled water and endogenous peroxidase activity was blocked with 0.3% hydrogen peroxide (Merck Millipore) for 20 minutes. Slides were rinsed in distilled water and antigen retrieval was performed in DAKO PT LINK with target retrieval solution pH 6.0 at 95°C for 10 minutes. After rinsing with phosphate buffered saline (PBS) the primary antibody was incubated overnight at room temperature and afterwards rinsed with PBS. Incubation of the secondary antibody (Envision anti-mouse HRP (DAKO)) was performed for 30 minutes at room temperature, followed by rinsing with PBS. Antibody binding was then visualized using 3,3'-diaminobenzidine (DAB, DAKO). Sections were counterstained with hematoxylin (Klinipath), rinsed in tap water, dehydrated and mounted with pertex. All slides were scanned using the Philips Ultra Fast Scanner 1.6 RA.

SCORING SYSTEM ••• CEA expression in cancer tissue was determined by immunohistochemical staining (brown) and scored for staining intensity (0: none, 1: weak, 2: moderate, 3: strong) and the fraction of positive tumor cells (1: $<10\%$, 2: $10\text{--}50\%$, 3: $50\text{--}80\%$, 4 $>80\%$). Homogeneity was defined when $>80\%$ of tumor cells stained positive for CEA (=score 4). All tissue specimens were scored by two independent observers (A.F.S. and L.B.); disagreements were resolved by consensus after reviewing the relevant slides.

STATISTICAL ANALYSIS ••• Statistical analysis was performed using SPSS version 23.0 software (SPSS, ©IBM Corporation). The concordance of serum CEA and CEA expression on tumor tissue and of pathological T (PT) stage and serum CEA was assessed using Spearman's test, defined as the correlation coefficient. The correlation between groups, based on an elevated or normal level of serum CEA and between smokers and non-smokers, was calculated using the Mann Whitney U test. A χ^2 test was used to compare homogeneity in PDAC tissues. In all tests, results were considered statistically significant at the level of $p < 0.05$.

RESULTS

PATIENT AND TUMOR CHARACTERISTICS ••• Patient and tumor characteristics are summarized in Table 1. In the pancreatic cancer cohort, 3 patients participated in the PREOPANC study protocol; 2 of them received preoperative chemoradiotherapy (CRT)¹⁵. In the rectal cancer cohort, 8 patients participated in the RAPIDO study protocol¹⁶. All serum CEA measurements were performed prior to the start of CRT. Median preoperative serum CEA of smoking PDAC patients was 3.8 (range 1.2–6.9), compared to 3.7 (range 0.6–23.8) for non-smokers ($p=0.50$). For rectal cancer patients, median preoperative serum CEA of smoking patients was 2.9 (range 1.0–16.9), compared to 2.7 for non-smokers (range 1.3–9.9; $p=0.68$). No significant correlation was found between PT stage and preoperative serum CEA ($p=0.61$, $\rho=0.09$ for PDAC patients, $p=0.95$, $\rho=0.02$ for rectal cancer patients).

CEA EXPRESSION AND CORRELATION TO SERUM CEA LEVEL

PDAC COHORT ••• The majority of tumors showed a heterogenous CEA expression pattern, whereas only 6/20 tumors showed homogeneous CEA expression ($>80\%$). CEA expression was mostly seen on the luminal surface of neoplastic glands and necrotic tissue; low levels of immunoreactivity were seen in the stromal tissue, while normal acini did not express CEA (Figure 1). A significant correlation was found between preoperative serum CEA levels and percentage of CEA-expressing tumor cells ($p=0.04$, $\rho=0.47$). This could not be shown for intensity of the staining ($p=0.21$, $\rho=0.29$). 15/20 tissues showed $>50\%$ CEA-expressing tumor cells and 16/20 tissues showed a high intensity of CEA expression (Table 2). When dividing the patients in groups of normal ($n=6$) and elevated serum CEA ($n=14$), no significant correlation between groups and percentage and intensity of stained tumor cells was found ($p=0.15$, $p=0.34$ respectively). However, all patients with tumors showing homogeneous CEA expression ($n=6$) had elevated serum CEA levels ($\chi^2=5.06$, $p=0.025$).

RECTAL CANCER COHORT ••• Almost all tumors (32/35, 91%) showed homogeneous CEA expression. CEA expression was found on luminal sides of malignant cells and in the majority of tumors, circumferential CEA staining was shown. Normal epithelium showed low levels of CEA immunostaining, which was far less than the CEA expression in cancer cells (Figure 2). No significant correlation was found between preoperative serum CEA and percentage and intensity of CEA-expressing tumor cells ($p=0.58$, $\rho=0.10$ and $p=0.17$, $\rho=0.24$ respectively). When dividing patients in groups of normal ($n=20$) and elevated serum CEA ($n=15$), again no significant correlation between groups and the percentage and intensity of CEA-expressing tumor cells was found (Table 2).

DISCUSSION

This study shows a significant correlation between serum CEA and the percentage of CEA-expressing tumor cells in PDAC tissue. Moreover, serum CEA levels were elevated in all PDAC patients with homogeneous CEA expression in the tumor (>3 ng/mL, $\chi^2 = 5.06$, $p=0.025$). These results suggest therefore that especially patients with elevated serum CEA levels could benefit from CEA-targeted agents. Importantly, normal acini did not show any expression of CEA. Personalized oncological care, to ensure that cancer patients benefit from targeted imaging and therapeutics, is already performed for other targets. For example, HER2-targeted drugs (i.e. trastuzumab) are recommended when $>30\%$ of tumor cells show a complete, circumferential and intense membrane staining¹⁷.

PDAC patient selection is justified as not all tissues express CEA. In the current study, only 6/20 tissues showed homogeneous CEA expression and 15/20 tissues showed expression in $>50\%$ of neoplastic pancreatic cells. Previous studies reported CEA expression in approximately 60–75% of PDAC tissues^{3,18}. Serum CEA measurements were performed using the Elecsys CEA assay (Roche Diagnostics), which is previously described to be specific for CEACAM5 as well as for NCA-2, the nonspecific cross reacting antigen-2¹⁹. NCA-2 is a truncated form of CEACAM5 with identical amino acid sequence, and therefore CEACAM5 was used as immunohistochemical tissue marker in this study²⁰. Several other CEACAM molecules have been previously described, each with a slightly different function^{21,22}. Gebauer et al.³ investigated CEACAM1, CEACAM5 and CEACAM6 as suitable biomarkers for PDAC in a tissue micro array (TMA; $n=252$). No significant correlation between elevated serum levels, e.g. >4.7 ng/mL, and tissue expression of one of these CEACAM subtypes could be shown. Yet, a significant correlation between CEACAM5 and CEACAM6 tissue expression and decreased overall and disease-free survival was demonstrated. The partly

different results compared to this study might be attributable to varying cut-off values for defining elevated serum CEA or differences in the staining or scoring protocol. Importantly, no correlation between serum CEA and homogeneity of CEA expression in PDAC tissues could be studied in this TMA study. No strict threshold of CEA tissue expression to ensure optimal applicability of CEA-targeted imaging or therapeutic agents has yet been defined. However, patients with homogeneous CEA expression are expected to benefit most from those agents.

In contrast to PDAC patients, no significant correlation between serum CEA and CEA tissue expression was found in the rectal cancer cohort. A possible cause for this finding might be the difference in vasculature and permeability of the two tumor types. Rectal tumors are generally well-vascularized and show a relatively good response to chemo(radio)therapy²³. PDAC shows poor blood supply and high amounts of stroma, possibly explaining the disappointing response to chemotherapy and the low 5-year survival rates of less than 5%²⁴. It can be hypothesized that CEA derived from rectal tumors accesses the bloodstream easier than CEA from PDAC, leading to higher CEA serum levels. However, no significant correlation between preoperative serum CEA and PT stage of tumors was found in the current study. Previous reports have indicated that several other factors, including tumor necrosis, smoking, benign liver disease and the location of the CEA receptor on the cell membrane, could also affect serum CEA levels^{25,26}.

Park et al²⁷ showed that CEA serum concentrations were significantly higher in patients with CEA-positive tumors than CEA-negative tumors, but this correlation could not be reproduced in other studies^{28–30}. It is nowadays accepted that rectal and colon cancer should be categorized as two different types of malignancies and treated differently. The current study differs from others as only rectal cancer patients were included. Nearly all tissues showed an intense and homogeneous expression compared to low expression on normal epithelium, independently of the neoadjuvant therapy given nor the preoperative serum CEA level. Although a relatively low number of rectal cancer patients was included, serum CEA levels, assessed prior to the start of preoperative CRT, are concordant with literature³¹. Thus, all rectal cancer patients, independent of their serum CEA level, might benefit from CEA-targeted agents.

A limitation of this small, retrospective study is that different intervals elapsed between measurement of the CEA serum concentrations and resection. Over- or underrating serum CEA levels, as a consequence of the timing of CEA measurement, could have influenced the outcome of the study. Moreover, it is possible that selection bias has occurred because not all serum CEA levels were measured in all subsequent patients between 2013–2016. Both of these issues could be avoided by

designing a prospective study in which serum CEA is measured directly prior to surgery. In addition, the effect of neoadjuvant therapy on serum CEA level and CEA expression on rectal and pancreatic cancer tissue should be studied further.

In conclusion, a significant correlation between serum CEA levels and percentage of CEA-expressing tumor cells in PDAC tissue was shown. PDAC patients that might benefit from CEA-targeted imaging or therapeutic agents can adequately be selected using serum CEA levels (>3 ng/mL). This finding can be used in the process of personalized cancer care. Selection based on serum CEA levels seems not useful in rectal cancer patients, as almost all show an intense, homogeneous CEA expression.

REFERENCES

- Nap M, Mollgard K, Burtin P, Fleuren GJ. Immunohistochemistry of carcino-embryonic antigen in the embryo, fetus and adult. *Tumour Biol.* 1988;9(2-3):145-153.
- Hammarstrom S. The carcinoembryonic antigen (CEA) family: structures, suggested functions and expression in normal and malignant tissues. *Semin Cancer Biol.* 1999;9(2):67-81.
- Gebauer F, Wicklein D, Horst J, et al. Carcinoembryonic antigen-related cell adhesion molecules (CEACAM) 1, 5 and 6 as biomarkers in pancreatic cancer. *PLoS One.* 2014;9(11):e113023.
- Li M, Li JY, Zhao AL, et al. Comparison of carcinoembryonic antigen prognostic value in serum and tumour tissue of patients with colorectal cancer. *Colorectal Dis.* 2009;11(3):276-281.
- Locker GY, Hamilton S, Harris J, et al. ASCO 2006 update of recommendations for the use of tumor markers in gastrointestinal cancer. *J Clin Oncol.* 2006;24(33):5313-5327.
- Bacac M, Fauti T, Sam J, et al. A Novel Carcinoembryonic Antigen T-Cell Bispecific Antibody (CEA TCB) for the Treatment of Solid Tumors. *Clin Cancer Res.* 2016;22(13):3286-3297.
- Boonstra MC, de Geus SW, Prevo HA, et al. Selecting Targets for Tumor Imaging: An Overview of Cancer-Associated Membrane Proteins. *Biomark Cancer.* 2016;8:119-133.
- Sahlmann CO, Homayounfar K, Niessner M, et al. Repeated adjuvant anti-CEA radioimmunotherapy after resection of colorectal liver metastases: Safety, feasibility, and long-term efficacy results of a prospective phase 2 study. *Cancer.* 2017;123(4):638-649.
- Duggan MC, Jochems C, Donahue RN, et al. A phase 1 study of recombinant (r) vaccinia-CEA(6D)-TRICOM and rFowlpox-CEA(6D)-TRICOM vaccines with GM-CSF and IFN-alpha-2b in patients with CEA-expressing carcinomas. *Cancer Immunol Immunother.* 2016;65(11):1353-1364.
- Bodet-Milin C, Faivre-Chauvet A, Carlier T, et al. Immuno-PET Using Anticarcinoembryonic Antigen Bispecific Antibody and ^{68}Ga -Labeled Peptide in Metastatic Medullary Thyroid Carcinoma: Clinical Optimization of the Pretargeting Parameters in a First-in-Human Trial. *J Nucl Med.* 2016;57(10):1505-1511.
- Schoffelen R, van der Graaf WT, Sharkey RM, et al. Pretargeted immuno-PET of CEA-expressing intraperitoneal human colonic tumor xenografts: a new sensitive detection method. *EJNMMI Res.* 2012;2:5.
- Boonstra MC, Tolner B, Schaafsma BE, et al. Preclinical evaluation of a novel CEA-targeting near-infrared fluorescent tracer delineating colorectal and pancreatic tumors. *Int J Cancer.* 2015;137(8):1910-1920.
- Vahrmeijer AL, Hutteman M, van der Vorst JR, van de Velde CJ, Frangioni JV. Image-guided cancer surgery using near-infrared fluorescence. *Nat Rev Clin Oncol.* 2013;10(9):507-518.
- Knutson S, Raja E, Bomgardner R, et al. Development and Evaluation of a Fluorescent Antibody-Drug Conjugate for Molecular Imaging and Targeted Therapy of Pancreatic Cancer. *PLoS One.* 2016;11(6):e0157762.
- Versteijne E, van Eijck CH, Punt CJ, et al. Preoperative radIOP chemotherapy versus immediate surgery for resectable and borderline resectable pancreatic cancer (PREOPANC trial): study protocol for a multicentre randomized controlled trial. *Trials.* 2016;17(1):127.
- Nilsson PJ, van Etten B, Hospers GA, et al. Short-course radiotherapy followed by neo-adjuvant chemotherapy in locally advanced rectal cancer—the RAPIDO trial. *BMC Cancer.* 2013;13:279.
- Wolff AC, Hammond ME, Hicks DG, et al. Recommendations for human epidermal growth factor receptor 2 testing in breast cancer: American Society of Clinical Oncology/College of American Pathologists clinical practice guideline update. *Arch Pathol Lab Med.* 2014;138(2):241-256.
- de Geus SW, Boogerd LS, Swijnenburg RJ, et al. Selecting Tumor-Specific Molecular Targets in Pancreatic Adenocarcinoma: Paving the Way for Image-Guided Pancreatic Surgery. *Mol Imaging Biol.* 2016;18(6):807-819.
- Hanada H, Mugii S, Takeoka K, et al. Early detection of colorectal cancer metastasis and relapse by recognizing nonspecific cross-reacting antigen 2 in commercial carcinoembryonic antigen assays. *Clin Chem.* 2009;55(9):1747-1748.
- Schee K, Flatmark K, Holm R, Boye K, Paus E. Investigation of nonspecific cross-reacting antigen 2 as a prognostic biomarker in bone marrow plasma from colorectal cancer patients. *Tumour Biol.* 2012;33(1):73-83.
- Simeone DM, Ji B, Banerjee M, et al. CEACAM1, a novel serum biomarker for pancreatic cancer. *Pancreas.* 2007;34(4):436-443.
- Kuespert K, Pils S, Hauck CR. CEACAMs: their role in physiology and pathophysiology. *Curr Opin Cell Biol.* 2006;18(5):565-571.
- Renehan AG, Malcomson L, Emsley R, et al. Watch-and-wait approach versus surgical resection after chemoradiotherapy for patients with rectal cancer (the OnCoRe project): a propensity-score matched cohort analysis. *Lancet Oncol.* 2016;17(2):174-183.
- Ilic M, Ilic I. Epidemiology of pancreatic cancer. *World J Gastroenterol.* 2016;22(44):9694-9705.
- Wagener C, Muller-Wallraf R, Nisson S, Groner J, Breuer H. Localization and concentration of carcinoembryonic antigen (CEA) in gastrointestinal tumors: correlation with CEA levels in plasma. *J Natl Cancer Inst.* 1985;67(3):539-547.
- Hamada Y, Yamamura M, Hioki K, Yamamoto M, Nagura H, Watanabe K. Immunohistochemical study of carcinoembryonic antigen in patients with colorectal cancer. Correlation with plasma carcinoembryonic antigen levels. *Cancer.* 1985;55(1):136-141.

- 27 Park JW, Chang HJ, Kim BC, Yeo HY, Kim DY. Clinical validity of tissue carcinoembryonic antigen expression as ancillary to serum carcinoembryonic antigen concentration in patients curatively resected for colorectal cancer. *Colorectal Dis.* 2013;15(9):e503-511.
- 28 Cosimelli M, De Peppo F, Castelli M, et al. Multivariate analysis of a tissue CEA, TPA, and CA 19.9 quantitative study in colorectal cancer patients. A preliminary finding. *Dis Colon Rectum.* 1989;32(5):389-397.
- 29 Nakagoe T, Sawai T, Ayabe H, et al. Prognostic value of carcinoembryonic antigen (CEA) in tumor tissue of patients with colorectal cancer. *Anticancer Res.* 2001;21(4B):3031-3036.
- 30 Nazato DM, Matos LL, Waisberg DR, Souza JR, Martins LC, Waisberg J. Prognostic value of carcinoembryonic antigen distribution in tumor tissue of colorectal carcinoma. *Arq Gastroenterol.* 2009;46(1):26-31.
- 31 Probst CP, Becerra AZ, Aquina CT, et al. Watch and Wait? Elevated Pretreatment CEA Is Associated with Decreased Pathological Complete Response in Rectal Cancer. *J Gastrointest Surg.* 2016;20(1):43-52.

Figure 1 Representative example of HE and CEA staining of pancreatic cancer tissue

CEA expression of tumor (T) tissue compared to adjacent normal (N) pancreatic tissue, derived from a patient with a preoperative serum CEA level <3ng/mL (A) and >3ng/mL (B; magnification 1x and 10x). The magnified image in A shows moderate CEA expression on the luminal side of neoplastic glands, while tumor tissue in image B shows an intense, circumferential CEA expression. The adjacent normal acini do not stain positive.

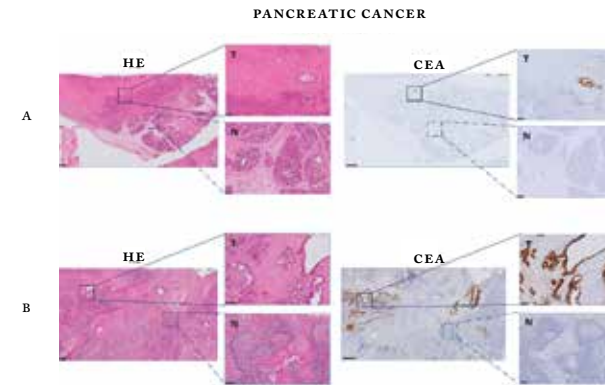


Figure 2 Representative example of HE and CEA staining of rectal cancer tissue

CEA expression of tumor tissue (T) compared to adjacent normal (N) rectal tissue, derived from a patient with a preoperative serum CEA level <3ng/mL (A) and >3ng/mL (B; magnification 1x and 10x). Both tumor tissues (A and B) show an intense, circumferential CEA expression, independent of the preoperative serum CEA level. Normal epithelium shows weak expression.

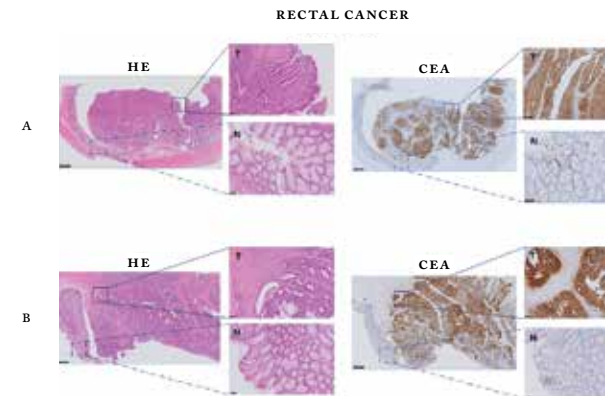


Table 1 Patient and tumor characteristics

		Pancreatic cancer	Rectal cancer
Included patients		n=20	n=35
Gender	Male	11 (55%)	22 (63%)
	Female	9 (45%)	13 (37%)
Age at diagnosis	Median age in years (range)	71 (51-86)	67 (42-78)
pT stage	1	2 (10%)	1 (3%)
	2	2 (10%)	13 (37%)
	3	7 (35%)	21 (60%)
	4	0 (0%)	0 (0%)
	Unknown	9 (45%)	0 (0%)
pN stage	0	8 (40%)	21 (60%)
	1	11 (55%)	13 (37%)
	2	1 (5%)	1 (3%)
pM stage	0	20 (100%)	35 (100%)
	1	0 (0%)	0 (0%)
	Angioinvasion	Yes	7 (35%)
	None	9 (45%)	27 (77%)
	Unknown	4 (20%)	8 (23%)
Neoadjuvant therapy	None	17 (85%)	18 (51%)
	PREOPANC study protocol	3 (15%)	n.a.
	Radiation therapy (25 x 2 Gray)	n.a.	7 (20%)
	RAPIDO study protocol	n.a.	8 (23%)
	Chemoradiation therapy	n.a.	2 (6%)
Smoking	Yes	7 (35%)	7 (20%)
	None	13 (65%)	11 (31%)
	Unknown	0 (0%)	17 (49%)
Tumor diameter (cm)	Median (range)	3 (0.9-6.1)	2.5 (1.2-6.0)
Differentiation grade	Well/moderate	3 (15%)	3 (9%)
	Moderate/poorly	14 (70%)	28 (80%)
	Unknown	3 (15%)	4 (11%)

p=pathological, n=number, CRT=chemo- and radiotherapy, n.a.=not applicable

Table 2 Percentage and intensity of stained tumor cells

Pancreatic cancer (N=20)	CEA serum level		
Percentage of stained tumor cells	<3ng/mL	>3ng/mL	Total
1 (<10%)	1	2	3
2 (10% - 50%)	1	1	2
3 (50% - 80%)	4	5	9
4 (>80%)	0	6	6
Intensity of staining			
0 (none)	0	0	0
1 (weak)	0	0	0
2 (moderate)	2	2	4
3 (strong)	4	12	16
Rectal cancer (N=35)	CEA serum levels		
Percentage of stained tumor cells	<3ng/mL	>3ng/mL	Total
1 (<10%)	0	0	0
2 (10% - 50%)	0	0	0
3 (50% - 80%)	1	1	2
4 (>80%)	19	14	33
Intensity of staining			
0 (none)	0	0	0
1 (weak)	0	0	0
2 (moderate)	2	1	3
3 (strong)	18	14	32

CRT = chemo- and radiotherapy; CEA = carcinoembryonic antigen; LN = lymph node; EPCAM = epithelial cell adhesion molecule; c-Met = tyrosine kinase protein Met

CHAPTER 8

BIOMARKER EXPRESSION IN RECTAL CANCER TISSUE BEFORE AND AFTER NEOADJUVANT THERAPY

Onco Targets Ther. 2018 Mar 23;11:1655-1664

LSF BOOGERD, MJM VAN DER VALK, MC BOONSTRA,
HAJM PREVOO, DE HILLING, CJH VAN DE VELDE, CFM SIER,
A FARIÑA-SARASQUETA AND AL VAHRMEIJER

ABSTRACT

PURPOSE ¶ Intraoperative identification of rectal cancer (RC) can be challenging, especially because of fibrosis after treatment with preoperative chemo- and radiotherapy (CRT). Tumor-targeted fluorescence imaging can enhance contrast between tumor and normal tissue during surgery. Promising targets for RC imaging are carcinoembryonic antigen (CEA), epithelial cell adhesion molecule (EPCAM) and the tyrosine-kinase receptor C-MET. The effect of CRT on their expression determines their applicability for imaging. Therefore, we investigated whether CRT modifies expression patterns in tumors, lymph nodes (LN) metastases and adjacent normal rectal tissues.

PROCEDURES ¶ Preoperative biopsies, primary tumor specimens and metastatic LNs were collected from 38 RC patients who did not receive CRT (cohort 1) and 34 patients who did (cohort 2). CEA, EPCAM and C-MET expression was determined using immunohistochemical staining and semi-quantified by a total immunostaining score, consisting of the percentage and intensity of stained tumor cells (TIS, range 0-12).

RESULTS ¶ In both cohorts CEA, EPCAM and C-MET were significantly higher expressed in more than 60% of tumor tissues compared with adjacent normal epithelium (T/N ratio, $p < 0.01$). EPCAM showed the most homogeneous expression in tumors, whereas CEA showed the highest T/N ratio. Most importantly, CEA and EPCAM expression did not significantly change in normal or neoplastic RC tissue after CRT, whereas C-MET levels changed ($p = 0.02$). Tissues of eight patients with a pathological complete response after CRT showed expression of all biomarkers with TIS close to normal epithelium.

CONCLUSION ¶ Histological evaluation shows that CEA, EPCAM and C-MET are suitable targets for RC imaging, because all three are significantly enhanced in cancer tissue from primary tumors or LN metastases compared with normal adjacent tissue. Furthermore, the expression of CEA and EPCAM is not significantly changed after CRT. These data underscore the applicability of C-MET and especially CEA, and EPCAM as targets for image-guided RC surgery, both before and after CRT.

INTRODUCTION

The cornerstone of rectal cancer (RC) treatment is surgical resection, performed via total mesorectal excision¹. Completeness of the surgical resection is pivotal for the prognosis of RC patients. A positive circumferential resection margin is associated with a high rate of local and distant recurrences, high morbidity and mortality^{2,3}. The introduction of neoadjuvant chemo- and radiotherapy (CRT) led to a significant decrease in the rate of irradical resections⁴. Still, a recent meta-analysis reported a positive resection margin rate of 14.7% after abdominoperineal excision and 27% after pelvic exenteration⁵, stressing the need for novel diagnostic imaging tools that can enhance contrast between cancer and adjacent normal/fibrotic tissue during surgery. An imaging modality that can fulfil this need is tumor-targeted fluorescence imaging⁶. This innovative technique can provide real-time intraoperative tumor visualization by selectively highlighting tumor cells.

Selection of tumor targets for imaging purposes depends on various characteristics including the expression pattern, localization of the biomarker in the cell and the tumor-to-normal (T/N) expression ratio^{7,8}. Prerequisite is a low or absent expression of a protein in normal tissue in combination with enhanced expression in cancer lesions. Promising targets for detection of RC are carcinoembryonic antigen (CEA), epithelial cell adhesion molecule (EPCAM) and the tyrosine-kinase receptor C-MET^{9,11}. The glycoprotein CEA is overexpressed in the vast majority of colorectal cancers (CRC) and has already been used for therapeutic and imaging purposes^{12,13}. Recently, an early phase clinical trial has been initiated utilizing a CEA-targeted fluorescent tracer for intraoperative detection of CRC (Netherlands Trial Register ID: 5673). EPCAM is a transmembrane glycoprotein, involved in cell-cell interactions and cell-stroma adhesion, and overexpressed in nearly all epithelial malignancies¹⁴. The recognition of EPCAM as one of the most promising, pluri-potent tumor markers has resulted in (pre)clinical testing of several EPCAM-targeted agents^{10,15,16}. First-in-human studies with an EPCAM-specific fluorescent agent to visualize various tumors during surgery are planned to start soon in our institution. C-MET, the receptor of hepatocyte growth factor (HGF), is involved in tumor cell proliferation and invasion, and its enhanced expression is associated with a poorer survival¹⁷. The upregulation of C-MET in (pre)malignant colorectal lesions supported the successful clinical testing of a C-MET targeted fluorescent peptide, i.e. GE-I37, for better endoscopic detection of colorectal adenomas^{11,18}.

Although several studies showed overexpression of CEA, EPCAM and C-MET in CRC tissues¹⁸⁻²⁰, the effect of CRT on protein expression is still unknown. This issue is however important for the reliable applicability of CEA-, EPCAM- and

C-MET-targeted fluorescent contrast agents for RC imaging, as the majority of RC patients receive neoadjuvant CRT. In addition, this knowledge can be utilized for application of CEA-, EPCAM or C-MET-targeted tracers for other imaging purposes, such as PET- or SPECT imaging. The aim of this study was to investigate whether CRT modifies expression of CEA, EPCAM and C-MET in RC tissues and in adjacent normal epithelium. Therefore we first studied the concordance in protein expression between diagnostic biopsies and tissue from primary resected adenocarcinomas and LN metastases of patients who did not receive neoadjuvant CRT, in order to establish that there are no significant differences between biomarker levels. Subsequently, the effect of CRT was studied in an additional cohort by correlating CEA, EPCAM and C-MET expression between biopsies, obtained prior to the start of CRT, versus primary tumors and metastatic LNS.

METHODS

TISSUE SAMPLES ••• Formalin-fixed paraffin-embedded (FFPE) tissue blocks from 72 patients, who underwent surgical resection of RC or polypectomy between 2000-2015, were obtained from the Pathology Department of the Leiden University Medical Center (LUMC) (Table 1). Medical records and pathology samples were retrospectively reviewed. Patients were divided into two cohorts based on their therapy: cohort 1 was defined by patients without neoadjuvant CRT whereas cohort 2 comprised the neoadjuvantly treated patients (Figure 1). CRT consisted of a combination of chemo- and radiotherapy, e.g. 25x2 Gray and Capecitabine with/without Avastin or 5x5 Gray with Capecitabine plus Oxaliplatin (RAPIDO study design)²¹. Available FFPE tissue blocks of diagnostic biopsy specimens, tumor resection material and metastatic LNS were collected. All biopsies from patients treated with neoadjuvant CRT were obtained via endoscopic procedures, prior to the start of CRT. Multiple biopsy specimens of individual patients were incorporated on one slide. Eight patients showed a pathological complete response (PCR) after CRT. These tissues were also included in the study to assess the expression of biomarkers on normal/fibrotic epithelium. All samples were handled in an anonymous fashion according to the national ethics guidelines ('Code for Proper Secondary Use of Human Tissue,' Dutch Federation of Medical Scientific Societies) and approved by the Institutional Ethics Committee of the Leiden University Medical Center.

IMMUNOHISTOCHEMISTRY ••• Based on hematoxylin-eosin-stained (HE) slides, a representative FFPE tissue block containing tumor and normal tissue from each patient was chosen by a board-certified pathologist (A.F.S.). After sectioning

the FFPE blocks in 4 µm slides, these were mounted on adhesive slides (Starfrost), deparaffinized using xylene and rehydrated in decreasing concentrations of ethanol. Subsequently, slides were rinsed with distilled (D1) water and endogenous peroxidase was blocked with hydrogen peroxidase 0.3% hydrogen peroxidase (Merck Millipore) for 20 minutes. Slides were rinsed in D1 water and antigen retrieval was performed in the DAKO PT LINK, Target Retrieval Solution pH6.0 at 95°C for 10 minutes. After rinsing with phosphate buffered saline (PBS), slides were stained with predetermined dilutions using monoclonal antibodies (MAB) against CEACAM5 (clone C1-P83-I, sc-23928 from Santa Cruz Biotechnology, 0.2 µg/m, dilution 1:2500), EPCAM (clone MOC-31 Acris Antibodies, dilution 1:10,000) and a polyclonal antibody against C-MET (polyclonal rabbit, Santa Cruz sc-10, 1 µg/ml, dilution 1:100). After overnight incubation with the primary antibodies, slides were incubated with the secondary antibody (Envision anti-mouse HRP (DAKO)) for 30 min, followed by diaminobenzidine solution (DAB+; DAKO Kit). All slides were counterstained with hematoxylin, dehydrated and finally mounted with pterex.

SCORING METHOD ••• All tumor tissues, metastatic LNS, normal appearing mucosae and fibrotic rectal tissues from patients who had a PCR after CRT were scored for expression of CEA, EPCAM and C-MET. The total immunostaining score (TIS) was calculated by multiplying the proportion score (PS) and intensity score (IS), as previously described²⁰. The PS represented the percentage of positively stained tumor cells and ranged between 0-4 (0=none; 1 <10%; 2=10-50%; 3=51-80%; 4>80%). The IS represented the intensity of the stained tumor cells and could range between 0-3 (0=no staining; 1=weak; 2=moderate; 3=strong). Subgroups were defined based on the calculated TIS: 0, no expression; 1-4, weak expression; 6-8, moderate expression; 9-12, intense expression. Homogeneous expression was defined when >80% of tumor cells, with a staining intensity of ≥1, showed expression of one of the biomarkers (PS=4). Evaluation of the IHC stainings was performed independently by two observers (A.F.S. and L.B.). All the sections with interobserver disagreement were discussed with a board certified pathologist until agreement was reached.

STATISTICAL ANALYSIS ••• Statistical analyses were performed using SPSS version 23.0 software (SPSS, © IBM Corporation, Somers NY, USA) and GraphPad Prism 6 (GraphPad, Software, Inc., La Jolla). For each patient, biomarker expression on biopsies, resected primary tumors and metastatic LNS was compared using the Mann-Whitney test. Differences in expression levels between cohort 1 (no CRT) and cohort 2 (CRT) were calculated using the Wilcoxon rank test. This test was also used to calculate differences in expression levels between tumor and adjacent normal

tissue per patient. Additionally, a Mann-Whitney test was performed to compare these analyses between patients of cohort 1 and 2. A Kruskal Wallis test was used to determine the differences in T/N ratio between all three biomarkers. In all tests, results were considered statistically significant at the level of $p < 0.05$.

RESULTS

Patient and tumor characteristics are summarized in Table 1. Briefly, thirty-eight patients did not receive neoadjuvant CRT (cohort 1). Of these patients, available biopsy specimens ($n=36$), primary tumor specimens ($n=38$) and metastatic LNS ($n=10$) were collected (Figure 1). In cohort 2, 34 patients treated with neoadjuvant CRT were included. Available biopsy specimens ($n=31$), obtained prior to the start of CRT, primary tumor specimens ($n=34$) and metastatic LNS ($n=7$) were collected. Eight out of 34 patients had a PCR after neoadjuvant CRT.

CEA, EPCAM AND C-MET EXPRESSION ••• Representative examples of CEA, EPCAM and C-MET staining in tumor tissue derived from a patient from cohort 1 are shown in Figure 2. CEA was mainly expressed on the apical side of cancer cells, while EPCAM and C-MET showed a more circumferential, membranous staining. Moreover, lymphoid cells, histiocytes and necrotic areas stained also positive for C-MET. Figure 3 shows similar representative stainings in a patient from cohort 2. All biomarkers showed some positivity in non-cancerous mucin producing cells in neoadjuvantly treated tissues. CEA, EPCAM and C-MET expression scores of all tumor tissues are shown in Table 2. The median TIS of all biomarkers in all tumor tissues was 12. In cohort 1, homogeneous expression of CEA, EPCAM and C-MET was found in respectively 28/38 (74%), 34/38 (89%) and 31/38 (82%) of the malignancies in resection material, which was significantly similar to the expression of CEA, EPCAM and C-MET in malignancies in resection material in cohort two, found in respectively 19/26 (73%), 24/26 (92%) and 22/26 (85%) of samples.

COMPARISON BETWEEN BIOMARKER EXPRESSION BEFORE AND AFTER CRT ••• The degree of concordance of CEA, EPCAM and C-MET expression between the various tumor tissues, i.e. biopsy, tumor in resection material and metastatic LN, is shown in Table 3. In cohort 1, >61% of biopsies showed concordant expression with their corresponding resected tumor. The majority of discordant scores were due to a difference in intense vs. moderate expression between the tumor tissues, i.e. 10/14 (71%) discordant scores for CEA and EPCAM, and 6/7 (86%) discordant scores for C-MET. There was no significant difference in expression of any of the

three biomarkers between endoscopically obtained biopsy specimens and resection specimens per individual patient ($p=0.43$ for CEA, $p=0.10$ for EPCAM and $p=0.41$ for C-MET). These data suggest that differences found between stainings in biopsies and resected material in cohort 2 are exclusively induced by CRT.

Also in cohort 2, the majority (>61%) of cases showed a concordant expression pattern when comparing biopsies and resection material, despite the fact that biopsies were obtained prior to the start of neoadjuvant CRT and primary tumors after CRT. The concordance between biopsies is shown in Table 2 and graphically displayed in Figure 4. No significant difference in CEA and EPCAM expression was found between the various tumor tissues per patient ($p=0.52$ for CEA, $p=0.11$ for EPCAM). However, C-MET expression appeared significantly different between biopsies and resected tumors ($p=0.02$). Again, most discordant expression scores between biopsies and primary tumors were due to minor differences in TIS between intense vs. moderate; 4/7 (57%) discordant scores for CEA, 5/6 (83%) for EPCAM and 7/9 (78%) for C-MET. Finally, when comparing all tumor tissues from patients who did not receive CRT with patients who did, no significant differences were found between expression in primary tumors and between expression in metastatic LNS (all p -values > 0.05). CEA, EPCAM and C-MET expression did not significantly differ between tumor tissues that showed no response after CRT and tissues that showed a partial pathological response.

COMPARISON OF BIOMARKER EXPRESSION BETWEEN CARCINOMA AND ADJACENT NORMAL TISSUE ••• Figure 5 shows the distribution of CEA, EPCAM and C-MET TIS in tumor tissues compared with normal adjacent epithelial tissues, from both patient cohorts together. All three biomarkers were significantly upregulated in cancer tissue compared to normal tissue of the same patient ($p < 0.01$ for CEA, EPCAM and C-MET). Median TIS expression in normal epithelium were respectively 4 (range 0-12) for CEA, 12 (range 0-12) for EPCAM and 8.5 (range 0-12) for C-MET. A significant difference between biomarkers was found using a Kruskal-Wallis test with the highest mean rank for CEA, followed by equal mean ranks for EPCAM and C-MET ($p < 0.01$).

EXPRESSION ON TISSUE WITH COMPLETE PATHOLOGICAL RESPONSE Median biomarker expression scores (TIS) in the tumor bed of resected tissue from patients with a PCR after neoadjuvant CRT were respectively 5 (range 1-12) for CEA, 10.5 (range 4-12) for EPCAM and 8.5 (range 4-12) for C-MET. CEA expression was seen on the surface of normal epithelium and alike EPCAM and C-MET, in mucin producing cells. The muscularis propria showed some expression of C-MET (probably non-specific binding).

DISCUSSION

Tumor-targeted fluorescence imaging has the potential to revolutionize the current practice of oncologic surgery by selectively highlighting neoplastic cells. This technique may be particularly useful during RC surgery, as clear tumor visualization is sometimes impaired by anatomic constraints such as a narrow pelvis. The present data confirm the results of previous studies that expression of the studied biomarkers CEA, EPCAM and C-MET is increased in tumor tissue as compared with normal mucosa from the same patient, and hence in principle could be used as targets for image-guided assistance during surgery. However, a substantial part of RC patients are nowadays treated with neoadjuvant CRT to induce down staging and to achieve local control²². Although the addition of CRT leads to a decrease in recurrence rates, it also causes massive tissue fibrosis which in turn hinders intraoperative tumor localization²³. The data presented here demonstrate that the expression of CEA and EPCAM does not significantly differ between endoscopically obtained diagnostic biopsies, resected primary tumors and LN metastases, in patients treated with or without neoadjuvant CRT. These results demonstrate the usability of these biomarkers for RC imaging. C-MET expression differed significantly between biopsies and resected tumors in cohort 2, which might reflect an effect of the CRT on protein expression, but could also be the result of a small sample size.

In the current study we showed that all three proteins are abundantly expressed in the vast majority of RC tissues, confirming previous studies with larger cohorts¹⁸⁻²⁰. Although IHC is not a fully quantitative technique, and results might depend on the selected antibodies and tissue fixation, the representative figures show that CEA and EPCAM seem to outperform C-MET with respect to staining intensity in tumors. Unlike CEA and EPCAM, which are involved in cell adhesion, C-MET is a tyrosine kinase receptor that becomes activated after binding of the hepatocyte growth factor. Due to the pivotal role of C-MET in cancer biology and overexpression in several cancer types, it is regarded as a promising target for molecular tumor imaging, including colorectal neoplasia^{11,24}. Still, the numbers of this receptor per tumor cell might be lower compared to adhesion molecules like CEA and EPCAM, as reflected in the expression scores within this study⁸.

A prerequisite for appropriate tumor targets in image-guided surgery is enhanced expression on tumor cells compared to adjacent normal tissue⁷. CEA and EPCAM are cell adhesion molecules and are both moderately expressed on normal cylindrical epithelium and goblet cells^{25,26}. Although EPCAM showed the highest amount of homogeneous tumor expression among all three biomarkers, the difference in the TIS between tumor and normal tissue was relatively low. This could

seem a disadvantage for EPCAM as a target. However, when analysing these data, one should take the limitations of IHC scorings into consideration when quantifying protein expression. For instance, a difference between 10,000 EPCAM molecules on a regular cell and 400,000 on a neoplastic cells would probably not be noticed by conventional IHC, but would be enough to discriminate tumor from normal tissue using fluorescence imaging. On the other hand, CEA has the disadvantage of being anchored to the cell membrane via a GPI-anchor, making it vulnerable for shedding in the bloodstream²⁷. As a result, high levels of soluble CEA could scavenge the intravenously administered targeting agent, being a disadvantage for CEA-based imaging.

Our group previously described the preclinical evaluation of respectively a fluorescent labelled EPCAM-specific MAB and a CEA-specific single-chain antibody fragment and showed successful fluorescent delineation of several tumor models, including CRC and peritonitis carcinomatosis^{9,10}. As already indicated in the previous paragraph, preclinical models can only partly mimic the human situation. The most important factor that influences the tumor-to-background ratio during clinical application of tumor-targeted agents will be the presence of the targeted receptor on adjacent normal cells. Both EPCAM and CEA expression are described to be confined to the basolateral surface of normal polarized epithelial cells, where these receptors might be less accessible for targeting by intravenous administered agents^{26,28,29}. When epithelial cells dedifferentiate into tumor cells, polarity is lost and CEA and EPCAM become expressed throughout the entire membrane. This phenomenon would be advantageous for tumor imaging. Especially for normal enterocytes, with a lifespan of 1-2 days, the continuous shedding of these cells into the bowel lumen would result in relatively low background fluorescence in normal mucosa, especially when imaging occurs a few days after tracer administration.

The main drawbacks of this study are the relatively low numbers of tissue sets and the use of semi-quantitative IHC. The collection of tumor tissue before and after CRT implies that both endoscopic diagnostic biopsy material and resection material of the same patient are available at the same institution. Our hospital is a reference hospital for some regional hospitals and therefore many of the diagnostic biopsies are taken elsewhere. Collecting the material is tedious and time consuming. Our approach of studying two cohorts of patients showed that the differences of expression of the three selected biomarkers before and after CRT were limited. IHC is relatively easy to perform, available at low costs compared to other diagnostic techniques, and provides information about the expression patterns of certain proteins in various cell types, which is pivotal information for imaging purposes. Although it is nowadays routinely used, IHC in most cases lacks standardization (pre-test variability) and variance in interpretation of the staining (post-test variability)²⁰. To minimize these

limitations, we performed IHC staining with validated antibodies and used a scoring method that was previously evaluated²⁰. Nevertheless, differences in expression could be observed by using various antibodies against the same target. Especially for c-MET, the use of a polyclonal antibody might difficult the comparison with other studies.

A promising application of CEA, EPCAM, or c-MET-targeted fluorescent agents might be the implementation during (endoscopic) surveillance of patients eligible for the Watch-and-Wait strategy (w&w), or during Transanal Endoscopic Microsurgery (TEM)^{30,31}. Over the last years, organ-preserving approaches for RC patients, such as the w&w strategy for patients with a complete clinical response (CCR) and TEM, are gaining interest³¹. As recent studies show a local regrowth rate up to 38% in patients selected for w&w, it seems that conventional imaging modalities are not able to select patients sufficiently³². Therefore, tumor-targeted fluorescence imaging during colonoscopies may assist in identification of a CCR, or residual tumor cells. This application would however only be valuable when markers are sensitive and specific enough to distinguish between normal tissue, fibrotic tissue and scattered tumor cells. In the eight tissues derived from patients with a PCR all biomarkers showed some expression in the resected fibrotic tumor bed, but considerably less than in the tumors. Larger studies are needed to confirm these findings and assess the expression of these and other biomarkers in patients with a PCR, both for primary and recurrent RC patients.

CONCLUSION

In conclusion, this study shows that CEA, EPCAM and c-MET are abundantly expressed in RC and LN metastases, and that modifications of protein expression by CRT in tumor or adjacent normal tissue are limited. Homogeneous expression in RC tissues of primary tumors and metastatic LNs was highest for EPCAM. But, based on staining of normal adjacent epithelium, CEA appeared the most distinctive biomarker. The data of the present study underscore a reliable applicability of CEA-, EPCAM- and c-MET-targeted imaging agents, which have recently been or will soon be used in clinical practice. A firm conclusion about which biomarker has the highest potential cannot be drawn based only on IHC or on animal models. Only comparative clinical trials can answer this question.

REFERENCES

- Heald, R. J. A new approach to rectal cancer. *Br J Hosp Med* 22, 277-281 (1979).
- Rickles, A. S. et al. High Rate of Positive Circumferential Resection Margins Following Rectal Cancer Surgery: A Call to Action. *Ann Surg* 262, 891-898 (2015).
- Nagtegaal, I. D. & Quirke, P. What is the role for the circumferential margin in the modern treatment of rectal cancer? *J Clin Oncol* 26, 303-312 (2008).
- Peeters, K. C. et al. The TME trial after a median follow-up of 6 years: increased local control but no survival benefit in irradiated patients with resectable rectal carcinoma. *Ann Surg* 246, 693-701 (2007).
- Simillis, C. et al. A Systematic Review to Assess Resection Margin Status After Abdominoperineal Excision and Pelvic Exenteration for Rectal Cancer. *Ann Surg*, 265(2):291-299 (2017).
- Vahrmeijer, A. L., Hutteman, M., van der Vorst, J. R., van de Velde, C. J. & Frangioni, J. V. Image-guided cancer surgery using near-infrared fluorescence. *Nat. Rev. Clin. Oncol* 10, 507-518 (2013).
- van Oosten, M., Crane, L. M., Bart, J., van Leeuwen, F. W. & van Dam, G. M. Selecting Potential Targetable Biomarkers for Imaging Purposes in Colorectal Cancer Using Target Selection Criteria (TASC): A Novel Target Identification Tool. *Transl Oncol* 4, 71-82 (2011).
- Boonstra, M. C. et al. Selecting Targets for Tumor Imaging: An Overview of Cancer-Associated Membrane Proteins. *Biomark Cancer* 8, 119-133 (2016).
- Boonstra, M. C. et al. Preclinical evaluation of a novel CEA-targeting near-infrared fluorescent tracer delineating colorectal and pancreatic tumors. *Int J Cancer*, Oct 15;137(8):1910-20 (2015).
- van Driel, P. B. et al. EPCAM as multi-tumour target for near-infrared fluorescence guided surgery. *BMC Cancer* 16, 884 (2016).
- Burggraaf, J. et al. Detection of colorectal polyps in humans using an intravenously administered fluorescent peptide targeted against c-MET. *Nat Med* 21, 955-961 (2015).
- Sahlmann, C. O. et al. Repeated adjuvant anti-CEA radioimmunotherapy after resection of colorectal liver metastases: Safety, feasibility, and long-term efficacy results of a prospective phase 2 study. *Cancer* 15;123(4):638-649 (2017)
- Schoffelen, R. et al. Development of an imaging-guided CEA-pretargeted radionuclide treatment of advanced colorectal cancer: first clinical results. *Br J Cancer* 109, 934-942 (2013).
- Trzpis, M., McLaughlin, P. M., de Leij, L. M. & Harmsen, M. C. Epithelial cell adhesion molecule: more than a carcinoma marker and adhesion molecule. *Am J Pathol* 171, 386-395 (2007).
- Loibner, H. et al. A randomized placebo-controlled phase II study with the cancer vaccine IG101 in patients with epithelial solid organ tumors (IG101/2-01). *J Clin Oncol* 22, 2619 (2004).
- Liao, M. Y. et al. An anti-EPCAM antibody EPAB2-6 for the treatment of colon cancer. *Oncotarget* 6, 24947-24968 (2015).
- Blumenschein, G. R., Jr., Mills, G. B. & Gonzalez-Angulo, A. M. Targeting the hepatocyte growth factor-cMET axis in cancer therapy. *J Clin Oncol* 30, 3287-3296 (2012).
- Di Renzo, M. F. et al. Overexpression and amplification of the met/HGF receptor gene during the progression of colorectal cancer. *Clin Cancer Res* 1, 147-154 (1995).
- Park, J. W., Chang, H. J., Kim, B. C., Yeo, H. Y. & Kim, D. Y. Clinical validity of tissue carcinoembryonic antigen expression as ancillary to serum carcinoembryonic antigen concentration in patients curatively resected for colorectal cancer. *Colorectal Dis* 15, e503-511 (2013).
- Spizzo, G. et al. EPCAM expression in primary tumour tissues and metastases: an immunohistochemical analysis. *J Clin Pathol* 64, 415-420 (2011).
- Nilsson, P. J. et al. Short-course radiotherapy followed by neo-adjuvant chemotherapy in locally advanced rectal cancer—the RAPIDO trial. *BMC Cancer* 13, 279 (2013).
- van de Velde, C. J. et al. EURECCA colorectal: multidisciplinary management: European consensus conference colon & rectum. *Eur J Cancer* 50, 1 e1-e34 (2014).
- Torres, M. L., McCafferty, M. H. & Jorden, J. The difficulty with localization of rectal cancer after neoadjuvant chemoradiation therapy. *Am Surg* 76, 974-976 (2010).
- Pool, M., van Dam, G. M. & de Vries, E. G. Emerging Opportunities for c-MET Visualization in the Clinic. *J Nucl Med* 53, 663-664 (2016).
- Hammarstrom, S. The carcinoembryonic antigen (CEA) family: structures, suggested functions and expression in normal and malignant tissues. *Semin Cancer Biol* 9, 67-81 (1999).
- Xie, X. et al. Expression pattern of epithelial cell adhesion molecule on normal and malignant colon tissues. *World J Gastroenterol* 11, 344-347 (2005).
- Boonstra, M. C. et al. Selecting Targets for Tumor Imaging: An Overview of Cancer-Associated Membrane Proteins. *Biomarkers in Cancer* 8, 15 (2016).
- Tiernan, J. P. et al. Carcinoembryonic antigen is the preferred biomarker for in vivo colorectal cancer targeting. *Br J Cancer* 108, 662-667 (2013).
- Ogura, E., Senzaki, H., Yoshizawa, K., Hioki, K. & Tsubura, A. Immunohistochemical localization of epithelial glycoprotein EGP-2 and carcinoembryonic antigen in normal colonic mucosa and colorectal tumors. *Anticancer Res* 18, 3669-3675 (1998).
- O'Neill, C. H., Platz, J., Moore, J. S., Callas, P. W. & Cataldo, P. A. Transanal Endoscopic Microsurgery for Early Rectal Cancer: A Single-Center Experience. *Dis Colon Rectum* 60, 152-160 (2017).
- Beets, G. L., Figueiredo, N. F. & Beets-Tan, R. G. Management of Rectal Cancer Without Radical Resection. *Annu Rev Med* (2016).
- Renchan, A. G. et al. Watch-and-wait approach versus surgical resection after chemoradiotherapy for patients with rectal cancer (the OnCoRe project): a propensity-score matched cohort analysis. *Lancet Oncol* 17, 174-183 (2016).

Figure 1 Overview of included tumor tissues

Described are the number of included specimens derived from patients who received no neoadjuvant CRT (cohort 1, $n=38$) and patients who did (cohort 2, $n=34$). In the primary tumor specimens, expression of biomarkers on normal epithelium was assessed when applicable. Biopsies were endoscopically obtained, prior to CRT (cohort 2). In cohort 1, 36 tumor sets were included consisting of biopsy material and primary resection specimens. Of these 36 patients, 10 tissues of LN metastases were included. In cohort 2, 31 sets were included consisting of biopsy material and primary resection specimens, including 4 with LN metastases. One patient with a LN metastasis had a CPR. Two LN metastases could only be correlated with expression in primary resection specimens, because biopsy material of these patients was lacking.

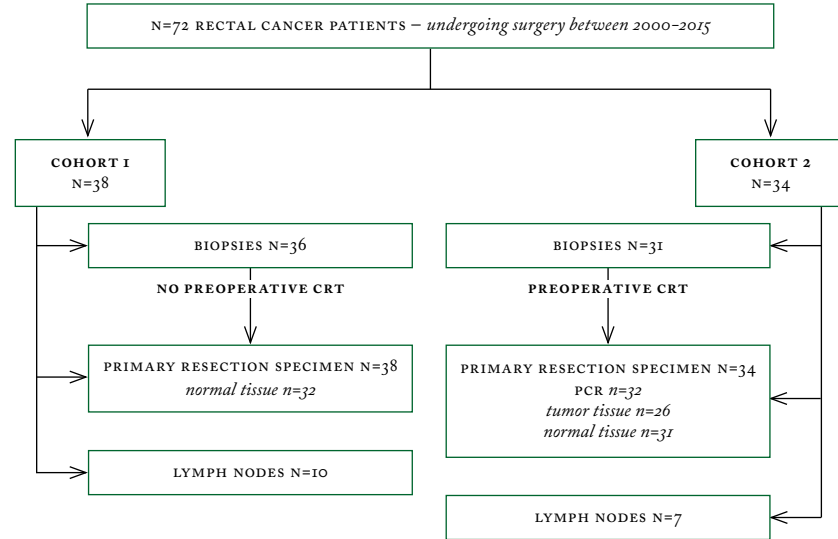


Figure 2 Representative images of CEA, EPCAM and C-MET expression on RC tissues of a patient who was not treated with CRT

- A Biopsy specimen (magnification 5x). All cancer cells show expression of all three biomarkers.
- B Primary tumor specimen (magnification 5x). The dotted arrow indicates normal epithelium and the other arrow indicates cancer tissue. A difference in intensity between tumor and normal tissue can be seen for all three biomarkers. This difference appears the highest for CEA, followed by EPCAM and C-MET.
- C Metastatic lymph node (magnification 5x). The arrow indicates the location of cancer cells, which are clearly visualized by EPCAM and CEA staining.

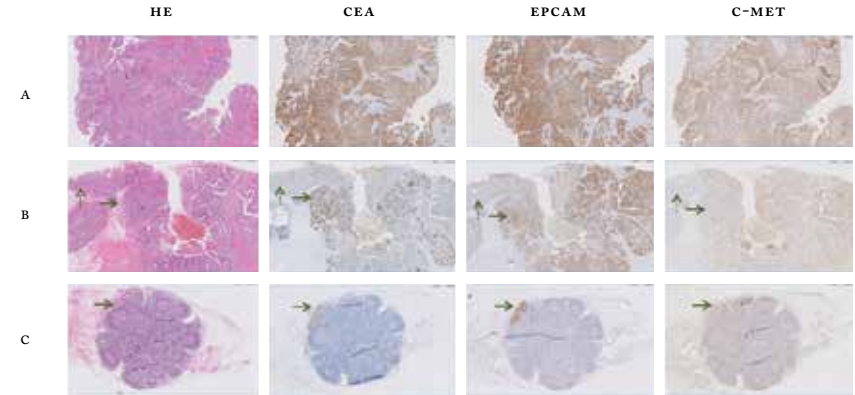


Figure 3 Representative images of CEA, EPCAM and C-MET expression on RC tissues of a patient who was treated with neoadjuvant CRT

- A Biopsy specimen (magnification 5x), obtained prior to the start of CRT, showing expression of all three biomarkers.
- B Primary tumor specimen (magnification 5x). The dotted arrow indicates normal epithelium and the other arrow indicates tumor tissue. A difference in intensity between tumor and normal tissue can be seen for all three biomarkers. This difference appears the highest for CEA.
- C Metastatic lymph node (magnification 5x). The arrow indicates the location of cancer cells, which are visualized by CEA, EPCAM and C-MET staining.

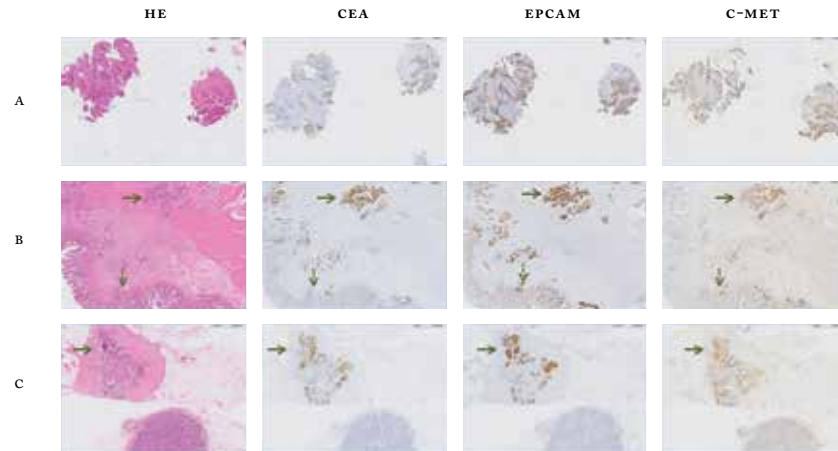


Figure 4 Difference in CEA, EPCAM and C-MET expression between biopsies, obtained prior to the start of CRT, and primary tumors

A horizontal line indicates the same level of expression between biopsy and primary tumor. For all biomarkers, the majority of tissues showed an intense expression (T1S of 12) in biopsies and corresponding primary tumor. The number of biopsy and tumor tissues with a certain expression score (T1S) are indicated next to the corresponding line.

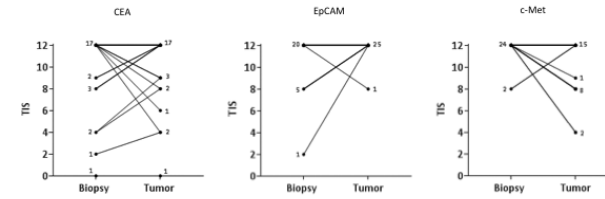


Figure 5 Tumor-to-normal tissue ratio for CEA, EPCAM and C-MET on primary resected tumors

Shown are correlations between tumor tissue and adjacent normal tissue in the same sample, per patient and per biomarker (both cohort 1 and cohort 2). All biomarkers were significantly upregulated in tumor tissue compared to adjacent normal epithelium. The T/N ratio was highest for CEA. The arrows indicate the number of tumor tissues that show an enhanced or decreased expression compared to adjacent normal epithelium; = refers to equal expression scores.

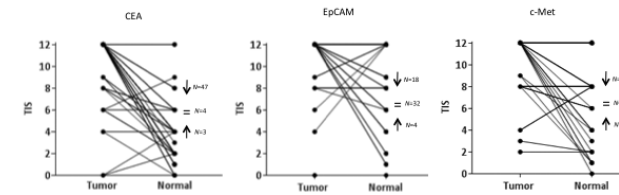


Table 1 Patient and tumor characteristics

	No CRT (N=38)	CRT (N=34)
Age at diagnosis, median years (range)	67 (36 - 87)	64 (26 - 76)
Gender, n		
male	25	21
female	13	13
Previous radiotherapy in area of rectum, n	3	2
Type of surgery performed		
low anterior resection	32	30
abdominoperineal resection	4	14
subtotal colectomy	1	0
polypectomy	1	0
Tumor size, median mm (range)	35 (5 - 120)	25 (1 - 70)
Primary tumor stage, n		
pT0	0	8
pT1	5	2
pT2	13	10
pT3	17	11
pT4	3	3
Nodal stage, n		
pN0	24	24
pN1	8	6
pN2	6	4
Metastatic stage, n		
pM0	32	32
pM1	6	2
Pathological response, n		
none	n.a.	9
partial	n.a.	17
complete	n.a.	8

*p=*pathological, *n=*number of patients, CRT = chemoradiotherapy

Table 2 Total immunostaining scores of all stained tumor tissues, derived from patients who did not (-) and patients who did (+) receive neoadjuvant CRT

Total Immunostaining Score (TIS) on tumor tissue N (%)					
CEA	No expression (TIS=0)	Weak expression (TIS=1-4)	Moderate expression (TIS=6-8)	Intense expression (TIS=9-12)	Total n tissues (-/+)
biopsies	- 0 (0%)	3 (8%)	10 (28%)	23 (64%)	36/31
	+ 1 (3%)	3 (3%)	6 (19%)	21 (68%)	
primary tumor	- 1 (3%)	1 (3%)	6 (16%)	30 (79%)	38/26
	+ 1 (4%)	1 (4%)	3 (12%)	21 (81%)	
LN metastases	- 0 (0%)	0 (0%)	0 (0%)	10 (100%)	10/7
	+ 0 (0%)	1 (14%)	0 (0%)	6 (86%)	
EPCAM					
biopsies	- 0 (0%)	2 (6%)	13 (36%)	21 (58%)	36/31
	+ 0 (0%)	1 (3%)	5 (16%)	25 (81%)	
primary tumor	- 1 (3%)	1 (3%)	4 (11%)	32 (84%)	38/26
	+ 0 (0%)	0 (0%)	1 (4%)	25 (96%)	
LN metastases	- 0 (0%)	0 (0%)	0 (0%)	10 (100%)	10/7
	+ 0 (0%)	0 (0%)	0 (0%)	7 (100%)	
C-MET					
biopsies	- 0 (0%)	3 (8%)	10 (28%)	23 (64%)	36/31
	+ 0 (0%)	0 (0%)	4 (13%)	27 (87%)	
primary tumor	- 0 (0%)	4 (11%)	4 (11%)	30 (79%)	38/26
	+ 0 (0%)	2 (8%)	8 (31%)	16 (61%)	
LN metastases	- 0 (0%)	1 (10%)	3 (30%)	6 (60%)	10/7
	+ 1 (14%)	1 (14%)	0 (0%)	5 (71%)	

Table 3 Degree of concordance of biomarker expression between various tumor tissues per patient

No CRT	CEA	EPCAM	C-MET
biopsy = tumor	22/36 (61%)	22/36 (61%)	28/36 (78%)
biopsy > tumor	5/36 (14%)	2/36 (6%)	2/36 (6%)
biopsy < tumor	9/36 (25%)	12/36 (33%)	6/36 (17%)
LN metastasis = tumor	9/10 (90%)	9/10 (90%)	7/10 (70%)
LN metastasis > tumor	1/10 (10%)	1/10 (10%)	1/10 (10%)
LN metastasis < tumor	0/10 (0%)	0/10 (0%)	2/10 (10%)
CRT			
biopsy = tumor	16/23 (70%)	17/23 (74%)	14/23 (61%)
biopsy > tumor	2/23 (9%)	1/23 (4%)	1/23 (4%)
biopsy < tumor	5/23 (22%)	5/23 (22%)	8/23 (35%)
LN metastasis = tumor	6/7 (86%)	7/7 (100%)	4/7 (57%)
LN metastasis > tumor	1/7 (14%)	0/7 (0%)	0/7 (0%)
LN metastasis < tumor	0/7 (0%)	0/7 (0%)	3/7 (43%)

CRT chemo- and radiotherapy, = indicates a concordant expression between the two tissues, > indicates up regulation of expression, < indicates down regulation of expression

PART III

CLINICAL TRANSLATION OF TUMOR-TARGETED FLUORESCENT TRACERS

CHAPTER 9

FOLATE RECEPTOR- α TARGETED NEAR-INFRARED FLUORESCENCE IMAGING IN HIGH-RISK ENDOMETRIAL CANCER PATIENTS: A TMA AND CLINICAL FEASIBILITY STUDY

Oncotarget. 2017 Dec 11;9(1):791-801

LSF BOOGERD*, CES HOOGSTINS*, KN GAARENSTROOM, CD DE KROON,
T BOSSE, E STELLOO, J VUYK, CJH VAN DE VELDE, PS LOW, J BURGGRAAF,
AND AL VAHRMEIJER

**shared first authorship*

ABSTRACT

OBJECTIVE ¶ Detection and resection of all malignant lesions is pivotal in staging and cytoreductive surgery (CRS) of endometrial cancer (EC). Intraoperative EC detection could be enhanced using OTL-38, a fluorescent-labelled folate receptor- α (FR α) targeted imaging agent. The objectives of this study were to investigate which subgroups of high-risk EC patients express FR α and assess feasibility of intraoperative EC detection using OTL-38.

METHODS ¶ Immunohistochemical (IHC) staining of FR α expression was performed on tissue micro arrays (TMA) of 116 patients with high-risk EC features. Patients with either serous or clear cell EC, planned for staging or CRS, were eligible for inclusion in the clinical study and received an intravenous dose of 0.0125 mg/kg OTL-38, 2-3 hours prior to surgery. Resected lesions, identified by standard-of-care and/or fluorescence imaging, were histopathologically assessed for FR α and tumor status.

RESULTS ¶ FR α expression on TMA was significantly correlated with tumor type ($p < 0.01$). Eighty-two percent of serous and clear cell carcinomas showed FR α expression. Four patients were enrolled in the clinical study. Using fluorescence imaging all omental ($N=3$) and lymph node (LN) metastases ($N=16$) could be clearly identified, including one otherwise undetected omental metastasis. However, false-positive fluorescence was identified in 17/50 non-metastatic LNs, caused by OTL-38 targeting of FR β , expressed by (tumor-associated) activated macrophages.

CONCLUSION ¶ This study describes high FR α expression in serous and clear cell EC and demonstrates the first experience of intraoperative FR α -targeted tumor detection in patients with these subtypes of EC. Although all metastases could be clearly identified using OTL-38, the role of tumor-associated macrophages should be further evaluated.

INTRODUCTION

Endometrial cancer (EC) can be categorized in type 1 and type 2, based on etiology and clinicopathologic features¹. Type 1 EC are commonly estrogen-dependent, low-grade, endometrioid adenocarcinomas, accounting for 80% of all EC. Type 2 EC account for the remaining 20% and represent a more aggressive, high-grade tumor type with a poorer prognosis^{2,3}. These tumors are generally non-endometrioid, i.e. serous or clear cell, and unrelated to estrogen exposure. High-risk EC is defined as a combination of several factors including non-endometrioid EC, more advanced disease stages/age, high-grade and lymphovascular space invasion⁴. Although EC is conventionally categorized in type I and II, improved understanding of the molecular landscape of EC has resulted in subdivision of EC in four molecular subtypes with improved prognostic significance, among others p53 mutant EC⁵. Each type and risk group of EC requires a different surgical approach because of distinctive tumor characteristics. For type 1, low-grade EC the extent of pelvic organ resection and lymphadenectomy depends on the tumor stage, whereas a complete staging is recommended for clinically early stage serous and clear cell carcinomas, due to higher rates of metastatic disease⁶. A complete surgical staging includes a total hysterectomy with bilateral salpingo-oophorectomy (BSO), pelvic and para-aortic lymph node sampling, omentectomy, and several peritoneal biopsies of predefined spots⁷. Depending on the presence of metastases during surgical staging, patients will either be monitored via follow-up or treated with adjuvant therapy¹.

Both during staging and cytoreductive surgery (CRS) of EC it is of utmost importance to identify tumor lesions with high accuracy. Surgeons are dependent on inspection and palpation (in case of open surgery) for intraoperative distinction between tumor and normal tissue. Histopathological analysis on frozen specimens obtained during the procedure can provide additional information, but is only performed on clinically suspicious lesions. Furthermore, non-suspect, but malignant lesions can easily be missed when visual inspection and palpation are the sole means for identification. An innovative technique that can assist in real-time intraoperative tumor detection is near-infrared (NIR) fluorescence imaging⁸. This technique is based on administration of a fluorescent agent and real-time detection of fluorescence using a dedicated NIR imaging system. A new era in the field of NIR fluorescence imaging has emerged with the clinical testing of tumor-targeted fluorescent contrast agents⁹. These agents consist of a tumor-targeting ligand, e.g. a peptide, antibody, nanobody etc., conjugated to a NIR fluorescent dye. One of the most promising agents currently available for clinical testing is OTL-38, a NIR fluorescent-labelled peptide targeting the Folate Receptor- α (FR α)¹⁰. The FR α , an isoform of the

folate receptor, is anchored on the cell membrane and binds folic acid with high affinity. Expression of *FR α* on normal tissue is restricted to the apical surface of few epithelial tissues. However, marked overexpression in several tumor types, including EC, makes the *FR α* an attractive candidate for targeted imaging and therapy^{11,12}.

Safety and feasibility of *FR α* -targeted tumor detection using OTL-38 have been demonstrated in ovarian and lung cancer^{10,13}. Application of OTL-38 in EC surgery could be especially valuable in high-risk EC patients, who have a high likelihood of extra-uterine disease⁷. In these high-risk EC patients, real-time fluorescence guidance with OTL-38 during staging and CRS may provide enhanced visualization and detection of more metastatic lesions. The aim of this study was to assess which high-risk EC patients could benefit from *FR α* -targeted imaging. Although general overexpression of *FR α* in EC was previously described^{12,14}, specific *FR α* expression in only high-risk EC patients, including both non-endometrioid and endometrioid EC, has not been demonstrated. Therefore, expression of *FR α* was assessed on a tissue micro array (TMA), consisting of 116 tissues derived from EC patients with high-risk features. Based on these results, feasibility of NIR fluorescence intraoperative tumor detection using OTL-38 was studied in patients with serous or clear cell EC, scheduled for staging or CRS.

RESULTS

TMA-STUDY

Tissue cores of 101 patients were suitable for assessment of *FR α* expression. Clinicopathological characteristics and expression scores are shown in Table 1. Figure 1 shows representative examples of weak, moderate and strong intensity of *FR α* expression, in both endometrioid and non-endometrioid cancer. *FR α* expression was found in 63% of endometrioid cancers and in 82% of non-endometrioid cancers. Strong *FR α* expression was found in 38% of all endometrioid cancers compared to 46% of non-endometrioid cancers. A significant correlation ($p < 0.01$) between the pattern of *FR α* expression, i.e. homogeneous vs. heterogenous, and tumor type was found. The majority of serous endometrial carcinomas (73%) showed homogeneous *FR α* expression, while clear cell carcinomas showed a more heterogenous *FR α* expression pattern (65%). Endometrioid cancers showed both homogeneous and heterogenous *FR α* expression in respectively 33% and 30% of all scored cases. Furthermore, a significant association between p53 status, i.e. wildtype or mutant, and *FR α* expression was found ($p = 0.01$). All (11/11) homogeneous *FR α* -expressing non-endometrioid cancers showed a mutant p53 status.

CLINICAL STUDY

PATIENT CHARACTERISTICS ••• Four patients with EC (serous carcinoma; $n=3$ and clear cell carcinoma; $n=1$) were included in the clinical study (Table 2). Three patients underwent a staging procedure and one patient CRS. The patient undergoing CRS (patient #4) was diagnosed with a large mass in the fundus uteri (5.5cm) and two suspect peritoneal depositions in the omentum (respectively 1.3cm and 2.8cm) on preoperative computed tomography imaging. CRS consisted of uterus extirpation, BSO and omentectomy.

SAFETY AND PHARMACOKINETICS ••• All patients received 0.0125mg/kg OTL-38 over 1 hour and no infusion was stopped or intermitted. Two patients experienced possibly related AES: one patient experienced a mild muscle spasm and another patient mild pruritus. Both AES were self-limiting. No clinically relevant changes in blood pressure or pulse rate were observed. The maximal concentration for each dose was obtained directly after the end of the infusion. The elimination half-life was approximately 86 min.

INTRAOPERATIVE FLUORESCENCE IMAGING ••• Intraoperative fluorescence imaging allowed clear detection of tumor lesions using an exposure time of less than 60 ms. During surgery a fluorescent signal arising from the uterus could be detected in all patients with the primary tumor still in situ, with a mean tumor-to-background ratio (TBR) of 6.4 (SD=4.7; range: 2.9-13, Table 3). However, after slicing of the resected specimen, adjacent uterine tissue without tumor (#1 and #2) appeared more fluorescent than the signal arising from the tumor (Figure 2). In patient #4, almost no normal uterine tissue was present because of the bulky size of the tumor. The intraoperative fluorescence signal therefore probably originated from the primary tumor, instead of from normal uterine tissue.

In two of four patients (#1 and #4) metastases were found in respectively 16/22 LNS and in three omental lesions. In the remaining two patients, no metastases were found during staging procedures. All histologically proven metastatic malignant lesions (19/19) could be identified by fluorescence imaging, with a mean TBR of 6.3 (SD=4.5; range 3.2 - 14.1) in metastatic LNS (16/19) and a mean TBR of 2.3 (SD=0.2; range 2.1 - 2.5) in omental metastases (3/19). Importantly, one omental lesion was not seen during visual inspection and only identified by fluorescence imaging. Histopathological analysis of this lesion revealed a small deposit of clear cell carcinoma. Fluorescence imaging enabled clear detection of all histologically proven metastatic LNS, even when these were located beneath a layer of peritoneum or other overlying tissue (Figure 2).

Furthermore, a total of 50 LNS were resected that did not contain tumor cells. Seventeen out of these 50 LNS were detected by fluorescence imaging (patient #1, #2 and #3). Mean TBR of these false-positive LNS was 2.5 (SD=1.3; range 1.5 – 6.2). No other false-positive lesions were identified, i.e. no fluorescence was detected in biopsies of the bladder, the diaphragm and recto-uterine (Douglas) pouch. Sensitivity, specificity and positive predictive value of fluorescence detection of LNS was 100% (16/16), 70% (39/56) and 48% (16/33) respectively.

HISTOPATHOLOGY ••• Histopathological analysis of EC lesions showed a circumferential staining pattern of FR α in malignant cells of both clear cell and serous cancer origin (Figure 3). FR α expression was also found in adjacent normal uterine epithelial cells and in adenomyosis tissue (patient #2, Figure 2), possibly explaining the weakened fluorescence intensity of uterine tumors compared to adjacent ‘normal’ uterine tissue.

In all metastatic LNS, an intense FR α expression was seen in lymph node follicles, while expression in sinuses was weak (Figure 3). In contrast, FR α expression was absent in all (fluorescent) false-positive LNS. Additional staining experiments however showed FR β expression in the sinuses of these LNS which explained the false-positive fluorescence signal. The FR β is expressed by activated macrophages and is also targeted by OTL-38 (Figure 4).

DISCUSSION

Prior to the clinical study, we first performed a TMA study with tissue of EC patients with high-risk clinical features to select those EC patients who may benefit most from FR α -targeted tumor imaging⁴. Optimally, selection of EC patients with homogeneous FR α expression would result in targeting of all FR α -expressing tumor cells and consequently, low chances to miss tumor lesions in the clinical setting. A significant association between FR α expression and tumor type was shown, with positive expression in the majority of non-endometrioid cancers (82%). Remarkably, 73% of serous type EC showed homogeneous FR α expression, which makes particularly this group of patients suitable for FR α imaging. Although a substantial part of high-risk EC patients (63%) also showed FR α expression, we chose to include only non-endometrioid cancer patients in this clinical proof-of-concept study. Non-endometrioid EC is by definition high-grade and all these patients require staging or CRS. Several other studies support our findings and show upregulation of FR α in non-endometrioid EC and a correlation with tumor grade^{12,14,15}. Limitations of the TMA part of this study are inherent to IHC analysis, such as variation in staining techniques, scoring

systems and quality of antibodies. Notwithstanding, results of the current study corroborated results of the TMA study by Brown Jones et al.¹⁴, who also showed a significant association between FR α overexpression and high-risk EC. Our study differs because FR α expression was evaluated among a subset of EC patients with high-risk features. Additionally, this is the first study to show a significant association between homogeneous FR α expression and a mutant P53 status in non-endometrioid EC. Routinely performed evaluation of the P53 status may therefore assist in patient selection for FR α -targeted agents. We did not perform a FR β staining on the TMA, because previous literature describes that FR β is more prevalent on stromal cells than on cancer cells^{16,17}. Yet, a systematic comparison between FR α and FR β expression on endometrial cancer tissues with enough stromal tissue may be interesting.

The most important prognostic factor for EC survival is the presence of LN metastases. Therefore, pelvic and para-aortic lymph node sampling is recommended as an integral part of a surgical staging procedure for a subset of EC patients with a high likelihood of metastatic disease, such as non-endometrioid EC patients⁶. The goal is to identify patients with nodal disease who will most likely benefit from adjuvant therapy¹⁸. The morbidity and mortality, costs and importantly, impact on patient survival associated with this procedure are however all subject to debate, especially in early stage EC patients¹⁹. In an attempt to better match the extent of the surgical staging procedure with the risk of LN metastasis, a surgical algorithm has recently been adopted for early stage EC patients²⁰. Another method that has been advocated as alternative staging procedure is sentinel lymph node (SLN) mapping. Recently published results of a large multicenter SLN study suggest high accuracy of SLN detection in 340 early EC patients using indocyanine green (ICG) as fluorescent tracer²¹. Cervical injection of ICG led to successful mapping of at least one SLN in 86% of patients and nodal metastases were correctly identified in 35 of 36 patients (97%). ICG is a safe and relatively inexpensive fluorescent dye, that has been extensively studied for SLN mapping in multiple tumor types, such as vulvar and cervical cancer^{22,23}. Although ICG proved its suitability as lymphatic tracer, it is not tumor-specific and does not bind to tumor cells. The use of ICG during gynecologic cancer surgery is therefore limited to the detection of SLNs. OTL-38 is an example of a tumor-targeted fluorescent tracer, that can selectively highlight tumor cells that express FR α ¹⁰. OTL-38 has therefore the potential to aid gynecologists in real-time detection of distant metastases, i.e. peritoneal metastases, as well as more reliable removal of metastatic pelvic and para-aortic LNS.

In the current study, all metastatic LNS were detected using fluorescence imaging with OTL-38. Importantly, LNS located below a layer of \pm 1cm of tissue, such as para-aortic LNS, could be clearly identified. Nevertheless, three out of four patients

showed false-positive LNS during staging procedures. The fluorescence signal arising in those LNS appeared related to expression of FR β , which is also targeted by OTL-38 as shown by histopathology evaluation. FR β is selectively expressed on activated macrophages and is therefore explored as imaging target to detect lesions of inflammatory conditions²⁴. Recently the role of FR β in tumor tissues has been elucidated showing FR β expression in tumor-associated macrophages²⁵. In a study of thousand tumor sections, Shen et al. showed that FR β is mainly expressed on tumor-associated macrophages in stromal cells¹⁷. Importantly, the percentage of positively stained cells correlated with tumor stage and LN involvement, suggesting that expression of FR β might be an indication of the metastatic potential of a tumor. Further research is needed to clarify whether the apparently non-malignant LNS identified with fluorescence imaging are involved in premetastatic niche formation. If so, resection of these LNS may yield clinical benefit. Thus, despite the fact that all metastatic LNS expressed FR α , the widespread implementation of OTL-38 for metastatic LN detection remains limited until the role of FR β is elucidated.

Although no clear intraoperative distinction between uterine tumor and background tissue could be made using OTL-38, this is not relevant in staging or CRS of EC because all patients undergo a total hysterectomy. Previous studies report on constitutive FR α expression on normal uterine epithelium, but high expression on various EC tumor tissues^{12,26}. An additional finding observed after histopathological analysis of uterine tissues was strong FR α expression in adenomyosis cells, which has been previously described in 17/18 endometriosis samples²⁷. Since the aim of surgery in severe endometriosis patients is to resect all visible lesions, it is plausible that OTL-38 may enhance intraoperative detection in those patients, enabling better patient outcome.

In conclusion, this study demonstrates the first application of OTL-38 for intraoperative tumor detection during staging and cytoreductive surgery in patients with either serous or clear cell EC. Prior to the clinical study, a TMA study on tissues from high-risk EC patients demonstrated a significant association between FR α expression and tumor type. In the clinical study, all malignant LNS and omental metastases could be clearly identified using OTL-38. However, until the role of FR β in false-positive LNS is unambiguously established, the added value of OTL-38 for detection of metastatic LNS is limited.

MATERIALS AND METHODS

TISSUE SELECTION ••• High-risk (stage IB-III) EC samples were collected from collaborating institutions within the *TransPORTEC* consortium, as previously described⁴. High-risk EC was defined using inclusion criteria for the *PORTEC3* study²⁸.

Specimen of 116 patients were included in this tissue micro array (TMA) study, and tissue microarrays contained 1-mm tumor and tumor/stroma cores in triplicate. Clinicopathological characteristics, including tumor type, stage, grade and p53 status of all cases have been described previously⁴.

IMMUNOHISTOCHEMICAL STAINING AND EVALUATION ••• Immunohistochemistry was performed as described previously using the monoclonal antibody (MAB) 26B3.F2 (certified Folate Receptor alpha IHC Assay Kit, Biocare Medical)²⁹. The MAB26B3.F2 is highly specific for FR α without cross-reactivity to the other FR, e.g. FR β , FR γ or FR δ . For validation of the staining protocol lung adenocarcinoma was used as positive control and normal liver as negative control.

Blinded, independent evaluation of IHC staining was performed by two observers (L.B. and C.H.). Discrepancies were resolved by reviewing the relevant scores with a board certified pathologist (T.B.). A tumor core was rejected and not included in the analysis if it was missing or if >75% of the core was insufficient for evaluation. Staining was scored as absent/weak (0), moderate (1+) or strong (2+). A positive FR α expression was defined when >5% of tumor cells showed a moderate or strong FR α expression. A core was considered negative when none or <5% of tumor cells showed FR α expression. The overall intensity of staining of a case was recorded for the intensity that was seen in the majority of cores. Homogeneity was defined when all three cores showed similar intensity of FR α expression.

CLINICAL STUDY ••• This trial was approved by the Medical Ethics Committee of the Leiden University Medical Center and was performed in accordance with the ethical standards of the Helsinki Declaration. Four patients with a high suspicion of primary serous or clear cell carcinoma, planned for either staging or CRS by laparotomy or laparoscopy, were included. Main exclusion criteria were pregnancy, history of anaphylactic reactions and impaired renal function (defined by EGFR<50 ml/min/1.73m²) or liver function (defined as values greater than 3x the upper limit of normal (ULN) for ALT, AST, or total bilirubin).

TRACER ADMINISTRATION AND SURGICAL PROCEDURE ••• Patients received a 1 hour intravenous infusion of 0.0125 mg/kg OTL-38, 2-3 hours before the start of surgery. The investigational product, OTL-38, has been extensively described¹⁰. Tolerability assessments (blood pressure, pulse, peripheral oxygen saturation, respiratory rate, ECG, temperature and skin assessments) and blood collection for pharmacokinetics and routine laboratory tests were performed regularly from just before administration up to 24 hours post-dosing. Adverse events (AEs) and use of concomitant medication were recorded. All surgical procedures were performed

by an experienced gynecological oncologist. First the surgical field was searched for metastases by usual visual and tactile methods (the latter only in case of open surgery). Thereafter, the open or laparoscopic Artemis imaging system was used to identify NIR fluorescent lesions as described previously³⁰. All tumor tissue identified, irrespective of the method, was resected if this was surgically feasible and clinically considered important by the operating gynecological oncologist. Each resected lesion was marked as fluorescent or non-fluorescent and as clinically suspected or not suspected for malignancy.

ANALYSIS ••• All resected lesions were routinely examined by an experienced pathologist for tumor status. A fluorescent tumor positive lesion was considered a true positive lesion, a fluorescent tumor negative lesion a false positive lesion and a non-fluorescent tumor positive lesion a false negative lesion. Additionally, immunohistochemical (IHC) staining for FR α was performed. IHC staining of FR β was performed to evaluate the cause of false positive fluorescence. Placenta was used as positive control for FR β staining. The negative control was assessed by using the secondary antibody only, without the primary antibody.

STATISTICAL AND IMAGE ANALYSIS ••• Statistical analysis was performed using the IBM SPSS for Windows 20.0 software. Correlation of patient and tumor characteristics, including p53-status, with FR α expression was assessed with t-test for continuous variables and with χ^2 test of Fisher's exact test for categorical variables. In all statistical tests, a p-value of <0.05 was considered statistically significant.

REFERENCES

- Amant F, Moerman P, Neven P, Timmerman D, Van Limbergen E and Vergote I. Endometrial cancer. *Lancet*. 2005; 366(9484):491-505.
- Hamilton CA, Cheung MK, Osann K, Chen L, Teng NN, Longacre TA, Powell MA, Hendrickson MR, Kapp DS and Chan JK. Uterine papillary serous and clear cell carcinomas predict for poorer survival compared to grade 3 endometrioid corpus cancers. *Br J Cancer*. 2006; 94(5):642-646.
- Bansal N, Yendluri V and Wenham RM. The molecular biology of endometrial cancers and the implications for pathogenesis, classification, and targeted therapies. *Cancer Control*. 2009; 16(1):8-13.
- Stelloo E, Bosse T, Nout RA, MacKay HJ, Church DN, Nijman HW, Leary A, Edmondson RJ, Powell ME, Crosbie EJ, Kitchener HC, Mileskin L, Pollock PM, Smit VT and Creutzberg CL. Refining prognosis and identifying targetable pathways for high-risk endometrial cancer; a TRANSPORT-EC initiative. *Mod Pathol*. 2015; 28(6):836-844.
- Cancer Genome Atlas Research N, Kandoth C, Schultz N, Cherniack AD, Akbani R, Liu Y, Shen H, Robertson AG, Pashtan I, Shen R, Benz CC, Yau C, Laird PW, Ding L, Zhang W, Mills GB, et al. Integrated genomic characterization of endometrial carcinoma. *Nature*. 2013; 497(7447):67-73.
- Colombo N, Creutzberg C, Amant F, Bosse T, Gonzalez-Martin A, Ledermann J, Marth C, Nout R, Querleu D, Mirza MR, Sessa C and Group E-E-ECCW. ESMO-ESGO-ESTRO Consensus Conference on Endometrial Cancer: diagnosis, treatment and follow-up. *Ann Oncol*. 2016; 27(1):16-41.
- Morice P, Leary A, Creutzberg C, Abu-Rustum N and Darai E. Endometrial cancer. *Lancet*. 2016; 387(10023):1094-1108.
- Vahrmeijer AL, Hutterman M, van der Vorst JR, van de Velde CJ and Frangioni JV. Image-guided cancer surgery using near-infrared fluorescence. *Nat Rev Clin Oncol*. 2013; 10(9):507-518.
- Zhang RR, Schroeder AB, Grudzinski JJ, Rosenthal EL, Warram JM, Pinchuk AN, Eliceiri KW, Kuo JS and Weichert JP. Beyond the margins: real-time detection of cancer using targeted fluorophores. *Nat Rev Clin Oncol*. 14(6):347-364 (2017)
- Hoogstins CE, Tummers QR, Gaarenstroom KN, de Kroon CD, Trimpos JB, Bosse T, Smit VT, Vuyk J, van de Velde CJ, Cohen AF, Low PS, Burggraaf J and Vahrmeijer AL. A Novel Tumor-Specific Agent for Intraoperative Near-Infrared Fluorescence Imaging: A Translational Study in Healthy Volunteers and Patients with Ovarian Cancer. *Clin Cancer Res*. 2016; 22(12):2929-2938.
- Cheung A, Bax HJ, Josephs DH, Ilieva KM, Pellizzari G, Opzoomer J, Bloomfield J, Fittall M, Grigoriadis A, Figini M, Canevari S, Spicer JF, Tutt AN and Karagiannis SN. Targeting folate receptor alpha for cancer treatment. *Oncotarget*. 2016; 7(32):5253-5257.
- O'Shannessy DJ, Somers EB, Smale R and Fu YS. Expression of folate receptor-alpha (FR α) in gynecologic malignancies and its relationship to the tumor type. *Int J Gynecol Pathol*. 2013; 32(3):258-268.
- Okusanya OT, DeJesus EM, Jiang JX, Judy RP, Venegas OG, Deshpande CG, Heitjan DF, Nie S, Low PS and Singhal S. Intraoperative molecular imaging can identify lung adenocarcinomas during pulmonary resection. *J Thorac Cardiovasc Surg*. 2015; 150(1):28-35 e21.
- Brown Jones M, Neuper C, Clayton A, Mariani A, Konecny G, Thomas MB, Keeney G, Hartmann L and Podratz KC. Rationale for folate receptor alpha targeted therapy in "high risk" endometrial carcinomas. *Int J Cancer*. 2008; 123(7):1699-1703.
- Allard JE, Risinger JI, Morrison C, Young G, Rose GS, Fowler J, Berchuck A and Maxwell GL. Overexpression of folate binding protein is associated with shortened progression-free survival in uterine adenocarcinomas. *Gynecol Oncol*. 2007; 107(1):52-57.
- O'Shannessy DJ, Somers EB, Wang LC, Wang H and Hsu R. Expression of folate receptors alpha and beta in normal and cancerous gynecologic tissues: correlation of expression of the beta isoform with macrophage markers. *J Ovarian Res*. 2015; 8:29.
- Shen J, Putt KS, Visscher DW, Murphy L, Cohen C, Singhal S, Sandusky G, Feng Y, Dimitrov DS and Low PS. Assessment of folate receptor-beta expression in human neoplastic tissues. *Oncotarget*. 2015; 6(16):14700-14709.
- Randall ME, Filiaci VL, Muss H, Spirto NM, Mannel RS, Fowler J, Thigpen JT, Benda JA and Gynecologic Oncology Group S. Randomized phase III trial of whole-abdominal irradiation versus doxorubicin and cisplatin chemotherapy in advanced endometrial carcinoma: a Gynecologic Oncology Group Study. *J Clin Oncol*. 2006; 24(1):36-44.
- Amant F and Trum H. Sentinel-lymph-node mapping in endometrial cancer: routine practice? *Lancet Oncol*. 2017; 18(3):281-282.
- Lefringhouse JR, Elder JW, Baldwin LA, Miller RW, DeSimone CP, van Nagell JR, Jr., Samoyoa LM, West DS, Dressler EV, Liu M and Ueland FR. Prospective validation of an intraoperative algorithm to guide surgical staging in early endometrial cancer. *Gynecol Oncol*. 145(1):50-54 (2017)
- Rossi EC, Kowalski LD, Scalici J, Cantrell L, Schuler K, Hanna RK, Method M, Ade M, Ivanova A and Boggess JF. A comparison of sentinel lymph node biopsy to lymphadenectomy for endometrial cancer staging (FIRE3 trial): a multicentre, prospective, cohort study. *Lancet Oncol*. 2017; 18(3):384-392.
- Beavis AL, Salazar-Marioni S, Sinno AK, Stone RL, Fader AN, Santillan-Gomez A and Tanner EJ, 3rd. Sentinel lymph node detection rates using indocyanine green in women with early-stage cervical cancer. *Gynecol Oncol*. 2016; 143(2):302-306.

23 Verbeek FP, Tummers QR, Rietbergen DD, Peters AA, Schaafsma BE, van de Velde CJ, Frangioni JV, van Leeuwen FW, Gaarenstroom KN and Vahrmeijer AL. Sentinel Lymph Node Biopsy in Vulvar Cancer Using Combined Radioactive and Fluorescence Guidance. *Int J Gynecol Cancer*. 2015; 25(6):1086-1093.

24 Yi YS. Folate Receptor-Targeted Diagnostics and Therapeutics for Inflammatory Diseases. *Immune Netw*. 2016; 16(6):337-343.

25 Puig-Kroger A, Sierra-Filardi E, Dominguez-Soto A, Samaniego R, Corcuera MT, Gomez-Aguado F, Ratnam M, Sanchez-Mateos P and Corbi AL. Folate receptor beta is expressed by tumor-associated macrophages and constitutes a marker for M2 anti-inflammatory/regulatory macrophages. *Cancer Res*. 2009; 69(24):9395-9403.

26 Wu M, Gunning W and Ratnam M. Expression of folate receptor type alpha in relation to cell type, malignancy, and differentiation in ovary, uterus, and cervix. *Cancer Epidemiol Biomarkers Prev*. 1999; 8(9):775-782.

27 van den Berg LL, Crane LM, van Oosten M, van Dam GM, Simons AH, Hofker HS and Bart J. Analysis of biomarker expression in severe endometriosis and determination of possibilities for targeted intraoperative imaging. *Int J Gynaecol Obstet*. 2013; 121(1):35-40.

28 Randomized Trial of Radiation Therapy With or Without Chemotherapy for Endometrial Cancer (PORTEC-3).

29 Boogerd LS, Boonstra MC, Beck AJ, Charehbili A, Hoogstins CE, Prevoo HA, Singhal S, Low PS, van de Velde CJ and Vahrmeijer AL. Concordance of folate receptor-alpha expression between biopsy, primary tumor and metastasis in breast cancer and lung cancer patients. *Oncotarget*. 2016; 7(14):17442-17454.

30 van Driel PB, van de Giessen M, Boonstra MC, Snoeks TJ, Keereweer S, Oliveira S, van de Velde CJ, Lelieveldt BP, Vahrmeijer AL, Lowik CW and Dijkstra J. Characterization and evaluation of the artemis camera for fluorescence-guided cancer surgery. *Mol Imaging Biol*. 2015; 17(3):413-423.

Figure 1 Representative examples of FR α expression status in endometrioid and clear cell endometrial cancer. Shown are tissue cores with respectively weak, moderate and strong intensity of FR α staining in endometrioid (A) and clear cell carcinoma (B). Magnification: 10x.



Figure 2 Fluorescence imaging of a primary uterine serous adenocarcinoma and of the metastatic lymph nodes.

- A Intraoperative identification of para-aortic, metastatic lymph nodes (dashed arrow), located beneath a layer of overlying tissue (patient #1). The normal arrow indicates the fluorescence signal arising from the uterus.
- B *Ex vivo* fluorescence imaging of the resected para-aortal lymph nodes (patient #1), that show a clear fluorescence signal.
- C *Ex vivo* fluorescence imaging of the bisected uterus (patient #1). The fluorescence signal, detected during surgery, appears to be mainly arising from normal adjacent background uterine tissue instead of the primary tumor.

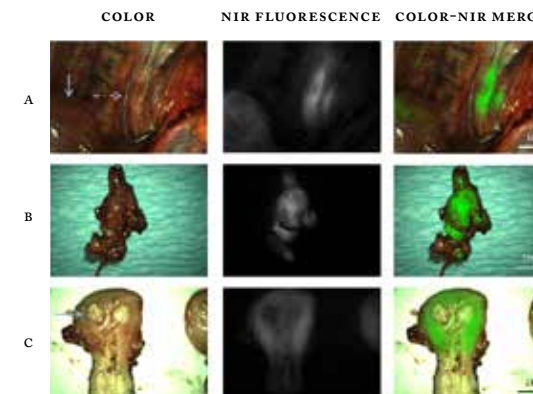


Figure 3 Histopathological evaluation of resected lesions

- A Immunohistochemical staining for FR α of a uterine tumor shows FR α expression in cancer cells (black arrow, patient #1) and in normal epithelial cells (dashed arrow). Magnification: 5x.
- B Immunohistochemical staining for FR α of non-malignant adenomyosis tissue of the uterus (patient #2). Magnification: 5x.
- C Immunohistochemical staining for FR α of a clinically suspect and fluorescent lymph node shows positive FR α expression in the lymph node follicles (patient #1). The FR α expression correlates with the presence of tumor cells. Magnification: 0.5x.
- D Immunohistochemical staining for FR α of a fluorescent omental lesion, that contained tumor cells, shows positive FR α expression (patient #4). Magnification: 2x.

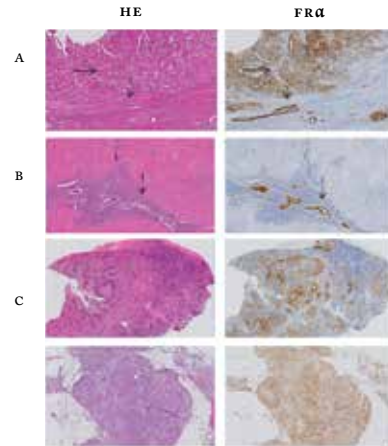


Figure 4 Histopathological evaluation of a false-positive lymph node

Shown are a NIR fluorescence image, haematoxylin & eosin (HE) staining, and FR α and FR β staining of a (fluorescent) LN that did not contain tumor cells. Fluorescence is mainly seen in the sinuses and not in the follicles. The magnified images (HE, FR α and FR β) show the lack of FR α staining, while the sinuses show a positive FR β staining. Magnifications: 1x and 10x.

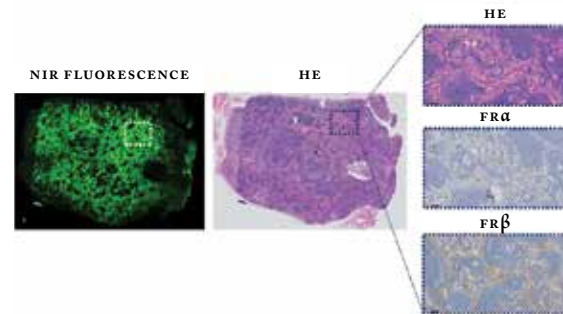


Table 1 Clinicopathologic patient characteristics in relation to FR α expression

	Total n (%)	FR α expression in tumor cells n (%)			P value
	(n=101)	absent	heterogenous	homogeneous	
Age					
<60	33 (33%)	15 (45%)	13 (39%)	5 (15%)	0.057
60-70	26 (26%)	6 (30%)	11 (42%)	9 (35%)	
>70	42 (42%)	11 (26%)	12 (29%)	19 (45%)	
FIGO stage 2009					
I	36 (36%)	15 (42%)	9 (25%)	12 (33%)	0.355
II	20 (20%)	5 (25%)	10 (50%)	5 (25%)	
III	35 (35%)	9 (26%)	13 (37%)	13 (37%)	
IV	9 (%)	3 (33%)	4 (44%)	2 (22%)	
Tumor type					
endometrioid	73 (72%)	27 (37%)	24 (33%)	22 (30%)	0.004
serous	11 (11%)	2 (18%)	1 (9%)	8 (73%)	
clear cell	17 (17%)	3 (18%)	11 (65%)	3 (18%)	
Grade					
1	11 (11%)	3 (27%)	5 (45%)	3 (27%)	0.082
2	5 (5%)	0 (0%)	1 (20%)	4 (80%)	
3	85 (84%)	29 (34%)	30 (35%)	26 (31%)	
Depth of myometrial invasion					
<50%	19 (20%)	4 (21%)	6 (32%)	9 (47%)	0.255
>50%	76 (80%)	28 (37%)	26 (34%)	22 (29%)	
Lymphovascular space invasion					
Absent	34 (40%)	15 (44%)	7 (21%)	12 (35%)	0.367
Present	48 (57%)	15 (31%)	19 (40%)	14 (29%)	
unknown	2 (2%)	1 (50%)	1 (50%)	0 (0%)	
Distant recurrence status					
Absent	67 (68%)	29 (43%)	19 (28%)	19 (28%)	0.004
Present	31 (32%)	3 (10%)	16 (52%)	12 (39%)	
Pelvic recurrence status*					
Absent	85 (88%)	29 (34%)	30 (35%)	26 (31%)	0.712
Present	12 (12%)	3 (25%)	4 (33%)	5 (42%)	
p53 status, endometrioid cancer					
Wildtype	56 (77%)	21 (38%)	20 (36%)	15 (27%)	0.472
Mutant	17 (23%)	6 (35%)	4 (24%)	7 (41%)	
p53 status, non-endometrioid cancer					
Wildtype	9 (32%)	3 (33%)	6 (67%)	0 (0%)	0.013
Mutant	19 (68%)	2 (11%)	6 (32%)	11 (100%)	

Table 2 Patient and tumor characteristics

Patient No.	Age	Type of Surgery	Diagnosis	Grade	Primary tumor in situ	Suspicion metastatic disease
1	53	Staging open surgery	Serous adenocarcinoma	III	Yes	Yes, enlarged suspect LNs
2	68	Staging laparoscopic	Serous adenocarcinoma	III	Yes	No
3	68	Staging laparoscopic	Serous adenocarcinoma	III	No	No
4	76	Cytoreduction open surgery	Clear-cell carcinoma	III	Yes	Yes, two omental lesions

LNs = lymph nodes

Table 3 Outcome of fluorescence imaging and histopathology

Patient No	Primary tumor		Lymph node		Omentum		Other biopsies	
	PA	Fluo.	PA	Fluo.	PA	Fluo.	PA	Fluo.
1	Malignant	Yes*	Malignant (16/22)**	Yes (all)	Benign	No	Benign	No
2	Malignant	Yes*	Benign	Yes (some)	Benign	No	Benign	No
3	n/a	n/a	Benign	Yes (some)	Benign	No	Benign	No
4	Malignant	Yes*	n/a	n/a	Malignant***	Yes (all)	n/a	n/a

Fluo: Fluorescent; n/a = not applicable;

* a fluorescence signal arising from the uterus was seen during surgery

** in 16/22 lymph nodes a macrometastasis was found;

*** two omental depositions were identified on preoperative imaging, but during surgery a third lesion was identified by NIR fluorescence imaging. Final histopathological analysis showed tumor cells in all three omental lesions.

CHAPTER 10

SAFETY AND EFFECTIVENESS OF SGM-101, A FLUORESCENT ANTIBODY TARGETING CARCINO-EMBRYONIC ANTIGEN, FOR INTRAOPERATIVE DETECTION OF COLORECTAL CANCER: A DOSE ESCALATION, PILOT STUDY

Lancet Gastroenterol Hepatol. 2018 Mar;3(3):181-191.

LSF BOOGERD*, CES HOOGSTINS*, DP SCHAAP, M KUSTERS, HJM HANDGRAAF, MJM VAN DER VALK, DE HILLING, FA HOLMAN, KCMJ PEETERS, JSD MIEOG, CJH VAN DE VELDE, A FARIÑA-SARASQUETA, I VAN LIJNSCHOTEN, B FRAMERY, A PÈLEGRIN, M GUTOWSKI, SW NIENHUIJS, IHJT DE HINGH, GAP NIEUWENHUIJZEN, HJT RUTTEN, F CAILLER, J BURGGRAAF AND AL VAHRMEIJER

*shared first authorship

ABSTRACT

BACKGROUND ¶ Tumour-targeted fluorescence imaging has the potential to advance current practice of oncological surgery by selectively highlighting malignant tissue during surgery. Carcinoembryonic antigen (CEA) is overexpressed in 90% of colorectal cancers and is a promising target for colorectal cancer imaging. We aimed to assess the tolerability of SGM-101, a fluorescent anti-CEA monoclonal antibody, and to investigate the feasibility to detect colorectal cancer with intraoperative fluorescence imaging.

METHODS ¶ We did an open-label, pilot study in two medical centres in the Netherlands. In the dose-escalation cohort, we included patients (aged >18 years) with primary colorectal cancer with increased serum CEA concentrations (upper limit of normal of >3 ng/mL) since diagnosis, who were scheduled for open or laparoscopic tumour resection. In the expansion cohort, we included patients (aged >18 years) with recurrent or peritoneal metastases of colorectal cancer, with increasing serum concentrations of CEA since diagnosis, who were scheduled for open surgical resection. We did not mask patients, investigators, or anyone from the health-care team. We assigned patients using a 3 + 3 dose design to 5 mg, 7.5 mg, or 10 mg of SGM-101 in the dose-escalation cohort. In the expansion cohort, patients received a dose that was considered optimal at that moment of the study but not higher than the dose used in the dose-escalation cohort. SGM-101 was administered intravenously for 30 min to patients 2 or 4 days before surgery. Intraoperative imaging was done to identify near-infrared fluorescent lesions, which were resected and assessed for fluorescence. The primary outcome was tolerability and safety of SGM-101, assessed before administration and continued up to 12 h after dosing, on the day of surgery, the first postoperative day, and follow-up visits at the day of discharge and the first outpatient clinic visit. Secondary outcomes were effectiveness of SGM-101 for detection of colorectal cancer, assessed by tumour-to-background ratios (TBR); concordance between fluorescent signal and tumour status of resected tissue; and diagnostic accuracy in both cohorts. This trial is registered with the Netherlands Trial Register, number NTR5673, and ClinicalTrials.gov, number NCT02973672.

FINDINGS ¶ Between January 2016 and February 2017, 26 patients (nine in the dose-escalation cohort and 17 in the expansion cohort) were included in this study. SGM-101 did not cause any treatment-related adverse events, although three possibly related mild adverse events were reported in three (33%) of nine patients in the

dose-escalation cohort and five were reported in three (18%) of 17 patients in the expansion cohort. Five moderate adverse events were reported in three (18%) patients in the expansion cohort, but they were deemed unrelated to SGM-101. No changes in vital signs, electrocardiogram, or laboratory results were found after administration of the maximum dose of 10 mg of SGM-101 in both cohorts. A dose of 10 mg, administered 4 days before surgery, showed the highest TBR (mean TBR 6.10 SD 0.42 in the dose-escalation cohort). In the expansion cohort, 19 (43%) of 43 lesions were detected using fluorescence imaging and were not clinically suspected before fluorescent detection, which changed the treatment strategy in six (35%) of 17 patients. Sensitivity was 98%, specificity was 62%, and accuracy of fluorescence intensity was 84% in the expansion cohort.

INTERPRETATION ¶ This study presents the first clinical use of CEA-targeted detection of colorectal cancer and shows that SGM-101 is safe and can influence clinical decision making during the surgical procedure for patients with colorectal cancer.

RESEARCH IN CONTEXT

EVIDENCE BEFORE THIS STUDY ¶¶¶ Tumour-targeted intraoperative fluorescence imaging can provide surgeons with real-time feedback about the location and extent of tumours, which might improve patient outcomes. A well-known tumour marker for colorectal cancer is carcinoembryonic antigen (CEA), which is overexpressed in the vast majority of colorectal cancer cells. Involvement of surgical margins (R+) is reported in up to 28% of primary colorectal cancer resections and up to 50% of recurrent rectal cancer resections. Moreover, 10% of patients with colorectal cancer develop peritoneal metastases, for whom cytoreductive surgery with hyperthermic intraperitoneal chemotherapy is the recommended surgical procedure. The extent of cytoreduction is directly associated with survival; therefore, maximal cytoreduction of small and otherwise undetected tumour lesions is important. CEA-targeted fluorescence imaging can be of added value in both locoregional and metastasised colorectal cancer. Our preclinical studies showed that a fluorescent anti-CEA monoclonal antibody, SGM-101, binds to CEA-positive tumours and its metastases after intravenous administration.

ADDED VALUE OF THIS STUDY ¶¶¶ This study describes the first clinical application of SGM-101 in patients with colorectal cancer for intraoperative detection of primary, recurrent, and peritoneal metastases. We showed that intravenous

administration of 10 mg of SGM-101 in patients with colorectal cancer is safe and tolerable, with the sensitivity needed to detect malignant lesions that would have otherwise been missed during surgery. Importantly, SGM-101 allowed detection of both superficially and more deeply seeded metastases. This study also suggests that intraoperative fluorescence imaging might guide surgeons to identify areas from which frozen sections should be obtained for intraoperative decision making.

IMPLICATIONS OF ALL THE AVAILABLE EVIDENCE ••• Application of CEA-targeted fluorescence imaging during colorectal cancer surgery can result in improved demarcation and detection of otherwise undetected malignant lesions. Although investigated in a small pilot study, SGM-101 can influence perioperative clinical decision making. Larger studies are needed to assess whether improved colorectal cancer detection influences R0 resection rates and results in more complete cytoreductive surgery, which should ultimately improve oncological outcomes.

INTRODUCTION

A new era in the field of near-infrared fluorescence-guided oncological surgery has commenced with the first clinical studies using tumour-specific fluorescent tracers¹. Fluorescence imaging can provide surgeons with real-time feedback about the location and extent of tumours, which might increase radical resection rates and improve patient outcomes. This technology uses clinically available monoclonal antibodies (eg, bevacizumab or cetuximab) or new tumour-specific ligands that are conjugated to a fluorophore and accumulate in tumours after intravenous administration². Subsequently, a dedicated near-infrared fluorescence imaging system enables detection of tumours in real-time during the procedure. Several tumour-targeted tracers have been tested in first-in-human studies, yielding promising results for intraoperative fluorescence detection of ovarian cancer, head and neck cancer, breast cancer, and peritoneal metastases of colorectal cancer³⁻⁶. However, no tracers have been investigated for fluorescence imaging of primary and recurrent colorectal cancer, although major advantages can be expected from this application.

The primary curative treatment for colorectal cancer is radical resection with clear margins (R0). Involvement of surgical margins (R+) is a poor prognostic factor for disease-free survival and overall survival, but is still reported in up to 28% of rectal cancer cases^{7,8}. In surgery for recurrent rectal cancer, an R0 resection is equally essential; this is generally achieved in 50-60% of cases, with 5-year survival up to 70%⁹. However, these procedures are challenging because of distorted pelvic anatomy after previous resections, the presence of multifocal tumour tissue, and

difficulty in distinction between fibrosis and tumour tissue after neoadjuvant therapy¹⁰. Globally, 10% of patients with colorectal cancer develop peritoneal metastases, for whom cytoreductive surgery with hyperthermic intraperitoneal chemotherapy is the recommended therapy, resulting in median overall survival of up to 32 months¹¹. The extent of cytoreduction is directly associated with survival; therefore, maximal cytoreduction of the numerous and often small tumour lesions is pivotal¹². With its potential to highlight small tumour lesions, tumour-targeted fluorescence-guided surgery can be of added value in both locoregional and metastasized colorectal cancer. Moreover, it could aid distinction between fibrosis and malignant tissue, which is often challenging in patients with rectal cancer who have had chemotherapy and re-irradiation or irradiation therapy.

Carcinoembryonic antigen (CEA) is a well known tumour marker and is highly expressed in colorectal cancer^{13,14}. Importantly, CEA expression in healthy tissue is on average 60 times lower than in tumour tissue, and the antigenic concentration of CEA on the surface of cancer cells is relatively high (10^5 - 10^6 antigens per cell)¹⁵. In this study, we describe SGM-101, a CEA-specific chimeric antibody conjugated to a fluorophore that emits near-infrared fluorescence. Preclinical studies showed that SGM-101 binds to CEA-positive colorectal cancer cells and its metastases after intravenous administration¹⁶. On the basis of these promising results with SGM-101, translation in a clinical study in patients with colorectal cancer is a logical next step. Therefore, in this study, we aimed to assess the tolerability of ascending doses of SGM-101 in patients with primary colorectal cancer, and to determine the best performing dose and dosing time for intraoperative fluorescence imaging. Additionally, these parameters were used in an expansion cohort of patients with colorectal cancer for intraoperative detection of recurrent tumours, including peritoneal metastases, and to assess whether SGM-101 could change patient management.

METHODS

STUDY DESIGN AND PATIENTS ••• We did an open-label, pilot study in two centres (Leiden University Medical Center, Leiden; and the Catharina Hospital Eindhoven, Eindhoven) in the Netherlands. We used a 3 + 3 dose escalating study design for those in the dose-escalation cohort only. This study was done in accordance with the Good Clinical Practice guidelines from the International Council for Harmonisation of Technical Requirements for Pharmaceuticals for Human Use, and the laws and regulations on drug research in humans of the Netherlands. The study was approved by a certified medical ethics review board (BEBO, Assen, Netherlands).

We included patients aged 18 years or older with a clinical diagnosis of primary colorectal cancer, with increased serum CEA concentrations (=upper limit of normal ULN of >3 ng/mL), who were scheduled for either open or laparoscopic surgical resection in the dose-escalation cohort. Additionally, we included patients aged 18 years or older who were diagnosed with recurrent or peritoneal metastases of colorectal cancer, with increasing serum CEA concentrations since diagnosis, and who were scheduled for open surgical resection in the expansion cohort. Staging of primary colon and rectal cancers was done according to standard protocol and included CT or MRI, or both. Staging of recurrent colon and rectal cancers, as well as peritoneal metastases, was done with use of either CT, MRI, or, when considered necessary, with PET-CT. No patients were excluded on the basis of preoperative imaging, but only patients eligible for surgical resection were included.

We excluded patients who were pregnant or breastfeeding, had a history of anaphylactic allergic reactions, had a serum CEA concentration of 300 ng/mL or more, had a diagnosis of another malignancy within the past 5 years (except adequately treated in-situ carcinoma of the cervix and basal or squamous cell skin carcinoma), and had anticancer therapy (except for routine preoperative radiotherapy for colorectal cancer) within 4 weeks before inclusion. Additionally, we excluded patients with only colorectal cancer who had abnormal laboratory test values for aspartate aminotransferase, alanine amino transferase, gamma-glutamyltransferase, or alkaline phosphatase concentrations that were more than five times the ULN; and total bilirubin concentrations more than two times the ULN. We excluded patients who had abnormal laboratory test values for serum creatinine concentrations more than 1.5 times the ULN, absolute neutrophil counts less than 1.5×10^5 cells per L, platelet counts less than 100×10^9 cells per L, or haemoglobin concentrations less than 4 mmol/L in women or 5 mmol/L in men. We also excluded patients with a known positive test for HIV infection, hepatitis B surface antigen, or hepatitis C virus antibody; patients with untreated serious infections; and those who had any condition that the investigator considered to be potentially compromising to the patients' wellbeing or the study objectives. Participants gave written informed consent to the investigators before screening to take part in the study.

PROCEDURES ••• In the dose-escalation cohort, we assigned patients using a 3 + 3 dose design to 5 mg, 7.5 mg, or 10 mg of SGM-101. In the expansion cohort, patients received a dose that was considered optimal at that moment of the study but not higher than the dose used in the dose-escalation cohort. We did not mask patients, investigators, or anyone from the health-care team and did not use placebo treatment.

SGM-101 consists of a chimeric monoclonal antibody that targets CEA covalently bound to the fluorophore BM-104. The tracer was manufactured by Novasep (Gosselies, Belgium) and supplied by Surgimab (Montpellier, France). Additional information about SGM-101 is provided in the appendix (p 1). On the basis of pre-clinical data¹⁶, a dose-escalation scheme of SGM-101 (5 mg, 7.5 mg, or 10 mg) was used (appendix p 1). We intravenously infused patients with SGM-101 for 30 min in a dedicated clinical research unit at least 2 days before surgery. Following each dose level, the collected data (ie, safety data and fluorescence intensity of tumour and background tissue using that dose of SGM-101) were reviewed jointly by the investigator and sponsor before ascending the dose level.

All surgical procedures were done by experienced oncological surgeons. First, the surgical field was explored using standard visual and tactile methods (for which tactile methods were done only during open surgery). Subsequently, the fluorescence imaging, which was done with the Artemis and Spectrum fluorescence imaging system (Quest Medical Imaging, Middenmeer, Netherlands; appendix p 1)¹⁷ was used to identify near-infrared fluorescent lesions. All lesions identified by visual and tactile methods or near-infrared fluorescence imaging were resected if it was surgically feasible and supported a clinical purpose (eg, adjustment in staging or treatment). If resection included surrounding structures, a frozen section was first assessed by an attending pathologist to confirm whether resection was needed. Each resected lesion was marked on a case report form as fluorescent or non-fluorescent, and as either clinically suspected for malignancy or not.

Following resection, fluorescence imaging of the wound bed was done to identify any remaining fluorescence. Fluorescence imaging of the resection specimen was done in the operating room and the pathology department. All resected specimens were assessed for fluorescence both before and after slicing, and localisation of fluorescence signal was recorded on macroscopic photographs. The slice containing the peak fluorescence signal of each patient undergoing surgery at the Leiden University Medical Center was additionally imaged with the Pearl imager (LI-COR Biosciences, Lincoln, NE, USA) to obtain ex-vivo tumour-to-background ratios (TBRs).

Additionally, we did tolerability assessments (ECG, blood pressure, pulse, peripheral oxygen saturation, respiratory rate, and temperature) at regular intervals starting directly before administration and continued up to 12 h after dosing. We repeated these measurements on the day of surgery, the first postoperative day, and the day of discharge from the hospital. Follow-up visits coinciding with clinical care took place at the day of discharge and the first outpatient clinic visit. Additionally, we recorded adverse events and the concomitant use of other medications throughout the study

period. We also collected blood samples from participating patients before and after dosing of SGM-101, and serum CEA concentrations were measured in these samples.

An experienced board-certified gastrointestinal pathologist did routine assessment of tumour status on all resected lesions following haematoxylin and eosin staining. The histopathological examination was considered the reference standard. Tumour status was correlated with the status of fluorescence, and immunohistochemistry staining was done to directly correlate CEA expression to fluorescence signal in formalin-fixed paraffin-embedded (FFPE) blocks with use of the Pearl imager (appendix pp 2, 3). A fluorescent lesion that was tumour positive was considered a true positive, a fluorescent lesion that was tumour negative was considered a false positive, and a non-fluorescent lesion that was tumour positive was considered a false negative. Using these classifications, we also evaluated sensitivity, which was calculated by dividing the number of true-positive lesions by the total number of resected tumour lesions; and specificity, which was calculated by dividing the true negative lesions by the total number of resected lesions without tumour involvement. Additionally, we evaluated the positive predictive value, which was calculated by dividing the number of true positives by the total number of true and false positives; and the negative predictive value, which was calculated by dividing the true-negative lesions by the total number of true and false-negative lesions.

OUTCOMES ••• The primary outcome was tolerability and safety of SGM-101, which was assessed with the use of routine clinical measures such as treatment-related adverse events, blood pressure, heart rate, body temperature, peripheral oxygen saturation, respiratory rate, skin examination, and routine laboratory assessments. Treatment-related adverse events were defined as any adverse event associated with the study procedure but not necessarily related to the study intervention (ie, SGM-101) for up to 10 days after surgery, using the National Cancer Institute Common Terminology Criteria for Adverse Events (version 4.03). Secondary outcomes were effectiveness of SGM-101 for detection of colorectal cancer, assessed by TBRs, concordance between fluorescent signal and tumour status of resected tissue, and diagnostic accuracy. Additionally, the amount of injected SGM-101 that was lost by binding to serum CEA was calculated by measuring serum CEA directly and after dosing in both cohorts.

STATISTICAL ANALYSIS ••• Due to the exploratory nature of this study, sample size was not based on statistical power considerations. TBR for fluorescence is reported as mean and SD. Patient characteristics are reported as median and IQR.

Fluorescence in tumour and normal tissues, measured on FFPE tissue blocks with the Pearl imager, was compared with the paired, non-parametric t test (ie, Wilcoxon rank test). A p value of less than 0.05 was considered significant. Data are summarised in a bar chart (mean range) and box plot (median IQR). Patients in the dose-escalation cohort were included in the primary analysis. Patients in the expansion cohort were analysed separately. We did all statistical analyses and generated graphs using GraphPad Prism (version 7.0)

This trial is registered with the prospective Dutch trial registry (Nederlands Trial Register), number NTR5673, and ClinicalTrials.gov, number NCT02973672.

ROLE OF THE FUNDING SOURCE ••• The study was designed by the investigators and approved by the sponsor, Surgimab. The funder of the study had no role in data collection, data analysis, data interpretation, or writing of the report. The corresponding author had full access to all the data in the study and had final responsibility for the decision to submit for publication.

RESULTS

Between January, 2016, and February, 2017, 26 patients were included in this study. Nine patients were included in the dose-escalation cohort and 17 patients were included in the expansion cohort. In two patients from the expansion cohort, the planned surgery was aborted because of unexpected tumour ingrowth in the anal sphincter in one of the patients who wanted only sphincter-saving surgery, and a high peritoneal carcinomatosis index in the other patient who was planned for cytoreductive surgery with hyperthermic intraperitoneal chemotherapy. Despite abortion of the surgical procedures, fluorescence imaging in the first patient was successfully done via transanal inspection with a laparoscope and in the second patient during exploratory laparotomy. Table 1 summarises the patient characteristics, surgical procedures, and histopathology results.

No serious adverse events were reported in the dose-escalation cohort of patients with primary colorectal cancer. Three possibly related mild adverse events were noted in three (33%) of nine patients in the dose-escalation cohort and five possibly related mild adverse events were reported in three (18%) of 17 patients in the expansion cohort. In the expansion cohort, five moderate adverse events were reported in three (18%) of 17 patients that were all regarded unrelated to the dosing of SGM-101 (Table 2). The most common serious adverse events were infections (three 60% of five events), paralytic ileus (one 20%), and pyelonephritis (one 20%). No changes in

vital signs, electrocardiogram, or laboratory results were found after administration of the maximum dose of 10 mg of SGM-101 in both cohorts.

The molecular weight of CEA is 2×10^5 Da and SGM-101 is 1.5×10^5 Da. The biggest change in serum CEA concentration before and after dosing was 40 µg/L. Considering a circulating blood volume of 5 L, this change means a total circulating amount of 200 µg (ie, 1.2×10^{20} Da or 6×10^{14} U). The total amount of injected SGM-101 was 5 mg (ie, 3×10^{21} Da or 2×10^{16} U). Thus, the amount of SGM-101 lost by binding to circulating CEA was 3%.

Of the nine patients in the dose-escalation cohort, the first three patients received a dose of 5 mg of SGM-101, administered 2 days before surgery. Because of substantial background fluorescence, probably as a consequence of high concentrations of the tracer in the systemic circulation, the interval between dosing and imaging was prolonged to 4 days. The next three patients received a dose of 7.5 mg, administered 4 days before surgery. The mean TBR of the resected specimens was 4.70 (SD 0.99) in the 5 mg dose group compared with 5.70 (SD 1.27) in the 7.5 mg dose group. Hence, the dose was further increased and the three subsequent patients received a dose of 10 mg, resulting in a mean TBR of 6.10 (SD 0.42). Separate tumour and background signals per dose group are shown in Figure 1A.

Fluorescence imaging was used to detect malignant lesions in three patients with colon adenocarcinomas and six patients with rectal adenocarcinomas, including two pathological complete responders. In four of nine patients, a fluorescent signal arising from the primary tumour could be detected during surgery with a mean TBR of 1.83 (SD 0.25; Table 3). These signals were all from three colon tumours (figures 2A, 2C) and one rectal tumour that was located near the anal verge and detected with transanal fluorescence imaging (TBR 1.52). The remaining five patients' rectal tumours could not be detected by intraoperative fluorescence imaging of the surgical field. Three of these rectal tumours showed a clear fluorescent signal during ex-vivo imaging of the sliced specimen (figures 3A, 3B). The last two specimens showed no fluorescence, which were confirmed as pathological complete responses by histopathological analysis.

Six metastases were detected with fluorescence imaging (mean TBR 1.74, SD 0.32): four colorectal liver metastases, one lymph node metastasis, and one omental lesion (figures 2B, 2D). All thirteen malignant primary and metastatic lesions showed co-localisation of fluorescence with CEA overexpression and tumour cells (Figure 3C). Immunohistochemistry staining of tumour tissues showed that CEA expression was strong in 80–100% of all tumour cells. Two false-positive fluorescent lesions were identified during surgery (mean TBR 1.62, SD 0.11): one lesion was classified as dysplasia of the urothelial lining of the bladder and one as a peritoneal lesion consisting

of particles of blue ink, caused by perforation of the bowel wall during endoscopic marking of the tumour. None of these lesions displayed CEA expression with immunohistochemistry staining. The diagnostic accuracy is shown in Figure 1B.

In the expansion cohort, the first patient received a dose of 5 mg of SGM-101 and the second patient received a dose of 7.5 mg, administered 2 days before surgery. The other 15 patients received a dose of 10 mg, 4 days before surgery. 44 malignant lesions were resected in 17 patients, of which 43 were fluorescent with a mean intraoperative TBR of 1.64 (SD 0.27; Table 3). The non-fluorescent malignant lesion was identified with a random biopsy during intraoperative analysis of a resection margin. Additional histopathological analysis of the part of the rectum where the biopsy was taken showed a microscopic metastasis in the fatty tissue with strong CEA expression.

In the expansion cohort, 19 (44%) of the 43 malignant lesions were only identified with fluorescence imaging and were not clinically suspected before fluorescent detection. Fluorescent tumour hotspots were located both superficially (eg, tumour spots in the bowel mesentery or ovary) and deeply (eg, retroperitoneal lymph nodes; Figure 4). 13 (68%) of the 19 lesions were detected in two patients undergoing cytoreductive surgery, followed by hyperthermic intraperitoneal chemotherapy. The other six (32%) additional malignant fluorescent hotspots were identified in four patients undergoing resection of recurrent colorectal cancer, mostly detected after resection of the tumour specimen at the pelvic wall. The original treatment strategy was altered in six (35%) of 17 patients because of intraoperative fluorescent detection of additional, otherwise undetected, malignant tissue.

Three (18%) of 17 patients had a pathological complete response after preoperative chemoradiotherapy. In two of these three patients, a fluorescent signal was still identified at the location of the suspected tumour (mean TBR 1.67, SD 0.19). One patient had a tumour mass near the left ovary, which appeared as an abscess during surgery. Both the abscess wall and abscess cavity were fluorescent during surgery, but did not contain malignant cells and were not CEA positive by immunohistochemical staining. The other patient with a pathological complete response had a tumour mass of 24 mm in diameter near the left iliopsoas muscle, which could be clearly identified during ex-vivo fluorescence imaging. Histopathological analysis revealed extensive necrosis, with mucin-producing cells that were positive for CEA, and scar tissue. Of the 14 patients with a malignancy, 13 had an intestinal-type adenocarcinoma. All these malignancies showed co-localisation of fluorescence and CEA expression on the malignant cells, with strong CEA staining. One patient had a poorly differentiated sarcomatous adenocarcinoma of the sacral bone; although the tumour was fluorescent during ex-vivo imaging (TBR 1.68), no CEA expression was found.

Ten false-positive lesions were identified with a mean TBR of 1.62 (SD 0.27), including lymph nodes, tissue adhered to the bowel, and at the rectal wall (marked during ex-vivo fluorescence imaging). Some CEA positivity was found in histiocytes within lymph nodes, as well as in fibrotic and chronic inflamed tissue. However, four (80%) of five assessed false-positive lesions did not show CEA expression. Ex-vivo analysis of FFPE blocks of all resected tissues from the expansion cohort showed a significantly higher fluorescence intensity in tumour tissue than in normal tissue (mean 0.51 SD 0.43 vs 0.24 SD 0.19; $p < 0.0001$; Figure 1C).

DISCUSSION

This study shows that intravenous administration of the CEA-specific near-infrared fluorescent tracer SGM-101 is safe, and provides successful detection of primary and recurrent colorectal cancer as well as peritoneal metastases. Intraoperative fluorescence imaging led to detection of otherwise undetected malignant tissue causing the treatment strategy to be altered in about a third of patients. Importantly, SGM-101 did not only identify superficially located cancer tissues (eg, small metastases in the omentum or bowel mesentery) but also identified more deeply seeded metastases (eg, retroperitoneal or para-aortic lymph nodes).

CEA is considered a favourable tumor target for colorectal cancer imaging^{14,18}, because it is highly expressed on colorectal cancer tissue, and importantly, expression patterns in rectal cancer are not modified after preoperative chemoradiotherapy¹⁹. However, CEA has several disadvantages as a tumour target, including expression on normal epithelium and the weak anchorage of CEA to the cell membrane. This weak anchorage results in shedding of soluble CEA into the bloodstream, which could serve as a scavenger source when injecting a CEA-targeted imaging agent. By measuring serum CEA concentrations in patients before and directly after dosing of SGM-101, we could conclude that 3% of the administered dose of SGM-101 was lost by binding to circulating CEA. Hence, almost all the injected probe was available for tumour targeting. The upper limit of circulating serum CEA concentration (300 ng/mL) as an exclusion criterion could therefore be abandoned in future studies. Assuming that increased concentrations of serum CEA represent upregulation of this marker in colorectal cancer tissue, serum CEA measurements were initially thought to benefit patient selection. However, a recent study²⁰ showed that 32 of 35 rectal cancer tissues showed intense CEA expression independent of the concentration of preoperative serum CEA. In the expansion cohort, this inclusion criterion was therefore adjusted, and patients with increasing serum CEA concentrations since diagnosis were also considered eligible. Although normal expression of CEA on the

healthy epithelium could be disadvantageous, this factor did not hinder discrimination between tumour and healthy tissue.

Histopathological analysis showed that some of the false-positive lesions detected contained mucin-producing cells, which express CEA. These lesions were only detected in patients with rectal cancer who had undergone re-irradiation, suggesting a relationship. Future immunohistochemistry studies should clarify the correlation between CEA expression and the subtype of colorectal cancer that contains mucin-producing cells or the effect of re-irradiation, or both. There are several hypotheses about why false-positive lesions appeared fluorescent during surgery. First, although the use of light in the near-infrared spectrum (700–900 nm) is associated with minimal auto fluorescence, it is plausible that collagen-rich structures, calcified spots, or the sacral bone could have caused false-positive fluorescence as a consequence of autofluorescence properties. Secondly, the enhanced permeability and retention effect, which results in accumulation of macromolecules (eg, SGM-101) as a consequence of hypervascularity and impaired lymphatic drainage, could play a part in false positivity^{21,22}. This effect is also considered the most likely cause for accumulation of indocyanine green in peritoneal metastases. Indocyanine green is a clinically available near-infrared fluorescent tracer and has been studied for intraoperative detection of peritoneal metastases of colorectal cancer and ovarian cancer^{23,24}. However, this tracer does not specifically bind to tumour cells and, importantly, small peritoneal metastases (<2 mm) are still avascular and not possible to detect via the enhanced permeability and retention effect²⁵. In an attempt to improve specificity, Harlaar and colleagues⁶ did a pilot study using a VEGF-A-targeting tracer in seven patients undergoing cytoreductive surgery for peritoneal metastases; although a high sensitivity was reported, specificity was only 53%.

The current dose-escalation study was done in patients with primary colorectal cancer. However, in both the dose-escalation and expansion cohorts, the time of administration of SGM-101 between the dosing groups differed - eg, the 5 mg dosing group was done 2 days before surgery, compared with 4 days before surgery in the 7.5 mg and 10 mg dosing groups in the dose-escalation cohort, possibly hampering a fair comparison. Moreover, the maximum tested dose was 10 mg of SGM-101, which did not cause any related adverse events. Higher dose concentrations need to be assessed in upcoming studies to investigate whether higher TBRs can be obtained while maintaining the good safety profile. Furthermore, not all tumours could be intraoperatively visualised. In three patients with rectal cancer and cT1-2 tumours, a fluorescence tumour signal was only visible after slicing of the resected specimen. Although use of near-infrared light allows detection of structures up to 1 cm in depth, the layer of mesorectum is apparently too thick to penetrate. In our opinion,

CEA-targeted fluorescence imaging during colorectal cancer surgery is therefore mainly useful to detect local and distant metastases, as well as locally advanced rectal cancers. Nonetheless, ex-vivo detection of a tumour-specific fluorescent signal underlines the potential added value of SGM-101 during transanal endoscopic microsurgery. Although different optical properties apply to the endoscopic situation compared with ex-vivo fluorescence imaging - eg, scattering and absorption of surrounding tissues - our results suggest that fluorescence imaging could improve the limited sensitivity of endoscopic assessment for residual tumour detection²⁶. The absence of fluorescence in two resected specimens with a pathological complete response underlines the role of SGM-101 application during watch-and-wait strategies after neoadjuvant treatment²⁷.

In the expansion cohort, patients with recurrent colorectal cancer and peritoneal metastases of colorectal cancer were included. Although a high sensitivity was reported, ten false-positive lesions were detected. An important lesson to bear in mind is that before substantial resections are done, frozen sections should be taken to ensure that there is no false positivity. SGM-101 can help surgeons to identify areas from which frozen sections should be obtained, which is normally very random without intraoperative imaging. The high negative predictive value indicates that if there is no fluorescence, there is no tumour if it is also clinically unsuspected. However, more deeply seeded tumours can be visualised only when the targeted area is first properly exposed. Targeted dual-modality imaging is currently being investigated to overcome the paucity of depth penetration of near-infrared light. This technique provides preoperative tumour detection through PET or single-photon emission CT imaging and intraoperative guidance towards deeper located targets via fluorescence imaging and the radioactive label. A recent preclinical study showed accurate preoperative and intraoperative detection of pulmonary micrometastases after intravenous administration of a dual-labelled CEA-targeted antibody²⁸.

Although there has been a rapid increase in the number of clinical trials using fluorescence imaging for cancer screening and detection, several barriers must be overcome before the technique can be widely used in everyday clinical practice². Besides funding and awareness, the translational process of tumour-targeted probes such as SGM-101 is a time consuming process with challenging regulatory affairs²⁹. Most importantly, not all currently available imaging devices have similar detection limits, which results in a scarcity of a fair comparison between these different systems, hampering reproducibility. A potential method to improve intraoperative distinction between malignant and non-malignant tissue might be the use of cutoff values - eg, the use of threshold by calculation of fluorescence with use of phantoms or reference standards^{30,31}. More research is needed to objectively compare imaging

devices and to determine the minimal amount of tumour cells that can be detected using a specific device³².

In conclusion, we showed that intravenous administration of SGM-101 is safe and provides successful detection of primary, recurrent, and metastasised colorectal cancer, leading to an altered treatment strategy in about a third of patients. Because completeness of tumour resection is associated with increased survival, SGM-101 could potentially improve the clinical outcome of patients undergoing surgery for colorectal cancer, including cytoreductive surgery and hyperthermic intraperitoneal chemotherapy. However, the results from this study have to be interpreted cautiously because of the small population and heterogeneity in doses and timing of fluorescence imaging after dosing. A larger clinical study is needed to assess whether these changes in the operative procedure might influence radical resection rates and completeness of cytoreductive surgery, which could ultimately result in improved local control and overall survival.

REFERENCES

- 1 Zhang RR, Schroeder AB, Grudzinski JJ, et al. Beyond the margins: real-time detection of cancer using targeted fluorophores. *Nat Rev Clin Oncol* 2017; 14: 347-64.
- 2 Tipirneni KE, Warram JM, Moore LS, et al. Oncologic procedures amenable to fluorescence-guided surgery. *Ann Surg* 2017; 266: 36-47.
- 3 van Dam GM, Themelis G, Crane LM, et al. Intraoperative tumor-specific fluorescence imaging in ovarian cancer by folate receptor- α targeting: first in-human results. *Nat Med* 2011; 17: 1315-19.
- 4 Rosenthal EL, Warram JM, de Boer E, et al. Safety and tumor specificity of cetuximab-IRDYE800 for surgical navigation in head and neck cancer. *Clin Cancer Res* 2015; 21: 3658-66.
- 5 Lamberts LE, Koch M, de Jong JS, et al. Tumor-specific uptake of fluorescent bevacizumab-IRDye800CW microdosing in patients with primary breast cancer: a phase I feasibility study. *Clin Cancer Res* 2017; 23: 2730-41.
- 6 Harlaar NJ, Koller M, de Jongh SJ, et al. Molecular fluorescence-guided surgery of peritoneal carcinomatosis of colorectal origin: a single-centre feasibility study. *Lancet Gastroenterol Hepatol* 2016; 1: 283-90.
- 7 Nagtegaal ID, Quirke P. What is the role for the circumferential margin in the modern treatment of rectal cancer? *J Clin Oncol* 2008; 26: 303-12.
- 8 Gravante G, Hemingway D, Stephenson JA, et al. Rectal cancers with microscopic circumferential resection margin involvement (Rt resections): survivals, patterns of recurrence, and prognostic factors. *J Surg Oncol* 2016; 114: 642-48.
- 9 Holman FA, Bosman SJ, Haddock MG, et al. Results of a pooled analysis of IORT containing multimodality treatment for locally recurrent rectal cancer: results of 565 patients of two major treatment centres. *Eur J Surg Oncol* 2017; 43: 107-17.
- 10 Dresen RC, Kusters M, Daniels-Goozen AW, et al. Absence of tumor invasion into pelvic structures in locally recurrent rectal cancer: prediction with preoperative MR imaging. *Radiology* 2010; 256: 143-50.
- 11 Razenberg LG, van Gestel YR, Creemers GJ, Verwaal VJ, Lemmens VE, de Hingh IH. Trends in cytoreductive surgery and hyperthermic intraperitoneal chemotherapy for the treatment of synchronous peritoneal carcinomatosis of colorectal origin in the Netherlands. *Eur J Surg Oncol* 2015; 41: 466-71.
- 12 Sugarbaker PH, Ryan DP. Cytoreductive surgery plus hyperthermic perioperative chemotherapy to treat peritoneal metastases from colorectal cancer: standard of care or an experimental approach? *Lancet Oncol* 2012; 13: e362-69.
- 13 Hammarstrom S. The carcinoembryonic antigen (CEA) family: structures, suggested functions and expression in normal and malignant tissues. *Semin Cancer Biol* 1999; 9: 67-81.
- 14 Tiernan JP, Perry SL, Verghese ET, et al. Carcinoembryonic antigen is the preferred biomarker for in vivo colorectal cancer targeting. *Br J Cancer* 2013; 108: 662-67.
- 15 Boonstra MC, de Geus SW, Prevoo HA, et al. Selecting targets for tumor imaging: an overview of cancer-associated membrane proteins. *Biomark Cancer* 2016; 8: 119-33.
- 16 Gutowski M, Framery B, Boonstra MC, et al. SGM-101: an innovative near-infrared dye-antibody conjugate that targets CEA for fluorescence-guided surgery. *Surg Oncol* 2017; 26: 153-62.
- 17 van Driel PB, van de Giessen M, Boonstra MC, et al. Characterization and evaluation of the artemis camera for fluorescence-guided cancer surgery. *Mol Imaging Biol* 2015; 17: 413-23.
- 18 van Oosten M, Crane LM, Bart J, van Leeuwen FW, van Dam GM. Selecting potential targetable biomarkers for imaging purposes in colorectal cancer using Target Selection Criteria (TASC): a novel target identification tool. *Transl Oncol* 2011; 4: 71-82.
- 19 Boogerd L, van der Valk M, Boonstra M, et al. Biomarker expression in rectal cancer tissue before and after neoadjuvant therapy. *Oncol Targets Ther* 2018; 23: 11655-1664.
- 20 Boogerd L, Vuijk FA, Hoogstins C, et al. Correlation between preoperative serum carcinoembryonic antigen levels and expression on pancreatic and rectal cancer tissue. *Biomark Cancer* 2017; 9: 1179299X1710016.
- 21 Maeda H, Wu J, Sawa T, Matsumura Y, Hori K. Tumor vascular permeability and the EPR effect in macromolecular therapeutics: a review. *J Control Release* 2000; 65: 271-84.
- 22 Matsumura Y, Maeda H. A new concept for macromolecular therapeutics in cancer chemotherapy: mechanism of tumoritropic accumulation of proteins and the antitumor agent smans. *Cancer Res* 1986; 46: 6387-92.
- 23 Liberale G, Vankerckhove S, Caldron MG, et al. Fluorescence imaging after indocyanine green injection for detection of peritoneal metastases in patients undergoing cytoreductive surgery for peritoneal carcinomatosis from colorectal cancer: a pilot study. *Ann Surg* 2016; 264: 1110-15.
- 24 Tummers QR, Hoogstins CE, Peters AA, et al. The value of intraoperative near-infrared fluorescence imaging based on enhanced permeability and retention of indocyanine green: feasibility and false-positives in ovarian cancer. *PLoS One* 2015; 10: e0129766.
- 25 Bergers G, Benjamin LE. Tumorigenesis and the angiogenic switch. *Nat Rev Cancer* 2003; 3: 401-10.
- 26 Kawai K, Ishihara S, Nozawa H, et al. Prediction of pathological complete response using endoscopic findings and outcomes of patients who underwent watchful waiting after chemoradiotherapy for rectal cancer. *Dis Colon Rectum* 2017; 60: 368-75.
- 27 Renehan AG, Malcomson L, Emsley R, et al. Watch-and-wait approach versus surgical resection after chemoradiotherapy for patients with rectal cancer (the OnCoRe project): a propensity-score matched cohort analysis. *Lancet Oncol* 2016; 17: 174-83.
- 28 Hekman MC, Rijkema M, Bos DL, et al. Detection of micrometastases using SPECT/fluorescence dual-modality imaging in a CEA-expressing tumor model. *J Nucl Med* 2017; 58: 706-10.
- 29 Tummers WS, Warram JM, Tipirneni KE, et al. Regulatory aspects of optical methods and exogenous targets for cancer detection. *Cancer Res* 2017; 77: 2197-206.
- 30 Burggraaf J, Kamerling IM, Gordon PB, et al. Detection of colorectal polyps in humans using an intravenously administered fluorescent peptide targeted against c-MET. *Nat Med* 2015; 21: 955-61.
- 31 Zhu B, Rasmussen JC, Sevcik-Muraca EM. A matter of collection and detection for intraoperative and non-invasive near-infrared fluorescence molecular imaging: to see or not to see? *Med Phys* 2014; 41: 022105.
- 32 Prince AC, Jani A, Korb M, et al. Characterizing the detection threshold for optical imaging in surgical oncology. *J Surg Oncol* 2017; Dec; 116(7): 898-906

Figure 1 Outcomes of fluorescence imaging in the dose-escalation and expansion cohort

- A Mean fluorescence intensity of tumour and background tissue per dose group of SGM-101 in the dose-escalation cohort. Error bars are the maximum fluorescence intensity measured.
- B Sensitivity, specificity, PPV, NPV, and accuracy of fluorescence imaging in the dose-escalation cohort. All resected tissues (either detected with visual inspection or with fluorescence imaging) were included in this analysis.
- C Mean fluorescence intensity of all resected lesions in the expansion cohort. On the basis of corresponding haematoxylin and eosin and CEA staining, regions of interest were drawn on fluorescent images and fluorescence between tumour and normal tissues was compared. The horizontal line in the box is the median fluorescence signal. The box refers to 50% of scores. Error bars are ranges.
- D Sensitivity, specificity, PPV, NPV, and accuracy of fluorescence imaging in the expansion cohort. All resected tissues (either with visual inspection or with fluorescence imaging) were included in this analysis. AU=arbitrary unit. N=total number of resected lesions. PPV=positive predictive value. NPV=negative predictive value. CEA=carcinoembryonic antigen

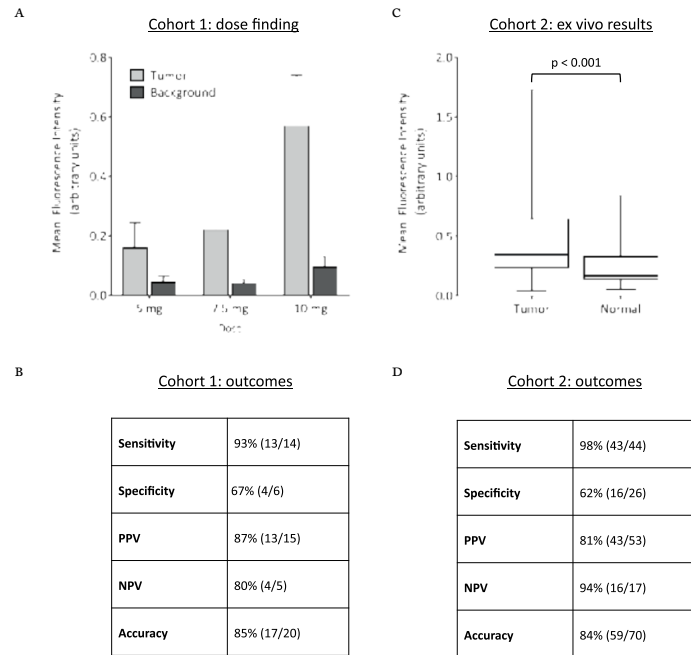


Figure 2 In-vivo and ex-vivo fluorescence imaging of a sigmoid cancer and synchronous liver metastasis

- A Intraoperative fluorescence imaging resulted in clear fluorescence detection of the primary tumour in the sigmoid.
- B Fluorescence detection of a synchronous liver metastasis.
- C Ex-vivo analysis of the primary sigmoidal cancer.
- D Ex-vivo analysis of the slices containing the liver metastasis, showing co-localisation of fluorescence with visual tumour location.

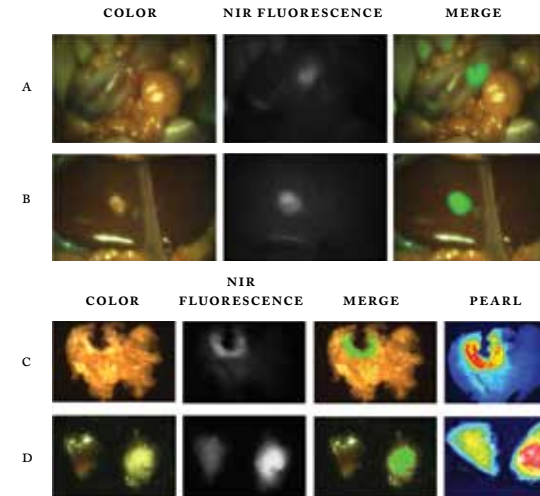


Figure 3 Ex-vivo fluorescence imaging of a primary rectal cancer

- A In this specimen (pT2), rectal cancer could not be detected during surgery. After cutting of the specimen, a clear fluorescent signal appeared.
- B Corresponding tumour slice, showing a fluorescence signal on the inside of the rectal wall.
- C Histopathological analysis of a tumour slice, showing co-localisation of tumour cells, CEA expression, and fluorescence. CEA=carcinoembryonic antigen.

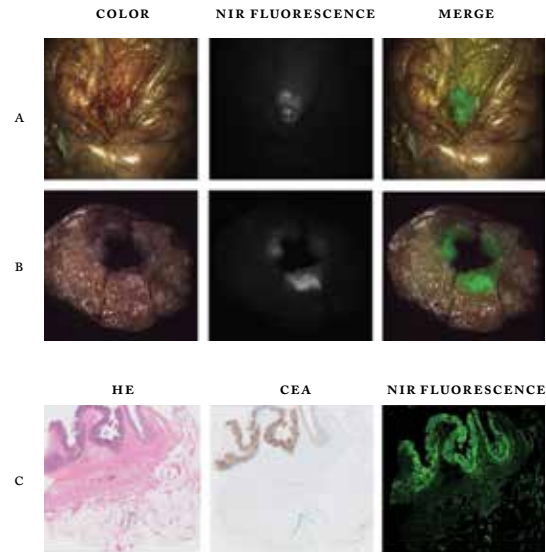


Figure 4 Intraoperative fluorescence detection of additional, otherwise undetected, metastases of colorectal cancer.

- A Identification of a fluorescent hotspot in the bowel mesentery, which was confirmed to contain malignant cells by frozen section analysis.
- B Intraoperative identification of two small additional fluorescent tumour hotspots in the omentum.
- C Intense fluorescence signal shown in the right ovary. Although the surgeon doubted if the ovary contained tumour cells, histopathological analysis revealed involvement of tumour cells.
- D Intraoperative fluorescence detection of retroperitoneal lymph nodes. Even below a layer of overlying tissue, metastasised lymph nodes can still be detected.

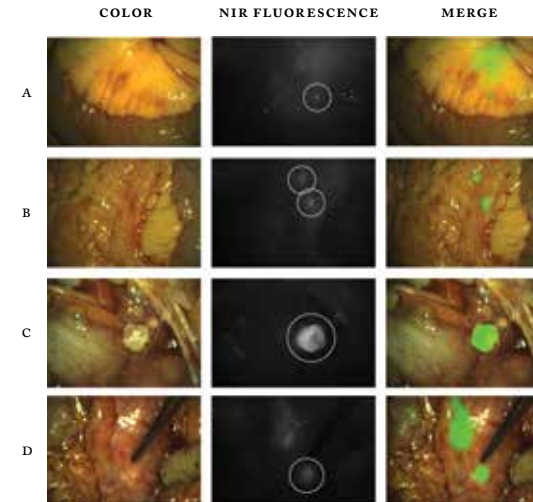


Table 1 Patient and tumour characteristics

	Dose-escalation cohort (N=9)	Expansion cohort (N=17)
Sex		
Men	5 (56%)	10 (59%)
Women	4 (44%)	7 (41%)
Age, median (range)	69 (65 - 72)	62 (55 - 67)
Median preoperative concentration of serum CEA (IQR;ng/mL)	4.0 (3.0 - 5.6)	4.3 (1.9 - 19.7)
Neoadjuvant therapy		
Yes	6 (67%)	14 (82%)
No	3 (33%)	3 (18%)
Type of surgery		
Abdominoperineal resection	2 (22%)	N/A
Low anterior resection	4 (44%)	N/A
Sigmoid resection	2 (22%)	N/A
Hemicolectomy	1 (11%)	N/A
Tumour recurrence locations		
Anastomotic recurrence	n/a	2 (12%)
Lateral recurrence*	n/a	3 (18%)
Unifocal recurrence elsewhere**	n/a	4 (24%)
Multifocal recurrence in small pelvis	n/a	4 (24%)
Peritoneal recurrence	n/a	4 (24%)
Method of surgery		
Open	4 (44%)	16 (94%)
Laparoscopic	4 (44%)	0
Transanal inspection	1 (11%)	1 (6%)
Additional intraoperative therapy		
Liver resection	1 (11%)	0
Intraoperative radiotherapy	0	10 (59%)
Hyperthermic intraperitoneal chemotherapy	0	4 (24%)
Tumour stage		
T0	2 (22%)	N/A
T1	1 (11%)	N/A
T2	1 (11%)	N/A
T3	5 (56%)	N/A
T4	0	N/A
Nodal stage		
N0	5 (56%)	N/A
N1	2 (22%)	N/A
N2	2 (22%)	N/A

Data are n (%), unless otherwise specified. CEA = carcinoembryonic antigen; NA = not applicable

* Tumours defined as a lateral recurrence were located in the obturator compartment or around the iliac vessels.

** Tumours defined as a unifocal recurrence elsewhere in the abdomen were located near the duodenal curve, between the bladder and prostate, in the rectovaginal septum or near the left iliopsoas muscle

Table 2

Dose escalation cohort	System organ class	Preferred term	Severity	Serious adverse event	Relationship to SGM-101	Occurrence
5.0 mg of SGM-101						
Patient 1						
day 3	Skin and subcutaneous disorders	Scar pain	Mild	No	Unrelated	Single occasion
day 6	Gastrointestinal disorders	Paralytic ileus	Mild	No	Unrelated	Single occasion
day 8	General disorders and administration site conditions	Pyrexia	Mild	No	Unrelated	Single occasion
day 17	Gastrointestinal disorders	Proctalgia	Mild	No	Unrelated	Single occasion
Patient 2						
day 4	Gastrointestinal disorders	Nausea	Mild	No	Unrelated	Single occasion
Patient 3						
day 20	Metabolism	Dehydration	Mild	No	Unrelated	Single occasion
7.5 mg of SGM-101						
Patient 4						
day 1	Skin and subcutaneous disorders	Rash	Mild	No	Possible	Intermittent
day 5	Undetermined	stirs	Moderate	No	Unrelated	Single occasion
day 6	Vascular disorders	Orthostatic-hypotension	Mild	No	Unrelated	Intermittent
Patient 5						
day 6	Gastrointestinal disorders	Nausea	Mild	No	Unrelated	Single occasion
10 mg of SGM-101						
Patient 7						
day 1	Nervous system disorders	Headache	Mild	No	Possible	Single occasion
day 4	Injury, poisoning, and procedural complications	Phlebitis	Mild	No	Unrelated	Intermittent
day 6	Gastrointestinal disorders	Nausea	Mild	No	Unrelated	Single occasion
Patient 8						
day 1	Gastrointestinal disorders	Abdominal discomfort	Mild	No	Possible	Intermittent
day 6	Musculoskeletal and connective tissue disorders	Muscle tightness	Mild	No	Unrelated	Single occasion
Patient 9						
day 1	Musculoskeletal and connective tissue disorders	Finger deformity	Mild	No	Unrelated	Single occasion
day 8	Cardiac disorders	Atrial-fibrillation	Mild	No	Unrelated	Single occasion
day 9	Skin and subcutaneous disorders	Decubitus ulcer	Mild	No	Unrelated	Single occasion
day 12	Infections	Wound infection	Mild	No	Unrelated	Single occasion

(continuation on next page)

Table 2 (continuation of previous page)

Expansion cohort	System organ class	Preferred term	Severity	Serious adverse events	Relationship to SGM-101	Occurrence
5.0 mg of SGM-101						
Patient 1						
day 3	Injury, poisoning and procedural complications	Scratch	Mild	No	Unrelated	Single occasion
day 5	Gastrointestinal disorders	Nausea	Mild	No	Unrelated	Intermittent
day 6	Vascular disorders	Scrotal haematoma	Mild	No	Unrelated	Single occasion
day 12	Gastrointestinal disorders	Paralytic ileus	Moderate	No	Unrelated	Single occasion
day 15	Infections	Urinary tract infection	Mild	No	Unrelated	Single occasion
day 23	Injury, poisoning and procedural complications	Renal injury	Moderate	Yes	Unrelated	Single occasion
7.5 mg of SGM-101						
Patient 2						
day 5	General disorders and administration site conditions	Flank pain	Mild	No	Unrelated	Single occasion
10 mg of SGM-101						
Patient 4						
day 6	Infections	Urinary tract infection	Mild	No	Unrelated	Single occasion
Patient 5						
day 28	Infections	Pyelonephritis	Moderate	No	Unrelated	Single occasion
Patient 7						
day 1	Nervous system disorders	Headache	Mild	No	Possible	Single occasion
Patient 9						
day 7	Infections	Urinary tract infection	Mild	No	Unrelated	Single occasion
Patient 11						
day 8	Infections	Pneumonia	Moderate	Yes	Unrelated	Single occasion
day 19	Infections	Abscess	Moderate	Yes	Unrelated	Single occasion
Patient 13						
day 1	Gastrointestinal disorders	Abdominal discomfort	Mild	No	Possible	Intermittent
day 1	Vascular disorders	Dizziness	Mild	No	Possible	Single occasion
day 1	Gastrointestinal disorders	Nausea	Mild	No	Possible	Intermittent
Patient 14						
day 1	Nervous system disorders	Headache	Mild	No	Possible	Single occasion

SIRS = systemic inflammatory response syndrome

Table 3 Malignant lesions detected with use of fluorescence imaging

Dose-escalation cohort	In vivo fluorescence	Ex vivo fluorescence
Primary tumours	4/7 (57%)	7/7 (100%)
Metastases	4/7 (57%)	6/7 (86%)
Expansion cohort		
All lesions	34/44 (77%)	43/44 (98%)

Data are n/N (%), for which N is the total number of resected lesions

PART IV

SUMMARY AND APPENDICES



CHAPTER II

**SUMMARY, DISCUSSION
AND FUTURE PERSPECTIVES**

SUMMARY

Near-infrared fluorescence imaging is a technique that can be used to selectively highlight certain structures during surgery. This includes structures that need to be spared (bile ducts, ureters) as well as structures that need to be resected (tumor tissue, sentinel lymph nodes). During the last decades, indications for fluorescence-guided surgery using the non-targeted fluorescent tracers ICG and MB have been explored. Currently, the focus has shifted towards development and clinical testing of novel tumor-specific fluorescent tracers. Several first-in-human studies with tumor-specific fluorescent tracers have shown promising results for selective tumor detection and resection. However, not all patients seem to benefit from this application. It is therefore of utmost importance to select vulnerable cancer patients prior to inclusion in studies and exposure to potentially harmful tumor-specific tracers.

This thesis first focuses on exploring indications of fluorescence guidance during hepato-pancreatico-biliary (HPB) surgery using ICG. Subsequently, novel tumor-targeted tracers are tested in preclinical studies and tailored tumor detection is evaluated. Finally, clinical studies with novel tumor-targeted tracers are presented for detection of colorectal- and endometrial cancer.

PART I: FLUORESCENCE-GUIDED HEPATO-PANCREATO-BILIARY SURGERY USING NON-TARGETED DYES

In **Chapter 2** a dose and time optimization study for fluorescence cholangiography is described. Literature reveals that over 1000 patients have been included in studies investigating fluorescence cholangiography during open, laparoscopic and robotic cholecystectomies. The vast majority of studies administrate a dose of 5 or 10mg ICG thirty minutes prior to fluorescence cholangiography. Yet, the optimal dose of ICG and timing of fluorescence imaging of bile ducts has never been properly investigated. Optimal would be a high fluorescent signal in bile ducts, while liver tissue in the background stains dark. This study shows that a prolonged interval (at least 3 hours) between ICG injection and intraoperative fluorescence cholangiography results in the highest contrast ratio between liver and bile ducts. This information can be applied in future studies aiming to prove the added value of fluorescence cholangiography in a randomized clinical trial.

Chapter 3 describes the application of ICG during associating liver partition and portal vein ligation for staged hepatectomy (ALPPS). This study demonstrates that fluorescence-imaging during ALPPS can provide real-time tumor margin assessment and can identify otherwise undetected tumor lesions.

Chapter 4 evaluates the use of near-infrared fluorescence guidance during laparoscopic detection and resection of occult liver tumors of various cancer types. Recurrence-free survival after radical resection of both primary and secondary liver tumors is rather low, suggesting that small malignant lesions are missed during surgical resection. We show that a variety of malignant liver tumors, such as cholangiocarcinoma, hepatocellular carcinoma and hepatic metastases of colorectal- and breast cancer and uveal melanoma, can be detected intraoperatively using ICG. Comparing sensitivity of all employed imaging techniques (CT, MRI, inspection, laparoscopic ultrasound and fluorescence imaging), we show that fluorescence imaging has the highest sensitivity for detection of small subcapsular located lesions (92.3%). Three additional, otherwise undetected, malignant lesions were identified by intraoperative fluorescence guidance only. Importantly, deeper located lesions could all be detected with laparoscopic ultrasound. All malignant lesions could be detected with the combined use of fluorescence imaging and laparoscopic ultrasound.

PART II: PRECLINICAL EVALUATION OF TUMOR TARGETS FOR FLUORESCENCE IMAGING

In **Chapter 5** the expression of Folate Receptor α (FR α) within biopsies, primary tumor specimens and metastases of lung and breast cancer is investigated. The FR α is a molecular target that is widely investigated for imaging and therapeutic purposes due to its high expression in several tumor types. In 2011 the first clinical trial with a tumor-specific fluorescent contrast agent was described by van Dam et al. using a FR α -targeting agent for ovarian cancer detection. Following this pioneering work, applications for FR α -targeted tumor detection are evaluated and investigated, among others for breast and lung cancer. In order to efficiently apply both FR α -targeted therapeutic and imaging agents, adequate patient selection regarding FR α expression is required. Moreover, information about concordance of FR α expression between several tumor lesions of an individual patient is pivotal to estimate efficacy and usability of these approaches. This study describes that false positivity of FR α expression on breast and lung cancer biopsies is limited to <5%, suggesting that biopsies can be reliably be used for patient selection. Moreover, high concordance rates of FR α expression between primary tumors and corresponding metastases of both tumor types was shown. High FR α expression was related with molecular subtypes of both cancers: in breast cancer, especially triple negative tumors show FR α expression, while in lung cancer patients adenocarcinoma shows higher expression than squamous cell carcinoma. The provided results can be used for patient selection, eventually leading to optimal personalized medicine and tailored tumor detection using fluorescent or nuclear agents.

Chapter 6 describes the preclinical validation of a novel Epithelial Cell Adhesion Molecule (EPCAM) targeted antibody fragment (EPCAM-F800) for fluorescence-guided tumor detection. EPCAM is considered as one of the most promising tumor-specific proteins due to its high expression on epithelial-derived cancers. EPCAM-F800 targets EPCAM with high specificity *in vitro*, which was also validated using *in vivo* blocking experiments with a 10x higher dose of unlabeled FAB. The optimal dose range for fluorescence tumor detection in mice was 1-5 nmol, which corresponds to a human equivalent dose of 0.2-0.8 mg/kg. Breast and colorectal tumors could be clearly visualized within 8h post injection and up to 96h, while the agent showed a homogeneous tumor distribution within 4h. Pharmacokinetic studies showed a blood half-life of 4.5h. EPCAM-F800 is currently translated for clinical use and first-in-human studies are expected to start in the near future.

In **Chapter 7** the levels of carcino-embryonal antigen (CEA) in preoperative serum is correlated with the expression of CEA on pancreatic- and rectal cancer tissue. Early phase clinical trials investigating CEA-targeted fluorescence tumor imaging are currently executed. It would be beneficial to select tumor patients with homogeneous CEA expression prior to exposure to a fluorescent labeled CEA-targeted tracer. This study demonstrates that most rectal cancer tissues (32/35) show homogeneous CEA expression, independent of serum CEA levels. In a small subset of pancreatic cancer patients (N=20), a correlation between serum CEA and expression in cancer tissue was found suggesting that selection of pancreatic cancer patients via serum CEA appears adequate.

In **Chapter 8** we investigated the expression of several promising biomarkers for rectal cancer and compared their expression before and after neoadjuvant therapy. Preoperative biopsies, primary tumor specimens and lymph node metastases of 38 rectal cancer patients who did not receive chemo-radiotherapy (CRT) were compared with 34 patients who did. Immunohistochemical analysis of CEA, EPCAM and C-MET expression showed that all were highly expressed on tumor tissue compared with normal epithelium. EPCAM showed the most homogeneous expression in tumors, while CEA showed the highest tumor-to-normal ratio. Importantly, CEA and EPCAM expression did not significantly change after CRT, whereas levels of C-MET did. These data underscore the applicability of C-MET, and especially CEA and EPCAM as targets for fluorescence-guided rectal cancer surgery both before and after CRT.

PART III: CLINICAL TRANSLATION OF TUMOR-TARGETED FLUORESCENT TRACERS

In **Chapter 9** the first clinical experience with a FR α -targeting agent in endometrial cancer is described. Detection and resection of all malignant lesions is pivotal in staging and in cytoreductive surgery of endometrial and ovarian cancer. In patients with high-risk endometrial cancer, application of a FR α -targeted imaging agent could be especially valuable, because of their relatively high likelihood of extra-uterine disease. First, expression of FR α was assessed in a tissue micro array (TMA) study consisting of tissue derived from high-risk EC patients to select patients who may benefit most from this application. A significant association between FR α and tumor type was seen, and 82% of serous and clear cell carcinomas showed FR α expression. In the clinical feasibility study, these patients were therefore enrolled. All lymph node and omental metastases could be clearly identified using OTL-38, but false-positivity was noticed in 17/50 non-metastatic lymph nodes, caused by OTL-38 targeting of FR β , expressed by tumor-associated macrophages. The role of FR β therefore needs to be further investigated before widespread implementation of OTL-38 in endometrial cancer patients.

Chapter 10 describes the clinical evaluation of a CEA-targeted near-infrared fluorescent tracer for intraoperative detection of primary and recurrent colorectal cancer, as well as their metastases. In this first-in-human study the tolerability and feasibility of SGM-101, a CEA-specific antibody conjugated to a fluorophore, is assessed. The dose escalation study in patients with primary colorectal cancer showed that highest tumor-to-background signals were obtained when administering 10mg SGM-101 four days prior to surgery and that no treatment-related adverse events occurred using this dose. In the expansion cohort, 17 patients suffering from recurrent or peritoneal metastases of CRC were included. 19 of 43 malignant lesions were identified using fluorescence imaging and were not clinically suspect before fluorescent detection. These lesions were mostly detected in patients undergoing cytoreductive surgery (13 out of 19 lesions). Larger studies are needed to investigate whether the use of SGM-101 might influence radical resection rates and completeness of surgery, which should ultimately result in improved local control and overall survival.

DISCUSSION AND FUTURE PERSPECTIVES

Fluorescence-enhanced surgical navigation has emerged as a promising technique to diminish iatrogenic damage during surgery, decrease morbidity and, potentially mortality rates. Although the technique exists for over twenty years, it is not yet

routine use in daily surgical practice. The question rises what pivotal steps are needed to move this field forward¹. Obviously, safety risks of fluorescent agents should be elucidated and potential benefits over existing practices should be demonstrated. The widely used non-targeted fluorescent dye indocyanine green (ICG) has an excellent safety profile². As described in this thesis, fluorescence cholangiography using ICG could theoretically prevent bile duct injury by highlighting the bile ducts during open, laparoscopic or robotic cholecystectomy. Prevention of bile duct injury is however a very difficult endpoint that requires huge amount of patients due its low incidence of 0.18-1.5%³. In an attempt to show the added value of fluorescence cholangiography, alternative endpoints are used in three randomized studies that are currently executed⁴. For example, the FALCON trial (clinicaltrials.gov number NCT02558556) evaluates the time to identification of the critical view of safety with and without use of ICG and, as secondary endpoint, prevention of bile duct injury.

The added value of fluorescence imaging during oncologic hepatic surgery is twofold: it can detect additional, otherwise undetected small tumors and it can provide real-time tumor margin assessment. Studies show that application of ICG results in detection of additional tumor lesions (this thesis,^{5,6}). These results are promising, but the question rises whether detection of these (mostly small) subcapsular malignancies influence the oncological outcome. When additional tumors are identified, these can be indicative of otherwise undetectable widespread metastases of the liver, or they can in fact cure the patient when resected. To answer this question, a retrospective case-control study was performed comparing long-term follow up after near-infrared (NIR) fluorescence-guided resection of colorectal liver metastases (CRLM) using ICG (N=86) vs. normal resection of CRLM (N=87). Use of NIR fluorescence guidance during surgical resection resulted in identification of significantly more tumors than the control cohort (25% vs 13%, $p=0.04$), as well as smaller tumors than compared with inspection, palpation or intraoperative ultrasound (3.2 ± 1.8 mm vs 7.4 ± 2.6 mm, $p < 0.001$). Separate analysis of the patients in whom additional metastases were found by NIR fluorescence imaging revealed that no liver recurrences occurred in 52% of patients within 3 years follow-up. Possibly, use of NIR fluorescence guidance has resulted in prevention of a recurrence in these patients. But, analysis of both cohorts showed that no significant changes in liver-specific recurrence-free survival, nor overall survival between were found. This is (most likely) the result of the study design; a study powered to show a significant difference of 7% would require a total of >1500 patients⁷. Prospective, larger multicenter studies should demonstrate the value of ICG-guided tumor detection and demarcation over the conventional techniques. Importantly, future study designs should take into account current advances in preoperative imaging modalities, such as gadoteric acid-enhanced MR imaging, leading to improved sensitivity for small sized tumor lesions⁸.

Recently the MIMIC trial has been initiated (Minimally invasive Indocyanin-guided Metastasectomy in patients with Colorectal liver metastases), a prospective multicenter study, aiming to show improved demarcation and hence, higher radical resection rates using fluorescence-enhanced surgical navigation. Potential other applications of ICG-guided liver tumor detection can be its use during laparoscopic staging procedures, for example to identify resectability of pancreatic cancers by identification of occult liver metastases⁹. Important limitations of ICG-guided liver tumor detection are inherent to the imaging technique. Only subcapsular tumors of maximally 8mm below the liver surface can be detected and it is therefore recommended to consider fluorescence imaging as complementary technique to laparoscopic ultrasound (this thesis). A possibly other imaging technique to identify more deeply located lesions is intraoperative photo-acoustic tomography, which combines the specific uptake of ICG with enhanced depth penetration¹⁰. This technique appears promising. Yet, there need to be technical advancements before it can be used in clinical practice.

A new era in the field of fluorescence-guided oncologic surgery has begun with the first clinical study in 2011 of van Dam et al. using a tumor-targeted fluorescent agent¹¹. Selection of tumor targets for imaging purposes depends on various characteristics such as (I) the upregulation of the biomarker on malignant cells compared to normal cells (II) localization on the cell membrane (III) actual number of targeted proteins available per cell (IV) percentage and distribution of expressing cells within a tumor¹². In the past decades, various promising tumor targets have been evaluated for fluorescence-guided tumor detection in preclinical studies of whom some have entered clinical trials. Examples are Folate Receptor- α (FRA)^{11,13}, Carcino-Embryonal Antigen (CEA)¹⁴, Epidermal Growth Factor Receptor (EGFR)¹⁵ and Vascular Endothelial Growth Factor (VEGF)¹⁶. Most of the tracers tested in clinical studies nowadays target membrane-bound proteins on malignant cells. Yet, future studies are awaited for showing the results of tracers that target not only malignant cells but also tumor-associated tissue at the invasive border of a tumor, e.g. stromal tissue. An example is CRGD-ZW800-I, a fluorescent labeled peptide that targets integrins associated with neo-angiogenesis. Preclinical evaluation has demonstrated real-time detection of multiple tumor types using CRGD-ZW800-I¹⁷. Other promising tracers targeting stromal tissue are cathepsin E, matrix metalloproteinases and UPAR^{18,19}.

Apart from the variety of targeted tumor molecules, there is also a wide variety of tumor-targeting ligands, e.g. peptides, antibodies, antibody fragments, nanobodies etc. Each targeting ligand has different properties and characteristics. Antibodies are believed to possess superior binding characteristics compared to smaller molecules, but their relatively large size (~150kDa) might result in heterogeneous tumor

distribution, complex pharmacokinetics, and long imaging lead-times (up to 72 h)²⁰. Antibody fragments (Fab fragments) are three times smaller and show more homogeneous tumor penetration. Moreover, they display shorter half-life times, a decreased immunotoxicity potential while they are large enough to maintain high plasma levels for optimal (tumor) distribution^{21,22}. Although smaller vehicles like nanobodies or peptides may result in even better pharmacokinetic properties (e.g. faster clearance)¹³, they can have lower stability and affinity than antibodies/Fab and more compromised by conjugation.

The idea that one target can be used for detection of all malignant cells in one tumor and in one patient appears too optimistic. It is therefore pivotal to understand the tumor landscape before exposing vulnerable cancer patients to (potentially harmful) novel agents in first-in-human studies. Different manners are performed to select patients and tumor tissue, such as analyzing biomarker expression on biopsy specimens or in preoperative obtained serum (this thesis). The work-up also includes determination of the effect of neoadjuvant therapy on biomarker expression, as well as the differences in biomarker expression between biopsies, local and distant metastases of tumors (this thesis). Current preclinical research focuses on addressing the difficulty of tumor heterogeneity. Combining multiple targets within one compound (bi-specific) may be a solution. Studies show that a so-called bi-paratopic target, e.g. an agent that targets two different epitopes on a biomarker, show considerably high specificity and sensitivity²³. Another way to address this problem is to simultaneously administer different fluorescent agents that fluoresce at various wavelengths. For example to combine administration of ICG (fluorescent at 700nm) and SGM-101 (fluorescent at 700nm) for detection of CRLM. Or, maybe even more interesting, combine the administration of a tumor-specific agent that targets membrane-bound malignant cells with the administration of an agent that targets stromal tissue at the invasive border.

One of the most important limitations of the technique of fluorescence-guided surgery is the limited depth penetration of NIR light of approximately 10mm. Tumor-specific multimodal imaging could overcome this issue. By conjugating a tumor-specific ligand with both a nuclear and fluorescent label, the location of the tumor can be preoperatively determined using SPECT/CT or PET imaging and intraoperatively by fluorescence and in case of a SPECT tracer, by a handheld Geiger counter. Proof-of-principle of this technique has been recently demonstrated by Hekman et al. showing clear pre- and intraoperative detection of renal cell carcinoma using an ¹¹¹Indium and fluorescent labeled antibody targeting carbonic anhydrase (¹¹¹In-DOTA-girentuximAb-IRDye800CW)²⁴. Another potential resolution for the limited depth penetration of NIR light is the extension beyond the NIR window

(700-900nm) into the so-called NIR-II optical window (1000-1700nm)²⁵. Using light in the NIR-II spectrum enables imaging of structures at centimeters depth due to reduced tissue scattering in the NIR-II spectrum²⁶.

The underlying principle of tumor targeting, combined with fluorescence imaging for tumor visualization can also be applied for therapeutic purposes and potentially, evaluation of therapeutic response. Tumor-targeted photodynamic therapy is a promising technique that induces cell death through light activation of a photosensitizer²⁷. Briefly, this technique requires a tumor-targeting ligand, conjugated to a fluorescent photosensitizer. After accumulation of the ligand in the tumor-target (for example an EGFR targeting nanobody) the tumor can be visualized using fluorescence imaging. Subsequently tumor margins can be locally illuminated leading to pronounced tumor necrosis and infiltration of immune cells²⁸. The therapeutic response can then be evaluated administering a fluorescent probe that targets tumor cell death, e.g. HQ4-DTPA, which has been recently described by Stammes et al²⁹.

The proof of principle of intraoperative fluorescence tumor detection has now been demonstrated for several tumor-specific fluorescent contrast agents in ovarian cancer^{11,13}, lung cancer³⁰, breast cancer³¹, head-and-neck cancer¹⁵, esophageal cancer¹⁶, pancreatic cancer¹⁴ and colorectal cancer patients³². Although all studies show promising results, it is important that results are critically evaluated before widespread implementation and/or testing in phase II/III studies. Diagnostic accuracy, the number of false positive lesions and even more important, false negative tumor lesions need to be properly investigated before moving on. This is underscored by the increasing interest in the field of fluorescence-guided pathology and elucidated by a recently described analytical framework for assessment of tracer uptake at resection borders on both a macroscopic and microscopic level³³.

As described in this thesis, application of SGM-101 led to detection of additional tumor tissue that resulted in one-third of these patients in a change of treatment plan. Obviously, large clinical studies are needed to confirm this finding and to assess whether the changes in the surgical procedure might influence radical resection rates and completeness of cytoreductive surgery. Ultimately this should result in improved local control and overall survival.

Clearly, not all tumors are amenable for application of fluorescence-guided surgery¹⁸. Solid tumors with high rates of positive resection margins as well as small tumor deposits that are easily missed by the naked eye are useful indications for this technique. The added value of tumor specific imaging during cytoreductive surgery (CRS) has been demonstrated in this thesis for colorectal cancer and in other studies for ovarian cancer^{11,13}. For both indications, literature suggests that the completeness of CRS is one of the most important prognostic factors for survival^{34,35}.

Only recently, Quenet et al. announced the first results of the randomized phase III Prodigé 7 trial, investigating the added benefit on survival of hyperthermic intraperitoneal chemoperfusion (HIPEC) to complete debulking, i.e. cytoreductive surgery, in patients with stage IV colorectal cancer³⁶. Surprisingly, median overall survival was not different between patients treated by CRS + HIPEC and patients treated by CRS alone (respectively 41.7 vs 41.2 months respectively). Importantly, the 60-day mortality rate was nearly double in the HIPEC + CRS patient group compared with the CRS group alone (24.1% vs. 13.6%). These results emphasize the potential importance of detection and resection of (often small sized) tumor lesions during CRS and the potential role of fluorescence guidance. Novel indications for fluorescence-enhanced tumor navigation also arise at the horizon. For example, application of rectal cancer detection during transanal endoscopic microsurgery or detection of residual/recurrent tumor tissue during surveillance colonoscopy of patients with a complete clinical response after neoadjuvant therapy³⁷. Response evaluation of neoadjuvant therapy is another promising application for multimodal tracers, for example in breast- or esophageal cancer.

Along with the increase of the number of clinically available fluorescent agents, numerous fluorescence imaging systems have been developed and are now clinically used³⁸. The increasing number of clinical studies, and more importantly, multicenter studies, require standards for quantification of the performance of clinically available imaging systems. Not all imaging systems share similar sensitivity (eg detection limits), which clearly hampers proper comparison between different centers and also progress of the research field. The Food and Drug Administration (FDA) and European Medicines Agency (EMA) have therefore expressed their preference that fluorescent tracers with imaging systems should be submitted as one package before market authorization³⁹. A resolution can be to use phantoms⁴⁰ or other performance tests like described by our research group to compare sensitivity between imaging systems⁴¹.

In conclusion, fluorescence-enhanced surgical navigation can revolutionize current surgical standards by highlighting structures during surgery and hence decrease iatrogenic damage and morbidity. The indications for ICG-guided surgery are still expanding, although the true added value is awaited from its application in large multicenter studies. Since the first clinical study with a tumor-targeted tracer, the research field really moved forward. Various tumor-targeted tracers already showed promising findings, resulting in detection and resection of otherwise undetected tumor tissue. Focus should now further be pointed to more intensive collaboration between fluorescence-guided research groups, standardization of the procedure and quality assurance.

REFERENCES

- Rosenthal, E. L. et al. Successful Translation of Fluorescence Navigation During Oncologic Surgery: A Consensus Report. *J Nucl Med* 57, 144-150 (2016).
- Benya, R., Quintana, J. & Brundage, B. Adverse reactions to indocyanine green: a case report and a review of the literature. *Cathet Cardiovasc Diagn* 17, 231-233 (1989).
- Tornqvist, B., Stromberg, C., Persson, G. & Nilsson, M. Effect of intended intraoperative cholangiography and early detection of bile duct injury on survival after cholecystectomy: population based cohort study. *BMJ* 345, e6457 (2012).
- Boogerd, L. S. F. et al. The Best Approach for Laparoscopic Fluorescence Cholangiography: Overview of the Literature and Optimization of Dose and Dosing Time. *Surg Innov* 24, 386-396 (2017).
- van der Vorst, J. R. et al. Near-infrared fluorescence-guided resection of colorectal liver metastases. *Cancer* 119, 3411-3418 (2013).
- Liberale, G. et al. Indocyanine green fluorescence-guided surgery after IV injection in metastatic colorectal cancer: A systematic review. *Eur J Surg Oncol* 43, 1656-1667 (2017).
- Handgraaf, H. J. M. et al. Long-term follow-up after near-infrared fluorescence-guided resection of colorectal liver metastases: A retrospective multicenter analysis. *Eur J Surg Oncol* 43, 1463-1471 (2017).
- Asato, N. et al. Comparison of gadoxetic acid-enhanced dynamic MR imaging and contrast-enhanced computed tomography for preoperative evaluation of colorectal liver metastases. *Jpn J Radiol* 35, 197-205 (2017).
- Handgraaf, H. J. M. et al. Staging laparoscopy with ultrasound and near-infrared fluorescence imaging to detect occult metastases of pancreatic and periampullary cancer. *Surg Endosc*, submitted (2018).
- Miyata, A. et al. Photoacoustic tomography of human hepatic malignancies using intraoperative indocyanine green fluorescence imaging. *PLoS One* 9, e112667 (2014).
- van Dam, G. M. et al. Intraoperative tumor-specific fluorescence imaging in ovarian cancer by folate receptor-alpha targeting: first in-human results. *Nat Med* 17, 1315-1319 (2011).
- Boonstra, M. C. et al. Selecting Targets for Tumor Imaging: An Overview of Cancer-Associated Membrane Proteins. *Biomark Cancer* 8, 119-133 (2016).
- Hoogstins, C. E. et al. A Novel Tumor-Specific Agent for Intraoperative Near-Infrared Fluorescence Imaging: A Translational Study in Healthy Volunteers and Patients with Ovarian Cancer. *Clin Cancer Res* 22, 2929-2938 (2016).
- Hoogstins, C. E. S. et al. Image-Guided Surgery in Patients with Pancreatic Cancer: First Results of a Clinical Trial Using sGM-101, a Novel Carcinoembryonic Antigen-Targeting, Near-Infrared Fluorescent Agent. *Ann Surg Oncol* 25, 3350-3357 (2018).
- Gao, R. W. et al. Safety of panitumumab-IRDYE800CW and cetuximab-IRDYE800CW for fluorescence-guided surgical navigation in head and neck cancers. *Theranostics* 8, 2488-2495 (2018).
- Nagengast, W. B. et al. Near-infrared fluorescence molecular endoscopy detects dysplastic oesophageal lesions using topical and systemic tracer of vascular endothelial growth factor A. *Gut*, 10.1136/gutjnl-2017-314953 (2017).
- Handgraaf, H. J. M. et al. Real-time near-infrared fluorescence imaging using CRGD-ZW800-1 for intraoperative visualization of multiple cancer types. *Oncotarget* 8, 21054-21066 (2017).
- Martelli, C., Lo Dico, A., Diceglie, C., Lucignani, G. & Ottobrini, L. Optical imaging probes in oncology. *Oncotarget* 7, 48753-48787 (2016).
- Boonstra, M. C. et al. uPAR-targeted multimodal tracer for pre- and intraoperative imaging in cancer surgery. *Oncotarget* 6, 14260-14273 (2015).
- Wittrup, K. D., Thurber, G. M., Schmidt, M. M. & Rhoden, J. J. Practical theoretic guidance for the design of tumor-targeting agents. *Methods Enzymol* 503, 255-268 (2012).
- Gratz, S. et al. Targeting osteomyelitis with complete 99mTc-besilesomAb and fragmented 99mTc-sulesomAb antibodies: kinetic evaluations. *QJ Nucl Med Mol Imaging* 60, 413-423 (2016).
- Watanabe, R. et al. Photoinmunotherapy targeting prostate-specific membrane antigen: are antibody fragments as effective as antibodies? *J Nucl Med* 56, 140-144 (2015).
- McCormack, E. et al. Bi-specific TCR-anti CD3 redirected T-cell targeting of NY-ESO-1- and LAGE-1-positive tumors. *Cancer Immunol Immunother* 62, 773-785 (2013).
- Hekman, M. C. et al. Tumor-targeted Dual-modality Imaging to Improve Intraoperative Visualization of Clear Cell Renal Cell Carcinoma: A First in Man Study. *Theranostics* 8, 2161-2170 (2018).
- Harmsen, S., Teraphongphom, N., Tweedle, M. F., Basilion, J. P. & Rosenthal, E. L. Optical Surgical Navigation for Precision in Tumor Resections. *Mol Imaging Biol* 19, 357-362 (2017).
- Antaris, A. L. et al. A small-molecule dye for NIR-II imaging. *Nat Mater* 15, 235-242 (2016).
- Sarcan, E. T., Silindir-Gunay, M. & Ozer, A. Y. Theranostic Polymeric Nanoparticles for NIR Imaging and Photodynamic Therapy. *Int J Pharm* (2018).
- van Driel, P. B. A. A. et al. EGFR targeted nanobody-photosensitizer conjugates for photodynamic therapy in a pre-clinical model of head and neck cancer. *J Control Release* 229, 93-105 (2016).
- Stammes, M. A. et al. The Necrosis-Avid Small Molecule HQ4-DTPA as a Multimodal Imaging Agent for Monitoring Radiation Therapy-Induced Tumor Cell Death. *Front Oncol* 6, 221 (2016).
- Predina, J. D. et al. A Phase I Clinical Trial of Targeted Intraoperative Molecular Imaging for Pulmonary Adenocarcinomas. *Ann Thorac Surg* 105, 901-908 (2018).

- 31 Lamberts, L. E. et al. Tumor-Specific Uptake of Fluorescent Bevacizumab-IRDYE800CW Microdosing in Patients with Primary Breast Cancer: A Phase 1 Feasibility Study. *Clin Cancer Res* 23, 2730-2741 (2017).
- 32 Harlaar, N. J. et al. Molecular fluorescence-guided surgery of peritoneal carcinomatosis of colorectal origin: a single-centre feasibility study. *Lancet Gastroenterol Hepatol* 1, 283-290 (2016).
- 33 Koller, M. et al. Implementation and benchmarking of a novel analytical framework to clinically evaluate tumor-specific fluorescent tracers. *Nat Commun* 9, 3739 (2018).
- 34 Sugarbaker, P. H. & Ryan, D. P. Cytoreductive surgery plus hyperthermic perioperative chemotherapy to treat peritoneal metastases from colorectal cancer: standard of care or an experimental approach? *Lancet Oncol* 13, e362-369 (2012).
- 35 Chang, S. J., Bristow, R. E. & Ryu, H. S. Impact of complete cytoreduction leaving no gross residual disease associated with radical cytoreductive surgical procedures on survival in advanced ovarian cancer. *Ann Surg Oncol* 19, 4059-4067 (2012).
- 36 Esquivel, J. Cytoreductive surgery and hyperthermic intraperitoneal chemotherapy for colorectal cancer: survival outcomes and patient selection. *J Gastrointest Oncol* 7, 72-78 (2016).
- 37 van der Valk, M. J. M. et al. Long-term outcomes of clinical complete responders after neoadjuvant treatment for rectal cancer in the International Watch & Wait Database (IWWDB): an international multicentre registry study. *Lancet* 391, 2537-2545 (2018).
- 38 AV, D. S., Lin, H., Henderson, E. R., Samkoe, K. S. & Pogue, B. W. Review of fluorescence guided surgery systems: identification of key performance capabilities beyond indocyanine green imaging. *J Biomed Opt* 21, 80901 (2016).
- 39 Tummers, W. S. et al. Regulatory aspects of Optical Methods and Exogenous Targets for Cancer Detection. *Cancer Res* 77, 2197-2206 (2017).
- 40 Zhu, B., Rasmussen, J. C., Litorja, M. & Sevik-Muraca, E. M. Determining the Performance of Fluorescence Molecular Imaging Devices Using Traceable Working Standards With SI Units of Radiance. *IEEE Trans Med Imaging* 35, 802-811 (2016).
- 41 Hoogstins, C. et al. Setting Standards for Reporting and Quantification in Fluorescence-Guided Surgery. *Mol Imaging Biol*, 10.1007/s11307-018-1220-0 (2018).

CHAPTER 12

NEDERLANDSE SAMENVATTING
CURRICULUM VITAE
DANKWOORD

Nabij-infrarode (NIR) fluorescentiebeeldvorming is een techniek die gebruikt kan worden om op een selectieve en specifieke manier anatomische structuren tijdens operatie op te laten lichten. Dit kunnen structuren zijn die gespaard moeten worden (galwegen, ureteren) of structuren die geresecteerd (tumoren, schildwachtklieren) dienen te worden. De afgelopen decennia zijn de indicaties voor fluorescentie-geleide chirurgie met behulp van de niet-tumor specifieke fluorescente stoffen indocyanine groen (ICG) en methyleen blauw (MB) uitgebreid onderzocht. Momenteel verschuift de aandacht in toenemende mate naar de ontwikkeling en het klinisch testen van tumor-specifieke fluorescente stoffen. Verscheidene first-in-human studies met tumor-specifieke fluorescente stoffen tonen hoopvolle resultaten voor selectieve tumor detectie. Echter, niet alle patiënten lijken baat te hebben bij deze toepassing. Het is daarom belangrijk om voorafgaand aan deelname in deze studies kwetsbare oncologische patiënten te selecteren om onnodige blootstelling aan potentieel schadelijke stoffen te voorkomen.

In dit proefschrift worden allereerst indicaties voor fluorescentiebeeldvorming met behulp van ICG onderzocht binnen de hepato-pancreatico-biliaire (HPB) chirurgie. Vervolgens wordt een aantal preklinische onderzoeken beschreven waarin tumor-specifieke fluorescente stoffen worden onderzocht en gepersonaliseerde tumordetectie wordt geëvalueerd. Tenslotte worden klinische studies beschreven waarin nieuwe tumor-specifieke fluorescente stoffen zijn onderzocht voor detectie van colorectaal- en endometrium carcinoom.

DEEL I: FLUORESCENTIE-GELEIDE HEPATO-PANCREATICO-BILIAIRE CHIRURGIE MET BEHULP VAN NIET-SPECIFIEKE FLUORESCENTE STOFFEN

In **hoofdstuk 2** wordt een onderzoek beschreven waarin de optimale dosis en de optimale tijd tussen toediening van ICG en fluorescentie cholangiografie wordt onderzocht. In de huidige literatuur is beschreven dat er meer dan 1000 patiënten zijn geïncludeerd in studies naar fluorescentie cholangiografie tijdens open, laparoscopische en robot cholecystectomie. De grote meerderheid van deze studies gebruikt een dosis van 5 of 10 mg ICG 30 min voorafgaand aan fluorescentie cholangiografie. De rationale voor de dosis en het tijdsinterval zijn nog niet onderzocht. In de optimale situatie zouden de galwegen een intens fluorescent signaal bevatten, terwijl de lever (achtergrond) donker zou zijn. De huidige studie toont dat een verlengd interval (ten minste 3 uur) tussen ICG toediening en intraoperatieve fluorescentie cholangiografie resulteert in de hoogste contrast ratio tussen lever en galwegen. Deze informatie kan worden toegepast in toekomstige gerandomiseerde studies die de meerwaarde van deze techniek moeten aantonen.

Hoofdstuk 3 beschrijft de toepassing van ICG tijdens associating liver partition and portal vein ligation for staged hepatectomy (ALPPS). Deze studie toont aan dat het gebruik van fluorescentiebeeldvorming tijdens ALPPS kan helpen in identificatie van tumorbegrenzing en van anderszins niet-gedetecteerde (kleine) tumoren.

Hoofdstuk 4 evalueert het gebruik van nabij-infrarode (NIR) fluorescentiebeeldvorming tijdens laparoscopische detectie en resectie van occulte levertumoren. De recidief-vrije overleving na radicale resectie van zowel primaire als secundaire levertumoren is relatief kort wat suggereert dat kleine maligne tumoren worden gemist ten tijde van operatie. Deze studie toont dat verschillende maligne levertumoren, zoals cholangiocarcinoom, hepatocellulair carcinoom en metastasen van colorectaal carcinoom, mamma carcinoom en oogmelanoom, gedurende de operatie gedetecteerd kunnen worden met behulp van ICG. Fluorescentiebeeldvorming heeft, vergeleken met alle andere gebruikte beeldvormende technieken zoals CT, MRI, inspectie en laparoscopische echografie, de hoogste sensitiviteit voor detectie van kleine subcapsulaire tumoren (92.3%). Drie additionele tumoren werden alleen gedetecteerd met behulp van fluorescentiebeeldvorming. Alle maligniteiten konden gedetecteerd worden door het gecombineerde gebruik van fluorescentiebeeldvorming en laparoscopische echografie. Deze bevinding suggereert dat beeldvorming tijdens de operatie kan bijdragen aan een meer radicale verwijdering van maligne laesies in de lever.

DEEL II: PREKLINISCHE EVALUATIE VAN TUMOR-SPECIFIEKE FLUORESCENTE CONTRASTSTOFFEN

In **hoofdstuk 5** wordt de expressie van Folaat Receptor α (FRA) onderzocht in bipten, primair tumorweefsel en metastasen van mamma- en longcarcinoom. FRA is een molecuul dat veelvuldig wordt onderzocht voor beeldvormende- en therapeutische doeleinden vanwege de hoge expressie op verschillende tumoren. In 2011 werd door van Dam et al. de eerste klinische studie beschreven met een tumor-specifieke fluorescente stof (een fluorescente stof aangrijpend op FRA) voor detectie van ovariumcarcinoom. Vervolgens zijn andere toepassingen voor FRA-doelgerichte tumordetectie geëvalueerd en onderzocht, onder andere in mamma- en longcarcinoom. Om zo efficiënt mogelijk zowel FRA-doelgerichte therapeutische als beeldvormende stoffen toe te passen, is adequate selectie van patiënten met betrekking tot FRA expressie nodig. Bovendien is informatie over de correlatie van FRA expressie tussen verschillende tumorweefsels van een individuele patiënt noodzakelijk om effectiviteit en bruikbaarheid van een stof aan te kunnen tonen. Deze studie beschrijft dat vals-positiviteit van FRA expressie op mamma- en longcarcinoom bipten beperkt is tot <5%. Dit suggereert dat bipten betrouwbaar kunnen worden gebruikt voor

patiënt selectie. Er werd eveneens een hoge correlatie aangetoond van *FR α* expressie tussen primaire tumoren en overeenkomende metastasen van beide tumortypes. Hoge *FR α* expressie bleek gecorreleerd aan moleculair subtype: in mammacarcinoom bleken met name triple negatieve tumoren *FR α* expressie te tonen, terwijl in niet-kleincellig longcarcinoom adenocarcinoom een hogere expressie toonde dan plaveiselcelcarcinoom.

Hoofdstuk 6 beschrijft de preklinische validatie van een nieuw Epithelial Cell Adhesion Molecule (EPCAM)-gericht antilichaam fragment (EPCAM-F800) voor fluorescentie-geleide tumordetectie. EPCAM wordt beschouwd als een van de meest veelbelovende tumor-specifieke eiwitten door de hoge expressie in epitheliale tumoren. EPCAM-F800 bindt aan EPCAM met hoge specificiteit in vitro, wat ook werd bevestigd door in vivo blocking experimenten met een 10x hogere dosering van onge-labeld antilichaam fragment. De optimale dosering voor fluorescente tumordetectie in muizen lag tussen 1-5 nmol, wat correspondeert met een humaan equivalente dosis van 0.2-0.8 mg/kg. Mamma- en colorectale tumoren konden duidelijk worden gevisualiseerd binnen 8u en tot 96u na injectie van EPCAM-F800, terwijl de stof al een homogene tumordistributie toonde binnen 4u. Farmacokinetische studies toonden een halfwaardetijd in bloed van 4.5h. Momenteel wordt EPCAM-F800 gereed gemaakt voor klinisch gebruik en first-in-human studies zullen binnenkort van start gaan.

In **hoofdstuk 7** wordt de waarde van carcino-embryonaal antigeen (CEA) in preoperatief serum vergeleken met expressie van CEA op pancreas- en rectumcarcinoom weefsel. Het zou gunstig zijn om oncologische patiënten met homogene CEA expressie voorafgaand aan inclusie met een fluorescent anti-CEA antilichaam te kunnen selecteren op basis van serum CEA. Deze studie toont dat de grote meerderheid van de rectumcarcinoom weefsels (32/35) homogene CEA expressie toont, onafhankelijk van serum CEA waarde. In een kleine groep van pancreascarcinoom patiënten (N=20) werd een correlatie gevonden tussen serum CEA en expressie op carcinoom weefsel, wat suggereert dat patiënt selectie voor deze ziekte via serum CEA wel adequaat zou zijn.

In **hoofdstuk 8** wordt de expressie van een aantal biomarkers voor rectumcarcinoom onderzocht waarbij ook de invloed van neoadjuvante therapie op deze expressie werd geëvalueerd. Preoperatieve bipten, primair tumorweefsel en lymfkliermetastasen van 38 patiënten die geen neoadjuvante chemoradiatie ondergingen werden vergeleken met weefsels van 34 patiënten die dit wel ondergingen. Immunohistochemische analyse van CEA, EPCAM en c-Met expressie toonde dat allen tot overexpressie kwamen op tumorweefsel ten opzichte van normaal epitheel. EPCAM toonde de meest homogene expressie in tumoren, terwijl CEA de hoogste tumor-tot-normaal ratio toonde. CEA en EPCAM expressie veranderde niet significant na neoadjuvante therapie, terwijl dit wel het geval was voor c-Met. Deze data benadrukken de toe-

pasbaarheid van c-Met, en vooral van CEA en EPCAM, als targets voor fluorescentie-geleide rectumchirurgie, zowel voor als na neoadjuvante chemoradiatie.

DEEL III: KLINISCHE TRANSLATIE VAN TUMOR-SPECIFIEKE FLUORESCENTE STOFFEN

Hoofdstuk 9 beschrijft de eerste klinische studie met een *FR α* -specifieke stof voor detectie van endometriumcarcinoom. Een cruciale stap in stagerings- en cytoreductieve chirurgie bij patiënten met endometrium- en ovarium carcinoom is de detectie en resectie van alle maligne tumoren. Met name in patiënten met een hoog-risico endometriumcarcinoom kan toepassing van een tumor-specifieke fluorescente stof van toegevoegde waarde zijn, aangezien zij relatief veel kans hebben op extra-uteriene ziekte. In de huidige studie werd allereerst expressie van *FR α* onderzocht in een tissue microarray (TMA) met weefsel van patiënten met hoog-risico endometriumcarcinoom. Een significante associatie tussen *FR α* en tumor type werd gezien; 82% van serous en heldercellig carcinoom toonde *FR α* expressie. In de klinische haalbaarheidsstudie werden vervolgens patiënten met deze tumor karakteristieken geïncludeerd. Alle lymfklier en omentale metastasen konden peroperatief worden geïdentificeerd met behulp van OTL-38 (een fluorescente stof aangrijpend op *FR α*). Echter, er werd ook een fluorescent signaal gezien in 17/50 lymfklieren die geen metastasen bevatten. Dit bleek te worden veroorzaakt door OTL-38 targeting van *FR β* ; deze receptor wordt tot expressie gebracht door tumor-geassocieerde macrofagen. De rol van *FR β* dient daarom eerst verder te worden onderzocht voorafgaand aan brede implementatie van OTL-38 tijdens chirurgie van patiënten met een endometriumcarcinoom.

Hoofdstuk 10 beschrijft de klinische evaluatie van een CEA-specifiek fluorescent antilichaam voor intraoperatieve detectie van primair-, recidief- en metastasen van colorectaal carcinoom. In deze first-in-human studie is de tolerabiliteit en haalbaarheid van SGM-101, een CEA-specifiek fluorescent antilichaam, onderzocht. De dosis-escalatie studie in patiënten met primair colorectaal carcinoom toonde dat de hoogste tumor-tot-normaal ratio werd behaald na toediening van 10 mg SGM-101 vier dagen voorafgaand aan operatie, en dat hierbij geen treatment-related adverse events (TRAE) optraden. In het tweede cohort werden 17 patiënten geïncludeerd met recidief of peritoneaal metastasen van colorectaal carcinoom. Negentien van de 43 maligne tumoren, die niet klinisch verdacht waren voorafgaand aan fluorescente detectie, werden eerst gedetecteerd met behulp van fluorescentiebeeldvorming. Deze tumoren waren vooral aanwezig in patiënten die cytoreductieve chirurgie ondergingen (13 van de 19 tumoren). Onderzoeken met grotere aantallen patiënten zijn nodig om te onderzoeken of het gebruik van SGM-101 kan leiden tot toename van het aantal radicale resecties, wat uiteindelijk kan resulteren in verbeterde lokale controle en algehele overleving.

LIST OF PUBLICATIONS

Boogerd LSF, Boonstra MC, Prevoo HAJM, Handgraaf HJM, Kuppen PJK, MacDonald GJ, Cizeau J, Premasukh A, Vinkenburg ML, Sier CFM, van de Velde CJH, Burggraaf J and Vahrmeijer AL. Fluorescence-guided tumor detection with a novel anti-epCAM targeted antibody fragment: preclinical validation. *Surg Oncol* 2019 (in press)

Hoogstins CES, Burggraaf JJ, Koller M, Handgraaf HJM, **Boogerd LSF**, van Dam GM, Vahrmeijer AL, Burggraaf J. Setting standards for reporting and quantification in fluorescence-guided surgery. *Mol Imaging Biol.* 2019 Feb;21(1):11-18.

Handgraaf HJM, Sibinga Mulder BG, Shahbazi Feshtali S, **Boogerd LSF**, van der Valk MJM, Fariña Sarasqueta A, Swijnenburg RJ, Bonsing BA, Vahrmeijer AL, Mieog JSD. Staging laparoscopy with ultrasound and near-infrared fluorescence imaging to detect occult metastases of pancreatic and periampullary cancer. *PLoS One.* 2018 Nov 13;13(11):e0205960.

Hoogstins CES, **Boogerd LSF**, Sibinga Mulder BG, Mieog JSD, Swijnenburg RJ, van de Velde CJH, Fariña Sarasqueta A, Bonsing BA, Framery B, Pèlegriñ A, Gutowski M, Cailler F, Burggraaf J, Vahrmeijer AL. Image-Guided Surgery in Patients with Pancreatic Cancer: First Results of a Clinical Trial Using SGM-101, a Novel Carcinoembryonic Antigen-Targeting, Near-Infrared Fluorescent Agent. *Ann Surg Oncol.* 2018 Oct;25(11):3350-3357.

Boogerd LSF, van der Valk MJM, Boonstra MC, Prevoo HAJM, Hilling DE, van de Velde CJH, Sier CFM, Fariña Sarasqueta A, Vahrmeijer AL. Biomarker expression in rectal cancer tissue before and after neoadjuvant therapy. *Oncotargets Ther.* 2018 Mar 23;11:1655-1664.

Boogerd LSF, Hoogstins CES, Gaarenstroom KN, de Kroon CD, Beltman JJ, Bosse T, Stelloo E, Vuyk J, Low PS, Burggraaf J, Vahrmeijer AL. Folate receptor- α targeted near-infrared fluorescence imaging in high-risk endometrial cancer patients: a tissue microarray and clinical feasibility study. *Oncotarget.* 2017 Dec 11;9(1):791-801.

Boogerd LSF, Hoogstins CES, Schaap DP, Kusters M, Handgraaf HJM, van der Valk MJM, Hilling DE, Holman FA, Peeters KCMJ, Mieog JSD, van de Velde CJH, Fariña-Sarasqueta A, van Lijnschoten I, Framery B, Pèlegriñ A, Gutowski M, Nienhuijs SW, de Hingh IHJT, Nieuwenhuijzen GAP, Rutten HJT, Cailler F, Burggraaf J, Vahrmeijer AL. Safety and effectiveness of SGM-101, a fluorescent antibody targeting carcinoembryonic antigen, for intraoperative detection of colorectal cancer: a dose-escalation pilot study. *Lancet Gastroenterol Hepatol.* 2018 Mar;3(3):181-191.

Handgraaf HJM, **Boogerd LSF**, Shahbazi Feshtali S, Fariña Sarasqueta A, Snel M, Swijnenburg RJ, Vahrmeijer AL, Bonsing BA, Mieog JSD. Intraoperative Near-Infrared Fluorescence Imaging of Multiple Pancreatic Neuroendocrine Tumors: A Case Report. *Pancreas.* 2018 Jan;47(1):130-133.

Hoogstins CES, Weixler B, **Boogerd LSF**, Hoppener DJ, Prevoo HAJM, Sier CFM, Burger JW, Verhoef C, Bhairosingh S, Fariña Sarasqueta A, Burggraaf J, Vahrmeijer AL. In Search for Optimal Targets for Intraoperative Fluorescence Imaging of Peritoneal Metastasis From Colorectal Cancer. *Biomark Cancer.* 2017 Aug 28;9:1179299

Boogerd LSF, Vuijk FA, Hoogstins CES, Handgraaf HJM, van der Valk MJM, Kuppen PJK, Sier CFM, van de Velde CJH, Burggraaf J, Fariña-Sarasqueta A, Vahrmeijer AL. Correlation Between Preoperative Serum Carcinoembryonic Antigen Levels and Expression on Pancreatic and Rectal Cancer Tissue. *Biomark Cancer.* 2017 May 17;9:1179299

Handgraaf HJM, **Boogerd LSF**, Höppener DJ, Peloso A, Sibinga Mulder BG, Hoogstins CES, Hartgrink HH, van de Velde CJH, Mieog JSD, Swijnenburg RJ, Putter H, Maestri M, Braat AE, Frangioni JV, Vahrmeijer AL. Long-term follow-up after near-infrared fluorescence-guided resection of colorectal liver metastases: A retrospective multicenter analysis. *Eur J Surg Oncol.* 2017 Aug;43(8):1463-1471.

Boogerd LSF, Handgraaf HJM, Huurman VAL, Lam HD, Mieog JSD, van der Made WJ, van de Velde CJH, Vahrmeijer AL. The Best Approach for Laparoscopic Fluorescence Cholangiography: Overview of the Literature and Optimization of Dose and Dosing Time. *Surg Innov.* 2017 Aug;24(4):386-396.

Handgraaf HJM, Boonstra MC, Prevoo HAJM, Kuil J, Bordo MW, **Boogerd LSF**, Sibinga Mulder BG, Sier CFM, Vinkenburg-van Slooten ML, Valentijn ARPM, Burggraaf J, van de Velde CJH, Frangioni JV, Vahrmeijer AL. Real-time near-infrared fluorescence imaging using CRGD-ZW800-1 for intraoperative visualization of multiple cancer types. *Oncotarget*. 2017 Mar 28;8(13):21054-21066.

Stegehuis PL, **Boogerd LSF**, Inderson A, Veenendaal RA, van Gerven P, Bonsing BA, Sven Mieog JSD, Amelink A, Veselic M, Morreau H, van de Velde CJH, Lelieveldt BP, Dijkstra J, Robinson DJ, Vahrmeijer AL. Toward optical guidance during endoscopic ultrasound-guided fine needle aspirations of pancreatic masses using single fiber reflectance spectroscopy: a feasibility study. *J Biomed Opt*. 2017 Feb 1;22(2):24001.

de Geus SW, **Boogerd LSF**, Swijnenburg RJ, Mieog JSD, Tummers WS, Prevoo HAJM, Sier CFM, Morreau H, Bonsing BA, van de Velde CJH, Vahrmeijer AL, Kuppen PJ. Selecting Tumor-Specific Molecular Targets in Pancreatic Adenocarcinoma: Paving the Way for Image-Guided Pancreatic Surgery. *Mol Imaging Biol*. 2016 Dec;18(6):807-819.

Boogerd LSF, Handgraaf HJM, Lam HD, Huurman VA, Fariña-Sarasqueta A, Frangioni JV, van de Velde CJH, Braat AE, Vahrmeijer AL. Laparoscopic detection and resection of occult liver tumors of multiple cancer types using real-time near-infrared fluorescence guidance. *Surg Endosc*. 2017 Feb;31(2):952-961.

Tummers QRJG, **Boogerd LSF**, de Steur WO, Verbeek FP, Boonstra MC, Handgraaf HJM, Frangioni JV, van de Velde CJH, Hartgrink HH, Vahrmeijer AL. Near-infrared fluorescence sentinel lymph node detection in gastric cancer: A pilot study. *World J Gastroenterol*. 2016 Apr 7;22(13):3644-51.

Boogerd LSF, Boonstra MC, Beck AJ, Charehbil A, Hoogstins CES, Prevoo HAJM, Singhal S, Low PS, van de Velde CJH, Vahrmeijer AL. Concordance of folate receptor- α expression between biopsy, primary tumor and metastasis in breast cancer and lung cancer patients. *Oncotarget*. 2016 Apr 5;7(14):17442-54.

Boogerd LSF, Handgraaf HJM, Lam HD, Braat AE, Baranski AG, Swijnenburg RJ, Frangioni JV, Vahrmeijer AL, Ringers J. Application of near-infrared fluorescence imaging during modified associating liver partition and portal vein ligation for staged hepatectomy. *Surgery*. 2016 May;159(5):1481-2.

Bongers PJ, **Boogerd LSF**, Handgraaf HJM, Hoogstins CES, van de Velde CJH, Burggraaf J, Vahrmeijer AL. Image-guided surgery using fluorescence: road to clinical translation of novel probes. *SPIE BIOS* 2016.

Handgraaf HJM, **Boogerd LSF**, Verbeek FP, Tummers QRJG, Hardwick JC, Baeten CI, Frangioni JV, van de Velde CJH, Vahrmeijer AL. Intraoperative fluorescence imaging to localize tumors and sentinel lymph nodes in rectal cancer. *Minim Invasive Ther Allied Technol*. 2016;25(1):48-53.

Boogerd LSF, Handgraaf HJM, Boonstra MC, Vahrmeijer AL and van de Velde CJH. Image-guided surgery. In: Poston GJ, Wyld L, Audisio A, editors. *Surgical Oncology: Theory and multidisciplinary Practice*. 2016.

Boogerd LSF, Handgraaf HJM, van de Velde CJH, Vahrmeijer AL. Image-guided surgery using near-infrared fluorescent light: from bench to bedside. *SPIE BIOS*. 2015;93110-UII

Boonstra MC, Tolner B, Schaafsma BE, **Boogerd LSF**, Prevoo HA, Bhavsar G, Kuppen PJ, Sier CFM, Bonsing BA, Frangioni JV, van de Velde CJH, Chester KA, Vahrmeijer AL. Preclinical evaluation of a novel cEA-targeting near-infrared fluorescent tracer delineating colorectal and pancreatic tumors. *Int J Cancer*. 2015 Oct 15;137(8):1910-20.

Handgraaf HJM, Verbeek FP, Tummers QRJ, **Boogerd LSF**, van de Velde CJH, Vahrmeijer AL, Gaarenstroom KN. Real-time near-infrared fluorescence guided surgery in gynecologic oncology: a review of the current state of the art. *Gynecol Oncol*. 2014 Dec;135(3):606-13.

Boogerd LSF, Perk LE and van Acker GJ. Pigtail stent for gallbladder drainage. *Ned Tijdschr Geneeskd*. 2014; 158:A7518

CURRICULUM VITAE

Noor Boogerd werd geboren op 5 april 1987 te Haarlem. In 2005 behaalde zij haar eindexamen aan het Stedelijk Gymnasium Haarlem, waarna zij startte met de studie Bouwkunde aan de Technische Universiteit Delft. Na twee jaar begon zij haar studie Geneeskunde aan het Leids Universitair Medisch Centrum (LUMC). Tijdens haar studie werkte zij onder andere op de Spoedeisende Hulp van het Reinier de Graaf Gasthuis in Delft. Daarnaast was zij actief lid van de Delftsche Studenten Vereniging dsc. Haar klinische stage deed zij op de kinderoncologie afdeling in het Khanti Children Hospital in Kathmandu (Nepal) en het coschap gynaecologie in Paramaribo (Suriname). Ten tijde van haar semi-arts stage chirurgie in het Haags Medisch Centrum zette zij klinisch onderzoek op naar transpapillaire galblaasdrainage. Haar wetenschappelijke stage volgde zij bij het Greenlight-onderzoeksteam naar fluorescente detectie van schildwachtklieren bij maagcarcinoom. Aansluitend hieraan begon zij in januari 2014 haar promotieonderzoek als arts-onderzoeker van de Image-Guided Surgery groep in het LUMC onder leiding van dr. A.L. Vahrmeijer (promotores: Prof. dr. C.J.H. van de Velde en Prof. J. Burggraaf). In die tijd schreef zij mee aan meerdere grants, waaronder die voor het KWF en KNAW. Daarnaast ontving zij een fellowship grant van de European Society of Surgical Oncology voor de ECCO-AACR-EORTC-ESMO workshop 'Methods in clinical cancer research' in Flims, Zwitserland.

In mei 2017 startte zij als ANIOS chirurgie in het voormalige MC Slotervaart (op-leider: dr S.C. Bruin) waar zij met veel plezier heeft gewerkt. In januari 2018 is zij begonnen met haar opleiding Chirurgie aan het Amsterdam UMC, locatie VUMC (op-leider: Prof. dr. D.L. van der Peet), waar zij momenteel werkzaam is.

DANKWOORD

Allereerst wil ik alle patiënten die hebben deelgenomen aan het klinische onderzoek hartelijk bedanken. Zonder hen was dit proefschrift er niet geweest. Ik heb veel respect voor alle patiënten die in emotionele tijden deelnemen aan (ons) onderzoek om de wetenschap verder te helpen.

Dr. Vahrmeijer, allerbeste Lex, bedankt voor het vertrouwen dat jij vanaf begin af aan in mij hebt getoond. Jij hebt mij vrijgelaten om verschillende onderzoeken op te zetten, waarbij alles op een creatieve manier mogelijk was. Ik heb veel van je geleerd en kijk uit naar de voortzetting van onze samenwerking!

Prof. Burggraaf, allerbeste Koos. Samen met jou hebben we de afgelopen jaren de first-in-human studies tot een hoger niveau gebracht. Werken op zaterdagen in het CHDR was nooit een kwelling door jouw plotselinge verschijning inclusief bloemen. Bedankt voor de leerzame discussies, (feestelijke) congressen en gastvrijheid op het CHDR.

Prof. van de Velde, beste professor. Ik beschouw het als een eer om onder uw leiding promotie onderzoek te hebben uitgevoerd. Uw staat van dienst heeft mij bijzonder geïnspireerd. Dank voor het vertrouwen, de begeleiding en de altijd verrassende anekdotes.

Prof. Frangioni, thank you for your support with our manuscripts. Dear Marty and Phil Low, thank you for the pleasant collaboration. I enjoyed working with you and discussing the future perspectives of OTL-38 during our trips abroad. Dr. Cailler, dear Françoise, thank you for the opportunity to investigate SGM-101 and assistance during the trial.

Chirurgen van het LUMC, gynaecologen en anesthesiologen: bedankt voor jullie medewerking tijdens onze klinische studies! Ook wil ik mijn dank uitspreken voor de pathologen die hebben meegewerkt aan ons onderzoek (in het bijzonder Arantza!). Margriet, Dorien, Graziella en alle nurse-practitioners van het CHDR: bedankt voor jullie hulp met includeren van patienten.

Green(dream)team, dankzij jullie was mijn promotietraject een feest! Joost, bedankt voor het stimuleren om onderzoek te doen bij Lex, jij hebt de deur voor mij geopend! Sven, Rutger-Jan, Merlijn, Bob, Floris, Denise: dank voor jullie hulp tijdens de studies. Mijn J3 kamergenoten: Mark, de preklinische koning! We hebben mooie tijden beleefd bij onze vrienden op de Eo, met als hoogtepunten onze EPCAM publicatie en natuurlijk jouw huwelijk afgelopen zomer. O, door jouw enthousiasme en discipline was je een voorbeeld voor mij als wetenschapsstage-begeleider. Hein,

bedankt voor het aanhoren van mijn verhalen, lachen om mijn goede grappen en natuurlijk ook de fantastische samenwerking! Lieve Char, mijn mede hottie, wat was het een feest om samen de laatste jaren de SGM-101 en OTL-38 studies te leiden. Lieve Babs (Babbel), wat een geluk dat jij ineens mijn nieuwe kamergenoot werd; ik heb heel veel van je (knorretje) lach genoten en kijk uit naar de roze ginto's! Maxime, Thomas, Marion, Kim en Ruben: de bal ligt nu bij jullie! Heel veel plezier met de (spannende) klinische studies die gaan komen. Kees, Marieke (Prevo) en Shadhvi: zonder jullie was dit proefschrift er niet geweest. Heel veel dank voor jullie hulp in het lab.

Prof. Rutten en de andere GE-chirurgen uit het Catharina ziekenhuis, bedankt voor de prettige samenwerking. Wij hebben ons altijd welkom gevoeld bij jullie en ik vind het heel leuk om te zien hoe jullie geïnspireerd zijn door de fluorescentie-beeldvorming. Miranda en Dennis, jullie wil ik in het bijzonder bedanken voor jullie bijdrage tijdens de SGM-101 studie.

Dank aan alle chirurgen van het MC Slotervaart en uiteraard ook mijn mede AIOS (Rutger, Pim, Marije, Patrick, Beaat, RJ en Hoda) en ANIOS voor het vertrouwen in mij tijdens mijn vuurdoop in de kliniek na mijn onderzoekstijd. De laatste periode was hectisch maar zeker ook bijzonder om met jullie mee te maken. Dank ook aan mijn huidige collega's van de chirurgie in het AUMC, locatie VUMC!

Lieve paranimfen. Marijk, aka Mary Temporary, wat ben ik blij dat jij vandaag naast mij staat op deze bijzondere dag. Dank voor je eindeloze steun, grappen en ontspannende danspassen in de woestijn (met Jo)! Lieve Joelle, jouw doorzettingsvermogen, nuchterheid en enthousiasme zijn uniek en aanstekelijk. Ik geniet enorm van de vele tijd die wij samen doorbrengen, of het nou hardlopend, skiënd of dansend is. Lieve Hippo's, wie had gedacht dat ik het zo naar mijn zin kon hebben in Delft? Ik had me geen leuker huis dan de Hippo kunnen wensen! Lieve Club ZO, heel veel dank voor de leuke en ontspannende momenten. Leonie, Jet en Charlotte: jullie steun is altijd heel waardevol voor mij geweest. Lieve Merel, my sister from another mister, life never gets boring with you! Dat geldt zeker ook voor mijn favoriete danspartners Jo & Leo! Lieve adinda, meik, amber & marijk: jullie betrokkenheid is goud waard!

Lieve pap en mam, bedankt voor jullie steun bij alle stappen die ik tot nu toe in het leven heb gezet. Lieve Erik, op naar een rooskleurige toekomst met Danielle samen! Ik ben zo trots op je! DJ, Emilie, Willem en Guus: wat een geluk om jullie familie te zijn. Ik waardeer het enorm dat jullie deur altijd voor mij open staat na een lange werkdag. Lieve Rein, niemand kan zo hard om mijn grappen lachen als jij, mij zo geruststellen en eindeloos veel vertrouwen in mij hebben. Op naar een leven vol avontuur samen!

